DTU Library

CO$_2$ Capture Dynamic and Steady-State Model Development, Optimization and Control: Applied to Piperazine and Enzyme Promoted MEA/MDEA

Gaspar, Jozsef

Publication date:
2016

Document Version
Publisher's PDF, also known as Version of record

[Link back to DTU Orbit](#)

CO2 Capture Dynamic and Steady-State Model Development, Optimization and Control

Applied to Piperazine and Enzyme Promoted MEA/MDEA

József Gáspár
PhD Thesis
September 2016

DTU Chemical Engineering
Department of Chemical and Biochemical Engineering
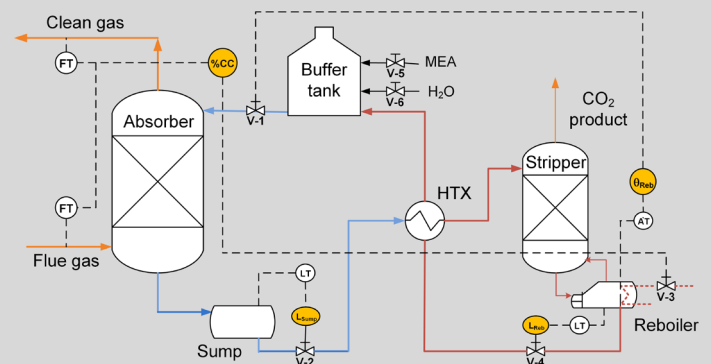
CO_2 Capture Dynamic and Steady-State Model Development, Benchmarking, Optimization and Control: Applied to Piperazine and Enzyme Promoted MEA/MDEA

Ph.D. Thesis
by
József Gáspár
2016

Center for Energy Resources Engineering
Department of Chemical and Biochemical Engineering
Technical University of Denmark
Kongens Lyngby, Denmark

Preface

This Thesis is submitted as partial fulfilment of the requirement for the Ph.D. degree at Technical University of Denmark (DTU). The work has been carried out at Center for Energy Resources Engineering, Department of Chemical and Biochemical Engineering from December 2012 to May 2016 under the supervision of Assoc. Prof. Philip Loldrup Fosbøl, Assoc. Prof. John Bagterp Jørgensen, Assoc. Prof. Kaj Thomsen and Assoc. Prof. Nicolas von Solms. The project was funded by DTU Chemical Engineering and the European Union's FP7 Research and Innovation programme as part of the OCTAVIUS project.

I would like to express my sincere gratitude to all my supervisors for their excellent guidance, valuable suggestions and continuous support on the research presented in this thesis. It has been a very rewarding experience for me to work with you. Philip thank you for always finding time for me and following my development closely and with great interest. My genuine thanks to all the members of Center for Energy Resources Engineering (CERE) for their moral support and for all the good times. I deeply cherish those memories. I am especially grateful to Anne Louise Biede for being patient and keeping our spirits up.

I want to thank Assist. Prof. Luis Ricardez Sandoval at University of Waterloo for the good collaboration, interesting discussions and his willingness to share his vast knowledge in the field of dynamic simulation and control during the period I spent there.

Finally, I want to thank my parents and my siblings for always pursuing me and supporting me to become the person I am today. Without your everlasting love and care I could not pursue my dreams. I am forever grateful. Carolina, I am grateful for you. I wasn't looking for you but I am very lucky I met you. I want to thank you for being next to me and loving me. I want to thank you for helping and supporting me.

I would like to dedicate this thesis to my family and to my love.

Jozsef Gaspar
May 2016
Kgs. Lyngby, Denmark

Summary

Despite the efforts and recent advances in renewable energy sources, the energy infrastructure is not yet ready to replace the fossil-fuel fired power plants with renewables. Thermal power plants represent the main energy supply and especially in developing countries, they are expected to dominate the market in the coming decades. However, the growing focus on mitigation of anthropogenic CO_2 requires integration of fossil-fuel fired power plant with CO_2 capture units. Post-combustion capture is the most mature capture technology and it is suitable for various processes in power plants, steel industry, cement production, and bio-chemical industry. However, to make CO_2 capture economically attractive, design of innovative solvents, optimization of operation conditions/process configuration and operational flexibility are of crucial importance.

This thesis aims to contribute to the development of efficient CO_2 post-combustion capture technology using alkanolamine solvents. Amine based CO_2 post-combustion capture is a reactive absorption process which implies complex mechanism of simultaneously occurring reaction and mass transport phenomena. Accordingly, first a simplified and easy to implement but general valid mass transfer model is developed and applied to single and parallel reactions systems, i.e. MEA, PZ and CA/MDEA. This mass transfer model uses existing correlations for mass and hydraulic characteristic and an enhancement factor to describe the acceleration of the mass transfer rate due to the reaction between CO_2 and amines. Afterwards, this sub-model together with the extended UNIQUAC thermodynamic model and correlations for physical properties is incorporated in a rate-based model for CO_2 absorption and desorption. The developed model is applied to MEA, PZ, PZ/K_2CO_3 and CA/MDEA and it is benchmarked against experimental pilot plant data and various models from independent research groups.

The validated steady-state model is used to determine set of optimal operation parameters for CO_2 capture post-combustion capture using PZ. This study accounts for the solubility window of PZ when determining the optimal and feasible operating conditions. The results are created in Aspen Plus using the hybrid CAPCO2 rate-based user model. This model considers slurry formation in the calculation of CO_2 mass transfer rate. The results show how the capture process needs to be operated up to 14% above the minimum achievable heat duty, to avoid clogging from solid formation. 5 molal PZ is the most promising trade-off between energy efficiency and solid-free operation with a specific reboiler duty of 3.22 GJ/t CO_2 at 0.34 lean loading.

Furthermore, this thesis presents a dynamic rate-based model for CO_2 absorption and desorption using MEA and PZ as solvent. This dynamic model is an extension of the steady-state model as it uses the same thermodynamic-, mass transfer-, kinetic- and physical property- modules. These modules are implemented in

Fortran and interfaced with the dynamic model which is implemented in Matlab. The developed model is used to investigate the transient behavior of a post-combustion plant using MEA and PZ. Moreover, a proportional-integral control structure is developed to investigate the controllability of the PZ based post-combustion plant compared to the MEA plant. The results reveal that PZ may be a better solvent than MEA as it can accommodate disturbances with less variability in the manipulated variables. However, control design alternatives and/or model based control structure should be developed to reduce the long settling time of the PZ plant compared to the MEA plant.

Dansk Resumé

Trods de mange nylige tiltag og fremskridt inden for vedvarende energikilder, er energiinfrastrukturen endnu ikke klar til at erstatte de fossilt fyrede kraftværker med vedvarende energi. Termiske kraftværker udgør den vigtigste energiforsyning, og især i udviklingslandene forventes de at dominere markedet i de kommende årtier. Men det stigende fokus på afhjælpning af menneskeskabt CO_2 kræver integration af fossilt fyrede kraftværk med CO_2-opsamlingsenheder. Post-forbrænding-opsamling er den mest modne opsamlingsteknologi, og den egner sig til forskellige processer i kraftværker, cementproduktion, stålindustrien, og den biokemiske industri. Men design af innovative solventer, optimering af driftsbetingelser/proceskonfigurering og operationel fleksibilitet er af afgørende betydning for, at CO_2-opsamling bliver økonomisk attraktiv.

Denne afhandling har til formål at bidrage til udviklingen af en effektiv post-forbrændings CO_2-opsamlingsteknologi ved hjælp alkanolamine solventer. Aminbaserede CO_2 post-forbrændingsopsamling er en reaktiv absorptionsproces, som indebærer komplekse mekanismer af simultant forekommende reaktions- og massetransportfænomener. Derfor er der i første omgang blevet udviklet en forenklet og let implementerbar, men generelt valid massetransportmodel, som er blevet anvendt til enkeltstående og parallelle reaktionssystemer, dvs. MEA, PZ og CA/MDEA. Denne masseoverføringsmodel benytter eksisterende korrelationer for masse og hydraulisk karakteristik, samt en forøgelsesfaktor til at beskrive accelerationen af massens overføringshastighed som følge af reaktionen mellem CO_2 og aminer. Efterfølgende er denne under-model og den udvidede UNIQUAC termodynamiske model og korrelationer for fysiske egenskaber blevet inkorporeret i en hastighedsbaseret model for CO_2-absorption og -desorption. Den udviklede model er blevet anvendt på MEA, PZ, PZ / K_2CO_3 og CA / MDEA og benchmarket mod data fra eksperimentelle pilotanlæg data og forskellige modeller fra uafhængige forskergrupper.

Den validerede steady-state model anvendes til at bestemme sæt af optimale driftsparametre for CO_2-opsamling efter forbrænding ved hjælp af PZ. Denne undersøgelse redegør for PZ's opløselighedsvindue, når optimale og gennemførlige driftsforhold fastsættes. Resultaterne er frembragt i Aspen Plus ved hjælp af den hybride CAPCO2 hastigheds-baserede brugermodel. Denne model tager højde for opslæmning i beregningen af CO_2 massetransporthastighed. Resultaterne viser, hvordan opsamlingsprocessen skal køre op til 14% over det mindst opnåelige varmekrav, for at undgå tilstopning pga. dannelse af faste strukturer. 5 molal PZ udgør det mest lovende tradeoff mellem energieffektivitet og drift uden problemer med dannelse af faste strukturer med en specifik kedelkrav på 3.22 GJ/t CO_2 ved 0.34 lean-loading.

Envidere præsenterer denne afhandling en dynamisk hastigheds-baseret model for CO_2-absorption og desorption med MEA og PZ som solvent. Denne dynamiske model er en udvidelse af steady-state modellen,

6

da den anvender samme moduler for termodynamik, masseoverførsel, kinetik og fysiske egenskaber. Disse moduler er implementeret i FORTRAN og interfacer med den dynamiske model, som er implementeret i Matlab. Den udviklede model benyttes til at undersøge transient opførsel i et post-afbrændingssanlæg, som benytter MEA og PZ. Derudover er en proportional-integral kontrolstruktur blevet udviklet med henblik på at undersøge kontrollerbarheden af PZ-baserede post-forbrændingsanlæg i forhold til MEA anlæg. Resultaterne viser, at PZ kan være et bedre solvent end MEA, da det kan håndtere forstyrrelser med mindre variation i de manipulerede variabler.

TABLE OF CONTENT

Chapter 1. Introduction

1.1 Energy production and CO_2 emissions

The CO_2 intensiveness of the energy sector creates concerns regarding changes in Earth's climate. Accordingly, policymakers and scientists are working on developing a sustainable energy infrastructure while meeting the energy demand of the growing population and limiting the changes in the climate.

According to the Fifth Assessment Report (AR5) by the Intergovernmental Panel on Climate Change (IPCC), CO_2 emissions from the energy sector will double or even triple by 2050 compared to the level of 14.4 Gt CO_2/year in 2010 . The rapid increase of CO_2 emissions is mainly due to the growing energy demand and increased use of coal in the global fuel mix. Currently, fossil fuels meet more than 80% of total primary energy demand and over 90% of energy-related CO_2 emissions are from combustion of fossil-fuels (Olivier et al., 2015; Yamaguchi, 2012). In addition to the CO_2 emissions, other greenhouse gases in smaller quantities such as methane, nitrous oxides and water are emitted by the power industry. These gases are less long-lasting in the atmosphere though with higher global warming potential (van der Hoeven, 2015). Consequently, replacing current world average coal-fired power plants with modern, highly efficient natural gas combined-cycle power plants or combined heat and power plants is essential to significantly reduce the greenhouse gas (GHG) emissions from the energy supply. Mitigating GHGs and especially the carbon intensity of the energy sector is a key component for stabilizing the climate and the level of CO_2 in the atmosphere (Pachauri et al., 2014).

As a result, renewable energy sources, e.g. hydropower-, solar-, wind- energy are the fastest growing sources of electricity and further growth of renewables is expected. According to the reference case of EIA (2013). Figure 1.1 shows that in 2015 5.3 trillion kWh electricity was produced worldwide by hydropower and non-hydropower renewables and it is expected to increase with a rate of 2.8 percent per year to 9.6 trillion kWh net electricity in 2040. The world non-hydropower electricity production is expected to double over the next 25 years by increasing from 1.5 trillion kWh to 3.4 trillion kWh. Approximately 80% of the predicted increase in renewable electricity productions will be generated by hydropower and wind power (van der

Hoeven, 2015). Non-hydropower renewable energy sources such as wind-, biofuel- and solar- energy may revolutionize the energy market, however the infrastructure is not ready to shut-down the fossil-fuel fired thermal power plants. Figure 1.1 highlights that after renewables, natural gas is the fastest growing source of electricity, with an expected increase of 2.5 percent per year. Although, coal-fired electricity generation will increase only by an annual average of 1.8% over the next 25 years, slowing down after 2020, coal still will dominate the future energy market. Coal is projected to remain the largest source of power generation through 2040, and subsequently the largest source of CO_2 emissions.
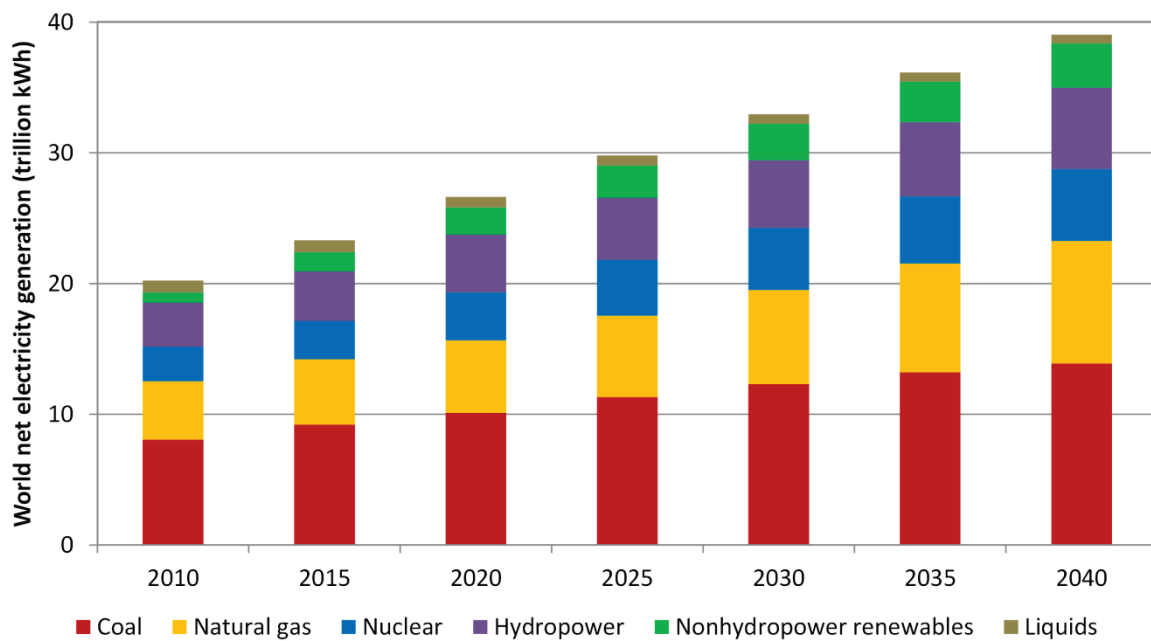
Figure 1.1. World net electricity generation by energy sources, 2010 – 2040 (EIA, 2013)

Therefore, effective action in the energy sector is essential to attack the climate change problem. On a global level, not one but the combination of different technologies will be needed to reach the zero CO_2 emission goal. Carbon capture and storage (CCS) is one of the key short and mid-term promising solutions. CCS technologies have the potential to reduce the lifecycle GHG emissions of fossil fuel power plants and to achieve low-CO_2 electricity supply. Moreover, combining bioenergy with CCS could supply energy with net negative CO_2 emissions (Mathews, 2008). While all of the components of CCS exist and are widely used by the fossil-fuel extraction and refining industry, the widespread and commercial implementation of CCS must be incentivized by governmental regulations and by reducing investment and operational cost of capture plants (Pachauri et al., 2014).

1.2 Amine CO$_2$ post-combustion capture

Numerous research and development projects are being conducted throughout the world on CCS. Post-combustion capture, pre-combustion capture and oxy-fuel process are the three main approaches investigated for CO$_2$ capture from the power industry (Figueroa et al., 2008; Rochelle, 2009; Wang et al., 2011). Post-combustion capture is particularly interesting as a retrofit option to existing power plants compared to the other two options. A post-combustion capture unit can be integrated into a power plant without fundamental changes in the power plant by modifying only the low-temperature steam part. In addition, post-combustion process achieves the highest degree of purity for the product CO$_2$ stream (>99.99%). Another advantage of this process is that all of the components are commercially available (Markewitz, 2015). However, these advantages come at the expense of efficiency reduction of the power generation process.

Several separation technologies are being developed for post-combustion capture, such as adsorption, cryogenic separation, physical absorption, membrane absorption, membrane-based separation and chemical absorption. Significant experience has already been acquired with aqueous alkanolamines based chemical absorption, which is commercially applied in industrial processes, e.g. ammonia production, natural gas treatment, refining industry, etc. The basic absorption-desorption technology for acid gas treating (amine scrubbing) was patented in 1930 by Bottoms (1930). This process consists of: (1) an absorber where an acid gas is removed from a gas stream at near ambient temperature using an aqueous amine solution and (2) a stripper tower where the CO$_2$ rich amine from the absorber is regenerated by stripping with water vapor at 100 to 120°C. The heat needed for CO$_2$ stripping is supplied in the reboiler. The lean regenerated amine solution is sent back to the absorber through the lean-rich heat exchanger and a cooler to bring its temperature down. Steam is recovered in the overhead condenser and fed back to the stripper whereas the CO$_2$ product gas leaves the stripper. The basic flowsheet of the process is presented in figure 1.2.

The amine scrubbing technology from the chemical industry cannot be directly transferred to the power generation process since the flue gas composition and its flow rate are very different in a power plant compared to other industrial processes (Markewitz, 2015). As a result, several research projects focus on developing and improving the amine CO$_2$ removal process in order to demonstrate its economic and technical feasibility for power plants' flue gas cleaning. For example, the European Commission has funded several research projects under the 6th and 7th Framework Program such as CASTOR, CESAR, iCAP, CAPRICE, OCTAVIUS, INTERACT. The main goal of these projects is to significantly reduce the he cost of CO$_2$ capture and to address issues related to geological storage. These projects involve development of reliable modeling tools, investigation of techno-economic feasibility as well as technology demonstration on pilot and industrial scale. These studies cover aspects related to steady-state and dynamic operation of the capture plant. In the United States of America, the Luminant carbon management program aims (1) to help

the deployment of CO_2 post-combustion removal by use of aqueous amines and (2) to improve the integration of carbon capture process with storage as well as enhanced oil recovery (Wang et al., 2011). Besides the pilot activities using MEA, PZ and PZ promoted K_2CO_3 respectively MDEA solvents, they research CO_2 rate kinetics and solubility, degradation of solvents and system modeling (Bishnoi and Rochelle, 2002, 2000; Dang and Rochelle, 2003; Ding et al., 2014; Dugas and Rochelle, 2011a; Freeman et al., 2009; Oyenekan and Rochelle, 2009; Sachde et al., 2013). Their most relevant contribution is the so called advanced flash stripper configuration using 5 and 8 molal PZ (Rochelle et al., 2011). A novel approach is the Carbon Capture Simulation Initiative (CCSI) with the purpose of developing and deploying state-of-the-art computational modeling and simulation tools to accelerate the commercialization of carbon capture technologies. These tools will increase confidence in designs, reducing the risk associated with incorporating multiple innovative technologies into new carbon capture solutions. The research in CCS in Australia is dominated by the Commonwealth Scientific and Industrial Research Organization (CSIRO). They concentrate on reducing and improving the efficiency of CCS, especially post-combustion capture in order to make it a viable option for Australia's energy future. The final goal of CSIRO is deploying large-scale demonstration projects that enable substantial reductions in emissions and provide a pathway for industry to adopt the technologies at full scale. The list of CCS activities is fairly long and they can be found elsewhere. An overview of some of the main activities is provided by Folger (2013); Pires et al. (2011); Wang et al. (2011) and at www.zeroco2.no/projects/list-projects/.
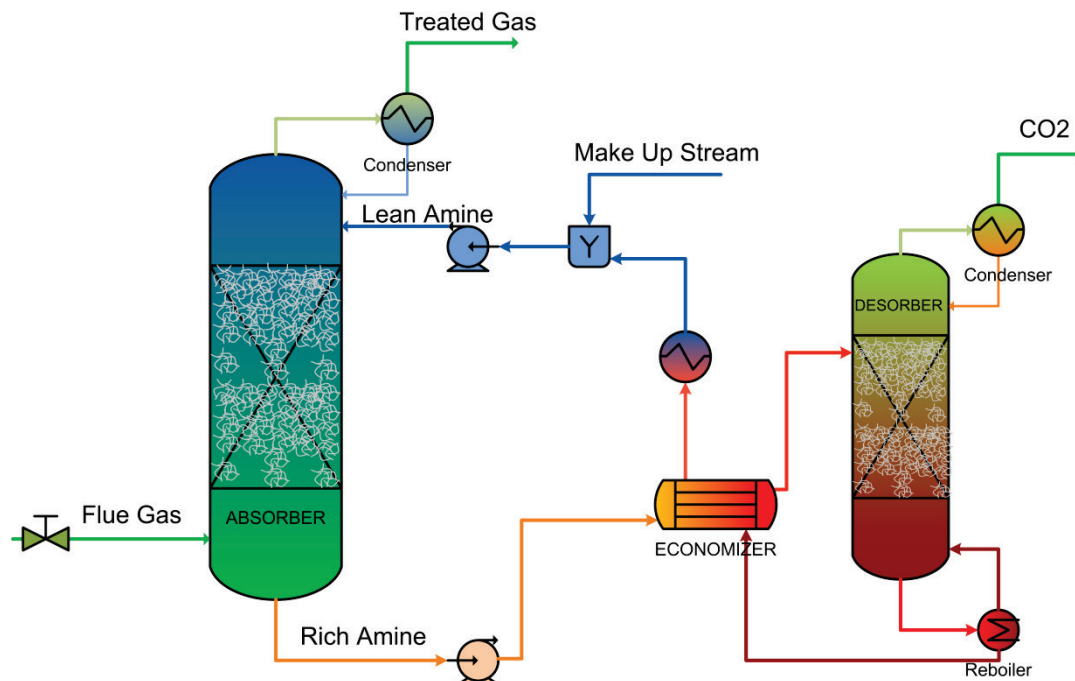
Figure 1.2. Process flow diagram for acid gas recovery from a flue gas by amine absorption

A possible pace of development for amine CO_2 post-combustion capture from power plants was discussed by Rochelle (2009) through an analogy to limestone slurry scrubbing. He showed that limestone scrubbing for flue gas desulfurization was first applied in 1936; however it was considered too expensive and too commercial for government-funded research and development in the 1960s. Nevertheless, this process was further developed and 60-250 MW prototypes were deployed in 1968. These prototypes formed the base for commercialization of 500+ MW capacity plants through the 1970s and beyond. Amine based post-combustion CO_2 removal from power plants was first identified in 1991 and similar to the limestone process, it was considered inefficient and too commercial for governmental support. The financial support shifted to other advanced technologies for CO_2 capture, however the interest in post-combustion capture has not been lost and great effort was invested in optimizing and reducing the cost of post-combustion capture. In the last 10-15 years, several bench and pilot scale studies demonstrated the technical feasibility of this process and optimized its economics. Post-combustion capture achieved an important milestone in 2014 with the Boundary Dam unit 3 (net capacity 120 MW) in Canada becoming the first commercial plant with integrated CO_2 capture. Another important milestone will be the upgrade of the Parish plant, Thompsons, Texas, USA with a post-combustion unit able to capture 90% of CO_2 from a 240 MW slip stream from the 610 MW unit. This project is scheduled to start at the end of 2016. Consequently, similar to the limestone scrubbing process, amine scrubbing was the first choice and still is the dominant technology for CO_2 capture from coal-fired power plants. However, further development of this technology is needed in order to develop more efficient systems by reducing the operational cost related to amine regeneration, compression, etc. Further research will make available the process at a lower capital cost by reducing the size of the absorber, heat exchangers, compressors, etc. It will also guarantee that power plants with integrated CO_2 capture will be able respond to changes in a volatile energy market.

1.3   Significance of the research

It is more and more recognized that CO_2 capture technologies will play an important role in mitigating the CO_2 emission rate of thermal power plants and stabilizing the climate. Solvent based post-combustion capture was the first choice for CO_2 capture from thermal plants and it is suitable for various processes in steel industry, cement production, and bio-chemical industry. As many times stated by Garry T. Rochelle, one of the leading researchers in the CO_2 capture field, solvent based post-combustion capture "is here to stay". Several studies confirmed that post-combustion capture is a competitive technology and it is the only capture alternative ready to be implemented on industrial scale.

Post-combustion capture is established but to make it economically attractive, development of innovative solvents, optimization of operating parameters and process design is of crucial importance. Thus, simulation and experimental studies intensively focus on these aspects to decrease the energy demand and the capital

cost of the capture plant. Detailed experimental trials are unfeasible and very expensive due to the abundance of potential blends of amines and the broad range of operating conditions encountered in post-combustion processes. Steady-state respectively dynamic modeling and simulation are consequently indispensable to develop, design, optimize and operate a post-combustion capture process. Thus, in addition to extensive experimental evaluation, accurate dynamic and steady-state models for both absorption and desorption are required to develop an energy efficient capture process using single and promoted solvents.

Solvent based post-combustion capture involves reactive absorption which implies a complex mechanism of both thermodynamic and chemical nature. Models for reactive absorption processes have to consider the simultaneously occurring reaction and mass transport phenomena. An important characteristic of CO_2 absorption and desorption is the variation of reaction rates, from low (slow reactions) to infinitely high (instantaneous reactions). Thus, the modeling of these mechanisms requires an adequate mass transfer model which is rigorous enough to incorporate all the complex aspects of reactive absorption and computationally manageable in order to enable plant-wide simulation and optimization. This mass transfer model couples to differential mass respectively energy conservation equations, to a thermodynamic model and correlations for physical and hydraulic properties. These sub-models represent the base of the dynamic respectively steady-state CO_2 absorption and desorption models. It can be seen that the resulting mathematical problem requires solving of a multi-coupled ordinary differential equations system and non-linear algebraic equations for a steady-state simulation and a multi-coupled partial differential equations system and non-linear algebraic equations for a dynamic simulation.

Although, the benchmark mono-ethanolamine CO_2 capture process has been extensively studied in the past, there is a lack of knowledge regarding dynamic and steady-state modelling, simulation and optimization of CO_2 post-combustion capture using novel solvents, e.g. piperazine, piperazine promoted solvents, enzyme enhanced amine solvents. These novel solvents have the potential to greatly reduce the energy demand of solvent regeneration and the capital cost of the capture unit. To fully explore the benefits and drawbacks of these novel systems, a general absorption respectively desorption model should be developed based on consistent modelling principles. To develop a reliable capture process model, all of the mentioned sub-models must be validated against experimental data followed by the validation of the column model against individual experimental data and finally against data from continuous operation in a pilot or industrial plant. After a simulator has been thoroughly validated, it can be used to evaluate process feasibility and economics, to study process alternatives, to optimize the design and the operation with respect to energy demand and operational constraints.

Furthermore, recently it has been recognized that dynamic studies are required to gain insight regarding the transient behaviour of a capture process, and to design operational strategies. Dynamic studies are essential

to identify potential bottlenecks during operation and to ensure operability of power plants with integrated CO_2 capture. Understanding of process dynamics is especially important in the coming dynamic energy market. Currently, most of the controllability and flexibility studies are performed using the baseline MEA solvent; however it is vital to understand similarities and differences in the operation of the MEA plant and better solvents, e.g. piperazine. Additionally, possible challenges which may emerge with novel solvent must be identified and tackled before large-scale deployment.

1.4 Research objectives

This work was performed to increase understanding of reactive absorption and to contribute to the development of efficient solvent based CO_2 post-combustion capture technology from a steady-state and dynamic point of view. Accordingly, the main research objectives are as follows:

1. To study mass transfer theories with the purpose of creating a practical but accurate model for simulation of parallel interacting reactions systems.
2. To create a standardized and consistent approach for steady-state and dynamic simulation of CO_2 post-combustion capture using in-house models and industrial process simulators.
3. To investigate the expected accuracy of steady-state and dynamic rate-based models.
4. To understand the importance of solid formation in modeling and performance evaluation of CO_2 post-combustion capture.
5. To reduce the energy consumption of the solvent regeneration unit.
6. To study the dynamic behaviour of the absorber and of the desorber using novel solvents.
7. To investigate the controllability of a pilot-scale post-combustion unit using novel solvents.

1.5 Research methodology

In order to achieve the specified objectives: (1) a theoretical and a modeling study has been performed to simulate, to optimize and to control a CO_2 post-combustion capture plant and (2) a novel enhancement factor model for CO_2 mass transfer rate calculation has been developed. Accordingly, the methodology of the present study is as follows:

1. To develop an enhancement factor model for CO_2 mass transfer rate calculation which applies to absorption, desorption and pinch conditions:
    1.1. To deduce the model for an *(m+n)-th* order single reversible reaction and multiple parallel reactions.
    1.2. To compare the model predictions against the numerical solution of the two-film model using the benchmark monoethanol-amine (MEA) solvent.

1.3. To apply the model for multiple parallel reactions using the innovative piperazine (PZ) and enzyme promoted methyl-di-ethanol-amine (MDEA) solvents.

2. To develop and validate a steady-state rate-based model for CO_2 absorption and desorption:

   2.1. To extend and to validate the CAPCO2 standalone model to novel solvents, i.e. PZ, PZ promoted K_2CO_3, MDEA, and carbonic anhydrase (CA) enhanced MDEA.

   2.2. To compare and to benchmark the model against experimental data and other process simulators.

   2.3. To implement an interface between the CAPCO2 model and industrial simulation engines for plant-wide process simulation using CAPE-OPEN and Aspen Custom Modeler (ACM).

3. To simulate and to optimize a PZ based CO_2 post-combustion capture process considering precipitation.

4. To develop a mechanistic dynamic rate-based model of a pilot-scale CO_2 post-combustion capture plant using MEA and PZ:

   4.1. To implement a mechanistic dynamic model of an MEA and PZ based CO_2 post-combustion capture process.

   4.2. To validate the dynamic model against experimental data.

   4.3. To compare the transient behaviour of the capture plant using MEA and PZ.

5. To develop and evaluate a proportional-integral control structure for a pilot-scale CO_2 capture plant using MEA and PZ.

1.6   Contribution and structure of the thesis

The present thesis presents steady-state and dynamic modeling, simulation, benchmarking, optimization and control of CO_2 post-combustion capture using amines. Additionally, it presents a novel enhancement factor model for CO_2 mass transfer rate calculation. These results have been published in 12 articles and they have been presented at prestigious conferences. These works represent the core of the thesis which is organized in seven chapters:

The General Method (GM) enhancement factor model for single and multiple parallel reactions is presented in **Chapter 2**. It is based on papers 2 and 4. First, the GM model is derived for a reversible *(m+n)*-th order, forward reaction kinetics and applied to CO_2-MEA-H_2O system. Then, the model is extended to multiple parallel reactions and it is applied to CO_2-PZ-H_2O and CO_2-CA/MDEA-H_2O parallel reactions systems. Finally, the GM model is implemented in the rate-based column model for PZ, PZ/K_2CO_3, CA/MDEA and MEA solvents for CO_2 absorption and desorption. Chapter 2 shows the GM model calculations against the numerical solution of the two-film model, previous enhancement factor models, respectively wetted-wall column experimental data. The results illustrate that the GM model overlap with the numerical solution of the two-film model, both at absorber and desorber conditions and for high driving force and pinch conditions

when using MEA as solvent. Moreover, a comparison to wetted-wall column data reveals that GM accurately predicts the CO_2 mass transfer rate when using piperazine respectively enzyme (CA) promoted MDEA solvents. This study shows that GM connects the Onda's approximation for reversible reactions with the van Krevelen's approach for instantaneous irreversible reactions and it eliminates many of the limitations of previous approaches. GM has a noticeable potential to enhance the accuracy of process simulators without significantly increasing the complexity of the numerical procedure.

Chapter 3 presents the development and validation of the absorption/desorption model. This chapter encapsulates papers 10 to 12. Chapter 3 provides a summary of relevant previous works. It presents the modeling basis and derives the model equations. The thermodynamic model, the numerical approach and the physical property correlations are also described in this chapter. The developed rate-based unit plugs into Aspen Plus using Cape-Open respectively Aspen Custom Modeler interfaces. The results demonstrate that the model consistently and accurately predicts the absorption and desorption process as well as the interaction between the units for all of the investigated solvents. This chapter also introduces a first-of-its-kind hybrid rate-based model for solid/slurry forming systems, i.e. PZ. The hybrid model includes the solid-liquid phase change when predicting the CO_2 mass transfer rates between the gas phase and the liquid phase. This study underlines that precipitation reduces the piperazine solvent CO_2 capture capacity by deactivating it. Consequently, the accurate description of the precipitation phenomenon is essential for realistic and accurate modeling of CO_2 absorption.

Chapter 4 shows a systematic and comprehensive evaluation of the absorption capacity and energy performance of a PZ based post-combustion CO_2 capture process. In addition, the energy penalty is minimized as part of the closed-loop multivariable optimization, taking into account the solubility window of piperazine. This chapter is based on papers 3 and 7. The results show how the capture process needs to be operated above the minimum achievable heat duty, to avoid potential clogging from precipitation. This chapter suggests solvent compositions which result in low heat requirement and solid-free operation.

Chapter 5 shows a mechanistic dynamic rate-based model for CO_2 absorption and desorption using MEA and PZ. It also compares the transient behaviour of an MEA and of a PZ plant for relevant operation scenarios, e.g. changes in the flue gas, lean solvent, heat supply, etc. This chapter encapsulates papers 5, 6, 8, and 9. The dynamic process model of the complete CO_2 capture plant is implemented in Matlab. This represents a unique feature since most of the current simulations available for this process have made use of standard software packages. The dynamic model is consistent with the steady-state model, using the GM enhancement factor model, the extended UNIQUAC thermodynamic model respectively mass transfer and hydraulic correlations.

Chapter 6 presents a decentralized control scheme and shows the performance of the PZ and MEA based CO_2 capture process for industrially-relevant operation scenarios, i.e. large load changes, malfunctioning of the lean-valve and limited heat supply. It is based on paper 1. This chapter shows that proportional-integral control structure can handle large changes in the capture plant's load for PZ and MEA when the manipulated variables do not reach their saturation limit. The results outline that in presence of shortages in the steam supply, the MEA plant controllers drive the system towards drying out/flooding while the CO_2 capture rate performance of the PZ plant reduces drastically. These findings suggest the need for model based control which can explicitly account for constraints in the process variables.

Chapter 7 summarizes the findings and gives recommendations for future work.

1.7 List of Research Papers and Conference Contributions

The following is a list of relevant papers and conference contributions to the thesis which has been performed by the author of this thesis:

Peer-reviewed articles:

1. **Gaspar, J.**, Ricardez-Sandoval, L.A.,, Jørgensen, J.B., Fosbøl, P.L. 2016. Controllability and Flexibility Analysis of CO_2 Post-combustion Capture Using Piperazine and MEA. International Journal of Greenhouse Gas Control 51, 276-289.

2. **Gaspar, J.,** Fosbøl, P.L. 2016. Practical enhancement factor model based on GM for multiple parallel reactions: Piperazine (PZ) CO_2 capture. Chemical Engineering Science (*accepted, 2016*).

3. **Gaspar, J.**, Fosbøl, P.L., 2016. Simulation and Multivariable Optimization of Post-combustion Capture Using Piperazine. International Journal of Greenhouse Gas Control 49, 227–238.

4. **Gaspar, J.**, Fosbøl, P.L., 2015. A General Enhancement Factor Model for Absorption and Desorption Systems: A CO_2 Capture Case-Study. Chemical Engineering Science 138, 203–215.

5. **Gaspar, J.**, Ricardez-Sandoval, L.A, Jørgensen, J.B., Fosbøl, P.L., 2016. Dynamic Simulation and Analysis of a Pilot-Scale CO_2 Post-combustion Capture Unit Using Piperazine and MEA. Proceedings of DYCOPS-CAB. IFAC (accepted).

6. **Gaspar, J.**, Gladis, A., Jørgensen, J.B., Thomsen, K., von Solms, N., Fosbøl, P.L., 2016. Dynamic Operation and Simulation of Post-Combustion CO_2 Capture. Energy Procedia 86, 205–214.

7. **Gaspar, J.**, von Solms, N., Thomsen, K., Fosbøl, P.L., 2016. Multivariable Optimization of the Piperazine CO_2 Post-Combustion Process. Energy Procedia 86, 229–238.

8. **Gaspar, J.**, Jorgensen, J.B., Fosbøl, P.L., 2015. Control of a Post-combustion CO_2 Capture Plant during Process Start-up and Load Variations. IFAC-PapersOnLine. IFAC 48, 580–585.

9. **Gaspar, J.**, Jørgensen, J.B., Fosbøl, P.L., 2015. A Dynamic Mathematical Model for Packed Columns in Carbon Capture Plants, Proceedings of ECC Conference. IFAC, http://www.ifac-papersonline.net/, pp. 2743–2748. doi:10.1109/ECC.2015.7330952.

10. **Gaspar, J.**, Thomsen, K., von Solms, N., Fosbøl, P.L., 2014. Solid Formation in Piperazine Rate-based Simulation. Energy Procedia 63, 1074–1083.

11. **Gaspar, J.**, Waseem Arshad, M., Ask Blaker, E., Langseth, B., Hansen, T., Thomsen, K., von Solms, N., Fosbøl, P.L. 2014. A Low Energy Aqueous Ammonia CO_2 Capture Process. Energy Procedia 63, 614–623.

12. Fosbøl, P.L., **Gaspar, J.**, Ehlers, S., Kather, A., Briot, P., Nienoord, M., Khakharia, P., Le Moullec, Y., Berglihn, O.T., Kvamsdal, H.M. 2014. Benchmarking and Comparing First and Second Generation Post Combustion CO_2 Capture Technologies. Energy Procedia 63, 27–44.

Conference contributions:

1. **Gaspar, J.**, Ricardez-Sandoval, L.A, Jørgensen, J.B., Fosbøl, P.L. Dynamic Simulation and Analysis of a Pilot-Scale CO_2 Post-combustion Capture Unit Using Piperazine and MEA. DYCOPS-CAB conference. 6-8 June 2016. Trondheim, Norway (oral presentation in the invited sessions).

2. **Gaspar, J.**, Gladis, A., Jørgensen, J.B., Thomsen, K., von Solms, N., Fosbøl, P.L. Dynamic Operation and Simulation of Post-Combustion CO_2 Capture. TCCS-8 conference. 16-18 June 2015. Trondheim, Norway (oral presentation).

3. **Gaspar, J.**, von Solms, N., Thomsen, K., Fosbøl, P.L. Multivariable Optimization of the Piperazine CO_2 Post-Combustion Process. TCCS-8 conference. 16-18 June 2015. Trondheim, Norway (oral presentation).

4. **Gaspar, J.**, Jørgensen, J.B., Ricardez-Sandoval, L.A., Thomsen, K., Fosbøl, P.L. 2016. Controllability and Flexibility Analysis of a CO_2 Capture Plant using MEA and Piperazine Promoted K_2CO_3. 3rd Post Combustion Capture Conference. 8-11 September 2015. Regina, Saskatchewan, Canada (oral presentation)

5. **Gaspar, J.**, Jorgensen, J.B., Fosbøl, P.L. Control of a Post-combustion CO_2 Capture Plant during Process Start-up and Load Variations. 9th ADCHEM conference. 7-10 June 2015. Whistler, British Columbia, Canada (oral presentation).

6. **Gaspar, J.**, Jørgensen, J.B., Fosbøl, P.L. A Dynamic Mathematical Model for Packed Columns in Carbon Capture Plants, ECC15 Conference. 15-17 July 2015. Linz, Austria (oral presentation)

7. **Gaspar, J.**, Thomsen, K., von Solms, N., Fosbøl, P.L. Solid Formation in Piperazine Rate-based Simulation. GHGT-12 conference. 6-9 October 2014. Austin, Texas, USA (poster).

8. **Gaspar, J.**, Waseem Arshad, M., Ask Blaker, E., Langseth, B., Hansen, T., Thomsen, K., von Solms, N., Fosbøl, P.L. 2014. A Low Energy Aqueous Ammonia CO_2 Capture Process. 6-9 October 2014. Austin, Texas, USA (oral presentation).

9. Fosbøl, P.L., **Gaspar, J.**, Ehlers, S., Kather, A., Briot, P., Nienoord, M., Khakharia, P., Le Moullec, Y., Berglihn, O.T., Kvamsdal, H.M. Benchmarking and Comparing First and Second Generation Post Combustion CO_2 Capture Technologies. 6-9 October 2014. Austin, Texas, USA (oral presentation).

10. **Gaspar, J.**, Thomsen, K., von Solms, N., Loldrup Fosbøl, P. Rate-based CO_2 Post-combustion Modeling in Aspen Plus using CERE Cape Open Modules. University of Texas Carbon Capture Storage (UTCCS-2). 27-29 January 2014. Austin, Texas (oral presentation).

11. **Gaspar, J.**, Thomsen, K., von Solms, N., Fosbøl, P.L. Interfacing Absorber and Desorber Columns for CO_2 Post-combustion Modelling. 7th Trondheim Conference on CO_2 Capture, Transport and Storage (TCCS-7). 4-6 June 2013. Trondheim, Norway (poster).

References

Bishnoi, S., Rochelle, G.T., 2002. Absorption of carbon dioxide in aqueous piperazine/methyldiethanolamine. AIChE J. 48, 2788–2799. doi:10.1002/aic.690481208

Bishnoi, S., Rochelle, G.T., 2000. Absorption of carbon dioxide into aqueous piperazine: reaction kinetics, mass transfer and solubility. Chem. Eng. Sci. 55, 5531–5543. doi:10.1016/S0009-2509(00)00182-2

Bottoms, R.R., 1930. Separating acid gases. U.S. Patent 1783901.

Dang, H.Y., Rochelle, G.T., 2003. CO2 absorption rate and solubility in monoethanolamine/piperazine/water. Sep. Sci. Technol. 38, 337–357. doi:10.1081/SS-12016678

Ding, J., Lin, Y.-J., Rochelle, G.T., 2014. Optimization of Stripping Piperazine with Variable Rich Loading. 12th Int. Conf. Greenh. Gas Control Technol. GHGT-12 63, 1842–1853. doi:http://dx.doi.org/10.1016/j.egypro.2014.11.192

Dugas, R.E., Rochelle, G.T., 2011. CO2 Absorption Rate into Concentrated Aqueous Monoethanolamine and Piperazine. J. Chem. Eng. Data 56, 2187–2195. doi:10.1021/je101234t

EIA, U.S., 2013. International Energy Outlook 2013 with Projections to 2040. Washington, US.

Figueroa, J.D., Fout, T., Plasynski, S., McIlvried, H., Srivastava, R.D., 2008. Advances in CO2 capture technology—The U.S. Department of Energy's Carbon Sequestration Program. Int. J. Greenh. Gas Control 2, 9–20. doi:10.1016/S1750-5836(07)00094-1

Folger, P., 2013. Carbon capture: a technology assessment.

Freeman, S.A., Dugas, R., Van Wagener, D., Nguyen, T., Rochelle, G.T., 2009. Carbon dioxide capture with concentrated, aqueous piperazine. Energy Procedia 1, 1489–1496. doi:10.1016/j.egypro.2009.01.195

Markewitz, P., 2015. Carbon Capture, Storage and Use, Carbon Capture, Storage and Use: Technical, Economic, Environmental and Societal Perspectives. Springer International Publishing, Cham. doi:10.1007/978-3-319-11943-4

Mathews, J.A., 2008. Carbon-negative biofuels. Energy Policy 36, 940–945. doi:10.1016/j.enpol.2007.11.029

Olivier, J.G.J., Muntean, M., Peters, J.A.H.W., 2015. Trends in global CO2 emissions: 2015 report. PBL Netherlands Environ. Assess. Agency Eur. Comm. Jt. Res. Cent. 1–78.

Oyenekan, B.A., Rochelle, G.T., 2009. Rate modeling of CO2 stripping from potassium carbonate promoted by piperazine. Int. J. Greenh. Gas Control 3, 121–132. doi:http://dx.doi.org/10.1016/j.ijggc.2008.06.010

Pachauri, R.K., Allen, M.R., Barros, V.R., Broome, J., Cramer, W., Christ, R., Church, J.A., Clarke, L., Dahe, Q., Dasgupta, P., Dubash, N.K., Edenhofer, O., Elgizouli, I., Field, C.B., Forster, P., Friedlingstein, P., Fuglestvedt, J., Gomez-Echeverri, L., Hallegatte, S., Hegerl, G., Howden, M., Jiang, K., Cisneroz, B.J., Kattsov, V., Lee, H., Mach, K.J., Marotzke, J., Mastrandrea, M.D., Meyer, L., Minx, J., Mulugetta, Y., O'Brien, K., Oppenheimer, M., Pereira, J.J., Pichs-Madruga, R., Plattner, G.-K., Pörtner, H.-O., Power, S.B., Preston, B., Ravindranath, N.H., Reisinger, A., Riahi, K., Rusticucci, M., Scholes, R., Seyboth, K., Sokona, Y., Stavins, R., Stocker, T.F., Tschakert, P., van Vuuren, D., van Ypserle, J.-P., 2014. Climate Change 2014: Synthesis Report. Contribution of Working Groups I, II and III to the Fifth Assessment Report of the Intergovernmental Panel on Climate Change. Cambridge University Press, Geneva, Switzerland.

Pires, J.C.M., Martins, F.G., Alvim-Ferraz, M.C.M., Simões, M., 2011. Recent developments on carbon capture and storage: An overview. Chem. Eng. Res. Des. 89, 1446–1460. doi:10.1016/j.cherd.2011.01.028

Rochelle, G., Chen, E., Freeman, S., Van Wagener, D., Xu, Q., Voice, A., 2011. Aqueous piperazine as the new standard for CO2 capture technology. Chem. Eng. J. 171, 725–733. doi:10.1016/j.cej.2011.02.011

Rochelle, G.T., 2009. Amine scrubbing for CO2 capture. Science (80-.). 325, 1652–1654.

Sachde, D., Chen, E., Rochelle, G.T., 2013. Modeling Pilot Plant Performance of an Absorber with Aqueous Piperazine. Energy Procedia 37, 1987–2001. doi:10.1016/j.egypro.2013.06.079

van der Hoeven, M., 2015. Energy and Climate Change.

Wang, M., Lawal, A., Stephenson, P., Sidders, J., Ramshaw, C., 2011. Post-combustion CO2 capture with chemical absorption: A state-of-the-art review. Chem. Eng. Res. Des. 89, 1609–1624. doi:10.1016/j.cherd.2010.11.005

Yamaguchi, M., 2012. Climate change mitigation : a balanced approach to climate change. Springer.

ZeroCO2.NO, n.d. List of CCS-projects [WWW Document]. URL http://www.zeroco2.no/projects/list-projects/ (accessed 5.12.16)

Chapter 2. Simultaneous mass transfer and reaction modeling

Part A. A general enhancement factor model for absorption and desorption systems: A CO_2 capture case-study

Abstract

This study derives a general method (GM) for reactive absorption and desorption calculation. It connects the Onda's approximation for reversible reactions with the van Krevelen's approach for instantaneous irreversible reactions. It is set-up for a reversible $(m+n)$-th order, forward reaction kinetics and applied for the CO_2-MEA-H_2O second order reversible system. The results show that the GM predicts the two-film theory within 2% accuracy and the surface renewal model within 10% accuracy, both at absorber and desorber conditions and for high driving force and pinch conditions. GM is compared to the ideas of van Krevelen, and Astarita & Savage. An analysis demonstrates how the GM model eliminates many of the limitations of previous approaches. It has a noticeable potential to enhance the accuracy of process simulators without sacrificing the simulation time. It could eliminate the need for conservative and uncertain design and therefore it will lead to more realistic cost estimations.

Keywords: Two-film model, surface renewal model, enhancement factor, mass transfer rate, CO_2 post-combustion capture.

2.A.1 Introduction

Important chemical processes like carbon capture, flue gas desulphurisation, synthesis gas purification, manufacturing of nitric acid, chlorination, hydrogenation, etc. all involve an absorption process to clean or upgrade the products. It may even require a desorption process to regenerate the solvents. These processes are usually carried out in gas-liquid contactors like packed columns, spray reactors, bubble columns, falling

film reactors etc. (King, 1966). Processes which are intensively used; however the principal modelling is still approximate.

More accurate and general models are needed for development of efficient and innovative equipment design, to upgrade the technical level and to perform better economic optimizations. The knowledge of hydrodynamics and non-ideal thermodynamics is essential (Versteeg, 2001). The description of reactive mass transfer resistance can still be improved. Current models are either computationally heavy or inaccurate approximations. A balance between accuracy and computational requirements needs to be found for industrial simulations and applications.

Three frameworks are typically used in the description of gas liquid hydrodynamics. These are the two-film theory, the penetration theory and the surface renewal model. Originally the film theory was developed by Lewis& Whitman (1924). The equations were setup assuming a stagnant film of liquid and a stagnant film of gas on the two sides of the interface. The resistance to mass transfer is concentrated in these layers and the transfer occurs by molecular diffusion. Higbie introduced the so called penetration theory (Higbie, 1935). This model assumes the gas-liquid interphase to be non-stagnant. Fluid elements rise from the liquid bulk to the interface where they remain for a period of time, the contact time. Subsequently the fluid orbits back into the solution. The theory proposed by Danckwerts (1951), is a modification of Higbie's model. It is known as the surface renewal theory and assumes a contact time distribution of the liquid elements. The models consider mass transfer through a laminar layer.

To solve a full numerical scheme using the above theories a number of mass and energy balances are needed to describe the system. These are typically formulated as non-linear partial differential equations. Even with the current technological advances, solving a full numerical scheme is still computationally heavy. One way to reduce the complexity of a mass transfer model is to introduce the enhancement factor, which is defined as the ratio of mass transfer from chemical absorption compared to physical absorption. It is therefore a relative factor which indicates the improvements of a reactive solvent compared to a physical non-reactive solvent. The enhancement factor is preferred in process simulations since it reduces the computational load. Several enhancement factor approximations were developed during the last century. One of the pioneering works is the simplified approach introduced by van Krevelen& Hoftijzer (1948). It describes the mass transfer rate of a reactive system in the pseudo-first order regime. Later, an algebraic method for a second-order reversible reaction was presented by Onda et al. (1970). Since then, various approximate models were derived for well-defined reaction regimes and reaction kinetics. Hogendoorn et al. (1997) proposed an explicit relation for reversible and finite rate reactions. This approximation has an adaptive tuning factor. These models are derived from the film theory. Another model is the interface-pseudo-first-order approximation (IPFO) used for CO2 capture modelling. This model assumes that as a consequence of fast kinetics, the concentration of

the species excluding CO2 is constant at its interface value. The IPFO model has been developed based on the eddy diffusivity theory (Al-Juaied, 2004; Freguia& Rochelle, 2003). The advantage of the Eddy theory over the penetration theory and the surface renewal theory is that it describes the dependence of the mass transfer coefficient on the diffusivity coefficient without introducing time as variable. Decoursey (1982) derived a relation for a first-order reaction. This model is based on the surface renewal theory and it assumes equal diffusivities for all of the reactants. Later it was generalized to systems with unequal diffusivities by Decoursey& Thring (1989). The performance of this approach was assessed by Winkelman, Brodsky, & Beenackers (1992). They have shown that the DeCoursey and Thring model can be used with a deviation up to 14%.

A Hatta number and the instantaneous enhancement factor are used in the calculations. The Hatta number is a relative parameter which compares the rate of reaction in a liquid film to the rate of diffusion. Thus a large Hatta value implies a much higher reaction rate compared to diffusion. Hence the reaction takes place mostly in the film. The instantaneous enhancement factor shows the intensification of a transfer phenomenon by an instantaneous and irreversible reaction. It corresponds to the asymptotic maximum limit of mass transfer enhancement.

Astarita& Savage (1980b) extended the absorption theory to desorption for systems which are first order with respect to the volatile component where the gas interface and bulk concentration are of the same magnitude. They demonstrated that the kinetics of the process play an important role in the mass transfer intensification, except for instantaneous reactions. Thus, the mentioned theories apply only for highly reactive solutions and for a limited loading range.

A new enhancement factor model can be developed by introducing simplifying assumptions for the film theory, the penetration theory or for the surface renewal model. Glasscock& Rochelle (1989) compared the above three frameworks in addition to the approximate film model. The approximate film model adjusts the instantaneous enhancement factor of the film theory to account for diffusivity differences of the species in the liquid film. It was concluded that the approximate film theory developed by Chang& Rochelle (1982) compares well to the surface renewal model and it is also equivalent to the penetration theory. The traditional two-film model on the other hand differs to the surface renewal model especially at high Hatta numbers and large differences in diffusivity. Chang& Rochelle (1982) substantiates that the main difference between the film theory and the surface renewal theory relies in the definition of the instantaneous enhancement factor. They have shown that the instantaneous enhancement factor of the film theory can be adjusted to estimate the surface renewal model within 10% accuracy. Therefore, it is expected that a film model based enhancement factor model can be extended to a surface renewal model, similar to the approach of Chang& Rochelle (1982).

The focus of the present paper is to develop a general approach for the calculation of the enhancement factor over wide temperature and loading ranges. It is intended in a two-film approach and extended to the surface renewal model. The proposed model covers the instantaneous, fast and intermediate reaction regimes for reversible reactions for both absorption and desorption. The model predictive capacity is assessed against the rigorous numerical solution of the film model and of the approximate film model. It is also compared against existing approximate models of van Krevelen& Hoftijzer (1948) and Astarita& Savage (1980a) model. The behaviour of the model is analysed through a CO_2 post-combustion case study, using the reactive MEA solvent. The improvements will be highlighted in terms of accuracy for start-up, normal and shut down operation for both, absorption and regeneration processes. This study presents a fast and simple to solve enhancement factor model and it demonstrates that the solution of the present model overlaps with the numerical solution of the film model.

2.A.2 Theory

2.A.2.1 The general method (GM)

This section describes a general method (GM) for the enhancement factor calculation of a reversible *(m+n)*-th order forward reaction where *m* and *n* are the reaction orders of the components. The kinetics is incorporated into the model in terms of the Hatta number and a simplified rate equation. It is derived using the reversible reaction (2.1), between a volatile gas, A, and a non-volatile solute, B resulting in products C and D:

$$v_A A + v_B B \rightleftharpoons v_C C + v_D D \tag{2.1}$$

The GM model can be derived for parallel non-interacting reactions and an approximate solution can be obtained for interacting systems. For non-interacting systems, each reaction contributes one additive term to the overall mass transfer enhancement. Therefore each reaction affects the mass transfer rate independently. The enhancement factor for the single reactions is derived for the individual reactions (Chang& Rochelle, 1982; Vanswaaij& Versteeg, 1992). Generally, multiple interacting reactions must be solved numerically. An approximate solution can be derived using the GM approach by assuming that the system consist of reactions with no kinetic interaction only thermodynamic interactions. In this case, the expression of the enhancement factor is derived for the individual reactions and they will be connected through the equilibrium constant. The GM model for parallel reactions is discussed in part B of this chapter.

The rigorous calculation of the mass fluxes according to the two-film mass transfer theory, suppose solving the differential equation system (2.2) to (2.5), which describes the differential mass balance according to Fick's law

$$D_A \frac{d^2 C_A}{dx^2} - \nu_A R = 0 \tag{2.2}$$

$$D_B \frac{d^2 C_B}{dx^2} - \nu_B R = 0 \tag{2.3}$$

$$D_C \frac{d^2 C_C}{dx^2} + \nu_C R = 0 \tag{2.4}$$

$$D_D \frac{d^2 C_D}{dx^2} + \nu_D R = 0 \tag{2.5}$$

where R is the reaction rate, ν_i are the stoichiometric coefficients, C_i is the concentration, and D_i is the diffusion coefficient of component i in the chemically loaded solution.

The boundary conditions (BC) necessary to solve the equation system are as follows:

BC1: At the gas-liquid interface, equilibrium is achieved instantaneously for the solute. Solvent and products are assumed non-volatile:

$$\frac{dC_j}{dx} = 0 \text{ where } j = B, C, D \text{ and } C_A = C_A^i \text{ at } x = 0$$

BC2: Equilibrium prevails in the liquid bulk:

$$C_j = C_j^b, \text{ for } x \geq \delta \text{ where } j = A, B, C, D.$$

The calculation of the mass transfer flux through the gas-liquid interface involves the determination of the concentrations at the interface (C_j^i). Evaluation of the mass fluxes according to the two-film theory requires the solution of the nonlinear-second order coupled boundary value problem, (2.2) to (2.5), with the conditions BC1 and BC2. The solution of this system is non-trivial. An analytical solution exists only for simple reaction kinetics such as the instantaneous irreversible reaction or the pseudo first order reaction.

The present work shows a general method to obtain a reduced order model based on the linearization of the two-film theory which is not restricted to simple reaction kinetics. The linearization of the system relies on bridging relations between the bulk and interface concentrations. These are obtained by eliminating the reaction term in (2.2) to (2.5). It reduces the second order differential equation system to a set of algebraic equations, resulting in much easier to solve model.

A linear equation is obtained by subtracting eq. (2.3) from eq. (2.2). The resulting relation is further simplified by integrating between 0 and δ, taking into account the boundary conditions:

$$D_A \nu_B \left(\frac{dC_A}{dx} - \frac{dC_A}{dx} \bigg|_{x=0} \right) - D_B \nu_A \frac{dC_B}{dx} = 0 \tag{2.6}$$

Based on Fick's first law and the definition of the E, the gas flux from the bulk to the interface is given by eq. (2.7). It describes the amount of A which diffuses from the interface towards the liquid.

$$\frac{dC_A}{dx} \bigg|_{x=0} = E \frac{D_A}{\delta} \left(C_A^i - C_A^b \right) \tag{2.7}$$

Substituting eq. (2.7) into (2.6) and rearranging the terms gives a correlation between concentration of A and B in the film and the enhancement factor, E:

$$D_A \nu_B \frac{dC_A}{dx} - D_B \nu_A \frac{dC_B}{dx} = - \frac{\nu_B E D_A \left(C_A^i - C_A^b \right)}{\delta} \tag{2.8}$$

The resulting equation, eq. (2.8), is the first bridging relation which establishes a correlation between the concentrations of the reactants at the interface and in the bulk. By integrating eq. (2.8) and applying the boundary conditions, BC1 and BC2, results in a relation of the enhancement factor as function of diffusivities and concentrations:

$$E = 1 + \frac{\nu_A D_B \left(C_B^b - C_B^i \right)}{\nu_B D_A \left(C_A^i - C_A^b \right)} \tag{2.9}$$

Finally, introducing the dimensionless compositions $y_A^b = C_A^b / C_A^i$ and $y_B^i = C_B^i / C_B^b$, gives a relation between the enhancement factor and the composition of the phases, as shown in eq. (2.10). It is a general equation which is true for all of the reaction regimes, from slow to instantaneous reaction. However, the non-volatile reactant concentration at the interface, y_B^i is not known and it cannot be measured. Thus the enhancement factor cannot be calculated directly from eq. (2.10). To solve it, a second equation is deduced below, which describes the relationship between E and y_B^i. It involves the use of (2.2) and introducing assumptions of the kinetics. Any kinetic expression can be used, however in this study the focus is the often used $r(C_A, C_B) = k C_A^m C_B^n$ expression.

$$E = 1 + \left(E_\infty^* - 1 \right) \frac{1 - y_B^i}{1 - y_A^b} \tag{2.10}$$

where E_∞^* is the instantaneous enhancement factor of the two-film approach and it is described by eq. (2.11). The instantaneous and irreversible enhancement factor is obtained from eq. (2.9) by setting C_B^i and C_A^b equal

to zero. This corresponds to a case of infinitely fast reaction, where the two reactants, A and B cannot exist together and the volatile component, A, is consumed immediately by the reaction with B:

$$E_\infty^* = 1 + \frac{v_A D_B C_B^b}{v_B D_A C_A^i} \tag{2.11}$$

Equation (2.12) and (2.13) are found by eliminating the reaction rate between (2.3) and (2.4), respectively (2.3) and (2.5). These describe the relationship between the concentration of the products respectively non-volatile component at the interface and in the liquid bulk. Applying the BCs and considering the dimensionless variables, $y_C^i = C_C^i / C_C^b$ and $y_D^i = C_D^i / C_D^b$, equivalent to y_B^i, gives:

$$y_C^i = 1 + \frac{v_C D_B C_B^b}{v_B D_C C_C^b}\left(1 - y_B^i\right) \tag{2.12}$$

$$y_D^i = 1 + \frac{v_D D_B C_B^b}{v_B D_D C_D^b}\left(1 - y_B^i\right) \tag{2.13}$$

The differential equations system of the film theory was reduced to a non-linear algebraic model by the use of bridging relations (2.9), (2.12) and (2.13) where (2.9) correlates the concentration of A and B while (2.12) and (2.13) express the concentration of the products, C and D, as function of B-reactant. When more products form, bridging relations expressing the concentration of the products as function of the concentration of the reactants are needed. These relationships show the correlation between the bulk and interface compositions with the enhancement factor. Therefore, E can be calculated with eq. (2.10) only if the interface concentration of the B-component is specified. The idea of the work below is to derive a correlation between E and C_B^i, based on kinetic considerations.

2.A.2.2 Enhancement factor for a reversible *(m+n)–th* order kinetics

The enhancement factor for an *(m+n)*-th order kinetics, eq. (2.1) is deduced below assuming equilibrium in the liquid bulk. The forward reaction rate for this kinetic is given by $r\left(C_A, C_B\right) = k C_A^m C_B^n$. The overall reaction rate is defined in eq. (2.14), where the dimensionless parameter, β, incorporates the reversibility of the process.

$$R = r\left(C_A, C_B\right)\left(1 - \beta\right), \text{ where } \beta = \frac{C_C^{v_C} C_D^{v_D}}{C_A^{v_A} C_B^{v_B} K_{eq}} \tag{2.14}$$

β is a relative parameter which relates the film and equilibrium compositions. The bulk compositions, $C_{i,b}$, appears in the equilibrium constant, $K_{eq} = C_{C,b}^{v_C} C_{D,b}^{v_D} \big/ C_{A,b}^{v_A} C_{B,b}^{v_B}$. These are known variables. The film composition can be expressed as function of C_B^i as shown in (2.12) and (2.13). For $\beta = 1$ the net reaction rate is zero, for $\beta < 1$ it is a case of absorption and $\beta > 1$ for desorption. How to determine β is described below. The reaction rate is transformed into a dimensionless function, $f(y_A, y_B) = y_A^m y_B^n$ and (2.2) is changed to a dimensionless form by introducing $C_A = y_A \cdot C_A^i$ and $x = \delta \cdot z$. The resulting differential equation is:

$$\frac{d^2 y_A}{dz^2} - v_A \frac{m+1}{2} Ha^2 f(y_A, y_B)(1-\beta) = 0 \qquad (2.15)$$

with the boundary conditions: $y_A(0) = 1$ and $y_A(1) = y_A^b$. Hikita & Asai (1964) linearized the rate equation of an $(m+n)$-th order kinetics and demonstrated that the Hatta number for this case is:

$$Ha = \frac{\sqrt{\frac{2}{m+1} k C_A^{m-1} C_B^n D_A}}{k_L} \qquad (2.16)$$

This study assumes that the reaction is fast enough to have a significant effect on the mass transfer rate. Slower processes have currently no practical industrial importance. This assumption involves the following two conditions which express how equilibrium holds in the bulk and the reaction takes place only in the film layer:

Condition 1. Assuming that the reaction reaches equilibrium in the vicinity of the interface, the concentration of the non-volatile components in the reaction and equilibrium terms can be replaced by their concentration at the interface, i.e. $y_B \approx y_B^i$, $y_C \approx y_C^i$, etc. Therefore the dimensionless parameter β is given by:

$$\beta \approx y_A^b \frac{y_{C,i}^{v_C} y_{D,i}^{v_D}}{y_A^{v_A} y_{B,i}^{v_B}} = \frac{y_A^*}{y_A^{v_A}} \qquad (2.17)$$

where y_A^* is defined as the composition of the A-component which will be in equilibrium with the interface concentration. Therefore, β can be expressed as function of y_A^* and y_A. From eq. (2.17) the equilibrium concentration of A is $y_A^* = y_{A,b}^{v_A} \cdot y_{C,i}^{v_C} y_{D,i}^{v_D} \big/ y_{B,i}^{v_B}$, where $y_{C,i}$ and $y_{D,i}$ are given in eq. (2.12) and (2.13). The value of y_A^* is found iteratively when it is introduced in the calculation of the enhancement factor. The relationship between y_A^* and E is discussed in the following.

Condition 2. The composition of the film at the bulk, $x = \delta$ $(z = 1)$, can be substituted by $y_A{}^*$, as follows:

$$y_A \to y_A^* \Rightarrow \frac{dy_A}{dz} = 0 \text{ at } z = 1 \tag{2.18}$$

Equation (2.15) can now be solved for any particular system with known kinetics. The kinetics are encapsulated in the normalized function $f(y_A, y_B)$ and $(1 - \beta)$ while the reaction regime is characterized by the Hatta number.

For the specified reaction kinetic, $f(y_A, y_B) = y_A^m y_B^n$, and introducing $p = dy/dz$, eq. (2.15) transforms to:

$$p \frac{dp}{dy} = v_A \frac{m+1}{2} Ha^2 y_B^n y_A^m (1 - \beta), \text{ where } \beta = \frac{y_A^*}{y_A^{v_A}} \tag{2.19}$$

with the following boundary conditions:

$$\text{BC3: } y_A = 1 \text{ and } p = \left. \frac{dy_A}{dz} \right|_{z=0} \text{ at the gas-liquid interface } (z = 0)$$

$$\text{BC4: } y_A \to y_A^* \text{ and } p = \frac{dy_A}{dz} = 0 \text{ in the bulk } (z = 1)$$

The boundary conditions, BC3 and BC4 are derived from BC1 and BC2 by introducing $y_A = C_A / C_A^i$ and $p = dy/dz$. The integration of eq. (2.19) between BC3 and BC4 gives an expression for the mass transfer flux through the interface, $\left. p \right|_{y_A=1} = \left. dy_A / dz \right|_{z=0}$:

$$\left. p \right|_{y_A=1} = \sqrt{\frac{v_A}{m}} Ha \cdot \sqrt{y_{B,i}^n \left(y_A^{*\,m+1} - (m+1) y_A^* + m \right)} \tag{2.20}$$

Similar to eq. (2.7), the diffusion of component A through the interface is expressed as function of the enhancement factor, shown by:

$$\left. p \right|_{y_A=1} = \left(\frac{dy}{dz} \right)_{z=0} = -E \left(1 - y_A^b \right) \tag{2.21}$$

and the expression of the enhancement factor is obtained by combining eq. (2.20) and (2.21), which for an *(m+n)*-th order reversible reaction gives:

$$E = \sqrt{\frac{v_A}{m}} \frac{Ha}{1-y_A^b} \sqrt{y_{B,i}^n \left(y_A^{*\,m+1} - (m+1) y_A^* + m \right)} \tag{2.22}$$

Eq. (2.10) and (2.22) form a system of nonlinear equations with two unknowns, E and y_B^i. Eliminating E leads to a single algebraic equation in y_B^i. The solution can be obtained numerically using methods such as the secant method, the Broyden method, or the Newton method, etc. The secant method is preferred; it does not require the evaluation of the derivative and needs only an initial interval for $y_B^i = C_B^i / C_B^b$. y_B^i is smaller than 1 for absorption and is greater than 1 for desorption. The lower limit for absorption and the upper limit for desorption is estimated assuming infinitely fast reaction where $y_A = 1$ and $\beta = 1$. For an infinitely fast reaction, the interface concentration of B $y_{B,i}^{v_B} \approx y_A^b y_{C,i}^{v_C} y_{D,i}^{v_D}$ is obtained by replacing (2.12) and (2.13) in (2.15) for $y_A = 1$ and $\beta = 1$. This relation holds for both absorption and desorption. It returns the lower limit for absorption and the upper limit for desorption. Hence the interval of interest is $\left(y_B^i, 1 \right)$ for absorption and $\left(1, y_B^i \right)$ for desorption. This method converges in 5 – 7 steps with a tolerance of 10^{-6} of E. Based on our simulations, GM reduces 1.5 to 4 times the computational time of the enhancement factor compared to the rigorous film model. This speed-up factor can differ from implementation to implementation. It is important to note that the time required to converge a CO_2 absorber and desorber will be much lower using the GM model than the numerical solver. Packed columns are solved iteratively. They are discrete systems and involve the calculation of all of the parameters, e.g. mass transfer properties, thermodynamic properties, etc. several times per iteration. Therefore, using the GM model reduces exponentially the simulation of a process.

2.A.2.3 Reversible second order reaction example

This section shows the enhancement factor for a second order and reversible reaction, as a specific case. The GM model is applied to the CO_2-MEA-H_2O system which is considered a base case in the CCS community. It uses one of the common kinetics in carbon capture modelling.

Equation (2.10) is a general relationship, when coupled with (2.22), enables the computation of the enhancement factor. Eq. (2.22) is valid for the *(m+n)*-th order reversible reaction and it reduces to a more compact and physical meaningful form when applied to the CO_2-MEA-H_2O system:

$$E = Ha \sqrt{y_B^i} \frac{1 - y_A^*}{1 - y_A^b}, \text{ where } B = MEA \text{ and } A = CO_2 \tag{2.23}$$

This equation is obtained by applying the second order reaction kinetics $f(y_A, y_B) = y_A y_B$ where $m = 1$ and $n = 1$ in (2.22). It can be seen from eq. (2.23) how the expression of the enhancement factor reduces to the Hatta number when the pseudo-first-order (PFO) approximation applies. The PFO approximation requires that the liquid phase driving force is small, $y_A^* = y_A^b$. This implies that the solute, B, concentration is approximately constant in the liquid film, $y_B^i = 1$, and the reaction products do not build up at the interface. In case of fast to slower reactions, such as the reaction of CO_2 and MEA at higher loadings, the enhancement factor is determined from (2.10) and (2.23). For the applied second order reaction kinetics, an analytical solution can be obtained by introducing (2.10) in (2.23) which results in a quadratic equation in Y, where $Y = \sqrt{y_B^i}$, as shown in (2.24). Finally, the enhancement factor is calculated by introducing the value of y_B^i in (2.10) or (2.23).

$$\left(1 - E_\infty^*\right) Y^2 + Ha \left(y_A^* - 1\right) Y + E_\infty^* - y_A^b = 0 \tag{2.24}$$

Equation (2.24) gives the ratio of the interface to bulk concentration. It can be shown, that only one of the solution is physically meaningful. It can be concluded that a general method (GM) was developed for the estimation of the enhancement factor. The present approach reduces the two-film model to one single algebraic equations and it can be solved analytically for simple reaction kinetics. An analytical solution for second order reaction kinetics is provided.

2.A.3   Enhancement factor models

This section discusses three of the commonly used enhancement factor models, namely the van Krevelen and Hoftijzer approach (van Krevelen& Hoftijzer, 1948), the Astarita & Savage model (Astarita& Savage, 1980a) and the approximate film model (Chang& Rochelle, 1982). These models were selected to outline the possibilities of improving enhancement factor calculations, to reach a scheme valid for both absorption and desorption conditions. Moreover, the Onda's approach is discussed since it represents the lower limit at which GM model applies. The equations of the models and assumptions are briefly discussed here.

2.A.3.1 The van Krevelen and Hoftijzer approach

One of the first approximate solutions for the enhancement factor calculation was introduced by van Krevelen& Hoftijzer (1948). Their method is based on the two-film theory. Originally, they considered a second order irreversible reaction and linearized the differential equation system. The relationship for the enhancement factor computation is presented in eq. (2.25). This is an often used equation for estimation of

enhancement factors using the knowledge of the instantaneous enhancement factor, E_∞^*. Notice the equation need to be solved iteratively, it is not explicit.

$$E = \frac{Ha\sqrt{\dfrac{E_\infty^* - E}{E_\infty^* - 1}}}{\tanh\left(Ha\sqrt{\dfrac{E_\infty^* - E}{E_\infty^* - 1}}\right)} \tag{2.25}$$

In order to calculate E, van Krevelen and Hoftijzer assumed that the concentration of the non-volatile components in the liquid boundary layer is constant and equal to their interface concentrations. Vanswaaij& Versteeg (1992) have shown that this assumption has limited application for a narrow stagnant film and for first-order reaction kinetics. Santiago& Farina (1970) demonstrated that the model accuracy is 3% for second order and irreversible reactions with Ha > 3.

Among others, Danckwerts (1970) and Hogendoorn et al. (1997) have shown that this model can be extended to reversible reactions and chemically loaded solutions. They indicated that the nonlinearity of real systems can be compensated for, by adjusting the instantaneous enhancement factor, E_∞^* and the Hatta number, *Ha*.

The intention of this work is not as suggested by Danckwerts (1970) and Hogendoorn et al. (1997) to tune the instantaneous enhancement factor. Rather an equal comparison basis is chosen where the van Krevelen and Hoftijzer approach is compared to the GM model without adjustments. In the following, the combination of eq. (2.10) and eq. (2.25) is addressed as the van Krevelen model.

2.A.3.2 The Astarita & Savage approach

The assumptions of the original van Krevelen model were modified by Astarita& Savage (1980a). They provided an analytical solution for the enhancement factor computation, based on the two-film theory. This model covers the reversible and instantaneous reactions regime. They also set up the differential equation schemes for the penetration theory. The time dependent equation system can be solved analytically only for simple reaction kinetics. The analytical solution for such cases has been presented by Olander (1960).

The analytical solution provided by Astarita and Savage is based on eqs. (2.26) – (2.28). This equation system shows that the enhancement factor depends on the interface composition which is not stoichiometrically accessible. The solution of equations (2.27) – (2.28) gives the extent of reaction which is correlated with the interface composition. Eq. (2.27) is a polynomial equation with more than one root. However just for one of the roots, the interface concentration will be non-negative (Astarita& Savage, 1980a). The instantaneous enhancement factor is calculated using eq. (2.11).

$$\xi = \left(E_\infty - 1\right)\left(C_A^i - C_A^b\right) \tag{2.26}$$

$$\Psi = \frac{C_A^i}{C_A^b} = \prod_j \left(1 - \frac{\nu_j \xi}{r_j C_j^b}\right)^{-\nu_j} \tag{2.27}$$

$$C_j^i = C_j^b - \nu_j \xi \tag{2.28}$$

where the ratio of the diffusion coefficients is $r_j = D_B / D_A$. Here the combination of eq. (2.25) and (2.26) is denoted the Astarita & Savage model. The solution is found by iteration.

According to (2.26) – (2.28), the enhancement factor depends only on the liquid bulk compositions and on the interface concentrations and it is independent of the thermodynamic equilibrium constant. Astarita& Savage (1980a) affirmed that the enhancement factor for an irreversible reaction can be approached asymptotically. They provided an analytical solution for three asymptotic cases: $\Psi >> 1$ for absorption, $\Psi << 1$ for desorption and $\Psi = 1 + \delta$ with $||\delta|| << 1$ for pinch regimes. The validity of this model was questioned by Bhattacharya& Ramachandran (1983). They emphasize that the irreversible asymptote is reached only for large values of the equilibrium constants. Katti (1992) concluded that the irreversible value of the enhancement factor is generally larger than the one calculated for reversible conditions and the error is especially severe near the industrially relevant pinch zone.

2.A.3.3 The approximate film (AF) model of the surface renewal theory

An approximation of the surface renewal model was introduced by Chang& Rochelle (1982). They investigated the differences between the two-film and the surface renewal models at various operational conditions and demonstrated that the simplicity of the two-film model and the accuracy of the surface renewal model can be combined. They show that the Danckwerts' surface renewal model reduces to the two-film model at equal diffusion coefficients of component A and B. The dissimilarities between the theories become more relevant for systems with large liquid or gas side resistance (large diffusivity differences) and for instantaneous or fast reactions regimes (high Hatta numbers). These findings suggest that the film theory is more adequate for stagnant fluids hydrodynamics while the surface renewal model is suitable for more turbulent flows.

Chang& Rochelle (1982) demonstrated that the numerical solution of the surface renewal theory can be approximated by the two-film theory by adjusting the instantaneous enhancement factor. The instantaneous enhancement factor according to the approximate film-model is:

$$E_\infty^* = \sqrt{\frac{D_A}{D_B}} + \frac{\nu_A C_B^b}{\nu_B C_A^i} \sqrt{\frac{D_B}{D_A}} \tag{2.29}$$

Comparing eq. (2.11) to (2.29), it can be seen that the instantaneous enhancement factor of the film theory is corrected by the square root ratio of the diffusion coefficients. Therefore (2.29) reduces to the film-theory instantaneous enhancement factor, eq. (2.11), for equal diffusivities. Chang& Rochelle (1982) compared the two solutions for various reaction types over a wide range of conditions. According to their analyses the approximate film model reproduces the surface renewal model within 10%.

In the following, the approximate film model for the surface renewal model will be addressed the AF model. It consists of eqs. (2.2) – (2.5) combined with eq. (2.29).

2.A.3.4 The interface-pseudo-first order model

The interface-pseudo-first order model (IPFO) reduces the rigorous Eddy mass transfer theory to a set of algebraic equations by introducing the concept of bridging relations, similar to the approach of this work. Glasscock& Rochelle (1989) have illustrated that the Eddy theory resembles the surface renewal and penetration theory for absorption within 5%.

The IPFO model considers that the reaction is fast enough and CO_2 reaches equilibrium with the solution near the interface and it assumes that the concentrations of the other species are constant at their interface value. These approximations are identical to the BC3 and BC4 conditions of the GM model.

The equation system for IPFO model has been set up for second order reversible reactions, first order with respect to the reactants in terms of mass transfer flux, N_A (Al-Juaied, 2004):

$$N_A = \sqrt{k_{2,\mathrm{B}} C_B^i D_A} \, \frac{p_A - p_A^*}{H_A} \tag{2.30}$$

One might note that eq. (2.30) and eq. (2.23) are similar. This is expected since both of the equations are derived from eq. (2.2). Similar to the GM model, IPFO can be solved iteratively and it requires an additional relationship to determine the interface concentration of B. The IPFO model uses eq. (2.31) which connects the loading, θ, at interface and in the bulk:

$$\theta^i = \frac{N_A}{k_{l,prod} C_B^T} + \theta^b \tag{2.31}$$

where the liquid side mass transfer coefficient of the products is $k_{l,prod} = k_{l,A} \sqrt{D_{prod}/D_A}$. It can be seen that the IPFO model uses the square root ratio of the diffusion coefficients, similar to the approximate film (AF) model. Therefore, it is expected that the IPFO model gives results comparable to the AF model.

2.A.3.5 The Onda approach

The above approximations are aimed at reactive systems. They tend to over-estimate the mass transfer rate for conditions of fast to slower reaction regimes. A counterpart was developed by Onda et al. (1970), which is accurate at these conditions. It is an approximate analytical solution for reversible reactions. The model assumes the film boundary concentrations identical to the equilibrium values which correspond to a reversible liquid bulk reaction. They used the same linearization technique for the reaction rate equations as Hikita& Asai (1964) and extended it to a *(m,n) – (p,q)*-th order reversible reaction, where *m* and *n* refer to the order of reactants while p and q to the order of the reverse reaction.

It was pointed out by Versteeg et al. (1989) that Onda's approach approximates the film model within 2% accuracy when *m = p*. However, the Onda solution is not feasible, i.e. the calculated enhancement factor is less than 1, for solute loadings significantly greater than zero and/or low equilibrium constants when the reverse reaction cannot be neglected. This might be due to the fact that the products, C and D are treated differently in the linearization of the reaction rate equation and the net reaction rate does not reduce to zero in the bulk of the liquid, although equilibrium is assumed to exist in the liquid bulk.

Although, the Onda's approach behaves fairly well for reversible reactions with relatively low Hatta numbers, CO_2 absorption and desorption systems are highly reactive and therefore the Onda's approximation does not apply for CO_2 capture simulation. For this reason, the Onda's model will not be considered for comparison in the present work. The GM model is a general approach aimed for mass transfer calculation accompanied by a reaction with a Hatta number greater than 3. It is important to keep in mind that Onda's model represents the asymptotical lower limit and the van Krevelen's model represents an upper limit at which the GM model applies.

2.A.4 Results and discussions

In the following, the accuracy of the GM model, the AF model (Chang& Rochelle, 1982), the van Krevelen (van Krevelen& Hoftijzer, 1948) and the Astarita & Savage (Astarita& Savage, 1980a) solutions are compared to the numerical solution of the two-film model. For illustration purposes the CO_2-MEA-H_2O system is considered. Note that the GM model is a general approach, usable for kinetic and stoichiometric setups, more complex than the CO_2-MEA-H_2O system. The van Krevelen approximation deals with absorption and the Astarita & Savage model is restricted to either absorption or desorption conditions, not

both. They are therefore of limited use. In order to highlight the significance of a general method, the above discussed approaches are evaluated for normal operating conditions as well as for process start-up and shut down conditions, at absorption and desorption conditions. The ranges of conditions under which these models have been compared are discussed in the following.

2.A.4.1 A system with finite reaction rate constant

This section presents the GM model compared to the film model for various equilibrium constants at low CO_2 loadings and for infinitely large gas-side mass transfer coefficient. The intent is to verify the GM model for various reversible conditions for gas-side controlled processes ($k_g \approx \infty$). Most of the chemical absorption processes are strongly influenced by liquid–side resistance. However, the contribution of the gas-side resistance becomes relevant in the more reactive top part of a packed column which is characterized by low loading. Note that similar conditions were extensively studied in the past, for example by Versteeg et al. (1989). In addition, this study also serves as a base case comparison of the GM model with a well-studied system.

The conditions for the comparative study are as follows: constant total amine concentration ($C_B^{tot} = 1000 \, mol/m^3$), constant low loading ($\phi = 10^{-3}$), and equal diffusivities of all species. For high values of the equilibrium constant this situation corresponds to an absorption followed by an instantaneous irreversible reaction with respect to mass transfer. The concentration of the amine as well as the loading of the solution in this case is relatively low and outside of the practical range, however the aim of this comparison is to highlight the shift of the reaction regime with the equilibrium constant. The actual value of the amine concentration is not relevant since it is kept constant for all of the cases. It can be regarded as a normalized concentration. The low loading value corresponds to gas-side controlled process.

Figure 2.A.1 presents the principle profile of the enhancement factor as function of the Hatta number at several equilibrium constant values. This figure demonstrates that the GM model compares well with the numerical solution of the film model. The maximum absolute relative deviation is 2.64%, with a standard deviation of 0.57%. The prediction is good in all cases of the slow, intermediate, fast and instantaneous reaction regimes. It has to be mentioned that the van Krevelen and the Astarita & Savage model behaves similarly good without introducing tuning parameters for the conditions shown in Figure 2.A.1.

The effect of the equilibrium constant on the enhancement factor is outlined in Figure 2.A.1. The enhancement factor increases with the equilibrium constant because the reverse reaction rate constant decreases. In other words, the forward reaction rate is much higher than the reverse reaction rate for large K-values, hence the system approaches irreversibility. Therefore, high equilibrium constant values correspond to absorption followed by an irreversible reaction. Consequently, very small equilibrium constant would

correspond to fast reaction followed by desorption. However, the loading of the solution is low, $\phi = 10^{-3}$ and therefore the inverse reaction followed by desorption is not possible.

It should be noted that the line $E = Ha$ is the pseudo-first order reaction scheme. For a pseudo-first order process, the reaction rate is sufficiently low or the resistance to mass transfer is small enough to maintain the concentration of one of the reactants relatively constant in the film. Therefore, the deviation from the pseudo-first order line indicates fast reaction compared to diffusion. The deviation from this line increases with Ha-value indicating that the diffusion limitation of mass transfer occurs. Note that high Ha-value corresponds to a fast or instantaneous reaction.

The limiting mechanism moves from diffusion to reaction rate controlled as the equilibrium constant, K, decreases. At low Ha and K-values the reaction rate becomes smaller than the diffusional transport. At this point the volatile gas, A, diffuses faster than it is consumed by the reaction which results in the decreased driving force. The drop of the driving force is due to saturation of the liquid with the gas. It can be seen in Figure 2.A.1 that for a reversible reaction, eg. at K=0.1, the asymptotic limit of the enhancement factor is around 3 while for an irreversible reaction, K=1000, the maximum value of the enhancement factor is approximately 100. High equilibrium constants correspond to fast or instantaneous regimes, where the volatile component is consumed instantaneously at the interface, or faster than it dissolves in the film. Further increase of the equilibrium constant does not significantly affect the asymptotic limit, as shown in Figure 2.A.1.
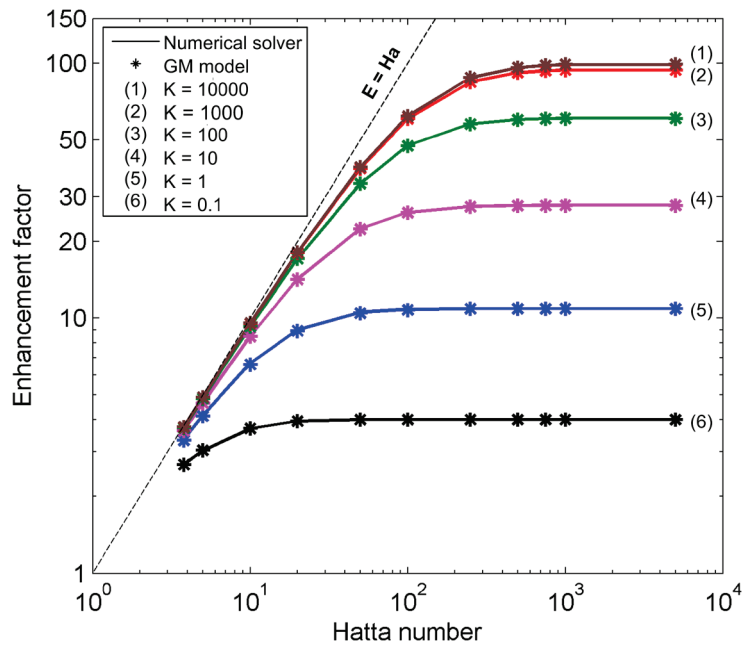
Figure 2.A.1. Enhancement factor as function of Hatta number for several equilibrium constants.

To summarize, the enhancement factor increases with the equilibrium constant and it behaves asymptotically at Hatta numbers greater than 200. The instantaneous enhancement factor is reached only for K-values greater than 1000 which correspond to irreversible instantaneous reaction. It can be concluded that the GM model and the numerical solution overlap indifferent of the equilibrium constant.

2.A.4.2 Absorption process modelling

Here the presented enhancement factor models are compared for absorption like conditions. The purpose is to demonstrate the need for an accurate model. The differences between the enhancement factors are shown for three cases defined in Table 2.A.1, covering common absorption conditions. Case 1 corresponds to low L/G ratio operation which might occur at shut down procedures or flexible operation when the amine flow is reduced. This could occur at hours of the day where the capture plant would be shut down to reach peak power production. The parameters of case 2 are characteristic for a normal operation with 90% capture rate. Case 3 is characterized by low CO_2 loading corresponding to column start-up with a mixture of fresh solvent and lean solution.

Table 2.A.1. Process conditions for the comparative simulations

Parameter	Case 1	Case 2	Case 3
Loading	0.27 – 0.48	0.27 – 0.47	0.003 – 0.250
Gas CO_2 composition (mol/m^3)	0.27 – 1.70	0.03 – 0.83	0.000 – 0.025
MEA concentration (mol/m^3)	170 – 2200	285 – 2250	2500 – 4950
Hatta number	45 – 160	35 – 110	115 – 165
y_{CO2}^b *	0.03 – 0.99	0.08 – 0.55	0.003 – 0.024

*dimensionless composition, $y_{CO2}^b = C_{CO2}^b / C_{CO2}^i$

Figure 2.A.2 to Figure 2.A.4 show the deviation of the van Krevelen, Astarita & Savage, and GM model compared to the numerical solution. These figures also present the ratio of the gas bulk to interface CO_2 concentration, $y_{CO_2}^b$. This variable can indicate the source of error in the models. It is a kind of driving force number. For an absorption process $y^b \in (0,1)$. At $y^b = 1$ the net transfer rate is zero and $y^b \approx 0$ corresponds to: (a) low driving force for absorption when $C_{CO2}^b \approx 0$ and C_{CO2}^i is finite or (b) high driving force when $C_{CO2}^i \approx \infty$ and C_{CO2}^b is finite. A performance overview is shown in Figure 2.A.5. The results demonstrate how the GM model performs well for wide ranges of loading and Hatta numbers.

The van Krevelen model generally over-predicts the enhancement factor, as shown in Figure 2.A.2 to Figure 2.A.4. This model deviates approximately 10 units for shut down and normal operation, seen in Figure 2.A.2

and Figure 2.A.3. Figure 2.A.4, at start-up, substantiates that the van Krevelen model overlaps with the GM model and it is accurate for these conditions. It corresponds to CO_2 absorption with fresh MEA where the amine film concentration can be assumed constant.

The performance of the Astarita & Savage model is often superior to the van Krevelen model, as shown in Figure 2.A.2 to Figure 2.A.4. Figure 2.A.2, at shut down operation, shows that the Astarita & Savage model and GM model overlap from the bottom to the middle section of the column. The deviation of the Astarita & Savage model increases from the middle to the top section, where $y_{CO_2}^b$ decrease correspondingly. The error is highest at the top section where $y_{CO_2}^b$ is almost zero. The model performs fairly well for normal operation, case 2, as shown in Figure 2.A.3, where $y_{CO_2}{}^b$ is approximately 0.45. It under-predicts the enhancement factor for start-up conditions of low $y_{CO_2}^b$, case 3, as shown in Figure 2.A.4. Figure 2.A.2 to Figure 2.A.4 demonstrates that the Astarita & Savage approach in general behaves well for $1 > y_{CO_2}{}^b > 0.35$.

The conclusions are substantiated by the results presented in Table 2.A.2. It shows the difference between the numerical solution, the pseudo first order reaction regime, $\Delta(Hatta) = E_{numeric} - Ha$, and the van Krevelen, Astarita & Savage and the GM model. It can be seen in Table 2.A.2 that the deviation of the van Krevelen approach increases as function of $\Delta(Hatta)$. The pseudo-first order line, $E=Ha$, indicates that the reaction rate and diffusion are of comparable order. Therefore, a higher $\Delta(Hatta)$ substantiates the growing importance of the diffusion limitation.

Table 2.A.2. Absolute error as function of the difference between the Hatta number and numerical solution

Δ(Hatta)*	Δ(van Krevelen)**	Δ(Astarita &Savage)**	Δ(GM model)**
0.05	0.05	0.08	0.02
0.50	0.30	4.64	0.06
5.70	3.10	4.18	0.00
9.80	6.90	0.62	0.03
14.5	8.90	1.89	0.06
20.8	8.60	0.98	0.15
30.2	8.30	1.80	0.07
35.3	10.8	1.50	0.09
41.8	13.8	12.6	0.16

* $\Delta(Ha) = |E_{num\ sol} - Ha|$ ** $\Delta(model) = |E_{num\ sol} - E_{model}|$

Table 2.A.2 outlines that the van Krevelen model behaves well for the pseudo first order scheme, $\Delta(Hatta) \to 0$ and it deviates from the numerical solution for conditions when the MEA bulk and film concentration differs, $\Delta(Hatta) > 0$. These conditions are specific for lower free amine concentrations when the reaction shifts from instantaneous to fast or slow reaction zone. In addition, the results presented in Table 2.A.2 highlights how the GM model and the Astarita & Savage model perform fairly well, independent of the $\Delta(Hatta)$ value.
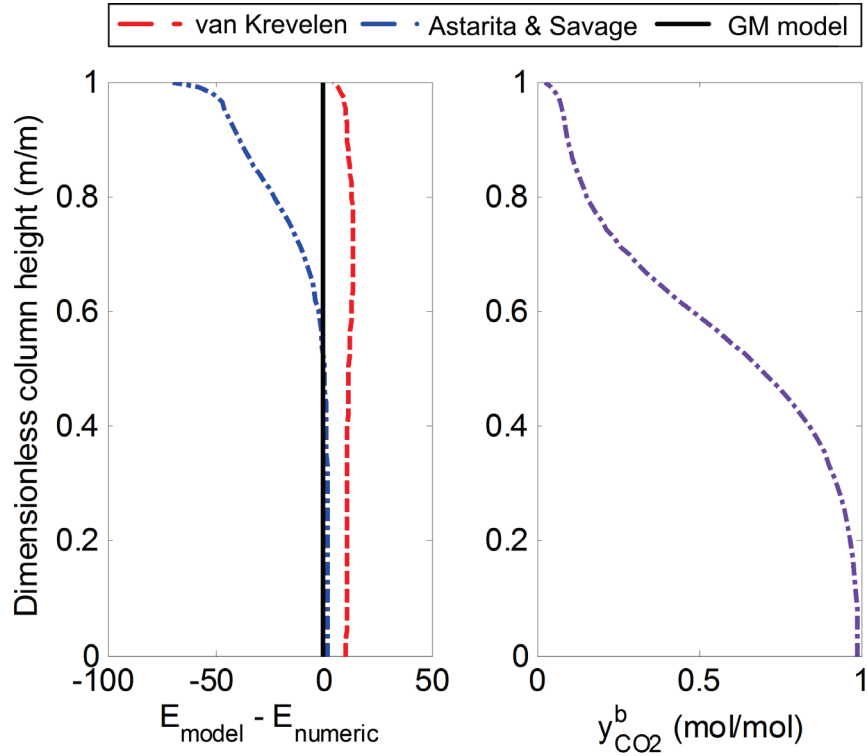
Figure 2.A.2. Enhancement factor as function of height (left) and corresponding ratio of the bulk to the interface CO_2 concentrations (right) for case 1
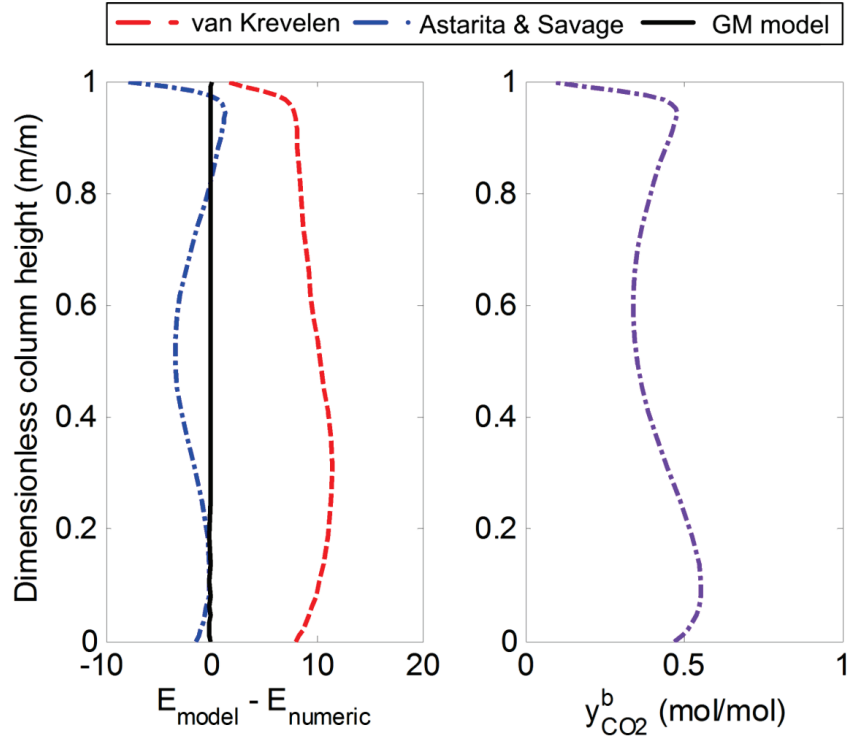
Figure 2.A.3. Enhancement factor as function of height (left) and corresponding ratio of the bulk to the interface CO_2 concentrations (right) for case 2
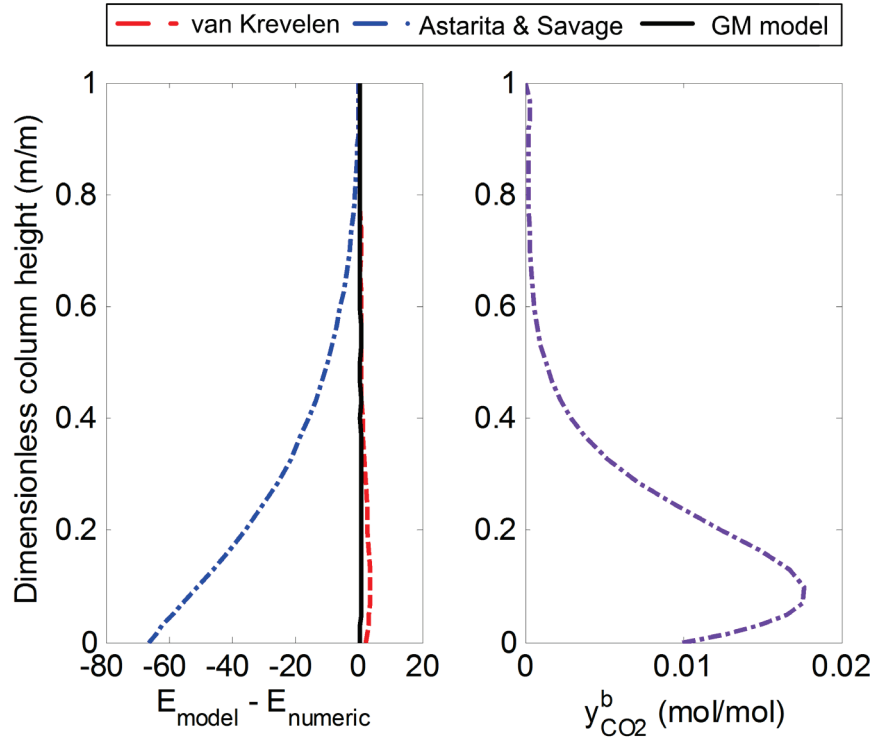
Figure 2.A.4. Enhancement factor as function of height (left) and corresponding ratio of the bulk to the interface CO_2 concentrations (right) for case 3

Figure 2.A.5 gives an overview. It summarizes the calculations for case 1, case 2 and case 3 for absorption process conditions, as shown in Figure 2.A.5a to Figure 2.A.5c. They represent the calculated enhancement factors as function of the numerical solution. The results are grouped into two categories according to y^b. Range 1 of high driving force, $y^b<0.3$, and range 2 for smaller driving forces, $0.3<y^b<1$.

Figure 2.A.5c exemplifies how the GM model overlaps the numerical solution, independent of the operational conditions. The average absolute relative deviation (AAD) is 0.299 % with a maximum relative deviation of 0.903 % and a standard deviation of 0.322%. The van Krevelen model presents similar behaviour with deviations up to 10 enhancement factor units. The model is slightly more reliable for range 1. The overall AAD from the numerical solution is 29.41%. The Astarita and Savage model is much more diverse. It overlaps range 2 very well but less good for range 1, as shown in Figure 2.A.5b. The AAD of this model is 25.93%.
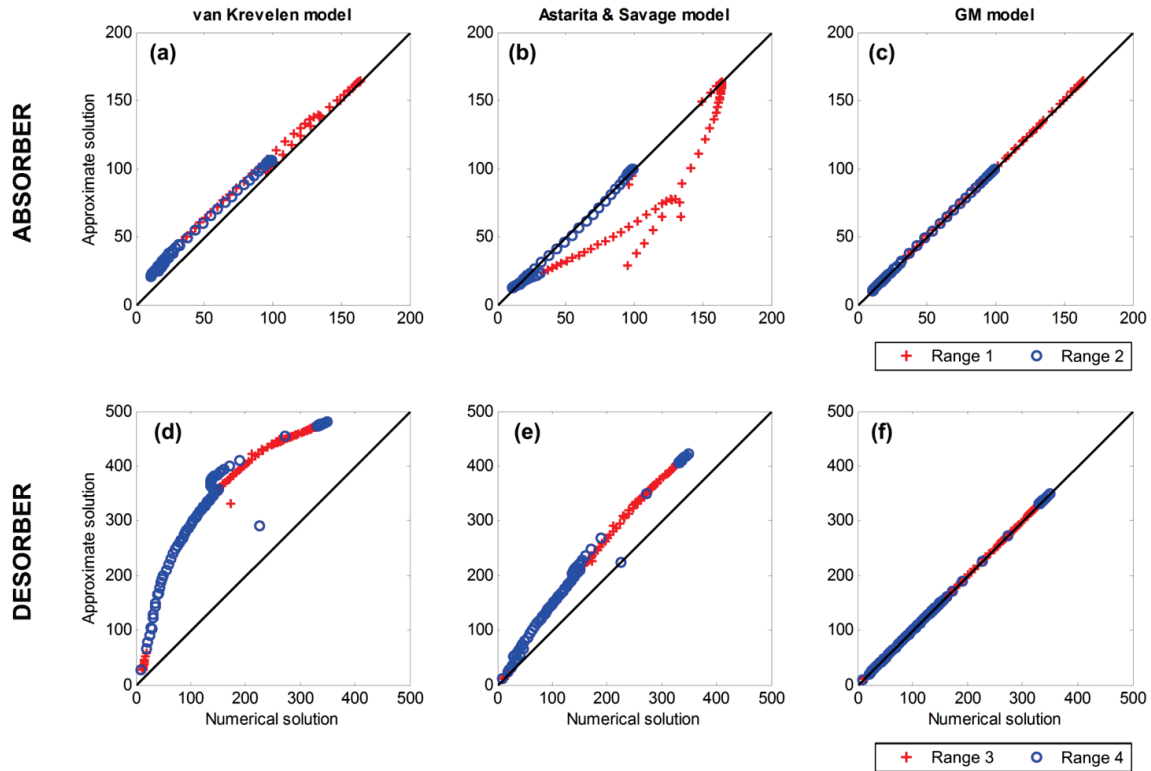
Figure 2.A.5. Enhancement factor as function of film model numerical solution
(***Range 1**: $y^b \leq 0.3$; **range 2**: $y^b \in (0.3,1)$; **range 3** $y^b \in (1,2)$; **range 4**: $y^b \geq 2$)*

The solution of the GM and of the film-model overlap for the entire range of absorption conditions. It can be concluded that the GM model is superior to the van Krevelen& Hoftijzer (1948) and Astarita& Savage (1980a and 1980b) model. GM is an accurate model for absorber design and optimisation. It may eliminate the need for more conservative design approaches, leading to economic benefits and optimal design and operational specifications.

2.A.4.3 Desorption process modelling

This section compares the accuracy of the van Krevelen& Hoftijzer (1948), Astarita & Savage (Astarita& Savage, 1980a; Astarita& Savage, 1980b) and GM enhancement factor model for desorption like process conditions. In order to emphasize the need for an accurate enhancement factor for desorption process modelling, three scenarios are studied in this work. The cases cover the whole operational window of a desorption process, from the pinch zone to high driving forces. Case 4 corresponds to optimal operation of a desorber, with a 90 % capture. Here optimal operation indicates a condition where the heat released by the condensation of water is consumed by the evaporation of an equivalent amount of CO2. The temperature is decreasing gradually from the bottom to the top of the column. The column operates at a point of minimal heat requirements. Case 5 can occur at reboiler malfunctioning or shut down procedure during flexible operation, when the amine regeneration percentage decreases. The reboiler temperature for case 5 is 6 °C below the optimal case 4 temperature. Case 5 results in high loadings and low bulk to interface concentration ratio, yCO2b. Case 6 is characterized by low rich loading. It might occur at start-up with a mixture of fresh solvent, resulting in a leaner rich solution. Figure 2.A.6 to Figure 2.A.8 show the enhancement factor results for case 4 to 6. The bulk to interface concentrations, yCO2b, are also shown. Note that for desorption, yCO2b >1, the asymptotic limit, yCO2b →∞, corresponds to high driving force. An overview of the results is shown in Figure 2.A.5.

Table 2.A.3. Process conditions for the comparative simulations

Parameter	Case 4	Case 5	Case 6
Loading	0.17 – 0.46	0.34 – 0.46	0.20 – 0.28
Gas CO_2 composition (mol/m^3)	0.20 – 4.80	3.5 – 19.5	0.10 – 0.90
MEA concentration (mol/m^3)	800 – 2800	1100 – 1700	2200 – 2800
Hatta number	180 – 470	220 – 350	320 – 490
y_{CO2}^{b} *	1.70 – 6.00	1.04 – 2.70	1.30 – 2.70

*dimensionless composition, $y_{CO2}^{b} = C_{CO2}^{b}/C_{CO2}^{i}$

From Figure 2.A.6 – Figure 2.A.8, it is evident that the size of the error on desorption of the van Krevelen and of the Astarita & Savage model is fairly high compared to absorption conditions, Figure 2.A.2– Figure 2.A.4. The GM model compares well with the numerical solution for all cases. The deviation is less than 2 enhancement factor units. Astarita& Savage (1980b) have shown the importance of the reaction kinetics for desorption process modelling. They demonstrated that the kinetics can be neglected only for the pseudo-first order reactions.

Generally, the van Krevelen model over-predicts the enhancement factor. The smallest deviations can be seen for case 5 in Figure 2.A.7 at lower reboiler temperatures. For case 4 and 6, Figure 6 and 8, the deviation

from the numerical solution is more than 100 enhancement factor units. These two cases both have a loading of 0.30 mole CO_2/ mole MEA at the top of the column and the ratio of the bulk to the interface concentration is less than 2. It can be concluded that the van Krevelen model over-predicts the enhancement factor for most process conditions. It behaves acceptable only for conditions close to the pinch, $y_{CO2}^{b} \cong 1$. Note an explanation could be that the van Krevelen approximation assumes constant or linear variation of the concentration in the film which is not valid for system with low free amine concentration. The Astarita & Savage model performs better than the van Krevelen model in the whole range. The average deviation between the numerical solution and the Astarita & Savage model for optimal operation, case 4 is 50 units with a maximum of 80 units at the bottom of the column, as shown in Figure 2.A.6. The Astarita & Savage model predicts fairly well the mass transfer phenomena for case 5, shown in Figure 2.A.7. The accuracy of the Astarita & Savage model for a low reboiler temperature and low lean loading is presented in Figure 2.A.8. The deviation for this case is nearly constant 70 units along the column height.
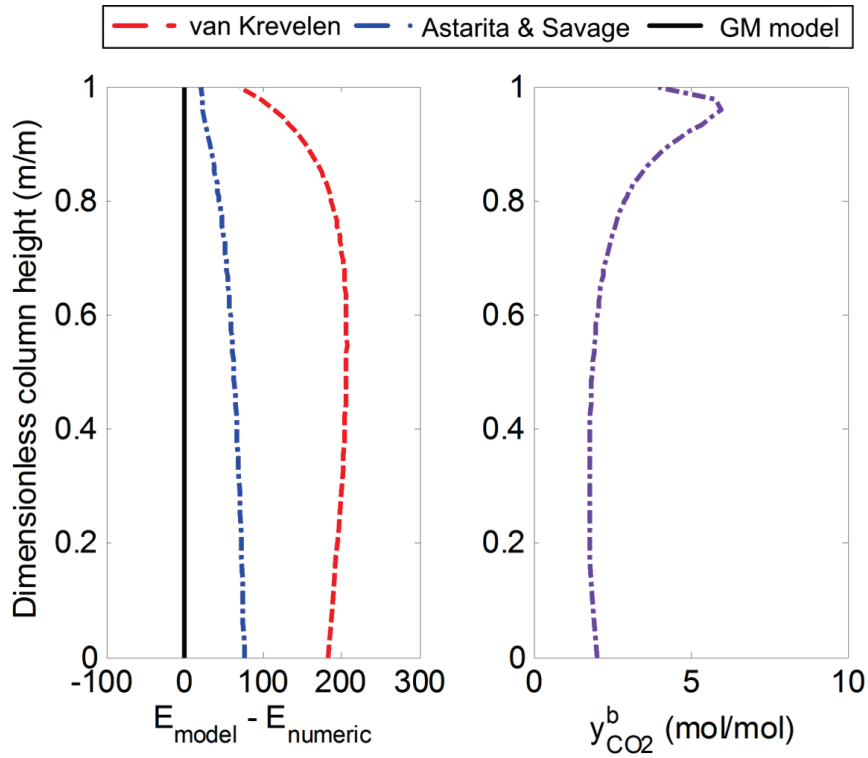
Figure 2.A.6. Enhancement factor as function of height (left) and corresponding ratio of the bulk to the interface CO_2 concentrations (right) for case 4
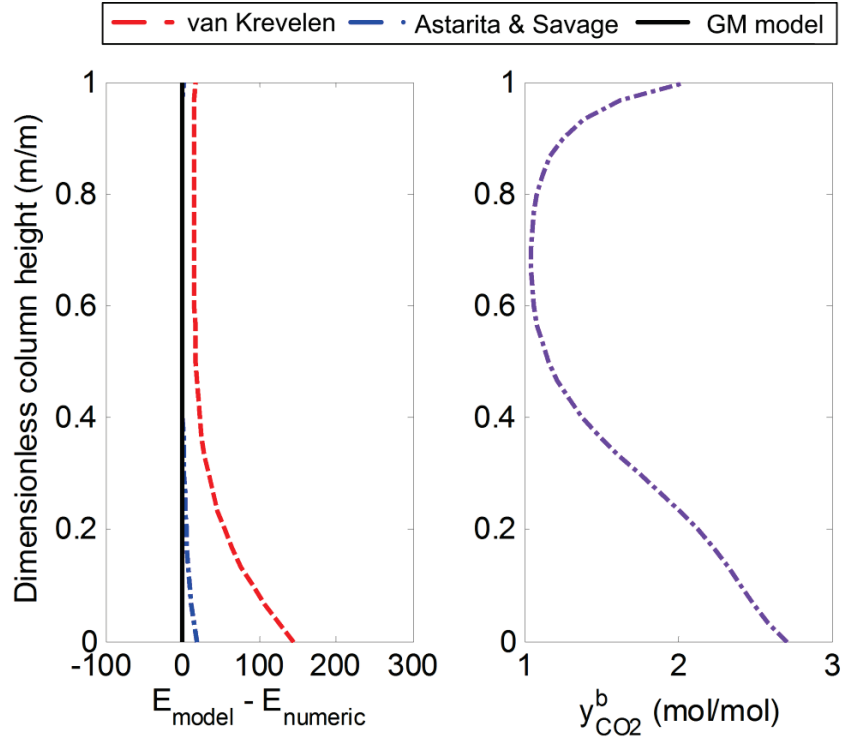
Figure 2.A.7. Enhancement factor as function of height (left) and corresponding ratio of the bulk to the interface CO_2 concentrations (right) for case 5
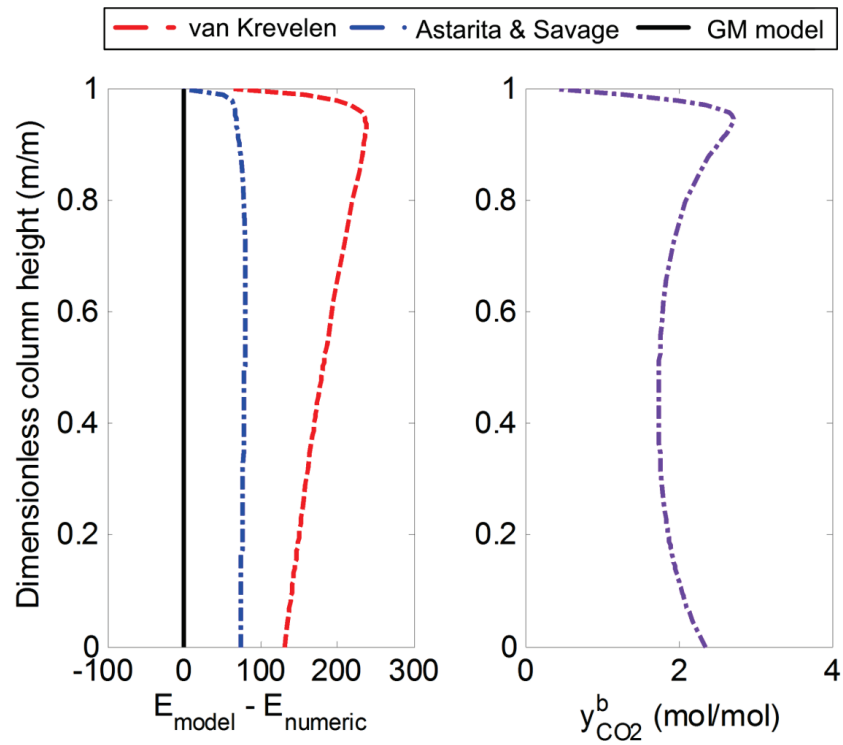
Figure 2.A.8. Enhancement factor as function of height (left) and corresponding ratio of the bulk to the interface CO_2 concentrations (right) for case 6

The assessment of the van Krevelen, Astarita & Savage and the GM model for desorption conditions is summarized in Figure 2.A.5d to Figure 2.A.5f. The accuracy of the models is analysed as function of y^b, where range 3 corresponds to low driving force with $y^b \in (1,2)$ and range 4 to high driving force, $y^b \geq 2$.

Figure 2.A.5d indicates how the van Krevelen model is over-predicting. The maximum absolute error is 243 units with an average absolute error of 158 units. Figure 2.A.5e shows that the Astarita and Savage enhancement model is superior to the van Krevelen approach. The maximum absolute deviation is 81 units with an average absolute error of 51 units. In summary, Figure 2.A.5d and Figure 2.A.5e highlight how the Astarita & Savage model performs better than the van Krevelen. The deviation from the numerical solution is most visible for the low driving forces, range 3. The Astarita & Savage model is acceptable when the bulk and the interface concentrations, C_B^b respectively C_B^i, are comparable and not near to zero.

The GM model performance is shown in Figure 2.A.5f. The average absolute deviation for desorption conditions is 0.070% with a maximum absolute deviation of 0.231% and a standard deviation of 0.057%. It can be concluded that the GM model predicts the enhancement factor well, also for desorption conditions. Therefore the GM model gives a reliable estimate for a post-combustion capture plant design. The van Krevelen and Astarita & Savage model under-predict the required column leading to a post-combustion plant with lower CO_2 capture rate. Therefore, the use of GM model leads to considerable savings and assures a more reliable optimization of the process conditions.

2.A.4.4 The general model of the surface renewal theory (GMAF)

This section focuses on the GM model comparison with the AF model and proposes a general model for the surface renewal model approximation. It has been demonstrated above that the GM model and the numerical solution of the two-film model agree well for both, absorption and desorption conditions. Moreover, the deviations between the two are negligible. Chang& Rochelle (1982) have shown that the film and surface renewal models differ mostly at high reactant diffusivity ratios and at high Hatta numbers. It only differs from the original film model in the limit of the instantaneous enhancement factor. This can be seen by comparing eq. (2.11) and eq. (2.29).

In this work a similar approach is developed called the GMAF model which is a combination of the GM and AF model. It is obtained by combining eq. (2.10) and eq. (2.23) with eq. (2.29). The GM model and the GMAF model is compared against the AF model for absorption and desorption process conditions, as shown in Figure 2.A.9a and Figure 2.A.9b. Note the original AF model was considered to deviate up to 10% (Chang& Rochelle, 1982). The conditions for the study are outlined in Table 2.A.1 and Table 2.A.3.

It was shown by Chang and Rochelle that the film model deviates from the AF model at high Hatta numbers. The current calculations indicate the same behaviour. Figure 2.A.9a outlines how the GM and the AF model overlap for absorption like conditions. However, the deviation increases significantly for desorption process conditions. Figure 2.A.9b presents the GM for surface renewal theory against the approximate film (AF) model. This figure demonstrates that the GMAF model approximates the surface renewal model as well as the AF model for absorption and for desorption conditions. The average absolute deviation between GMAF and AF model is 0.82 % with a maximum absolute deviation of 0.25 %.

In addition, we have compared the IPFO model to the approximate film model. This analysis reveals that the IPFO model, similar to GMAF, agrees fairly well with the AF model. The absolute relative deviations are up to 2.34% for absorption conditions. At desorption like conditions, the difference between the two models is somewhat higher. The deviations are up to 15%.

The source of these discrepancies between IPFO and AF might be the underlying mass transfer model. The IPFO model is based on the Eddy theory which predicts the surface and penetration theory within 5% (Glasscock& Rochelle, 1989). The AF model build on the film model and it deviates up to 10% from the penetration and surface renewal theory (Chang& Rochelle, 1982). It can be concluded that these results agree well with the findings presented in Figure 9 and suggest that GMAF model as well as the IPFO model can be used to predict the surface renewal model and the penetration theory.
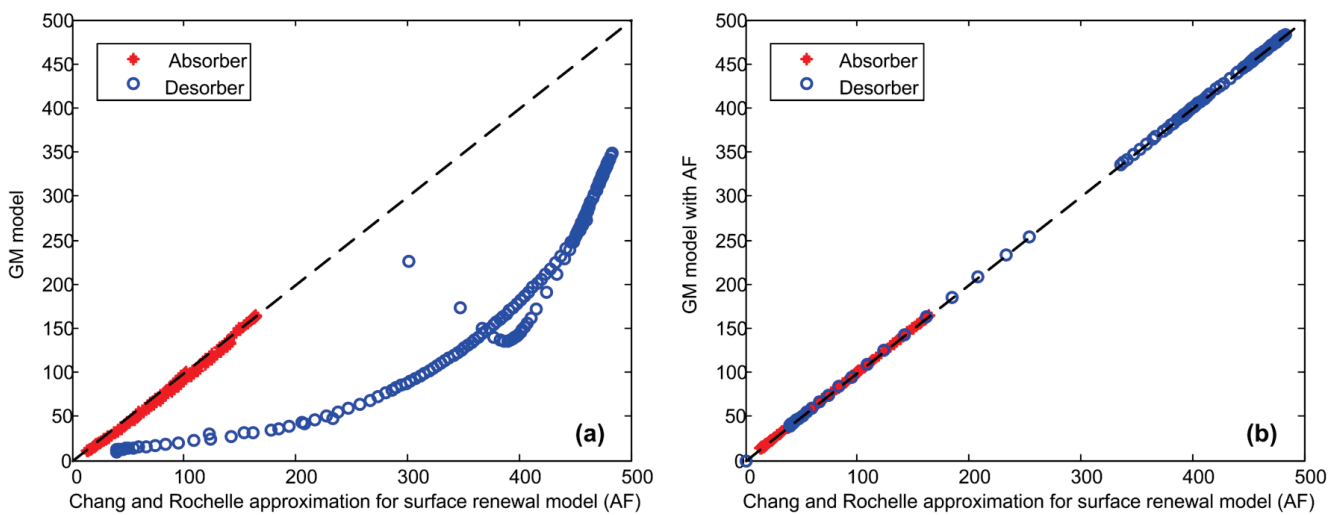
Figure 2.A.9. Enhancement factor of (a) GM model and (b) GM model with AF model against the approximate film (AF) model of Chang and Rochelle

It can be concluded that the GM model predicts the enhancement factor well for absorption conditions and under-predicts for desorption, compared to the AF model. The GM model can be extended to the surface

renewal model, becoming the GMAF model. The benefit of the GMAF model compared to the full surface renewal model is the simplicity of the solution and therefore it is less computationally heavy.

2.A.5 Conclusions

The present work develops a general method (GM) for enhancement factor calculation. The model is compared with the van Krevelen and the Astarita & Savage model. The results are shown in terms of deviations between the approximate solutions and a rigorous numerical solution. The numerical model used for the comparison is based on the two-film theory. Although the main focus of this work is the film theory, a separate section is dedicated to the GM model evaluation and adjustment to the surface renewal model. The behaviour of the GM and GMAF model for absorption and desorption process conditions is evaluated for CO_2 capture modelling. However the enhancement factor model is set up in a general form to make it easily extendable to other systems with various kinetics and stoichiometry.

The analysis of the results reveals that the van Krevelen model deviates in the prediction of the enhancement factor at high loadings and low MEA concentrations at absorption like conditions. The comparison of the enhancement factor calculations also reveals that the accuracy of the results is uncertain for desorption conditions. It was shown that the magnitude of the error can increase to the order of ten's in case of desorption modelling. The increase of the error is possibly due to the linearization technique used by van Krevelen and Hoftijzer. This model was developed for irreversible reactions which strictly valid in the applied CO_2-MEA-H_2O system.

The Astarita and Savage model generally performs better than the van Krevelen model, due to the improvement of the linearization assumption. However, the Astarita and Savage model inherits some of the limitations of the van Krevelen approach. For absorption conditions the model tends to under-predict while for desorption like conditions it often over-predicts the enhancement factor. In case of absorption the error is highest at near zero gas phase CO_2 concentration. This is an important limitation of the model, as the flue gas CO_2 composition is generally less than 1 % at the top part of the column. The limitations of the model is more pronounced for the desorption case. The error of the model is the highest near to the pinch zone which is relevant to the industry. It can be due to the overestimation of the irreversible value of the enhancement factor compared to the one calculated for reversible conditions.

The comparison of the GM model with the numerical solver highlights that it can be used to calculate the enhancement factor for both, absorption and desorption process conditions. The model is derived for an *(m+n)*-th order and reversible reaction kinetics and applied for the CO_2-MEA-H_2O second order reversible system. An equilibrium assumption in the liquid film has to be fulfilled. However, slower processes where this is relevant have currently no industrial importance.

Generally, the approximate models presented in the literature can be used for some specific systems or operational ranges. Therefore they are of restricted use. It is demonstrated through a case study that the developed GM model predicts the enhancement factor for both, absorption and desorption conditions very well. The GM model can be applied in both the film model scenario and surface renewal model. The average absolute relative deviation between the GM model and two-film model is less than 0.5%. The average absolute relative deviation compared to the surface renewal model is less than 1%. Thus it can be used reliably for both absorption and desorption in the film and surface renewal approach. As a result, many of the limitations of the previous models have been considerably improved. The high accuracy and simplicity of the GM model makes it suitable not only for engineering calculations but also for advanced process analyses and optimization.

The GM model relies on computation of a single algebraic equation while the two-film model requires the solving of a second order differential equation system. Hence, GM model is less computationally heavy. Furthermore, it can be used for approximation of the surface renewal model, without increasing the complexity. The GM model can enhance crucially the accuracy of process simulators. In this way, a conservative design can be eliminated and consequently the cost of equipment can be optimised. From an economic point of view, it can reduce the cost of process scale-up.

Nomenclature

A,B,C,D	Reactants respectively products
C_i	Molar concentration of component i (mol/m^3)
D_i	Diffusion coefficient of component i (m^2/s)
dx	Grid increment (m)
E	Enhancement factor (-)
E_∞	Instantaneous /Asymptotic enhancement factor
Ha	Hatta number
K_{eq}	Chemical equilibrium constant
k	Reaction rate constant
k_L	Partial mass transfer coefficient on the liquid side (m/s)
m, n	Order of reaction
N_A	Mass transfer flux through the gas liquid interface (mol/m^{2}s)
r	Reaction rate (mol/m^{3}s)
R	Reaction term (mol/m^{3}s)
x	Spatial coordinate (m)
y_i	Dimensionless composition of component i in the film
y_A*	composition of A-component at equilibrium

Greek symbols

ν	Reaction order/ Stoichiometric coefficient
ϕ	Loading (mole CO_2 /mole Amine)
ξ	Extent of reaction as defined by Astarita & Savage
δ	Film thickness according to the film model (m)
β	Dimensionless parameter in the reaction rate eq.
Ψ	Dimensionless composition defined by Astarita & Savage
Δ	Absolute deviation

Subscripts/Superscripts

∞	Assymptotic or infinit
*	Equilibrium
b	Bulk
0	Bulk
i	Interface
tot	Chemically free plus bounded amine

Acknowledgments

References

Al-Juaied, A., Mohammed (2004). Carbon Dioxide Removal from Natural Gas by Membranes in the Presence of Heavy Hydrocarbons and by Aqueous Diglycolamine®/Morpholine.

Astarita, G., & Savage, D. W. (1980a). Gas-Absorption and Desorption with Reversible Instantaneous Chemical-Reaction. *Chemical Engineering Science, 35*, 1755-1764.

Astarita, G., & Savage, D. W. (1980b). Theory of Chemical Desorption. *Chemical Engineering Science, 35*, 649-656.

Bhattacharya, A., & Ramachandran, P. A. (1983). Comparison of Enhancement Factor for Reversible and Irreversible Instantaneous Reactions. *Chemical Engineering Science, 38*, 472-473.

Chang, C. S., & Rochelle, G. T. (1982). Mass-Transfer Enhanced by Equilibrium Reactions. *Industrial & Engineering Chemistry Fundamentals, 21*, 379-385.

Danckwerts, P. V. (1970). Gas-Liquid reactions. *McGraw-Hill Chemical Engineering Series*.

Danckwerts, P. V. (1951). Significance of Liquid-Film Coefficients in Gas Absorption. *Industrial and Engineering Chemistry, 43*, 1460-1467.

Decoursey, W. J. (1982). Enhancement Factors for Gas-Absorption with Reversible-Reaction. *Chemical Engineering Science, 37*, 1483-1489.

Decoursey, W. J., & Thring, R. W. (1989). Effects of Unequal Diffusivities on Enhancement Factors for Reversible and Irreversible Reaction. *Chemical Engineering Science, 44*, 1715-1721.

Freguia, S., & Rochelle, G. T. (2003). Modeling of CO2 capture by aqueous monoethanolamine. *AIChE Journal, 49*, 1676-1686.

Glasscock, D. A., & Rochelle, G. T. (1989). Numerical-Simulation of Theories for Gas-Absorption with Chemical-Reaction. *AIChE Journal, 35*, 1271-1281.

Higbie, R. (1935). The rate of absorption of a pure gas into a still liquid during short periods of exposure. *Transactions of the American Institute of Chemical Engineers, 31*, 365-389.

Hikita, H., & Asai, S. (1964). Gas absorption with (m,n)-th-order irreversible chemical reaction. *International Journal of Chemical Engineering, 4*, 332-340.

Hogendoorn, J. A., Vas Bhat, R. D., Kuipers, J. A. M., van Swaaij, W. P. M., & Versteeg, G. F. (1997). Approximation for the enhancement factor applicable to reversible reactions of finite rate in chemically loaded solutions. *Chemical Engineering Science, 52*, 4547-4559.

Katti, S. (1992). Gas-Absorption and Desorption with Reversible Instantaneous Chemical-Reaction. *Chemical Engineering Science, 47*, 2125-2127.

King, C. J. (1966). Turbulent Liquid Phase Mass Transfer at a Free Gas-Liquid Interface. *Industrial & Engineering Chemistry Fundamentals, 5*, 1-&.

Lewis, W. K., & Whitman, W. G. (1924). Principles of gas absorption. *Industrial and Engineering Chemistry, 16*, 1215-1220.

Olander, D. R. (1960). Simultaneous Mass Transfer and Equilibrium Chemical Reaction. *AIChE Journal, 6*, 233-239.

Onda, K., Sada, E., Kobayash.T, & Fujine, M. (1970). Gas Absorption Accompanied by Complex Chemical Reactions .1. Reversible Chemical Reactions. *Chemical Engineering Science, 25*, 753-&.

Santiago, M. D., & Farina, I. H. (1970). Mass Transfer with Second Order Reaction - Numerical Solution. *Chemical Engineering Science, 25*, 744-&.

van Krevelen, D. W., & Hoftijzer, P. J. (1948). Kinetics of gas-liquid reactions - I. General theory. *Recueil, 67*, 563-586.

Vanswaaij, W. P. M., & Versteeg, G. F. (1992). Mass-Transfer Accompanied with Complex Reversible Chemical-Reactions in Gas-Liquid Systems - an Overview. *Chemical Engineering Science, 47*, 3181-3195.

Versteeg, G. F. (2001). Gas-liquid reactions. Influence of liquid bulk and mass transfer on process performance. *PhD thesis*.

Versteeg, G. F., Kuipers, J. A. M., Vanbeckum, F. P. H., & Vanswaaij, W. P. M. (1989). Mass-Transfer with Complex Reversible Chemical-Reactions .1. Single Reversible Chemical-Reaction. *Chemical Engineering Science, 44*, 2295-2310.

Winkelman, J. G. M., Brodsky, S. J., & Beenackers, A. A. C. M. (1992). Effects of Unequal Diffusivities on Enhancement Factors for Reversible-Reactions - Numerical-Solutions and Comparison with Decoursey Method. *Chemical Engineering Science, 47*, 485-489.

Part B. A general enhancement factor model (GM) for multiple parallel reactions: Mass transfer rate of piperazine (PZ) CO₂ capture

Abstract

Reactive absorption is a key process for gas separation and purification and it is the main technology for CO_2 capture. Thus, reliable and simple mathematical models for mass transfer rate calculation are essential. Models which apply to parallel interacting and non-interacting reactions, for all industrially relevant reaction regimes must be developed and validated against experimental measurements.

In a previous work, we presented the general model (GM) enhancement factor model for *(m+n)-th* order reversible reactions and validated it against the numerical solution of the two-film model for absorption, desorption and pinch conditions.

In this work, we extend the GM model to multiple parallel reactions. We deduce the model for piperazine (PZ) CO_2 capture and we validate it against wetted-wall column measurements using 2, 5 and 8 molal PZ for temperatures between 40°C and 100°C and CO_2 loadings between 0.23 and 0.41 mol CO_2/2 mol PZ. We demonstrate that the zwitterion based kinetic describes well the reaction between CO_2 and PZ accounting for the carbamate and bicarbamate reactions. Here we prove the GM model for piperazine and MEA but the theory is general and expectedly accurate for various amines, blends of amines and promoted amines with similar kinetics. It is also expectedly accurate for complex reaction mechanisms in other parallel chemical systems.

Furthermore, we compare the GM model and the numerical solution of the complete two-film model predictions to MEA wetted-wall data and we prove that it is safe to assume that GM and the two-film model give practically identical results. We demonstrate that the expected predictability of CO_2 mass transfer rates using off-the-shelf correlations generally is ±20%.

Keywords: *GM enhancement factor; parallel reactions; wetted-wall validation; model uncertainty; CO_2 post-combustion capture; piperazine.*

2.B.1   Introduction

Reactive absorption is a widespread process used for gas purification, product cleaning, separation, etc. Amine based reactive absorption has been used for decades in the refining industry and the chemical industry. Currently, it is the leading technology for post-combustion CO_2 capture. However, traditional

solvents such as mono-ethanol-amine (MEA), di-ethanol-amine (DEA) have an undesirably high energy demand and they are economically unfeasible for large scale post-combustion capture.

The continuous search for a better solution led us to innovative solvents, to blends of amines and/or promoted amine solvents, e.g. aqueous piperazine, PZ/MDEA, enzyme/MDEA and PZ/K_2CO_3. These solvents have several advantageous over the benchmark MEA solvent, such as higher CO_2 cycling capacity and lower regeneration energy demand (Puxty et al., 2009). But the kinetics between CO_2 and the solvents as well as the effect of the reaction on mass transfer rate needs further analysis. In order to accelerate the development of CO_2 capture technologies and various reactive absorption processes, accurate mass transfer models are needed (Versteeg, Van Dijck, & Van Swaaij, 1996). Models are essential to fully understand the competing phenomena of diffusion and multiple reactions respectively to design and optimize the solvent of tomorrow.

An important but not fully developed topic is mass transfer accompanied by multiple interacting and non-interacting parallel reactions. Multiple reactions are non-interacting if only one or no components are common between the reactions, e.g. reaction between CO_2 and MEA producing carbamate. Chang& Rochelle (1982) have shown that for non-interacting reaction systems, each reaction contributes individually to the overall increase of the mass transfer rate. Consequently, existing enhancement factor models, e.g. GM model (Gaspar& Fosbøl, 2015), DeCoursey model (Decoursey& Thring, 1989), Astarita and Savage model (Astarita& Savage, 1980), van Krevelen model (van Krevelen& Hoftijzer, 1948), etc. apply to non-interacting multiple reactions.

Multiple interacting reactions are more complex. Two reactions are considered to interact if two or more components are common between the reactions, e.g. both CO_2 and PZ participate in two separate reactions to produce the carbamate and bicarbamate ions. The reactions no longer contribute independently to the acceleration of the mass transfer rate. Hence, the distribution of the components between the reactions must be considered in the material balance. Vanswaaij& Versteeg (1992) showed that exact description of a system consisting of two parallel reactions with a moderate and a low equilibrium constant can be obtained only numerically by solving the complete two-film model. Similar conclusion was drawn by Glasscock & Rochelle (1989). However, the numerical treatment of a mass transfer model requires simultaneous computation of differential equations and non-linear algebraic equations coupled with a thermodynamic model. This is computationally-demanding and it is not feasible for industrial process simulation.

Simplified models are employed to describe industrial mas transfer processes involving reactive absorption. Generally, an enhancement factor describes the intensification of mass transfer due to the reaction compared to a non-reacting solvent. The enhancement factor is an approximation of the rigorous mass transfer model under simplifications of the reaction kinetics, flow regime and mass transfer rate determining step. Under

these simplifications the mass transfer model can be reduced to simple algebraic equations which require significantly less computational resources.

The so called interface-pseudo-first order (IPFO) approximate model for MEA CO_2 capture calculation, accounting for the reaction between CO_2 and MEA respectively CO_2 and OH^-, was introduced by Freguia& Rochelle (2003). This model assumes that the reactions are fast and all of the species, excluding CO_2, are constant at their interface values. The allocation of CO_2 absorption rates between the reactions is arbitrary and it depends on the equilibrium constants of the reactions. Later, this model has been demonstrated for the aqueous diglycolamine solvent (DGA) and blends of morpholine and DGA by Al-Juaied (2004). This implementation includes two respectively three parallel reactions. Al-Juaied (2004) compared the model against wetted wall column data and the rigorous Eddy diffusivity model. He concluded that the reaction of DGA with CO_2 is dominant at low loadings but diffusion of reactants and products becomes an important phenomenon at high loadings, in the instantaneous reactions zone. A similar work on PZ was performed by Dugas (2009) and Dugas & Rochelle (2011). They successfully implemented a thermo-molecular kinetics based mass transfer model and compared the model against wetted wall column data for PZ and MEA. Furthermore, Dugas & Rochelle (2011) show how the liquid film resistance increases with CO_2 loading due to the changing PZ and $PZCOO^-$ concentrations. They showed that the system behaves pseudo-first order at low CO_2 loadings and it experiences diffusion resistance at high CO_2 loadings when depletion of the reactants occurs.

In a previous work, we have shown that various approximate models have been developed for CO_2 mass transfer rate prediction using single reactions. However, most of these models apply only for limited process conditions, such as instantaneous reaction, irreversible reaction, slow reaction, pseudo-first order reaction, etc. Industrial processes cover a broader range and a general mass transfer model is essential to avoid significant differences between simulation and plant measurements (Gaspar& Fosbøl, 2015). Previously, we presented and illustrated the reliability of the GM model for single reversible reactions. We demonstrated that GM eliminates many of the limitations of existing models, e.g. the Astarita and Savage model, the van Krevelen model. It predicts the rigorous two-film model within 2% accuracy and the surface renewal model within 10% accuracy for the reaction between CO_2 and MEA (Gaspar& Fosbøl, 2015).

In the present work we take a step forward. Here, we propose a simple model to determine the mass transfer rate enhancement for multiple parallel reactions. Parallel reactions are common in gas cleaning processes, such as CO_2 capture using the currently emerging promising solvents, e.g. piperazine, enzyme promoted tertiary amine solvents, blends of amine solvents. The proposed model builds on the previously presented GM model (Gaspar& Fosbøl, 2015). It assumes that only thermodynamic interaction exists between the components, where CO_2 is distributed per equilibria between the reactions. We present the equation system

for the piperazine CO_2 capture process and we show the good agreement between the model and wetted wall column measurements for the 2, 5 and 8 molal PZ solvents. The proposed model accounts for two parallel reactions: the formation of the carbamate and bicarbamate ions. It is essential to include both of the reactions since the contribution of the bicarbamate forming reaction is greater than 30% at high CO_2 loading, especially for 2 molal PZ solution. In addition, we validate the GM model using the benchmark 30 wt.% monoethanolamine solvent and we analyze the effect of parameter uncertainties, i.e. diffusion coefficient, rate constant, CO_2 bulk concentration, on the model outputs.

2.B.2   Model basis

This section discusses the GM enhancement factor model for single reactions and multiple parallel reactions. In a previous work, we have deduced the GM model for an *(m+n)-th* order single reversible reaction and illustrated the model for MEA CO_2 capture process simulation (Gaspar& Fosbøl, 2015). Here, we exemplify GM model for an *(1+1)-th* order reversible reaction, i.e. $A + B \rightarrow Products$, which is typical for second order kinetics in CO_2 capture and we extend the mass transfer model to *N* parallel reactions. We expect the approach is similarly applicable to *N* reactions of *(m+n)-th* order. The mass transfer model is exemplified for the innovative PZ solvent, used in CO_2 post-combustion capture processes. The kinetics of the reaction between CO_2 and PZ respectively CO_2 and MEA, the thermodynamic model and the physical properties entering the CO_2 mass transfer flux calculation are also discussed.

2.B.2.1 Reaction kinetics

The reaction kinetics of CO_2 with amines depends on the type of amine (primary, secondary, tertiary, etc.) and on process conditions (temperature, CO_2 loading, etc.). This reaction can occur in various absorption regimes, e.g., slow, fast, intermediate and instantaneous. Therefore, in-depth knowledge of the reaction mechanisms and corresponding rate constants is required. A typical rigorous mechanism consists of several parallel, simultaneous and/or competing reactions. Implementation of such mechanism in a mass transfer model is a laborious task and it results in significant increase of the computational time. As a consequence, simplified kinetics is usually proposed. Here, we apply a simplified approach for the reaction of CO_2 with piperazine assuming two parallel reactions and we briefly present the reaction between CO_2 and MEA assuming one single reaction.

Kinetics of CO_2 capture by MEA

Versteeg et al. (1996) outlined that CO_2 reacts with MEA according to second-order kinetics. It is first order with respects to the reactants. In addition, they showed that good agreement exists between the reaction rate constants obtained by different researchers. This second order rate constant is:

$$k_{2,MEA} = 4.4 \cdot 10^8 \exp\left(-\frac{5400}{T}\right) \left[\frac{m^3}{mol \cdot s}\right]$$

(2.32)

Keep in mind that a common approach for determining the parameters in eq. (2.32) is by applying the pseudo-first order approximation (PFO). At these conditions the enhancement factor is identical to the Hatta number. The PFO approximation requires that: (1) the liquid phase driving force is small and (2) the reaction between CO_2 and MEA is fast, thus the reaction occurs in a small fraction of the boundary layer and CO_2 reaches equilibrium with the solution. These assumptions imply that the interface concentration of MEA and of the reaction products can be approximated with their bulk concentrations. Thus, the concentration of all of the species, excluding CO_2, is constant in the liquid film. Essentially the reaction becomes first order with respect to CO_2 at constant amine concentration.

The assumptions of the PFO do not hold at all conditions: (1) at low CO_2 loadings a large amount of free-MEA is available to react, thus a very large driving force is necessary to break this assumption. These conditions are industrially irrelevant. (2) However at high CO_2 loadings, the free-MEA concentration is small; thus, only at small driving forces the film MEA concentration remains constant. These conditions occur in the bottom of an absorption column. As a consequence, the driving force at which the PFO approximation holds reduces when CO_2 loading increases. Consequently, eq. (2.32) results in greater discrepancies at high CO_2 loadings.

Kinetics of CO_2 capture by PZ

The kinetics of the reaction between CO_2 and PZ is more complex. In aqueous solutions, PZ forms various reaction products with CO_2. Derks et al. (2006) showed that the major contributors to the overall observed absorption rate are reactions (2.33) and (2.34), producing the carbamate and the bicarbamate ions:

$$CO_2 + PZ \xrightarrow{H_2O} PZCOO^- + H_3O^+$$

(2.33)

$$CO_2 + PZCOO^- \xrightarrow{H_2O} PZ\left(COO^-\right)_2 + H_3O^+$$

(2.34)

Furthermore, Derks et al. (2006) outlines that the reaction between CO_2 and the hydroxyl ion is negligible since the forward rate constant and the hydroxyl ion concentration are much smaller than the piperazine concentration and the rate constant of (2.33). Furthermore, they demonstrate that it is reasonable to disregard the reaction between CO_2 and PZH^+, since the forward reaction rate constant is a few order of magnitude smaller compared to the reaction rate constant of (2.33). As a consequence, we include reactions (2.33) and (2.34) when determining the CO_2 mass transfer rate through the gas-liquid interface.

We implement second-order reaction kinetics, first order in reactants, i.e. CO_2, PZ, and PZCOO$^-$, as described by Derks et al. (2006). The selection of the rate constant values for reaction (2.33) and (2.34) is not as straightforward as for MEA. First of all, only limited rate data is available in the open literature for the PZ system, especially for highly loaded solutions. Another source of uncertainty is the methodology used to interpret the experimental data. A common approach is to back-calculate the rate constant using the PFO approximation. But, Derks et al. (2006) demonstrated that the value of the rate constant significantly varies when using different enhancement factor models and the PFO approximation may not hold for the piperazine system. Gaspar et al. (2014) have shown how published $k_{2,PZ}$ values differ significantly between experiments. The deviations between experimental data as well as correlations are especially high at desorption conditions. Therefore, in the present work we use $k_{2,PZ}$ from Gaspar et al. (2014), which is a compilation of several experimentally measured and published correlations:

$$k_{2,PZ} = 7.734 \cdot 10^8 \exp\left(-\frac{5054.34}{T}\right) \left[\frac{m^3}{mol \cdot s}\right] \tag{2.35}$$

The kinetic experiments to determine $k_{2,PZ}$ were carried out in the pseudo-first order regime. In this reaction regime the concentration of PZ does not decrease noticeably when reacting with CO_2. Therefore, the concentration of the carbamate ion at the interface is small and the contribution of reaction (2.34) to the overall reaction is negligible. However, at conditions of interest for the CO_2 capture process, the formation of the bicarbamate ion, reaction (2.34), has to be accounted for, as shown by Derks et al. (2006). The rate constant of this reaction, $k_{2,PZCOO^-}$ is not available in open literature. Its value has been estimated using the Brönsted relation (Derks et al., 2006; Dugas& Rochelle, 2011) and it is:

$$k_{2,PZCOO^-} = 5.414 \cdot 10^8 \exp\left(-\frac{5054.34}{T}\right) \left[\frac{m^3}{mol \cdot s}\right] \tag{2.36}$$

One can see that several uncertainties have to be accounted for when implementing the kinetics of PZ CO_2 capture. The agreement between mass transfer models and experimental measurements is subject to these uncertainties.

2.B.2.2 Mass transfer with simultaneous single and multiple reactions

This section presents the equations system of the GM enhancement factor model for single *(1+1)-th* order reactions and show an approach to account for multiple reactions when determining the overall mass transfer rate enhancement. The basis of the current approach is the two-film model, thus the mass transfer rate through the gas liquid interphase, $J_{CO_2,gl}$ is:

$$J_{CO_2, gl} \simeq \frac{1}{1/k_{CO_2}^g + H_{CO_2}/E_{overall} k_{CO_2}^l}\left(p_{CO_2} - p_{CO_2}^*\right) \tag{2.37}$$

$k_{CO_2}^g$ and $k_{CO_2}^l$ are the partial mass transfer coefficients for the gas side and for the liquid side, H_{CO_2} is the Henry law constant and $E_{overall}$ denotes the overall enhancement factor. The overall enhancement factor includes the intensification of the mass transfer rate from all of the participating reactions. The driving force for mass transfer is the difference between the partial pressure of CO_2 in the gas phase, p_{CO_2} and the equilibrium partial pressure of CO_2 exerted from the liquid phase, $p_{CO_2}^*$.

The gas side and liquid side mass transfer coefficients for wetted wall columns must be determined experimentally (Dugas, 2009). For packed columns various correlations exist which account for packing and flow regime characteristics. Two of the most common models are Billet& Schultes (1999) and Rocha, Bravo, & Fair (1996).

The GM enhancement factor model for single reactions

This section presents the GM model equation system for kinetics resembling the reactions between CO_2 and PZ, i.e. the *(1+1)-th* order single reactions (2.33) and (2.34). Here, we briefly describe the GM model. For more details, regarding development of the model and solution methodology see the work of Gaspar& Fosbø, (2015).

According to (Gaspar& Fosbøl, 2015), the two film model can be expressed in terms of an enhancement factor, as shown in eq. (2.38). This equation applies for all of the reactions regimes. This equation depends on the instantaneous enhancement factor, E_∞^*, and the dimensionless compositions $y_{CO_2}^b$ and y_B^i. The mathematical development was illustrated by (Gaspar& Fosbøl, 2015).

$$E = 1 + \left(E_\infty^* - 1\right)\frac{1 - y_B^i}{1 - y_{CO_2}^b} \tag{2.38}$$

where B refers to a base, e.g. *PZ, PZCOO⁻*. The instantaneous enhancement factor, E_∞^*, shows the intensification of a transfer phenomenon by an instantaneous and irreversible reaction. It corresponds to the asymptotic maximum limit of mass transfer enhancement. It is given by eq. (2.39). The dimensionless compositions represent the ratio between the bulk and the interface concentrations and they are: $y_{CO_2}^b = C_{CO_2}^b/C_{CO_2}^i$ and $y_B^i = C_B^i/C_B^b$.

$$E_\infty^* = 1 + \frac{D_B C_B^b}{D_{CO_2} C_{CO_2}^i} \tag{2.39}$$

where D_B and D_{CO2} are the diffusion coefficients of a base B. e.g. *PZ, PZCOO*⁻ respectively CO_2. C_B^b and $C_{CO_2}^i$ denote the concentration of the base in the liquid bulk respectively the concentration of CO_2 at the gas-liquid interphase. $C_{CO_2}^i$ is calculated using the extended UNIQUAC thermodynamic model. Practically, the thermodynamic model provides the liquid phase and the gas phase equilibrium CO_2 concentration and pressure. The ratio of the two gives a so called apparent Henry coefficient. This is applied to convert the bulk CO_2 partial pressure to interface concentration.

Equation (2.38) has two unknowns, E and y_B^i. In order to solve it, we introduce a second relationship accounting for the *(1+1)-th* order reaction kinetics. According to the work of Gaspar& Fosbøl (2015), the enhancement factor for this reaction type is:

$$E = Ha \sqrt{y_B^i} \frac{1 - y_{CO_2}^*}{1 - y_{CO_2}^b} \tag{2.40}$$

$y_{CO_2}^*$ represents the composition of CO_2 which would be in equilibrium with the interface concentration: $y_{CO_2}^* = y_{CO_2}^b \, y_P^i y_R^i / y_B^i$, where *P* and *R* refer to reaction products and *B* is PZ respectively PZCOO⁻. The Hatta number, *Ha*, entering eq. (2.40) is according to Hikita& Asai (1964):

$$Ha = \frac{\sqrt{k_2 C_B^b D_{CO_2}}}{k_L} \tag{2.41}$$

Now, the enhancement factor for the single reactions can be determined by solving the system of algebraic non-linear equations (2.38) and (2.40). The solution strategy is discussed in Gaspar& Fosbøl (2015). The enhancement factor for MEA is obtained similar to the above described. The equations system is described in Gaspar& Fosbøl (2015) and they are not discussed here.

Enhancement factor model for parallel reactions

A calculation method for complex systems with parallel reactions is presented here. Models for parallel reactions are of great importance in reactive absorption processes. Modeling of these processes requires solving of a rigorous mass transfer model which consists of partial differential equations and a kinetic respectively a thermodynamic model (Versteeg et al., 1996). The numerical solution of these rigorous

models is computationally heavy for plant-wide process simulation. Though, here we propose a model which is rigorous enough to include all the relevant aspects of reactive absorption and simple enough to enable an easy and practical implementation of the process.

The model is based on the assumption that only thermodynamic interaction exists between the reactions and the acceleration of mass transfer rates due to each reaction is distributed per equilibria. The coupling between the individual reactions is through the underlying thermodynamic model which provides the bulk compositions in the expression of y_{CO2}^*. Accordingly, the enhancement factor for each reaction is calculated identical to a single reaction-system for each reaction independently and the overall mass transfer intensification is the combined effect of the individual reactions. Therefore, the overall enhancement factor is:

$$E_{overall} = 1 + \sum_{j}^{N}\left(E_j - 1\right)$$
(2.42)

where E_j is the enhancement factor of single reaction j and N is the number of participating reactions. Essentially, the total intensification of mass transfer rate is obtained by combining eq. (2.42) with the GM enhancement factor model for single reactions.

In the following we apply this approach for CO_2 absorption and desorption rate calculations using 2, 5 and 8 molal piperazine solvents. The accuracy of the model is shown against wetted wall column measurements. Chang& Rochelle (1982) demonstrated that eq. (2.42) represents the exact solution for non-interacting parallel reaction-systems and here we show that it applies to multiple parallel reactions as well.

2.B.3   Thermodynamic and physical properties

The extended UNIQUAC thermodynamic model proposed by Thomsen, Rasmussen, & Gani (1996) provides the liquid-vapour equilibrium and the thermal properties of the electrolyte system. The phase equilibrium is calculated in a γ-φ approach coupled with equilibrium speciation reactions. Therefore, liquid phase activity coefficients are calculated with the extended UNIQUAC model, and the gas phase fugacity coefficients are estimated with the Soave-Redlick-Kwong equation of state. A detailed description of the equation system and derived properties is given by Thomsen et al. (1996) and Thomsen& Rasmussen (1999). A validation of the model against experimental PZ data is shown by Fosbøl, Maribo-Mogensen, & Thomsen (2013).

Table 2.B.1 presents the physical properties used in the mass transfer model. These originate from the open literature. The diffusion coefficient of CO_2 in PZ and MEA solutions is obtained from the $N_2O:CO_2$ analogy (Versteeg et al., 1996). We assume that the diffusion coefficients of the products are identical to the diffusion

coefficient of PZ respectively MEA. The viscosity of the solvent is obtained from the work of Rochelle et al. (2011) and Cheng, Meisen, & Chakma (1996). The gas and liquid side mass transfer coefficients entering eq. (2.37) originate from Dugas (2009).

Table 2.B.1. Physical property correlations

Physical property	Reference
Diffusivity coefficient of CO_2 and N_2O in water	(Versteeg et al., 1996)
Diffusivity coefficient of CO_2 in MEA solution	(Versteeg et al., 1996)
Diffusivity coefficient of CO_2 in PZ solution	(Dugas& Rochelle, 2011)
Diffusivity coefficient of MEA in MEA solution	(Snijder et al., 1993)
Diffusivity coefficient of PZ in PZ solution	(Dugas& Rochelle, 2011)
Density of MEA solution	(Weiland et al., 1998)
Density of PZ solution	(Gaspar et al., 2015)
Viscosity of MEA solution	(Cheng et al., 1996)
Viscosity of PZ solution	(Dugas, 2009)

2.B.4   Results and discussions

The focus of this section is on investigating the agreement between the proposed model for parallel reactions and wetted-wall column data. First, we perform an uncertainty analysis to understand the effect of key parameters, i.e. diffusion coefficient, rate constant and CO_2 loading on mass transfer rate predictions. Secondly, we compare the GM model against wetted-wall data using 30 wt% (7 molal) MEA. Finally, we compare the proposed enhancement factor model for parallel interacting reactions, i.e. GM model combined with eq. (2.42), to wetted-wall column data using 2, 5 and 8 molal PZ solutions. The experimental data originates from Dugas (2009).

Table 2.B.2 gives an overview of the experimental conditions for the wetted wall column measurements from Dugas (2009) for both solvents, MEA and PZ. It illustrates how the campaign covered a broad range of CO_2 loadings and temperatures on both absorption and desorption. The CO_2 loading of the solvent was between 0.23 and 0.50 mol CO_2/mol alkalinity at 40, 60, 80 and 100°C. For each condition of CO_2 loading and temperature, six CO_2 partial pressures were tested: the lowest partial pressure was pure solvent using nitrogen; the highest partial pressure was double the calculated equilibrium CO_2 partial pressure of the solution; and four measurements at partial pressures uniformly distributed between the two extremes were performed. This design assures similar fluxes in magnitude for CO_2 absorption and desorption. It is worth

noting that most of the measured CO_2 fluxes are within ± 0.005 mol/m^{2}s. The few remaining data corresponds to very high driving forces.

Table 2.B.2. Input specifications for the wetted-wall column measurements

Parameter	Unit	MEA	PZ
Number of experimental data		69	212
Amine concentration	mol/kg water	7	2, 5, 8
Amine concentration	wt.%	30	15, 30, 41
CO_2 loading	mol/mol alk.*	0.23 – 0.50	0.23 – 0.41
Temperature	°C	40 – 100	40 – 100
Driving force	kPa	-18.7 – 20.5	-38.6 – 28.3
CO_2 molar flux	mol/m^{2}s	-0.016 – 0.013	-0.1 – 0.019

* mol/mol alk. corresponds to mol CO_2/mol MEA respectively mol CO_2/ 2 mol PZ

The published data by Dugas (2009) was screened for potential outliers. For this, the experimental flux measurements were represented versus the driving force. This analysis revealed that 7 points unexpectedly deviate from the observed trend. Moreover, the same points presented relative absolute deviations above 100% from the GM calculated values. Thus, these 7 points were eliminated from the total of 288.

2.B.4.1 Validation of the GM model for MEA-CO$_2$ capture

Before discussing the accuracy of the GM model for PZ-CO$_2$ capture, we perform a parametric uncertainty analysis by varying diffusion coefficient, reaction rate constant and CO$_2$ loading. This analysis is performed using the rigorous two-film model and the baseline MEA solvent. Afterwards, we compare the GM model for MEA-CO$_2$ capture to wetted-wall column measurements. The rigorous two-film model refers to the numerical solution of the two-film model.

Parametric uncertainty analysis of the model

This section presents how uncertainties in the rate constant, the diffusion coefficient of CO$_2$, and the CO$_2$ loading influences the CO$_2$ mass transfer rate using MEA. This analysis is performed with the rigorous two-film model. The effect of parameter uncertainties is quantified in terms of relative CO$_2$ flux, Δ:

$$\Delta = \frac{J_{CO_2,gl}\left(k_{2,MEA,\text{default}} + \delta, D_{CO2,\text{default}} + \delta, \theta_{\text{default}} + \delta\right)}{J_{CO_2,gl}\left(k_{2,MEA,\text{default}}, D_{CO2,\text{default}}, \theta_{\text{default}}\right)}$$

(2.43)

where the subscript "*default*" refers to the value calculated with the inlet conditions specified in table 2.B.2 and δ represent the uncertainty limit of the respective parameter, e.g. rate constant, diffusion coefficient, and CO_2 loading. Thus, $\Delta < 1$ reflects a decrease of the mass transfer rate, $\Delta = 1$ shows that there is no dependency between mass transfer rate and the varied parameter, and $\Delta > 1$ shows an increase in the CO_2 flux. In this analysis δ was selected to reach a relative CO_2 flux (Δ) between 0.8 and 1.2. Note that the rate constant, the diffusion coefficient of CO_2, and the CO_2 loading are varied one by one to determine the isolated effect of these parameters on the model prediction. The results are summarized in figures 2.B.1 and 2.B.2.

Figure 2.B.1 shows the relative CO_2 flux for $\delta = \pm40\%$ change in the reaction rate constant ($k_{2,MEA}$) and $\delta = \pm25\%$ change in the CO_2 diffusion coefficient (D_{CO2}) as function of CO_2 partial pressure. Practically, the increase of the partial pressure corresponds to the increase of the driving force for CO_2 mass transfer. The effect of the reaction rate constant and the CO_2 diffusion coefficient on the prediction uncertainty is divided in three zones as function of E_∞^*/Ha : $E_\infty^*/Ha \leq 1$ corresponds to instantaneous reaction regime (zone 1); $1 < E_\infty^*/Ha \leq 2$ resembles intermediate reaction regime (zone 2) and $E_\infty^*/Ha > 2$ matches fast reaction regime (zone 3). In this analysis, zone 1 and zone 2 corresponds to high temperature (T > 80°C) and higher CO_2 loading ($\theta > 0.30$) conditions.

Figure 2.B.1 illustrates that both parameters, $k_{2,MEA}$ and D_{CO2}, have a strong effect on the mass transfer flux. A higher rate constant, $k_{2,MEA,default} + 40\%$, which corresponds to larger reaction rates results in greater CO_2 flux ($\Delta > 1$) and vice-versa. This is expected since CO_2 absorption and desorption using MEA is typically fast to instantaneous. This figure also shows that an error of $\delta = \pm25\%$ in the value of the rate constant results in an expected mass transfer model certainty of 5 to 15% in zone 3 ($E_\infty^*/Ha > 2$) and it results in an accuracy up to 5% in zone 1 ($E_\infty^*/Ha \leq 1$).

Equations (2.39) and (2.41) show that the instantaneous enhancement factor inversely depends on D_{CO2} and the Hatta number is proportional to the square route of D_{CO2}. Therefore, in the fast reaction regime ($E_\infty^*/Ha > 2$) in figure 2.B.1, an over-predicted diffusion coefficient ($D_{CO2,default} + 25\%$) results in slightly over-predicted CO_2 flux ($\Delta > 1$). However, in the intermediate to instantaneous regimes ($E_\infty^*/Ha \leq 2$), $\delta = \pm25\%$ results in under-prediction of the CO_2 flux ($\Delta < 1$)). Figure 2.B.1 shows that at greater CO_2 partial pressure, above 20 kPa, an uncertainty of $\delta = \pm25\%$ leads to an error of 10 – 20% in the CO_2 flux prediction. Thus, this analysis shows that uncertainty of the kinetic parameter has a high impact on model prediction at low driving force and uncertainty of the diffusion coefficient has a high impact on model predictions at high driving force.

Figure 2.B.2 shows the sensitivity of the mass transfer flux with respect to the CO_2 bulk concertation. It illustrates that an uncertainty of $\delta = \pm 0.01$ in the CO_2 loading value leads to an error of 5% of the predicted flux up to a loading of 0.35 mol/mol. Above this value, Δ increases exponentially. Thus, the dependency between CO_2 bulk concentration and calculated CO_2 flux is greater at higher CO_2 loadings.
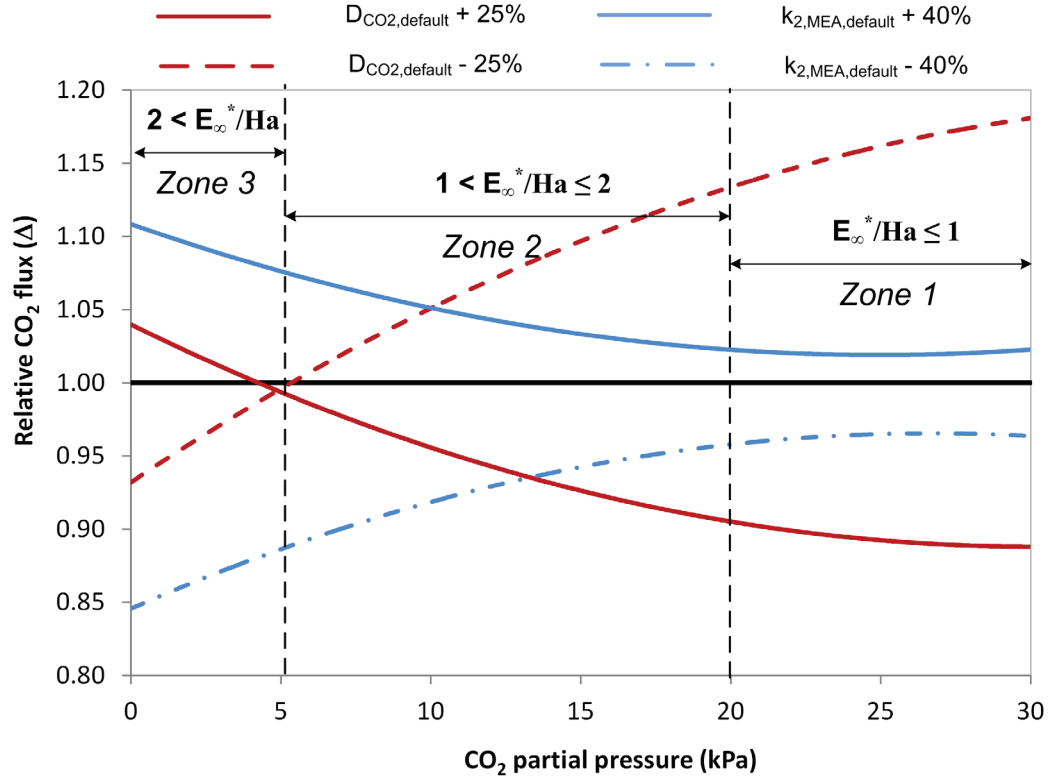
Figure 2.B.1. Effect of diffusion and kinetic characteristics on prediction uncertainty
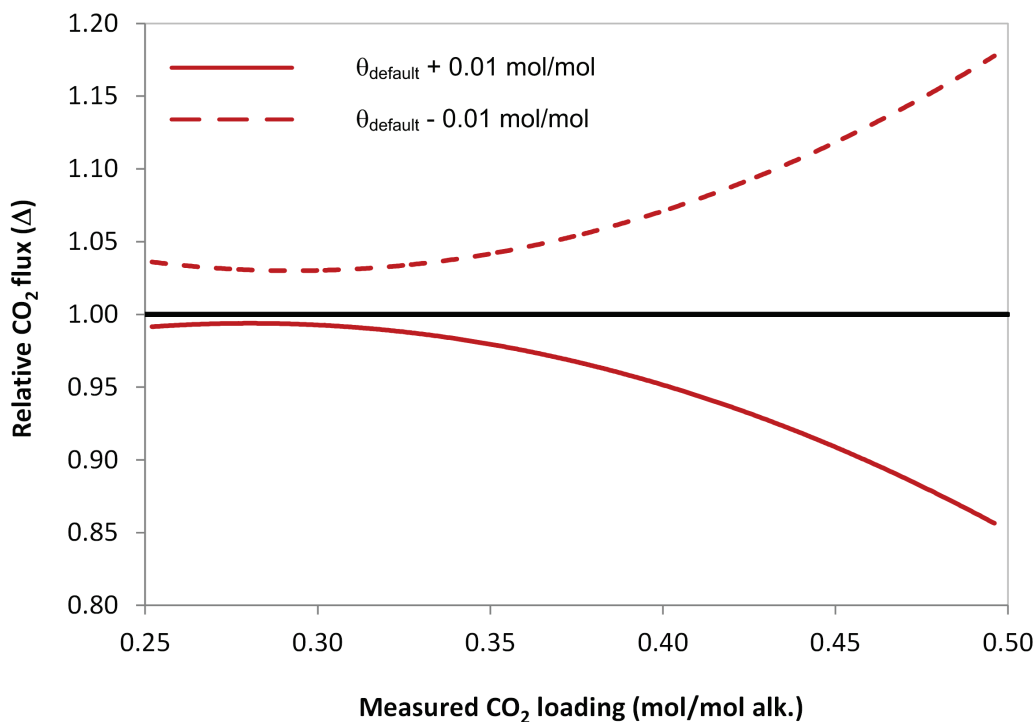
Figure 2.B.2. Effect of CO_2 loading uncertainty on prediction accuracy

It can be concluded that an uncertainty in the value of the diffusion coefficient, the reaction rate constant and the CO_2 loading has a great impact on the calculated CO_2 flux. This uncertainty analysis showed that the expected accuracy range of the calculated CO_2 flux is between 5-20% when assuming an uncertainty limit ±40% of the reaction rate constant or ±25% of the diffusion coefficient respectively a variability of ±0.01 mol/mol of the loading value.

Comparison of model to MEA wetted-wall column measurement

In this section, we compare the wetted-wall column measurements (Dugas, 2009) to the GM model calculations. Previously, the GM model was compared against the numerical solution of the film model using MEA for absorption, desorption and pinch conditions by Gaspar& Fosbøl (2015). It was shown that GM predicts the film model within an accuracy of 2%. The present analysis reveals that the discrepancy between the numerical solution of the two-film model and the GM model are less than 1% for all of the points compared (table 2.B.2). Thus, it is safe to assume that GM and the numerical solution of the two-film model overlap. Note, the correlations are taken off-the-shelf without any additional adjustment

Figure 2.B.3 shows the GM calculated CO_2 flux versus the measured values. It demonstrates that model and experiments agree. The absolute relative deviations (ARD) between the experimental data and GM model predictions are generally less than 20% with a mean absolute relative deviation (MARD) of 22.1%. In

addition, the analysis reveals that there are no visible systematic deviations between model and measurements with respect to temperature.

Figure 2.B.3 shows how the discrepancy between model and experiment is more noticeable at high CO_2 fluxes, above 0.005 mol/m^{2}s and at very low CO_2 fluxes, below 0.0005 mol/m^{2}s. High CO_2 mass transfer rates were recorded at CO_2 loadings above 0.40 mol/mol. Conditions at which a loading uncertainty limit of 0.01 mol/mol produces an accuracy range of 5 – 20% (see figure 2.B.2). Low CO_2 flux measurements correspond to very small CO_2 partial pressures when the model predictions strongly depend on the rate constant (see figure 2.B.1).

It can be concluded that GM accurately predicts the wetted-wall column using the described kinetics for MEA. We expect slightly higher deviations for the PZ solvent due to greater uncertainties of parameters, e.g. diffusion coefficients, rate constant, viscosity correlations as well as the use of a simplified kinetics. In addition, the use of an approximate overall enhancement factor for multiple parallel reactions, eq. (2.42) may be reflected in greater scatter between predictions and experiment.
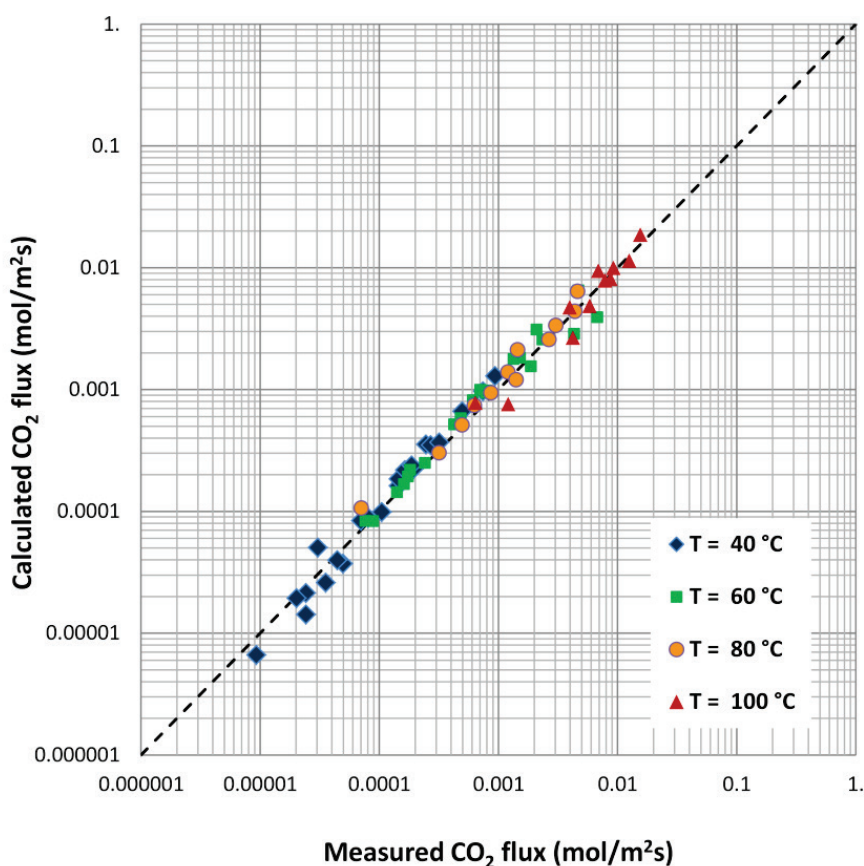

Figure 2.B.3. Predicted versus measured CO_2 flux for 7 molal MEA at different CO_2 loading and temperatures

2.B.4.2 Validation of the GM model for PZ-CO$_2$ capture

This section shows the GM model predictions against wetted wall column measurements for 2, 5 and 8 molal PZ solutions. We implement the GM model and we use the property correlations from table 2.B.1 with the extended UNIQUAC thermodynamic model. Similar to the analysis on MEA, none of the parameters are adjusted to match the experimental data. Our intention is not to determine a new rate constant to match the experiment. Instead an objective evaluation is preferred in order to investigate the expected accuracy of the model for CO$_2$ mass transfer rate calculation.

Figure 2.B.4 to 2.B.6 show the calculated CO$_2$ mass transfer rates versus measurements using 2, 5 and 8 molal PZ at different temperatures. The temperature and CO$_2$ loading range resembles both, absorption and desorption conditions. This figure underlines that the agreement between the GM model and experiment is good. None of the data sets, varying by temperature and amine concentration, show significant deviations from the mean. The absolute relative deviation (ARD) between predictions and measurements generally is less than 20% for 2 and 5 molal PZ and it is less than 25% for 8 molal PZ. The mean absolute relative deviations (MARD) are: 19.32% at 2 molal, 20.28% at 5 molal and 27.84% at 8 molal. This is remarkably considering the range of conditions and the confidence level of the reaction rate constants (Gaspar et al., 2014). Note, the correlations are taken off-the-shelf without any additional adjustment.

Figure 2.B.4 to 2.B.6 demonstrate that CO$_2$ absorption and desorption flux varies with changing temperature and CO$_2$ loading. The fluxes are the smallest at 40°C and 0.24 CO$_2$ loading and they are the largest at 100°C, as expected. It can be seen that the model potentially under-predicts the CO$_2$ flux at 40°C and 0.24 CO$_2$ loading, especially below 0.0001 mol/m^{2}s CO$_2$ flux. At these conditions the system approaches the pseudo-first order regime and the rates are the limiting factors. Figure 2.B.1 outlined that at these conditions, the calculated mass transfer rate strongly depends on the rate constant value. An uncertainty limit of ±40% results in expected errors up to 20%. Figure 2.B.4 to 2.B.6 show that, the model over-predicts the measurements at 100°C using 5 respectively 8 molal PZ, especially above 0.01 mol/m^{2}s when the systems becomes controlled by diffusion and rates are near instantaneous. At these conditions, the mass transfer flux predictions strongly depend on the value of the diffusion coefficient. An uncertainty limit of ±25% in the diffusion coefficient, results in errors up to 15% (figure 2.B.1).These findings are in agreement with the results on MEA, figure 2.B.3. Consequently, the deviations between model and experiment at low and high CO$_2$ fluxes may be due to inaccuracy of the rate constant and the CO$_2$ diffusion coefficient.

The deviations between calculations and measurements are the lowest for the 5 molal solution. The model slightly under-predicts the experiment using 2 molal PZ and slightly over-predicts the CO$_2$ rates at 8 molal. It may be due to the accuracy of the viscosity correlation. The viscosity considerably changes with respect to PZ content and it directly influences the diffusion coefficient.

Other significant difference between the 2 and the 8 molal PZ solutions is the contribution of reaction (2.34) to the overall mass transfer enhancement. Reaction (2.33) is the dominant term but the contribution of (2.34) becomes greater than 30% above 0.30 CO_2 loading. The importance of reaction (2.34) is more noticeable for the 2 molal solution. Therefore, an erroneous rate constant for reaction (2.34) has a greater impact on the mass transfer flux using 2 molal solution compared to 8 molal solution.
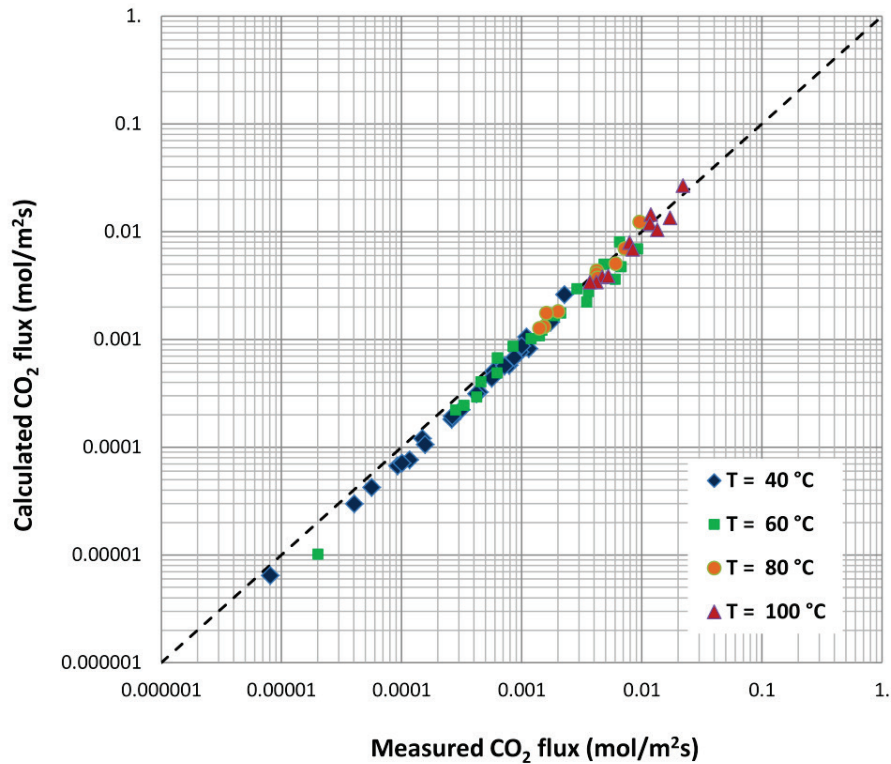

Figure 2.B.4. Predicted versus measured CO_2 flux for 2 molal PZ at different CO_2 loading and temperatures
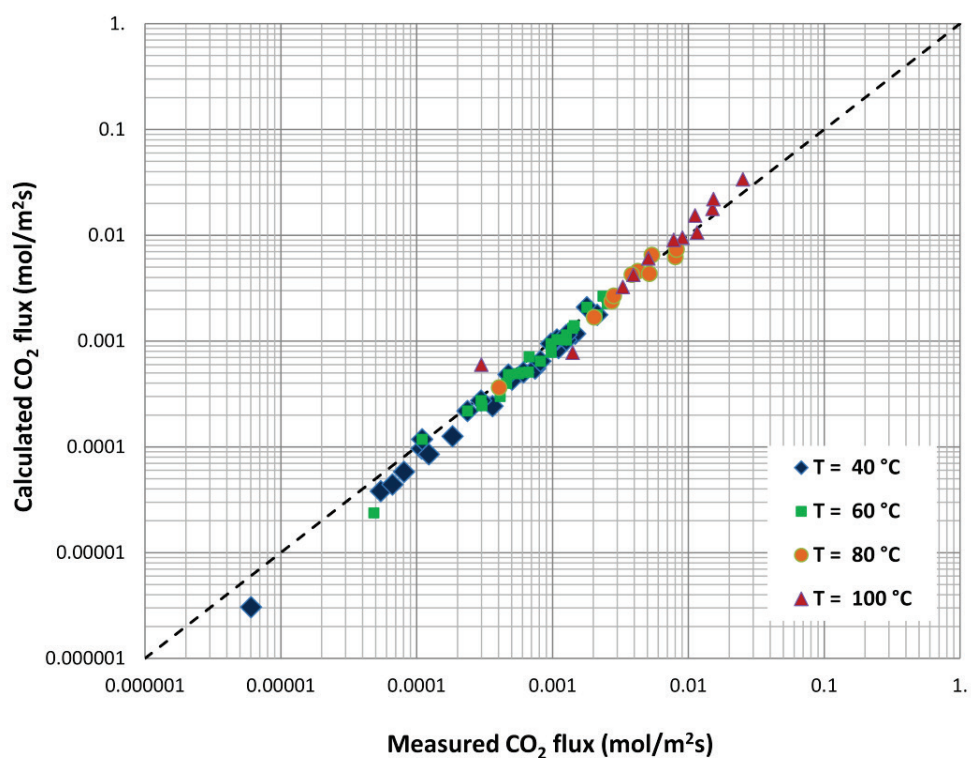
Figure 2.B.5. Predicted versus measured CO_2 flux for 5 molal PZ at different CO_2 loading and temperatures
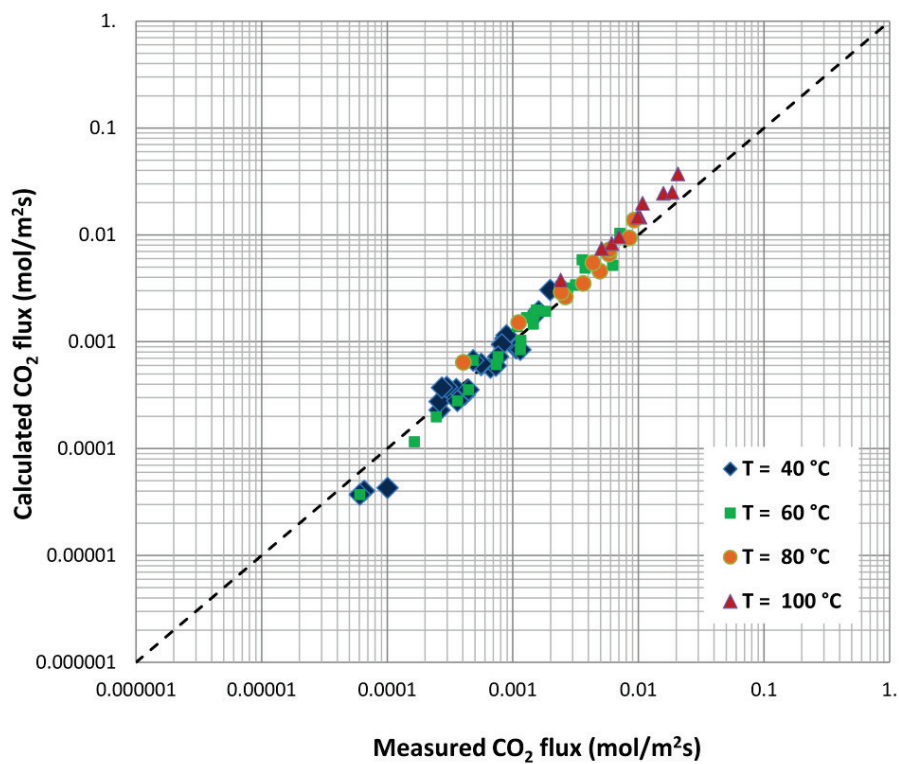

Figure 2.B.6. Predicted versus measured CO_2 flux for 8 molal PZ at different CO_2 loading and temperatures

It can be concluded that the proposed model predicts well the CO_2 absorption and desorption rates for a broad temperature and CO_2 loading range using 2, 5 and 8 molal PZ solutions. The accuracy of the PZ model is comparable with the accuracy of the MEA model, generally within ±20%. We expect that this approach can be applied to other solvents which can be represented as combination of several *(m+n)-th* order reversible reactions, such as amines, blends of amines, and promoted reactions, etc.

2.B.5   Conclusions

A reliable enhancement factor model for interacting and non-interacting multiple parallel reactions was developed and compared to wetted-wall experimental data for 2, 5 and 8 molal PZ respectively 30 wt.% MEA solutions. This model simplifies the two-film mass transfer model, reducing it to a system of algebraic equations. It uses the GM enhancement factor model (Gaspar& Fosbøl, 2015) to calculate the mass transfer rate enhancement of the individual reactions and proposes the distribution of the CO_2 reaction rates between the parallel reactions, i.e. reaction of CO_2 and PZ respectively CO_2 and PZCOO-, as function of their equilibrium constant. Furthermore, this work demonstrated that the zwitterion kinetics accurately describes the reaction mechanisms between CO_2 and PZ respectively CO_2 and MEA. The wetted-wall measurements generally are predicted within an accuracy of 20% when including the formation of the carbamate and bicarbamate ions for the PZ solvent and the formation of the carbamate ion for MEA.

The proposed model has been validated against 281 experimental measurements for absorption and desorption conditions: temperatures between 40°C and 100°C and CO_2 loadings between 0.23 and 0.5 mol/mol alkalinity using PZ and MEA (Dugas, 2009). The analysis showed the good agreement between model predictions and measurements. The relative deviations between model and experiment generally are within ±20% for both solvents. The discrepancy is greater at very high and low CO_2 transfer rates. Moreover, the results showed that the GM model slightly under-predicts the experimental data for the 2 molal solvent and it slightly over-predicts for the 8 molal solvent. The best fit was seen for the 5 molal PZ respectively 7 molal MEA solutions. Overall the agreement is good, considering the range of the conditions and accounting uncertainties related to the rate constants, physical properties as well as the measurement accuracy.

Furthermore, we analysed the model uncertainty with respect to the accuracy of the CO_2 diffusion coefficient, the reaction rate constant and the CO_2 bulk concentration. This analysis showed that the expected accuracy of approximate enhancement factor models is within ±20% assuming and uncertainty limit of ±25% of the diffusion coefficient, ±40% of the rate constant and a confidence interval of ±0.01 mol/mol in the CO_2 loading value. This analysis outlined that the uncertainty of the model prediction exponentially increases above a CO_2 loading of 0.35. Furthermore, this analysis showed that at CO_2 partial pressures below 5 kPa, a ±40% uncertainty of the reaction rate constant translates to a model accuracy of 10–15%. On the other hand, at higher CO_2 partial pressures, the certainty of the diffusion coefficient correlation dominates the accuracy

of the model prediction. A ±25% uncertainty limit of the CO_2 diffusion coefficient results in an expected accuracy of 15–20%.

In this work we demonstrated that GM works well for MEA and PZ but we expect that it applies to other single and parallel reactions which can be approximated with multiple *(m+n)-th* order reversible reactions, e.g. reaction of CO_2 with blends of amines, promoted amines, etc.

References

Al-Juaied, A., Mohammed (2004). Carbon Dioxide Removal from Natural Gas by Membranes in the Presence of Heavy Hydrocarbons and by Aqueous Diglycolamine®/Morpholine.

Astarita, G., & Savage, D. W. (1980). Gas-Absorption and Desorption with Reversible Instantaneous Chemical-Reaction. *Chemical Engineering Science, 35*, 1755-1764.

Billet, R., & Schultes, M. (1999). Prediction of mass transfer columns with dumped and arranged packings - Updated summary of the calculation method of Billet and Schultes. *Chemical Engineering Research & Design, 77*, 498-504.

Chang, C. S., & Rochelle, G. T. (1982). Mass-Transfer Enhanced by Equilibrium Reactions. *Industrial & Engineering Chemistry Fundamentals, 21*, 379-385.

Cheng, S., Meisen, A., & Chakma, A. (1996). Predict amine solution properties accurately. *Hydrocarbon Processing, Hydrocarbon Process, 75*, 81-84.

Decoursey, W. J., & Thring, R. W. (1989). Effects of Unequal Diffusivities on Enhancement Factors for Reversible and Irreversible Reaction. *Chemical Engineering Science, 44*, 1715-1721.

Derks, P. W. J., Kleingeld, T., van Aken, C., Hogendoom, J. A., & Versteeg, G. F. (2006). Kinetics of absorption of carbon dioxide in aqueous piperazine solutions. *Chemical Engineering Science, 61*, 6837-6854.

Dugas, R. E. (2009, December). Carbon Dioxide Absorption, Desorption and Diffusion in Aqueous Piperazine and Monoethanolamine. *, University of Texas at Austin*.

Dugas, R. E., & Rochelle, G. T. (2011). Modeling CO2 absorption into concentrated aqueous monoethanolamine and piperazine. *Chemical Engineering Science, 66*, 5212-5218.

Fosbøl, P. L., Maribo-Mogensen, B., & Thomsen, K. (2013). Solids Modelling and Capture Simulation of Piperazine in Potassium Solvents. *Energy Procedia, 37*, 844-859.

Freguia, S., & Rochelle, G. T. (2003). Modeling of CO2 capture by aqueous monoethanolamine. *AIChE Journal, 49*, 1676-1686.

Gaspar, J., & Fosbøl, P. L. (2015). A general enhancement factor model for absorption and desorption systems: A CO2 capture case-study. *Chemical Engineering Science, 138*, 203-215.

Gaspar, J., Gladis, A., Jørgensen, J. B., von Solms, N., Thomsen, K., & Fosbøl, P. L. (2015). Dynamic Operation and Simulation of Post-Combustion CO2 Capture. *Energy Procedia, Proceddings of the 8th Trondheim Conference on Capture, Transport and Storage (TCCS8)*.

Gaspar, J., Thomsen, K., von Solms, N., & Fosbøl, P. L. (2014). Solid Formation in Piperazine Rate-based Simulation. *Energy Procedia, 63*, 1074-1083.

Glasscock, D. A., & Rochelle, G. T. (1989). Numerical-Simulation of Theories for Gas-Absorption with Chemical-Reaction. *AIChE Journal, 35*, 1271-1281.

Hikita, H., & Asai, S. (1964). Gas absorption with (m,n)-th-order irreversible chemical reaction. *International Journal of Chemical Engineering, 4*, 332-340.

Puxty, G., Rowland, R., Allport, A., Yang, Q., Bown, M., Burns, R., Maeder, M., & Attalla, M. (2009). Carbon Dioxide Postcombustion Capture: A Novel Screening Study of the Carbon Dioxide Absorption Performance of 76 Amines. *Environmental science & technology, 43*, 6427-6433.

Rocha, J. A., Bravo, J. L., & Fair, J. R. (1996). Distillation columns containing structured packings: A comprehensive model for their performance .2. Mass-transfer model. *Industrial & Engineering Chemistry Research, 35*, 1660-1667.

Rochelle, G., Chen, E., Freeman, S., Van Wagener, D., Xu, Q., & Voice, A. (2011). Aqueous piperazine as the new standard for CO2 capture technology. *Chemical Engineering Journal, 171*, 725-733.

Snijder, E. D., te Riele, J. M., Versteeg, G. F., & van Swaaji, W. P. M. (1993). Diffusion coefficients of several aqueous alkanolamine solutions. *Journal of Chemical and Engineering Data, 38*, 475-480.

Thomsen, K., & Rasmussen, P. (1999). Modeling of vapor–liquid–solid equilibrium in gas–aqueous electrolyte systems. *Chemical Engineering Science, 54*, 1787-1802.

Thomsen, K., Rasmussen, P., & Gani, R. (1996). Correlation and prediction of thermal properties and phase behaviour for a class of aqueous electrolyte systems. *Chemical Engineering Science, 51*, 3675-3683.

van Krevelen, D. W., & Hoftijzer, P. J. (1948). Kinetics of gas-liquid reactions - I. General theory. *Recueil, 67*, 563-586.

Vanswaaij, W. P. M., & Versteeg, G. F. (1992). Mass-Transfer Accompanied with Complex Reversible Chemical-Reactions in Gas-Liquid Systems - an Overview. *Chemical Engineering Science, 47*, 3181-3195.

Versteeg, G. F., Van Dijck, L. A. J., & Van Swaaij, W. P. M. (1996). On the kinetics between CO2 and alkanolamines both in aqueous and non-aqueous solutions. An overview. *Chemical Engineering Communications, 144*, 113-158.

Weiland, R. H., Dingman, J. C., Cronin, D. B., & Browning, G. J. (1998). Density and viscosity of some partially carbonated aqueous alkanolamine solutions and their blends. *Journal of Chemical and Engineering Data, 43*, 378-382.

Part C. General Method (GM) applied to Carbonic Anhydrase enhanced MDEA (CA/MDEA)

2.C.1 Introduction

Aqueous amine solution based reactive absorption is the state-of-the-art technology for CO_2 post-combustion capture. Especially primary and secondary amines showed potential for this technology at industrial scale due to their fast reaction with CO_2 compared to tertiary amines. However, an advantage of tertiary amines is their significantly lower regeneration energy demand compared to primary and secondary amines. Primary and secondary amines require smaller absorption towers while tertiary amines assure lower stripping energy demand. As a result, various blends of primary/secondary amines and tertiary amines have been proposed in recent years to combine their advantages: fast reaction and lower heat of desorption. An example is the blend of MDEA and MEA or MDEA and PZ. In these blends, MEA respectively PZ do not act only as promoter but they form stable carbamates, thus significantly increasing the regeneration energy requirement of the blend compared to MDEA.

A newly emerging alternative for CO_2 post-combustion capture is the use of biocatalyst (enzyme) carbonic anhydrase (CA) to increase the CO_2 absorption rate. Enzymes promoted tertiary amines appear to be the ideal solution for CO_2 capture, being the combination of fast absorption and low regeneration energy. Enzymes act as real biocatalyst assuring fast CO_2 absorption (smaller absorption tower) and they do not alter the positively low heat of stripping of tertiary amines (lower regeneration energy demand).

Alper and Deckwer (1980) were one of the first to investigate the effect of carbonic anhydrase on CO_2 absorption kinetics in a continuous stirred tank reactor and a wetted wall column using different buffer solvents, i.e. KH_2PO_4 + Na_2HPO_4, Na_2HPO_4 + Na_3PO_4 and $NaHCO_3$ + Na_2CO_3. They observed a linear dependency between enzymatic CO_2 hydration reaction rate and enzyme concentration and a first order reaction regime with respect to CO_2. They also showed that decreasing the pH to 6.6 significantly decreases the activity of the enzyme. Later, Vinoba et al., (2013) compared CO_2 absorption rates using alkanolamine solutions (MEA, DEA, MDEA and AMP) of 5 wt.% respectively 10 wt.% with and without enzyme at temperatures ranging from 10 to 60 °C. They concluded that MDEA presents the greatest absorption enhancement with enzyme, followed by AMP, DEA and MEA. Moreover, they illustrated that the absorption rate decreases with respect to temperature when using AMP, DEA and MEA solutions and it rises up to 40°C and then decreases at higher temperatures using MDEA as solvent.

Similar approach was adopted by Penders-van Elk et al., (2016, 2015, 2013, 2012). They experimentally confirmed that carbonic anhydrase significantly enhances the absorption of CO_2 in aqueous alkanolamine

solutions. Penders-van Elk et al. (2012) outlined that when enzyme is present in an MDEA solution, the concentration of MDEA does not noticeably influence the absorption rate of CO_2. Practically, the enzyme accelerates the reaction of CO_2 with water and does not enhance the reaction between CO_2 and MDEA. Furthermore, Penders-van Elk et al., (2013) investigated the effect of enzyme concentration respectively temperature on the absorption rate. They showed that at low enzyme concentration the absorption rate linearly increases with respect to enzyme concentration, while at higher enzyme concentrations it deviates from linear dependency. They described the effect of enzyme on the reaction rate by an enzyme concentration and temperature dependent Langmuir-Hinshelwood type empirical expression for the reaction rate constant. In addition, they showed that temperature weakly influences the overall absorption rate; however the reaction rate constant of the enzyme catalysed reaction decreases with increasing temperature. Penders-van Elk et al. (2013) suggested that this behaviour may be due to instantaneous deactivation of the enzyme.

In a recent study, Kunze et al., (2015) investigated the capacity of a biocatalyst carbonic anhydrase (CA) to increase the CO_2 absorption rate when combined with different solvents: 30 wt.% MEA, 30 wt.% MDEA, 30 wt.% DEEA and 10 wt.% K_2CO_3. They showed that MDEA and K_2CO_3 are promising solvents for use with CA biocatalyst/enzyme. The addition of 0.2 wt.% CA increased the CO_2 absorption flux by a factor greater than 4. They also showed the technical feasibility of the enzyme enhanced solvent concept in a pilot scale packed column. The agreement between the laboratory scale and the pilot scale experiments was deemed satisfactory and no undesired effects of foaming, aggregation or clogging was observed during these experiments. Moreover, they determined mass transfer parameters using wetted-wall column measurements. In this study, the reaction mechanism of CA with CO_2 is considered a black box, assuming that CA exclusively accelerates the reaction between CO_2 and H_2O. They proposed to include the influence of enzyme on the reaction kinetics in a pseudo-first order reaction rate constant.

Most of the research and development involving enzymes in CO_2 capture processes have focused on discovery of robust enzymes, protein engineering for better stability and investigation of the enzyme accelerated reaction kinetics (Kunze et al., 2015; Li et al., 2013; Penders-van Elk et al., 2015; Sharma et al., 2011; Ye and Lu, 2014; Yong et al., 2015; Zhang et al., 2011). The next logical step is to develop an accurate and easy-to-implement mass transfer model. Such a model is essential to develop, optimize and scale-up a carbonic anhydrase accelerated CO_2 capture process.

Accordingly, this subsection demonstrates the General Method (GM) enhancement factor model for the CA-enzyme enhanced MDEA system (CA/MDEA). The proposed model accounts for two parallel reactions: the reaction between CO_2 and MDEA and the enzyme catalysed hydration of CO_2. The GM model predictions are compared against wetted-wall column experimental data using MDEA and CA enhanced MDEA

solvents. The experiments cover a broad range of operating conditions: 15 to 50 wt.% MDEA, 0 to 0.57 mol/mol CO_2 loading and temperatures between 25 and 55 ºC.

2.C.2   Reaction kinetics

Tertiary amines such as MDEA cannot react directly with CO_2 contrary to primary and secondary amines. Primary and secondary amines form carbamate when reacting with CO_2 while tertiary amines (MDEA) react with CO_2 through base catalysis of the CO_2 hydration reaction:

$$CO_2 + MDEA : H_2O \underset{}{\overset{k_{MDEA}}{\rightleftharpoons}} HCO_3^- + MDEAH^+ \tag{2.44}$$
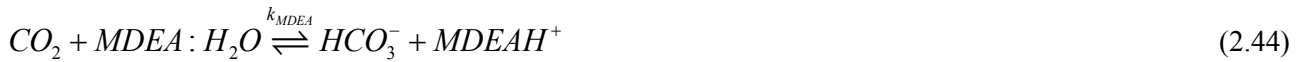
The reaction between CO_2 and MDEA is overall second order and it is first order with respect to reactants (Penders-van Elk et al., 2013). The concentration of H_2O can be assumed constant since its concentration is much greater than the concentration of CO_2 and MDEA; therefore the kinetic rate expression is: $R_{MDEA} = k_{MDEA} C_{MDEA} C_{CO_2}$. The reaction rate constant, k_{MDEA} originates from Versteeg et al. (1996):

$$k_{MDEA} = 3.82 \cdot 10^5 \cdot \exp\left(-\frac{5080}{T(K)}\right) \frac{mol}{m^3 s} \tag{2.45}$$

Additionally, CO_2 reacts with hydroxide ion and water. Based on the reaction rate constants respectively hydroxide ion concentration in MDEA solution, these reactions are negligible compare to reaction (2.44) (Kunze et al., 2015; Penders-van Elk et al., 2012; Pinsent et al., 1956). As a result, the overall reaction rate for CO_2 absorption in MDEA is fully determined by the rate of reaction (2.44).

Carbonic anhydrase (CA) is a very efficient catalyst. It accelerates the formation of bicarbonate ion and the release of a proton by converting water to active hydroxyl ion. Penders-van Elk et al. (2012) showed that CA enhances the reaction of carbon dioxide with water and it does not enhance the reaction of CO_2 with MDEA. Thus, the complex mechanism of enzyme catalysed CO_2 absorption practically can be accounted for by reaction (2.46). The complete reaction mechanism and set of reactions can be found in Astarita et al. (1981), Monteiro et al. (2015) and Penders-van Elk et al. (2012).

$$CO_2 + 2H_2O : CA \underset{}{\overset{k_{CA}}{\rightleftharpoons}} HCO_3^- + H_3O^+ \tag{2.46}$$

The reaction rate of carbonic anhydrase catalysed CO_2 hydration reaction can be expressed by Michaelis-Menten kinetics:

$$R_{H_2O:CA} = \frac{k_{cat}}{K_M + C_{CO_2}} C_{CA} C_{CO_2} C_{H_2O} \tag{2.47}$$

where the Michaelis-Menten constant K_M (mol·m⁻³) shows the CO_2 concentration, C_{CO2}, (mol·m⁻³) at which the enzyme reaction rate is halved. k_{cat} is the so-called turnover number and C_{CA} is the concentration of the enzyme (mol·m⁻³). Since the CO_2 concentration is usually very low at absorption conditions compared to the Michaelis Menten constant (Penders-van Elk et al., 2012; Pierre, 2012), eq. (2.47) can be further simplified using a k_{enz} (m³·mol⁻¹·s⁻¹) instead of the Michaelis Menten description. This simplification leads to:

$$R_{H_2O:CA} = k_{enz} C_{CA} C_{CO_2} C_{H_2O} = k_{enz}^{app} C_{CO_2} C_{H_2O} \tag{2.48}$$

Based on the work of Gladis et al. (2015), in this work we use the empirical expression (2.49) for the enzyme reaction rate constant.

$$k_{enz}^{app} = \frac{k_{CA,1}}{1 + \dfrac{C_{HCO_3^-}}{k_{CA,2}}} C_{CA} \tag{2.49}$$

where $k_{CA,1}$ respectively $k_{CA,2}$ are temperature dependent adjustable parameters and the term $C_{HCO_3^-}/k_{CA,2}$ accounts for the enzyme deactivation by the bicarbonate ion.

In this work, the overall reaction rate is given by the contribution of the parallel reactions (2.44) and (2.46) which are overall second order and first order with respect to reactants.

2.C.3   Mass transfer rate calculation

The model for the CO_2 mass transfer rate calculation in MDEA respectively CA enhanced MDEA is presented in this section. The base for this model is the General Method (GM) enhancement factor model providing the acceleration of CO_2 absorption/desorption rate in reactive systems compared to physical and non-reactive systems. This model includes the reaction between MDEA and CO_2, reaction (2.44) respectively the enzyme promoted hydration reaction of CO_2, reaction (2.46). Thus, it applies to systems with and without enzyme. The model used for CA/MDEA has been successfully applied and validated for calculation of CO_2 mass transfer rate using piperazine in subsection 2B, accounting for two parallel reactions, i.e. formation of the carbamate and bicarbamate ions.

Similar to the model for CO_2 capture in piperazine, we assume that only thermodynamic interaction exists between the two reactions and the acceleration of the mass transfer rate due to each reaction is distributed per

equilibria. Thus, the coupling between the individual reactions is through the underlying thermodynamic model which provides the bulk compositions of the reactants and products. Consequently, the acceleration of the mass transfer rate due to reactions (2.44) and (2.46) is calculated identical to a single reaction-system for each reaction independently. The overall mass transfer intensification is the combined effect of the individual reactions, as shown in eq. (2.50). Note that for MDEA without enzyme, the reaction rate constant, eq. (2.49) reduces to zero and $E_{R_{H_2O:CA}}$ equals 1.

$$E_{overall} = E_{R_{MDEA}} + E_{R_{H_2O:CA}} - 1 \tag{2.50}$$

where $E_{R_{MDEA}}$ and $E_{R_{H_2O:CA}}$ are the enhancement factors for reactions (2.44) and (2.46). These are *(1+1)-th* order reactions where 1 mol of CO_2 reacts with ν_B moles of base B (*B = MDEA:H$_2$O and H$_2$O:CA*). According to the GM model, the enhancement factor for this type of single reaction is the solution of the equations system (2.51) and (2.52).

$$E_{R_i} = Ha_{R_i} \sqrt{y^i_{B,R_i}} \frac{1 - y^*_{CO_2,R_i}}{1 - y^b_{CO_2}} \tag{2.51}$$

$$E_{R_i} = 1 + \left(E^*_{\infty,R_i} - 1\right) \frac{1 - y^i_{B,R_i}}{1 - y^b_{CO_2}} \tag{2.52}$$

where E_{R_i} is the enhancement factor of the *R_i-th* individual reaction: $E_{R_i} = E_{R_{MDEA}}$ respectively $E_{R_i} = E_{R_{H_2O:CA}}$. Equations (2.51) and (2.52) form a system of nonlinear equations with two unknowns, E_{R_i} and y^i_{B,R_i}. Eliminating E_{R_i} leads to a single algebraic equation in y^i_{B,R_i} which can be solved numerically using methods such as the secant method, the Broyden method, the Newton method, etc. The solution methodology is presented in subsection 2A.

The Hatta number (Ha_{R_i}) and instantaneous enhancement factor (E^*_{∞,R_i}) entering equations (2.51) and (2.52) are:

$$Ha_{R_i} = \frac{\sqrt{k_{R_i} C^b_B D_{CO_2}}}{k_L} \tag{2.53}$$

$$E^*_{\infty,R_i} = 1 + \frac{D_B C^b_B}{\nu_B D_{CO_2} C^i_{CO_2}} \tag{2.54}$$

D_B and D_{CO_2} are the diffusion coefficients of B respectively CO_2. C_B^b and $C_{CO_2}^i$ denote the concentration of the base in the liquid bulk respectively the concentration of CO_2 at the gas-liquid interphase; the dimensionless parameter $y_{CO_2}^b = C_{CO_2}^b / C_{CO_2}^i$ is given by the extended UNIQUAC thermodynamic model. In eqs. (2.44) and (2.46), the CO_2 dimensionless compositions which would be in equilibrium with the interface concentration, y_{CO_2,R_i}^* is:

$$y_{CO_2,R_i}^* = y_{CO_2,b} \frac{y_{P_1,R_i} y_{P_2,R_i}}{y_{B,R_i}^{v_B}}$$

(2.55)

where $P1$ and $P2$ refer to reaction products and B is MDEA respectively H_2O:CA. y_{P_1,R_i}^i and y_{P_2,R_i}^i are given by:

$$y_{P_j,R_i}^i = 1 + \frac{D_B C_B^b}{v_B D_{P_j} C_{P_j}^b} \left(1 - y_{B,R_i}^i\right)$$

(2.56)

where $j=1$ and 2. Note, the stoichiometric coefficient of B, v_B equals 1 for reaction (2.44) and v_B equals 2 for reaction (2.46).

The obtained overall enhancement factor, $E_{overall}$, is used to determine the CO_2 mass transfer flux across the gas-liquid interface according to:

$$J_{CO_2,gl} \simeq \frac{1}{1/k_{CO_2}^g + H_{CO_2}/E_{overall}k_{CO_2}^l} \left(p_{CO_2} - p_{CO_2}^*\right)$$

(2.57)

$k_{CO_2}^g$ and $k_{CO_2}^l$ are the partial mass transfer coefficients for the gas side and for the liquid side and H_{CO_2} is the Henry law constant. The overall enhancement factor includes the intensification of the mass transfer rate from reactions (2.44) and (2.46). The driving force for mass transfer is the difference between the partial pressure of CO_2 in the gas phase, p_{CO_2} and the equilibrium partial pressure of CO_2 exerted from the liquid phase, $p_{CO_2}^*$. The gas side and liquid side mass transfer coefficients for the wetted wall column at Technical University of Denmark was determined experimentally by Gladis et al. (2015).

2.C.4 Thermodynamic and physical properties

The extended UNIQUAC thermodynamic model provides the bulk composition of the liquid phase and the equilibrium partial pressure of CO_2 in MDEA respectively CA enhanced MDEA solvents (Thomsen et al., 1996). The adjustable parameters determined for the MDEA-CO_2-H_2O system are used for both solvents,

with and without enzyme (Sadegh et al., 2015). Correlations for diffusion coefficients, density and viscosity of the MDEA-CO_2-H_2O system originate from Glibstrup (2015). Glibstrup (2015) evaluated various experimental datasets and re-fitted the existing correlations to better resemble those data. These correlations determined for the solvent without enzyme were used for the enzyme promoted system. Similar approach was adopted by Kunze et al. (2015). Moreover, Penders-van Elk et al. (2012) performed a N_2O solubility experiment and showed that the physical solubility of CO_2 is not altered by the addition of enzyme. To our knowledge, there are no other studies investigating the influence of enzyme on the properties of amine solutions. Consequently, we assume that enzyme will not alter nor the phase equilibrium neither the physical properties of the system. This seems a reasonable assumption considering that the concentration of the enzyme is very small, up to 1 wt.% CA in this study.

2.C.5 Results and discussions

This section shows the validation of the mass transfer model against wetted-wall column experimental data for MDEA and CA-enzyme enhanced MDEA solutions. The model predictions are compared against a large number of experimental data covering a broad range of CO_2 loadings, between 0 and 0.54 mol CO_2/mol MDEA, at temperatures of 25°C, 40°C and 55°C, for both absorption and desorption of CO_2. The experiments were carried out at different MDEA respectively enzyme concentrations. Table 2.C.1 gives an overview of the experimental conditions for the wetted wall column measurements. The experiments were carried out at Center for Energy Resources Engineering (CERE), Technical University of Denmark by Ph.D. student Arne Gladis (Gladis et al., 2015).

The experimental data was screened for outliers. First, the measurements corresponding to the lowest partial pressure were eliminated since the CO_2 concentration was low, near the detection limit of the concentration probe. Furthermore, the measured CO_2 flux was represented versus the driving force. Generally, the dependency between mass transfer flux and driving force is linear since the experiments were carried out in the pseudo-first order reaction regime. Thus, the points greatly deviating from this line are most probably outliers and they were eliminated. Note that the points deviating from the linear trend presented relative absolute deviations above 100% from the GM calculated values.

Table 2.C.1. Input specifications for the wetted-wall column measurements

Parameter	Unit	MDEA	CA enhanced MDEA
Number of experimental data		80	256
Amine concentration	mol/kg water	4	1, 4, 8
Amine concentration	wt.%	30	15, 30, 55
Enzyme (CA) concentration	mol/m^3	0	0.05, 0.1
CO_2 loading	mol/mol	0 – 0.53	0 – 0.54
Temperature	°C	25, 40, 55	25, 40, 55
Driving force	kPa	-93 – 33	-45 – 30
CO_2 molar flux	mol/m^2s	-0.003 – 0.003	-0.01 – 0.01

2.C.5.1 Validation of the GM model for MDEA-CO_2 capture

This section shows the wetted-wall column measurements using MDEA compared to the GM model calculations. The focus is on verifying the model predictive capacity for CO_2 mass transfer rate with slow reacting solvents (MDEA) for absorption and desorption using off-the-shelf correlations.

Figures 2.C.1 and 2.C.2 show the calculated CO_2 flux as function of measured values at different CO_2 loadings and temperatures of 25ºC, 40ºC and 55ºC. These figures underline that the relative deviations are generally within ±25%, indifferent of loading and temperature. The mean absolute relative deviation (MARD) is 20.1%. Figure 2.C.1 shows that only a few points at 0.03 CO_2 loading are visibly outside of the ±25% accuracy range when the model under-predicts the measured values. A possible explanation is the high susceptibility of CO_2 towards very lean MDEA solution, which may result in additional dissolution of CO_2 from air during sampling and analysis. This leads to under-predicted CO_2 flux. Note that unloaded and very lean solutions are not relevant for the CO_2 capture business. The model slightly under-predicts the experiment at high loadings (≥ 0.36) and temperatures of 40 ºC respectively 55 ºC. The uncertainty analysis in subsection 2A showed the strong dependency between loading and calculation accuracy. A variability of *±0.01* in the CO_2 loading leads to exponential increase of the error with respect to loading. However, more data is needed to representatively evaluate the model behaviour at desorption.
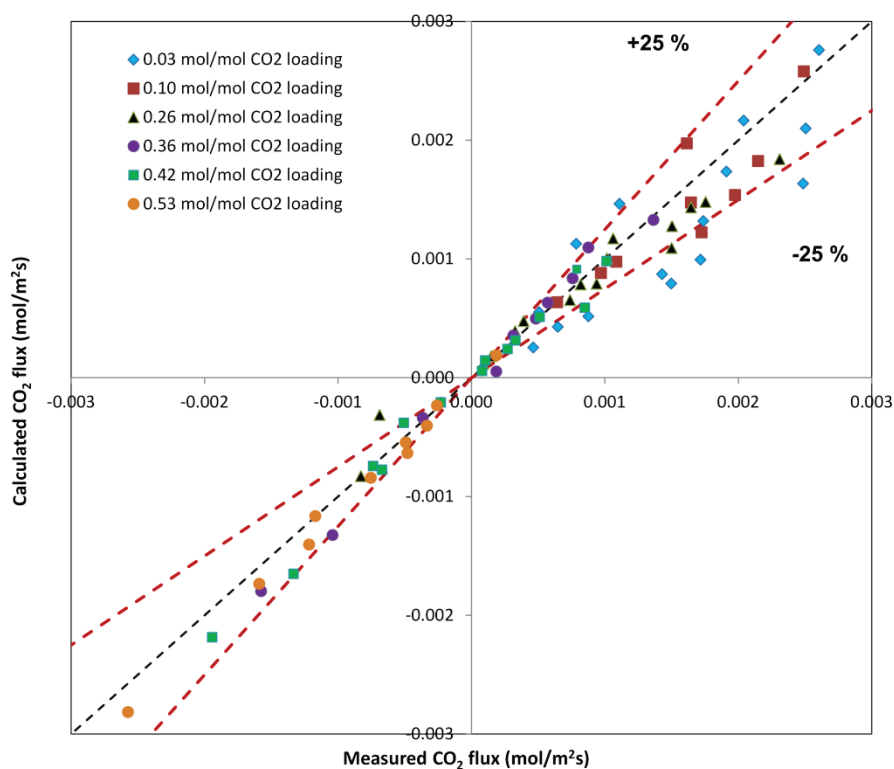
Figure 2.C.1. Predicted versus measured CO_2 flux for 30 wt.% MDEA solution at different CO_2 loadings
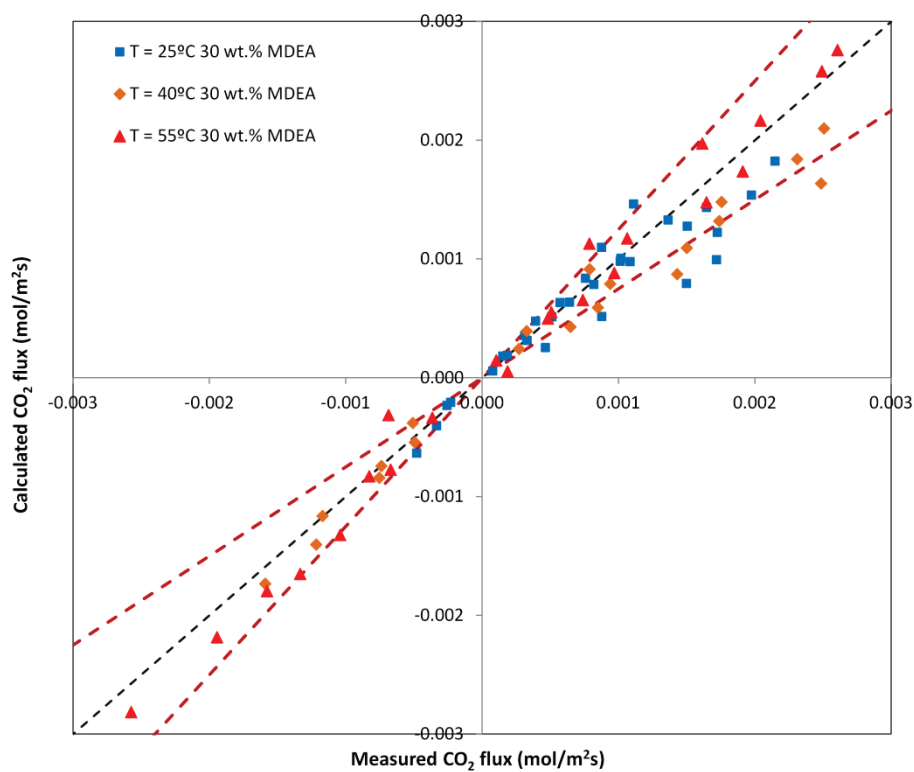

Figure 2.C.2. Predicted versus measured CO_2 flux for 30 wt.% MDEA solution at different temperatures

In summary, it can be concluded that GM accurately predicts CO_2 absorption and desorption rates using the described kinetics for MDEA, reaction (2.44). Figures 2.C.1 and 2.C.2 demonstrate that the deviations between calculations and measurements are not systematic with respect to loading and temperature for absorption conditions. The agreement between model and desorption experiments is deemed satisfactory good; however further experimental investigation is required for CO_2 desorption to have a representative overview of the model's accuracy.

2.C.5.2 Validation of the GM model for CA enhanced MDEA-CO_2 capture

The estimation of the kinetic parameters for the enzyme catalysed CO_2 hydration reaction and the comparison of the GM mass transfer model to experimental data is presented in this section. The mass transfer model includes the reactions (2.44) and (2.46). The accurate calculation of the mass transfer rate is based on physical property correlations reported in the literature and the extended UNIQUAC model. The expression of the reaction rate constant for MDEA originates from literature (Versteeg et al., 1996). Only the adjustable parameters, $k_{CA,1}$ and $k_{CA,2}$ for the reaction rate constant in (2.49) were fitted to match the experimental data.

$k_{CA,1}$ and $k_{CA,2}$ kinetic parameters of eq. (2.49) were fitted simultaneously by minimizing the mean absolute relative deviation (MARD) between the calculated and measured CO_2 transfer rates. Gladis et al. (2015) experimentally showed that temperature only weekly influences the CO_2 mass transfer rate; however the reaction rate constant of the enzyme catalysed reaction decreases with increasing bicarbonate concentration. Moreover, the present study showed that addition of a temperature dependent term in the expression of $k_{CA,1}$ only slightly improves the fit between model and experiment. Subsequently, to avoid fitting of experimental noise and for model simplicity, $k_{CA,1}$ is set to a scalar value, $k_{CA,1} = 5.87 \cdot 10^{-1}$ $(m^3/mol \cdot s)$, while the bicarbonate deactivation parameter is:

$$k_{CA,2} = 2.68 \cdot 10^{-4} \cdot \exp\left(4.62 \cdot 10^{-2} \cdot T(K)\right) \; \left(mol / m^3\right) \tag{2.58}$$

The resulting model with the above kinetic parameters fits the experimental mass transfer rates within ±25% with an MARD of 18.5%. None of the datasets, varying by temperature respectively CO_2, MDEA or enzyme concentration, deviate significantly from the mean. The agreement between the model and experiment is very good, considering the large number of data and the wide range of experimental conditions. This is demonstrated in figures 2.C.3 to 2.C.5.

Furthermore, we investigated the importance of reaction (2.44) for modeling of CO_2 capture using CA enhanced MDEA solvent. This analysis was performed by setting $E_{R_{MDEA}}$ to 1 and simultaneously adjusting

$k_{CA,1}$ and $k_{CA,2}$ to match the experimental data, similar to the above methodology. The resulting kinetic parameters, $k_{CA,1}$ = $9.27 \cdot 10^{-1}$ $(m^3/mol \cdot s)$ and $k_{CA,2} = 0.0026 \cdot \exp\left(3.76 \cdot 10^{-2} \cdot T(K)\right) \left(mol / m^3\right)$, reproduce the experiment with a MARD of 17.5%. The agreement between the model and experiment is similar between the single and multiple reaction approach. These findings suggest that the mass transfer model can be simplified by eliminating the reaction between CO_2 and MDEA but the kinetic parameters should be used only in the investigated range of enzyme and MDEA concentrations. Therefore, in this study we include both of the reactions (2.44) and (2.46), in order to keep the model generally applicable to solutions without enzymes and/or very low enzyme concentrations.

Figure 2.C.3 illustrates the fit between the model and experiment for 30 wt.% MDEA + 0.1% CA solution at different CO_2 loadings. The agreement between the model and experiment is good. Some of the data are a bit under- and some of the data are a bit over-predicted by the model. Only a few point deviates noticeably from the mean at 0.03 and 0.54 CO_2 loadings, similar to the results for MDEA without enzyme (figure 2.C.1). However, the error is not systematic with respect to loading. Figure 2.C.4 demonstrates the good agreement between GM and wetted wall data using 30 wt.% MDEA and different enzyme concentrations (0.05% respectively 0.1% CA) for temperatures of 25ºC, 40ºC and 55ºC. The agreement between model and experiment is as expected, within the ±25% for both, absorption and desorption. Only a few points deviate visibly from the mean, although the deviations are not systematic with respect to temperature or enzyme concentration. It suggests that these points are outliers. Figures 2.C.3 and 2.C.4 show that GM describes well the effect of CO_2 loading, temperature and enzyme concentration on CO_2 mass transfer rate.
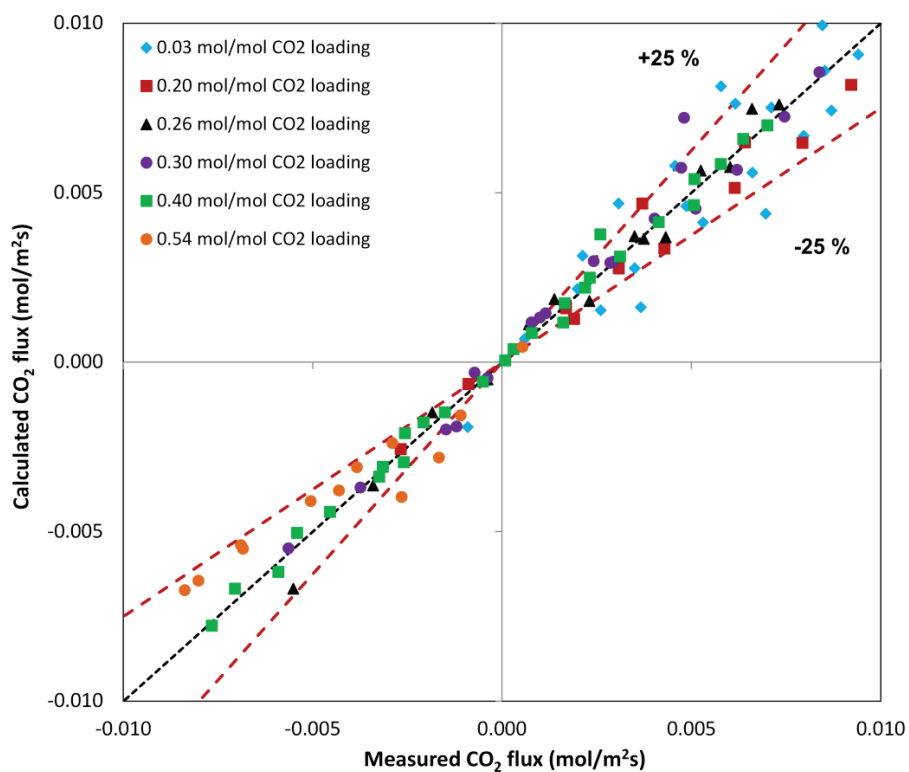
Figure 2.C.3. Predicted versus measured CO_2 flux using 30 wt.% MDEA + 0.1% CA at different loadings
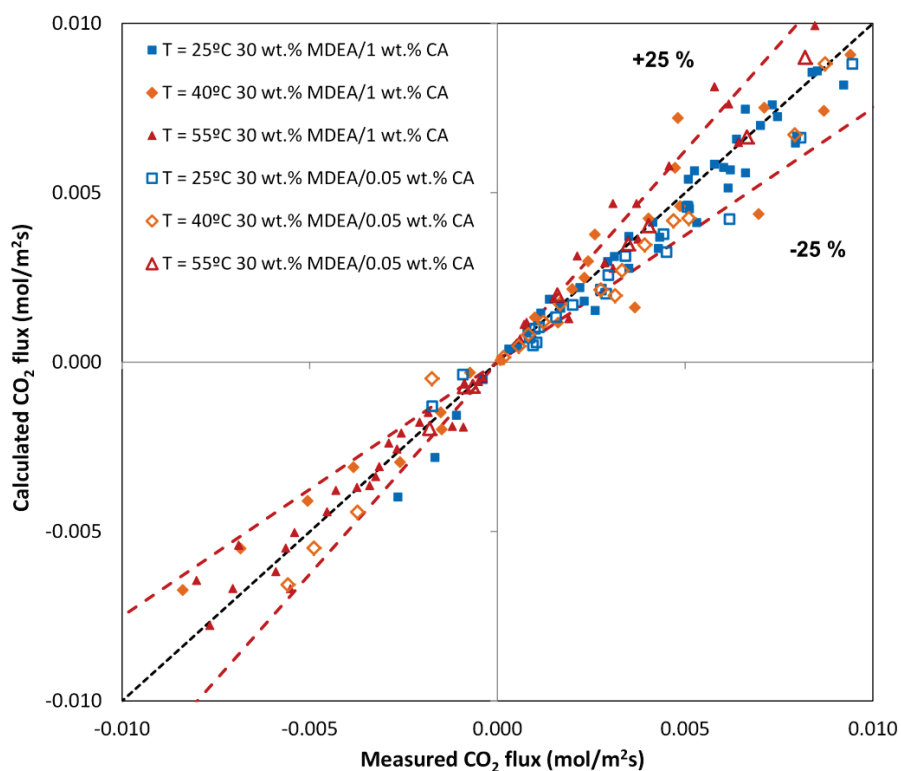
Figure 2.C.4. Predicted versus measured CO_2 flux using 30 wt.% MDEA + 0.05 and 0.1% CA at different temperatures

Figure 2.C.5 shows calculated versus measured mass transfer rates at different MDEA concentrations and 0.05% CA enzyme concentration. This is a logarithmic-scale plot; subsequently the absolute of the negative (desorption) mass transfer rates is represented. This figure demonstrates the good agreement between model and experiment. The MARD is 17.9% with absolute deviations generally less than 25%. Only 6 points deviate noticeably from the mean. They correspond to different CO_2 loadings and temperatures and for absorption respectively desorption. Thus, the model accounts for the effect of MDEA concentration on the mass transfer rate and the deviations are not systematic with respect to MDEA concentration.
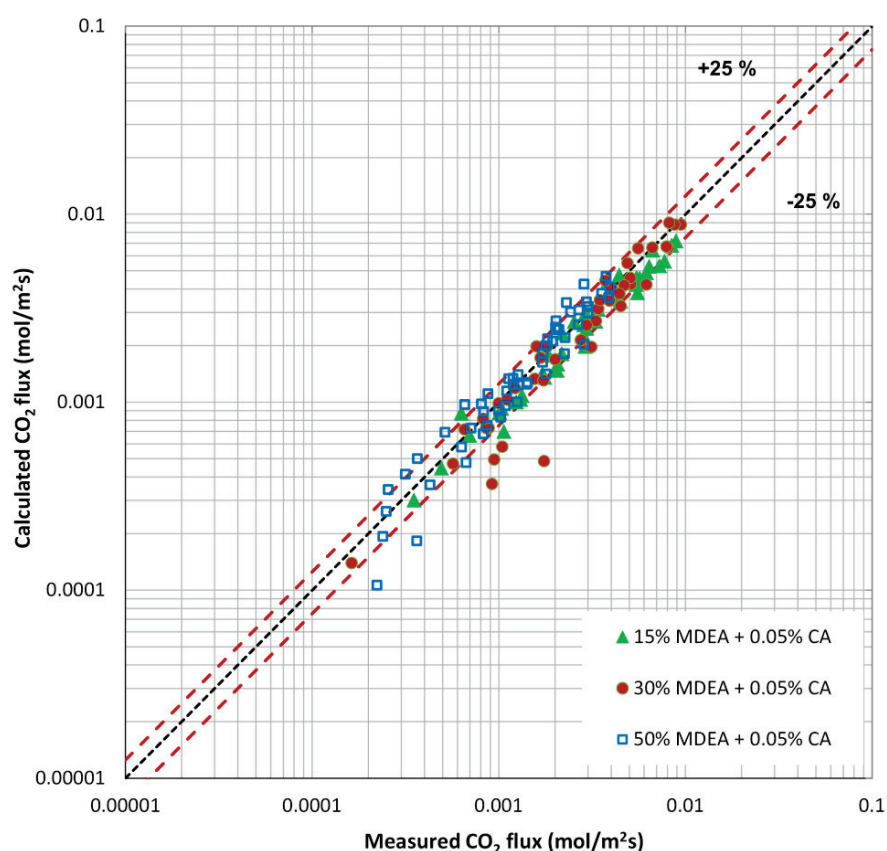
Figure 2.C.5. Predicted versus measured CO_2 flux for 15, 30 and 50 wt.% MDEA + 0.05% CA solutions

Based on these findings, it can be concluded that the simplified Michaelis Menten kinetics represents adequately the CA enhanced MDEA system in the investigated enzyme and CO_2 concentration range. The agreement between model and experiment is satisfactory, without systematic deviations with respect to loading, temperature, MDEA concentration or enzyme concentration.

2.C.6 Conclusions

An accurate mass transfer calculation approach based on the General Method (GM) enhancement factor model has been applied for calculation of CO_2 absorption and desorption rates in a wetted-wall column using MDEA and carbonic anhydrase (CA) enhanced MDEA solvents. This model reduces the differential equations system of the two-film mass transfer model to a set of algebraic non-linear equations. It includes two parallel reactions: (1) the reaction between CO_2 and MDEA and (2) the CA catalysed CO_2 hydration reaction. The distribution of CO_2 reaction rates between the two reactions is as function of their equilibrium constant. This approach has been verified for piperazine in subsection 2B.

The developed model has been compared to a large number of wetted-wall column measurements for both, CO_2 absorption and desorption. The experiments are predicted generally within an accuracy of ±25% with a mean absolute relative deviation (MARD) of 20.1% for MDEA respectively 18.5% for CA enhanced MDEA systems. This study showed that the simplified Michaelis Menten expression (2.49) with $k_{CA,1}$ and $k_{CA,2}$ adjustable kinetic parameters accurately predicts the CO_2 mass transfer rate using CA enhanced MDEA as solvent. This model uses off-the-shell correlations for physical properties in combination with the extended UNIQUAC thermodynamic model. The model calculations using MDEA as solvent are pure predictions using the second order reaction-rate constant from Versteeg et al. (1996).

Here, we demonstrated that GM works well for CA enhanced MDEA but we expect that it applies to other enzyme catalysed systems such as K_2CO_3 which can be approximated with multiple *(m+n)-th* order reversible reactions.

References

Alper, E., Deckwer, W.-D., 1980. Kinetics of absorption of CO2 into buffer solutions containing carbonic anhydrase. Chem. Eng. Sci. 35, 549–557. doi:10.1016/0009-2509(80)80003-0

Astarita, G., Savage, D.W., Longo, J.M., 1981. Promotion of Co2 Mass-Transfer in Carbonate Solutions. Chem. Eng. Sci. 36, 581–588. doi:10.1016/0009-2509(82)80025-0

Gladis, A., Gundersen, M.T., Fosbøl, P.L., Woodley, J.M., von Solms, N., 2015. Carbon dioxide absorption rate intensification by carbonic anhydrase for different solvent types. 3rd Post-Combustion Capture Conf.

Glibstrup, J., 2015. Enzymes promoted rate-based amine CO2 capture model development and simulation.

Kunze, A.-K., Dojchinov, G., Haritos, V.S., Lutze, P., 2015. Reactive absorption of CO2 into enzyme accelerated solvents: From laboratory to pilot scale. Appl. Energy 156, 676–685. doi:10.1016/j.apenergy.2015.07.033

Li, B., Duan, Y., Luebke, D., Morreale, B., 2013. Advances in CO2 capture technology: A patent review. Appl. Energy 102, 1439–1447. doi:10.1016/j.apenergy.2012.09.009

Monteiro, J.G.M.-S., Knuutila, H., Penders-van Elk, N.J.M.C., Versteeg, G., Svendsen, H.F., 2015. Kinetics of CO2 absorption by aqueous N,N-diethylethanolamine solutions: Literature review, experimental results and modelling. Chem. Eng. Sci. 127, 1–12. doi:10.1016/j.ces.2014.12.061

Penders-van Elk, N.J.M.C., Derks, P.W.J., Fradette, S., Versteeg, G.F., 2012. Kinetics of absorption of carbon dioxide in aqueous MDEA solutions with carbonic anhydrase at 298K. Int. J. Greenh. Gas Control 9, 385–392. doi:10.1016/j.ijggc.2012.04.008

Penders-van Elk, N.J.M.C., Fradette, S., Versteeg, G.F., 2015. Effect of pKa on the kinetics of carbon dioxide absorption in aqueous alkanolamine solutions containing carbonic anhydrase at 298K. Chem. Eng. J. 259, 682–691. doi:10.1016/j.cej.2014.08.001

Penders-van Elk, N.J.M.C., van Aken, C., Versteeg, G.F., 2016. Influence of temperature on the kinetics of enzyme catalysed absorption of carbon dioxide in aqueous MDEA solutions. Int. J. Greenh. Gas Control 49, 64–72. doi:10.1016/j.ijggc.2016.02.021

Penders-van Elk, N.J.M.C.M.C., Hamborg, E.S., Huttenhuis, P.J.G.G., Fradette, S., Carley, J.A., Versteeg, G.F., 2013. Kinetics of absorption of carbon dioxide in aqueous amine and carbonate solutions with carbonic anhydrase. Int. J. Greenh. Gas Control 12, 259–268. doi:10.1016/j.ijggc.2012.10.016

Pierre, A.C., 2012. Enzymatic Carbon Dioxide Capture. ISRN Chem. Eng. 2012, 1–22. doi:10.5402/2012/753687

Pinsent, B.R.W., PEARSON, L., ROUGHTON, F.J.W., 1956. The Kinetics of Combination of Carbon Dioxide with Hydroxide Ions. Trans. Faraday Soc. 52, 1512–1520. doi:10.1039/tf9565201512

Sadegh, N., Stenby, E.H., Thomsen, K., 2015. Thermodynamic modeling of CO2 absorption in aqueous N-Methyldiethanolamine using Extended UNIQUAC model. Fuel 144, 295–306. doi:10.1016/j.fuel.2014.12.002

Sharma, A., Bhattacharya, A., Shrivastava, A., 2011. Biomimetic CO_2 sequestration using purified carbonic anhydrase from indigenous bacterial strains immobilized on biopolymeric materials. Enzyme Microb. Technol. 48, 416–26. doi:10.1016/j.enzmictec.2011.02.001

Thomsen, K., Rasmussen, P., Gani, R., 1996. Correlation and prediction of thermal properties and phase behaviour for a class of aqueous electrolyte systems. Chem. Eng. Sci. 51, 3675–3683. doi:http://dx.doi.org/10.1016/0009-2509(95)00418-1

Versteeg, G.F., Van Dijck, L.A.J., Van Swaaij, W.P.M., 1996. On the kinetics between CO2 and alkanolamines both in aqueous and non-aqueous solutions. An overview. Chem. Eng. Commun. 144, 113–158. doi:10.1080/00986449608936450

Vinoba, M., Bhagiyalakshmi, M., Grace, A.N., Kim, D.H., Yoon, Y., Nam, S.C., Baek, I.H., Jeong, S.K., 2013. Carbonic anhydrase promotes the absorption rate of CO2 in post-combustion processes. J. Phys. Chem. B 117, 5683–5690. doi:10.1021/jp401622c

Ye, X., Lu, Y., 2014. CO2 absorption into catalyzed potassium carbonate–bicarbonate solutions: Kinetics and stability of the enzyme carbonic anhydrase as a biocatalyst. Chem. Eng. Sci. 116, 567–575. doi:10.1016/j.ces.2014.05.040

Yong, J.K.J., Stevens, G.W., Caruso, F., Kentish, S.E., 2015. The use of carbonic anhydrase to accelerate carbon dioxide capture processes. J. Chem. Technol. Biotechnol. 90, 3–10. doi:10.1002/jctb.4502

Zhang, S., Zhang, Z., Lu, Y., Rostam-Abadi, M., Jones, A., 2011. Activity and stability of immobilized carbonic anhydrase for promoting CO2 absorption into a carbonate solution for post-combustion CO2 capture. Bioresour. Technol. 102, 10194–201. doi:10.1016/j.biortech.2011.09.043

Chapter 3. Steady-state rate-based model for CO_2 absorption and desorption

3.1 Introduction

This chapter presents the developed steady-state rate-based model for CO_2 absorption and desorption. The developed model is applied to piperazine (PZ), piperazine promoted potassium-carbonate (PZ/K_2CO_3), carbonic anhydrase enhanced methyl-di-ethanol-amine (CA/MDEA) and the benchmark monoethanol-amine (MEA). Additionally, the CAPE-OPEN and the Aspen Custom Modeler (ACM) interfaces are implemented to connect the CO_2 capture model to Aspen Plus process simulator. The developed rate-based model is validated against several experimental dataset for absorption and desorption and the complete Aspen Plus CO_2 post-combustion process model is compared to pilot measurements to investigate the accuracy of the plant-wide model. Simulation and validation of the individual absorber/desorber model and of the plant-wide post-combustion capture model is essential to increase confidence in computer aided process design and optimization, and to understand the interactions between various units.

3.1.1 Review of rate-based models for CO_2 absorption and desorption

Solvent based CO_2 post-combustion capture is the technology of choice for exhaust gas cleaning. Numerous studies appeared in the last two decades on modelling and simulation of this process, especially using the benchmark MEA solvent. The most relevant developments in modelling of CO_2 absorption and desorption without aiming to discuss all of the published models are summarized in this section.

The complexity and accuracy of the developed CO_2 capture models mainly depend on the approach used for determining the CO_2 mass transfer flux across the gas-liquid interface and on the complexity of the applied thermodynamic model. Greater complexity always results in exponential increase of the computational load. Therefore, a trade-off between accuracy and model complexity must be considered when developing a plant-

wide model. The ideal usable model is rigorous enough to include all the complex aspects of reactive absorption and simple enough to enable an easy and practical implementation of the process.

Kenig et al. (2001) presented the evolution of model complexity for reactive absorption modeling. An adaptation of their classification is shown in figure 3.1. This figure illustrates that there are two approaches for simulation of absorption and desorption: the equilibrium-based model and the rate-based model. The simplest model (model 1) is the classical equilibrium stage model which assumes infinitely fast mass transfer and reaction at equilibrium within each stage. The accuracy of model 1 improves by considering the liquid bulk and/or liquid film reaction kinetics (model 2). The equilibrium stage extended by the consideration of kinetically controlled reactions (model 2) is physically inconsistent; though it has been applied in the past (Mores et al., 2011). The accuracy of absorption/desorption models greatly improves by including the reaction kinetics in the description of mass transfer phenomenon. Lawal et al. (2009) have shown that the rate-based approach is more realistic for simulation of CO_2 capture since in practice phase equilibrium is not attained in the column. Moreover, an important benefit of rate-based models (model 3 to 5) is that the process dynamics and mass transfer capacity are directly included using correlations for pressure drop, hold-up and mass transfer resistance. Thus, composition, temperature, and flow rates are related to geometrical characteristics and operating conditions, allowing the scale-up design. There are three variants of rate-based models, depending on the complexity of the kinetic model. The simplest rate-based model (model 3) assumes chemical reactions at equilibrium. This model significantly improves by including an enhancement factor to determine the mass transfer rate with simultaneous chemical reaction (model 4). Enhancement factor models are approximation of rigorous mass transfer models, e.g. two-film model, penetration model and surface renewal model. Conclusively, the accuracy of the rate-based model noticeably depends on the accuracy of the enhancement factor model (Gaspar and Fosbøl, 2015; Tobiesen et al., 2007). At the highest level of complexity, model 5, reaction kinetics is calculated directly. This model implements reaction rates directly into the transport and balance equations in the film and the bulk of the fluid; thus it considers mass transfer resistances, electrolyte thermodynamics, reaction kinetics and the column configuration.
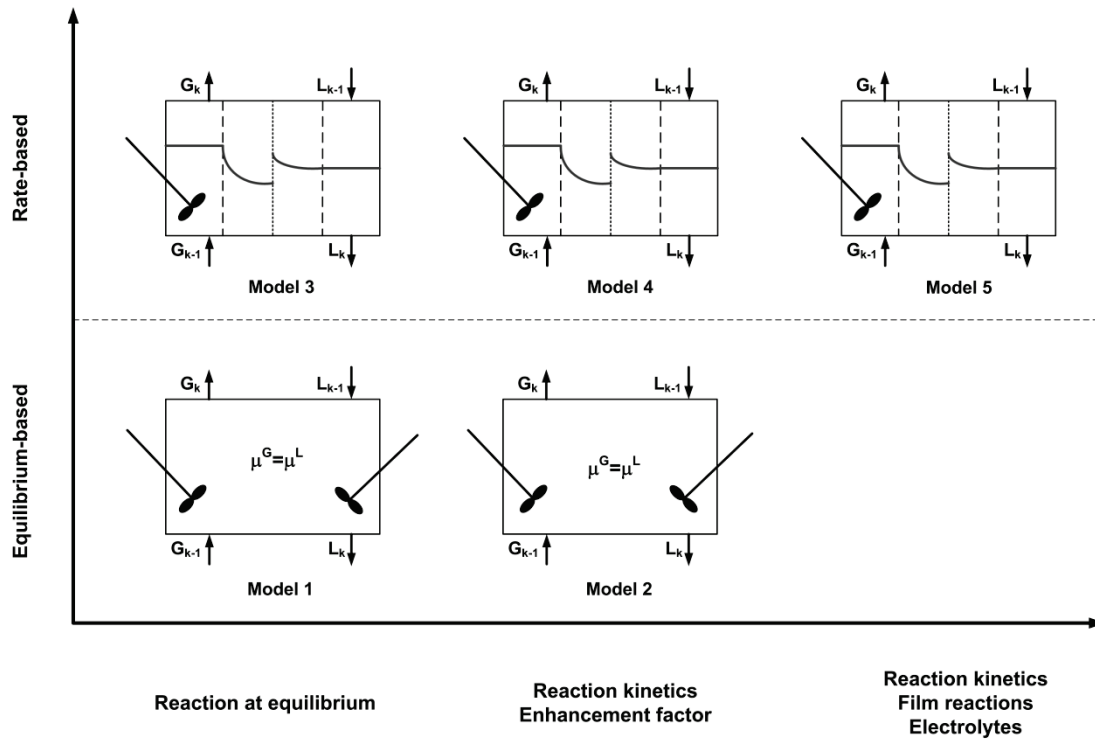
Figure 3.1. Absorption and desorption model complexity, adopted from Kenig et al. (2001)

Several papers presented models for CO_2 capture covering all of the above modeling approaches, mostly applied to MEA and for absorption. Model 4 is the most common and accepted approach in the carbon capture and storage community (Koronaki et al., 2015). An overview of representative implementations is provided in the following.

One of the pioneering models for gas absorption and stripping was developed by Pandya (1983), based on the widely accepted concepts proposed by Treybal (1969) and Danckwerts (1970). Pandya (1983) set up the differential component mass and energy balances assuming ideal gas and ideal liquid phase behavior. He presented only a calculation example using MEA as solvent, and he did not compare the model predictions against experimental data. Tontiwachwuthikul et al. (1992) applied Pandya's model for CO_2 absorption using NaOH and MEA as solvent. They compared the model predictions against pilot-scale experimental data. This model calculates the composition and temperature of the gas phase and of the liquid phase along the column height. It uses the Onda et al. (1968) mass transfer model and an explicit expression for the enhancemnt factor for second-order and irreversible reaction in the liquid film (Wellek et al., 1978). Later, Gabrielsen developed a rate-based model for CO_2 absorption using MEA and AMP (Gabrielsen, 2007; Gabrielsen et al., 2006). This model is similar with Tontiwachwuthikul's model, however it includes total mass balances to describe the changes in the gas and in the liquid flow rates. Additionally, it uses temperature and composition dependent correlations for physical and thermal properties. These correlations account for non-idealities of the liquid phase. Gabrielsen's model has been used to investigate the effect of

mass transfer respectively enhancement factor correlations on model predictions by Faramarzi et al. (2010). Faramarzi et al. (2010) have shown that different mass transfer correlations show similar trends; however the performance of the model significantly depends on the applied correlations for mass-transfer parameters and for reaction rate calculation. The mass transfer model of Rocha et al. (1996, 1993) in combination with a pseudo-first-order reaction constant showed smaller deviation compared to the investigated experimental measurements. This model has been extended to desorption using MEA as solvent by Fosbøl et al. (2009).

Khan et al. (2011) also developed a rate-based model for CO_2 absorption using MEA. This model is based on fast second-order kinetics and takes into account the mass transfer resistance. Similar to previous works, Khan et al. (2011) used empirical correlations for key thermodynamic and transport properties. They compared model predictions against pilot scale and industrial scale experimental data from Aroonwilas and Veawab (2004), Pintola et al. (1993) and Tontiwachwuthikul et al. (1992). Khan et al. (2011) showed that the model is in good agreement with those measurements. Additionally, they analyzed the impact of different mass transfer correlations on the model prediction and concluded that the Onda et al. (1968) model provides better predictions than the penetration theory of Higbie (1935) and the correlations of Rocha et al. (1996, 1993). These findings are to some extent contrary to the results of Faramarzi et al. (2010). Gaspar and Cormos (2012) and Cormos and Gaspar (2012) demonstrated that the suitability of mass transfer and hydraulic correlations depends on various factors, e.g. flow conditions, packing type, amine type, etc. As a result, a general conclusion on the accuracy of mass transfer and hydraulic correlations cannot be established. To increase confidence in models, they should be benchmarked against several experiments performed on different columns, different packing types and for a broad range of operation conditions.

The above studies usually include results only for CO_2 absorption. A CO_2 absorption and desorption simulation software capable of simulating the closed-loop flowsheet of a complete CO_2 post-combustion capture process is developed by Tobiesen et al. (2008, 2007). This model is applied to the benchmark MEA solvent. Tobiesen's implementation combines two types of interfacial mass transfer models: an enhancement factor model based on the film theory, and the rigorous penetration model. The driving force for absorption and desorption is accounted for by using CO_2 activities. Both, the absorption and desorption model has been validated against experimental data outlining the good agreement between model and experiment (Tobiesen et al., 2008, 2007).

Recently, innovative solvents such as piperazine, piperazine promoted amines and enzyme enhanced reactive solvents are in focus. Piperazine presents several advantages over the base case MEA solvent such as low degradation, high reaction rate and it may reduce the regeneration energy demand by 20% (Freeman et al., 2010; Rochelle et al., 2011). Piperazine is a promising promoter for MDEA and K_2CO_3 due to its rapid formation of carbamates with CO_2 (Bishnoi and Rochelle, 2002; Cullinane and Rochelle, 2004; Dang and

Rochelle, 2003). An absorber model for 8 molal piperazine was developed in Aspen Plus$^{®}$ RateSep™ by Plaza and Rochelle (2011). This model uses the *5deMayo* thermodynamic model implemented in the electrolyte NRTL framework of Aspen Plus (Frailie et al., 2011) and the kinetic model proposed by Dugas and Rochelle (2011a) respectively Cullinane and Rochelle (2006). It uses FORTRAN subroutines to override the Aspen Plus built-in correlation for interfacial area and viscosity. The model has been compared to pilot plat data showing the good agreement between model and experiment (Plaza and Rochelle, 2011; Plaza, 2011). Similar approach was adopted and validated for desorption simulation using 8 molal PZ by Van Wagener et al. (2013). This model also uses the *5deMayo* thermodynamic model in combination with the RADFRAC unit of Aspen Plus$^{®}$. Van Wagener et al. (2013) modelled the stripper with rate-based calculations in 30 stages assuming instantaneous reactions at equilibrium (model 3). The absorber model of Plaza and Rochelle (2011) and the stripper model of Van Wagener et al. (2013) has been integrated by Frailie (2014) in order to simulate and optimize the entire absorption-desorption cycle using 8 molal PZ. Furthermore, Frailie (2014) implemented a rate-based model in Aspen Plus for 7 m MDEA/2 m PZ and 5 m MDEA/5 m PZ using user-supplied FORTRAN subroutines to calculate thermodynamic and kinetic properties in addition to density, viscosity, and binary diffusivity correlations. He concluded that the 7 m MDEA/2 m PZ solvent has a considerably higher CO_2 capacity and lower cost of CO_2 capture compared to PZ when operating the absorber at low temperature, 20ºC. However, this model has not been compared to experimental data. A similar modeling approach for CO_2 stripping was adopted by Oyenekan and Rochelle (2009) for the PZ promoted K_2CO_3 system. They highlighted that a "short and fat" column requires less equivalent work than a "tall and skinny" column because of its lower pressure drop and less temperature change. However, there is a limitation in developing models in Aspen Plus, due to its closed-structure. Currently, there is no popular rate-based model for promoted systems.

A newly developing alternative for CO_2 post-combustion capture is the use of enzyme to increase the CO_2 absorption rate of otherwise slow reacting liquid absorbents, e.g. MDEA, K_2CO_3. Enzymes are renewable, non-volatile and biodegradable catalysts. Carbonic anhydrases (CA) in particular are the most promising class of enzymes for improving reactive CO_2 absorption. They are considered to be the fastest as well as most selective biocatalyst known for the hydration of CO_2 (Lu et al., 2011). CA enhanced tertiary amines have the potential to assure fast CO_2 absorption (smaller absorption tower) and they do not alter the positively low heat of stripping of tertiary amines (lower regeneration energy demand).

3.1.2 The need for general and accurate models using novel solvents

Nowadays a marathon is going on among researchers to find single and promoted solvents with improved properties, such as low degradation rate, less corrosion, higher CO_2 capacity and lower energy demand. Detailed experimental trials are often unfeasible and expensive due to the large number of possible amine

formulations and the broad operation range encountered in post-combustion capture. Thus, computer-based process models have emerged as indispensable tools for solvent respectively process design and optimization.

We have shown that modeling principles are relatively well established and demonstrated using the benchmark MEA solvent, but only a few models and simulation studies exist for novel solvents and promoted systems. General rate-based models with accurate mass transfer and kinetic models, applicable to single and promoted solvents in a wide range of operating conditions should be developed and thoroughly validated. Only benchmarked models can be used with confidence to compare the absorption capacity and energy performance of solvents, to assess technical and economic feasibility, to study process alternatives and to optimize the operating conditions.

Moreover, a challenging phenomenon has been observed when using piperazine as solvent and/or promoter. Piperazine and blends of piperazine may precipitation at process conditions of interest for CO_2 capture triggering the shut-down of the plant. The risk of precipitation is high especially in lean solutions, at process start-up, during solvent mixing, or in the condensing reflux sections of the stripper. These potential hazardous scenarios have to be identified in order to minimize the risk of equipment clogging. Additionally, the effect of slurry formation on the energy performance and CO_2 capacity of the solvent should be investigated and included in simulation studies. Currently, there is no popular rate-based model for CO_2 post-combustion process simulation which addresses the issue of precipitation. The growing interest for systems with solid formation, e.g. PZ, NH_3, K_2CO_3 calls for more realistic models. Precipitation must be included in the description of transfer phenomena and in the calculation of the equilibrium composition since solid formation changes the absorption capacity of the solvent.

This chapter presents a general model for the simulation of the absorption/desorption cycle and applies to various single and promoted solvents. It also introduces a first-of-its-kind hybrid rate-based model for modeling of precipitating systems.

3.2   Rate-based model for CO_2 absorption and desorption

This section presents the steady-state rate-based model for CO_2 absorption and desorption applied to PZ, PZ/K_2CO_3, MDEA, CA/MDEA and MEA. The model is based on the equation system proposed by Gabrielsen (2007). It consists of flow and transport equations describing the flow rate, composition and temperature of the gas phase and of the liquid phase. In the development of the model the following assumptions were considered:

- All of the reactions take place in the liquid film and the liquid bulk is at equilibrium.
- The gas-liquid interface is at equilibrium.
- Gas phase is ideal due to low pressure.
- The amine is non-volatile.
- The effective mass and heat transfer area are the same.
- Radial distribution of temperature, composition and fluxes are neglected; plug flow is considered.
- Heat loss to the surroundings is negligible.

The rate-based model is based on the plug-flow-reactor model and it is formulated as a boundary value problem (BVP) with fixed inlet conditions. The gas stream composition, temperature and molar flow are specified at the bottom while the liquid stream characteristics are specified at the top of the column. The mass and energy balances are set up around an infinitesimal small volume element with a cross section area of S and a wetted packing area of a. The mass and energy balance equations are listed in Table 3.1.These conservation equations, a system of ordinary differential equations, are coupled with non-linear algebraic equations providing the mass transfer and the hydraulic parameters, e.g. partial mass transfer coefficients, hold-up, effective mass transfer area and pressure drop. The mathematical formulation of these independent terms is discussed in the followings. Temperature and composition dependent correlations for physical properties entering the mass transfer calculations such as viscosity, diffusivity, surface tension and density are taken from the open-literature. The model uses the extended UNIQUAC thermodynamic model for vapor-liquid-solid equilibria (VLSE) and thermal properties calculation. The General Model (GM) enhancement factor model describes the acceleration of mass transfer rate due to the reaction between the amine and CO_2. In the following the developed model will be referred to as CAPCO2 model.

Table 3.1. Mass and energy conservation equations - CAPCO2 model

---

Total mass balances for the gas phase and for the liquid phase

$$\frac{dG}{dz} = -(J_{CO_2,gl} + J_{H_2O,gl})aS \tag{3.1}$$

$$\frac{dL}{dz} = -J_{H_2O,gl}aS \tag{3.2}$$

Component mass balances for the gas phase and for the liquid phase

$$G\frac{dy_{CO_2}}{dz} = -y_{CO_2}\frac{dG}{dz} - J_{CO_2}aS \tag{3.3}$$

$$G\frac{dy_{H_2O}}{dz} = -y_{H_2O}\frac{dG}{dz} - J_{H_2O}aS \tag{3.4}$$

$$L\frac{dx_{CO_2}}{dz} = -x_{CO_2}\frac{dL}{dz} - J_{CO_2}aS \tag{3.5}$$

$$L\frac{dx_{H_2O}}{dz} = -x_{H_2O}\frac{dL}{dz} - J_{H_2O}aS \tag{3.6}$$

Energy balances for the gas phase and for the liquid phase

$$GC^G_{p,tot}\frac{dT_G}{dz} = -\left(\frac{dG}{dz}C^G_{p,tot} + aS\left(C^G_{p,H_2O}J_{H_2O} + C^G_{p,CO_2}J_{CO_2}\right)\right)T_G - qaS \tag{3.7}$$

$$LC^L_{p,tot}\frac{dT_L}{dz} = C^L_{p,tot}T_L\frac{dL}{dz} - aS\left(\left(C^L_{p,H_2O}T_G + \Delta_{vap}H_{H_2O}(T_L)\right)J_{H_2O} + \left(C^L_{p,CO_2}T_G + \Delta_{CO_2,diss}H(T_L)\right)J_{CO_2}\right) - qaS \tag{3.8}$$

Pressure drop equation (Rocha et al., 1993)

$$\frac{dP}{dz} = \frac{dP_{dry}}{dz}\left[\frac{1}{1 - K_2 h_L}\right]^5 \tag{3.9}$$

$$\frac{dP_{dry}}{dz} = \frac{f\rho_g U_{ge}^2}{Sg_{eff}} \tag{3.10}$$

G and L denote the total gas and liquid flows in mol/s; y_i and X_i represent the composition of the gas respectively liquid phase, where i is CO_2 and H_2O; T_G and T_L refer to the gas respectively liquid temperature. The solvent flow rate and composition are expressed on a CO_2-free basis: L gives the flow rate of water plus amines and X_i represents the amount of component i per moles of water plus amines. We adopt this approach to overcome uncertainties related to the accuracy of physical property correlations of CO_2 loaded solutions. The transport of species between the gas phase and the liquid phase is described by the flux J_{CO2} for CO_2 absorption/desorption and J_{H2O} for H_2O condensation/evaporation. By convention, the mass transfer between

the phases is bi-directional: positive sign shows mass transfer from gas to liquid, i.e. absorption or condensation and negative sign refers to desorption and evaporation. The pressure drop per volume of element, dP/dz in eqs. (3.9) and (3.10) is calculated with the model of Rocha et al. (1993). This correlation takes into account the liquid hold up, h_L, and the dry pressure drop, dP_{dry}. The dry pressure drop gives the change in pressure in a packed column without solvent. It depends on the gas phase density, ρ_g, velocity, U_{ge}, and on the friction factor, f. The heat transferred by conduction, q, is calculated with $q = h_G (T_G - T_L)$ using the Chilton-Colburn analogy for the heat transfer coefficient, h_G (Gabrielsen, 2007).

3.3   Mass transfer model

The phenomenon of coupled chemical reaction and mass transfer across the gas-liquid interface is described according to the two-film theory. The film theory assumes a stagnant film of liquid and a stagnant film of gas on each side of a gas-liquid interface. The resistance to mass transfer is concentrated in these layers and mass transfer between the two films occurs by molecular diffusion. Accordingly, the molar flux of component $i = CO_2$ and H_2O across the gas-liquid interface is:

$$J_{i,gl} = K_i^g \left(p_i - p_i^* \right)$$

(3.11)

where K_i^g is the overall mass transfer coefficient where i equals CO_2 and H_2O. The driving force for mass transfer is expressed as the difference between the partial pressure of component i in the gas phase, p_i and the equilibrium partial pressure of component i, p_i^*. The extended UNIQUAC thermodynamic model provides the equilibrium partial pressure for CO_2 and H_2O.

The overall mass transfer coefficient includes the resistance opposed by the liquid plus the gas film. In this work, we assume that the liquid side resistance to water diffusion is negligible since the liquid phase mainly consists of water. Consequently, the overall mass transfer coefficient of water equals the gas side mass transfer coefficient of water, $K_{H_2O}^g = k_{H_2O}^g$. The overall mass transfer coefficient of CO_2 is:

$$\frac{1}{K_{CO_2}^g} = \frac{1}{k_{CO_2}^g} + \frac{H_{CO_2}}{E_{overall} k_{CO_2}^l}$$

(3.12)

$k_{CO_2}^g$ and $k_{CO_2}^l$ are the partial mass transfer coefficients for the gas side and for the liquid side. They are calculated with the Rocha et al. (1996) (when using MEA, PZ, PZ/K$_2$CO$_3$) and Billet and Schultes (1999) (when using MDEA and CA/MDEA) mass transfer correlation model. The Henry solubility parameter, H_{CO_2} is determined using the extended UNIQUAC thermodynamic model and the overall enhancement factor, $E_{overall}$ is provided by the GM model. The overall enhancement factor shows the acceleration of CO_2

absorption/desorption rate due to the reactions between CO_2 and amines. Chapter 2 presents the enhancement factor model for single reactions and multiple parallel reactions and it demonstrates for CO_2 capture using MEA, PZ and CA/MDEA. The kinetic model for PZ/K_2CO_3 is described in Appendix A.

3.4 Extended UNIQUAC thermodynamic model

A thermodynamic model is required during the solution of the BVP problem, equations (3.1) to (3.10), for the description of the vapour-liquid-solid equilibrium (VLSE) and thermal properties, e.g. equilibrium pressures, activity coefficients, Henry's constant, heat capacities and enthalpy of absorption/desorption. Tobiesen et al. (2008, 2007) have shown that the equilibrium model is vital for obtaining good absorber simulation results, in particular at high loadings and it is even more important for desorption since all of the reaction and transport rates are much higher. They have concluded that small deviations of about 5% in the activity coefficient of water results in considerable changes in the overall stripping. Thus, the use of an accurate thermodynamic model for a broad range of operating conditions (25 to 150 °C, 0.1 to 0.5 CO_2 loading) is vital for CO_2 absorption and especially desorption simulation.

This works uses the extended UNIQUAC thermodynamic model in the description of the vapor-liquid-solid equilibria (VLSE) and thermal properties. The extended UNIQUAC model is a Gibbs excess energy model which applies the thermodynamic γ-φ convention. The extended UNIQUAC model is used for liquid phase activity coefficients while the SRK equation gives the gas phase non-idealities. The extended UNIQUAC model was developed from the well-known UNIQUAC model by adding a Debye-Hückel term to correct for the electrostatic interactions between the ions in the liquid. A detailed description of the equation system and derived properties of the Gibbs excess model was previously presented (Thomsen et al., 1996). The method for VLSE calculation is presented by Thomsen and Rasmussen (1999). The fitting of the parameters were performed against a large database at Center for Energy Resources Engineering and applied in numerous CO_2 capture related projects, like the chilled ammonia capture process (Darde et al., 2012), or the novel ammonia capture process (Gaspar et al., 2014), and etc. The parameters regressed for MEA-H_2O-CO_2, MDEA-H_2O-CO_2 and $PZ/K_2CO_3/CO_2$ systems are used in the present work to account for the interactions between the ions and for the interactions between molecules (Faramarzi et al., 2009; Fosbøl et al., 2013; Sadegh et al., 2015). These works demonstrate the very good agreement between the extended UNIQUAC thermodynamic model and several experimental dataset.

3.5 Physical properties

This section summarizes the physical property correlations, i.e. diffusivity coefficients, density, viscosity, surface tension and thermal conductivity entering the mass and heat transfer respectively hydraulic models. A general and robust model for both, CO_2 absorption and desorption requires an accurate estimation of these

properties for broad loading and temperature ranges: 0.1 – 0.5 mol CO_2/ mol alkalinity, and 25 – 150 °C. Accordingly, significant effort was invested in securing the validity of these properties. Several correlations and experimental data were compared and combined to generalize them for absorption and desorption conditions. Finally, with the help of three master and bachelor students, the developed correlations were validated for the above conditions (Faramarzi et al., 2010; Gabrielsen, 2007; Gaspar et al., 2016b; Glibstrup, 2015; Nielsen, 2015; Poulsen, 2014). This methodology assures the suitability of the correlations for CO_2 absorption as well as for desorption. Table 3.2 summarizes these correlations.

Table 3.2. Physical property correlations for the gas phase and for the liquid phase

Gas phase	Solvent	Source
Thermal conductivity of the gas mixture	All	(Mason, 1958; Reid et al., 1987)
Diffusivity coefficient of CO_2 and N_2O in water	All	(Versteeg et al., 1996)
Diffusivity coefficient of CO_2 and H_2O in air	All	(Reid et al., 1987)
Viscosity of gas mixture	All	(Reid et al., 1987)
Heat capacity of gas components	All	(Reid et al., 1987)
Liquid phase		
Diffusivity coefficient of CO_2 in solution	MEA	(Versteeg et al., 1996)
	PZ	(Dugas and Rochelle, 2011b)
	MDEA	(Glibstrup, 2015)
	PZ/K_2CO_3	(Nielsen, 2015)
Diffusivity coefficient of amine in solution	MEA	(Snijder et al., 1993)
	PZ	(Dugas and Rochelle, 2011a)
	MDEA	(Glibstrup, 2015)
	PZ/K_2CO_3	(Nielsen, 2015)
Density of amine solution	MEA	(Weiland et al., 1998)
	PZ	(Gaspar et al., 2016b)
	MDEA	(Glibstrup, 2015)
	PZ/K_2CO_3	(Nielsen, 2015)
Viscosity of amine solution	MEA	(Cheng et al., 1996)
	PZ	(Dugas and Rochelle, 2009)
	MDEA	(Glibstrup, 2015)
	PZ/K_2CO_3	(Nielsen, 2015)
Surface tension of amine solution	MEA	(Vazquez et al., 1997)
	PZ	(Gaspar et al., 2016b)
	MDEA	(Glibstrup, 2015)
	PZ/K_2CO_3	(Nielsen, 2015)

3.6 A hybrid CO₂ capture model for precipitating solvents

This section presents the hybrid CAPCO2 rate-based model (hCAPCO2) which directly accounts for slurry formation in packed columns. This model is applied to CO_2 capture using PZ. Precipitation can be imagined as apparent removal of active components, e.g. PZ, H_2O from the solution. As a result, the precipitated solid is not present in the liquid phase and it is not free to react with the dissolved CO_2. Solutions with less active components will absorb less CO_2. Therefore, the real concentration of the liquid phase needs to be considered in the transfer flux calculation as it will be demonstrated in the following.

To account for the deactivation of the active components due to precipitation, the equations describing solid formation are integrated into the system of differential equations (3.1) to (3.10). This model combines an equilibrium and a rate-based approach. The amount of solid is estimated assuming equilibrium between the liquid phase and the solid phase using the extended UNIQUAC model. The CO_2 mass transfer rate through the gas-liquid interface is described by eq. (3.11). One can see that compared to traditional rate-based models, the hybrid CAPCO2 model includes the solid-liquid phase change when predicting the CO_2 mass and heat transfer fluxes between the gas phase and the liquid phase. The concentration of the dissolved active components, x_i^{real} and dissolved CO_2 is back-calculated from the initial concentration, x_i^{app} using the precipitated amount, n_i^{solid}, as shown in (3.13) and (3.14). The total liquid molar flow also changes and it is calculated according to (3.15).

$$x_i^{real} = \frac{x_i^{app} L^{app} - n_i^{solid}}{L^{real}}, \text{ where } i = PZ, H_2O \tag{3.13}$$

$$x_{CO_2}^{real} = \frac{x_{CO_2}^{app} L^{app}}{L^{real}} \tag{3.14}$$

$$L^{real} = L^{app} - \sum_j n_j^{solid} \text{ where } j = \text{solid components} \tag{3.15}$$

In (3.13) to (3.15), "real" refers to the composition respectively flow rate of the liquid phase excluding solids while "app" indicates total composition, assuming no precipitation. The effect of slurry formation on the absorption capacity of a PZ solid precipitating solvent is discussed in the following.

3.7 Numerical solution of the capture model

The mathematical formulation of the resulting CO_2 capture model is a two point boundary value problem (BVP) in a single dimension. This model needs to be discretized in the spatial domain in order to solve with

BVP solvers. A variety of methods exists for the discrete representation of the derivative operator. However, most of the methods are variations and combination of three well-known methods: the finite difference method, the finite volume method and the finite element method. In this work, the finite difference method (FDM) has been applied. The FDM is widely used in computer simulations because of its simplicity and intuitive approach. The FDM method represents the spatial derivatives in discrete grid points. The derivatives at the grid points are estimated using the neighbouring points. It has been shown that FDM is robust and efficient for various problems especially for 1D representation, such as the developed CO_2 capture model (LeVeque, 2007).

Figure 3.2 presents the solution scheme for the hybrid CO_2 capture model. The hybrid CO_2 capture model includes slurry/solid formation in the calculation of the CO_2 mass transfer rate. Essentially, the hybrid capture model consist of the core gas-liquid rate-based model (CAPCO2), represented by the blue box in figure 3.2 and it extends to solid-liquid-gas systems by directly including solid formation in the mass and energy balance equations (green box in figure 3.2). For non-precipitating solvents, e.g. MEA, MDEA the hybrid capture model reduces to the traditional CAPCO2 model. This model has been implemented in FORTRAN, including all of the sub-models for mass transfer and hydraulic correlations as well as the extended UNIQUAC thermodynamic model.

The underlying mass and energy conservation equations and additional sub-models for mass transfer and thermodynamic calculations are the same for the hybrid model and the CAPCO2 model. This coupled system of differential equations and algebraic equations is solved iteratively, using a damping factor algorithm. The use of a damping factor guarantees the robustness and convergence of the model for both absorption and desorption conditions. This approach requires an initial solution at the first iteration. This solution is updated each iteration by slowly eliminating the damping factor. The initial solution should be realistic and further give physically meaningful values throughout the iterations. This numerical approach requires several iterations and may be computationally heavy but assures the convergence of the model nevertheless of the stiffness. Note that the stiffness of the problem depends on the given inputs. It varies from light to very stiff system with high gradient differences for desorption. The complexity of the BVP is increased by the non-constant boundary conditions for the stripper with integrated reboiler configuration. The presented solution procedure is general for absorption and desorption modelling.
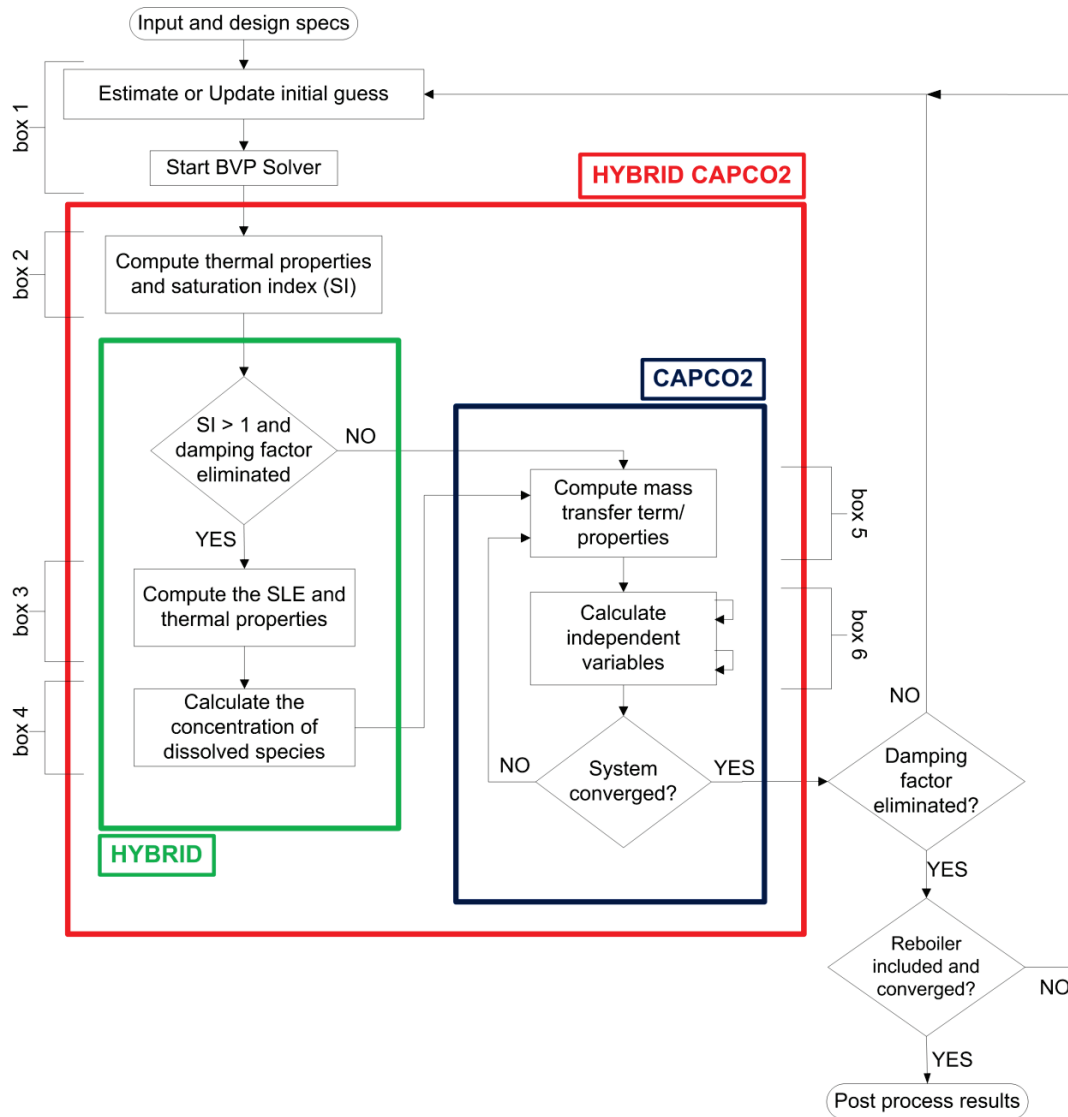
Figure 3.2. Structure and numerical solution methodology of the developed rate-based model

Figure 3.2 shows that the solution procedure starts with the estimation of an initial solution using a uniform grid with 30 elements. The initial solution at these grid points is obtained assuming inefficient column, i.e. CO_2 and water mass transfer rates equal zero. Then, the length of the grid is recalculated each iteration, obtaining a non-uniform mesh. Typically, the number of elements varies between 30 and 300. The advantage of using adaptive grid is the higher order accuracy and computational savings compared to algorithms with fixed and uniform grid (LeVeque, 2007; Tobiesen, 2006). The solution of the problem is updated each iteration by slowly eliminating the damping factor. The current solution is used to compute thermal properties and the saturation index, box 2 in figure 3.2. The saturation index (SI) indicates the presence of solid formation when is greater than 1. A bubble calculation routine provides the saturation index, but this routine does not provide the amount of solids. It only indicates if precipitation occurs. Therefore, a second TP-flash calculation (box 3) is performed when SI>1 to determine the solid-liquid-vapor composition. This

composition enters equations (3.13) - (3.15), represented by box 4. Note that the bubble point routine is preferred to determine if solid forms before actually calculating the solid-liquid equilibria since the bubble point routine is much faster compared to the TP-flash calculation. Thus, this approach assures that at solid-free conditions, the solution is obtained faster. Moreover, this approach allows merging of the hybrid model and CAPCO2 model without additional increase of the CAPCO2 model's computational heaviness. Figure 3.2 shows that for solid free-conditions and non-precipitating systems, the solution procedure continues with the computation of the mass transfer terms (box 5) and other independent variables, e.g. enhancement factor, heat flux, etc. (box 6). The solution of the model for a given estimates of the column profile is determined in an inner loop, returning the composition, temperature and flow rate at each grid point along the packed column. An outer recycle loop is used to close the mass and energy balances around the reboiler. The reboiler is represented by a TP-flash.

Furthermore, figure 3.2 shows that the hybrid part of the model is called only when the damping factor is eliminated, i.e. a solution of the model is obtained. This approach was adopted due to two reasons: (1) Initially, the column profiles are generated for zero CO_2 and H_2O mass transfer rates resulting in conditions at which precipitation generally occurs, i.e. unrealistically low temperature and CO_2 loading. However, as the damping factor reduces and the column profiles are closer to the steady state values, the solid formation is less or none. (2) Solid formation results in sudden changes of the liquid phase composition; thus precipitation introduces discontinuities in the column profiles. These discontinuities may lead to convergence issues. Therefore, the applied approach minimizes the time required to converge systems with slurries and it keeps the robustness respectively speed of the original CAPCO2 model by eliminating the time-demanding TP-flash calculations (box 3).

3.8   Results and discussion

The validation of the developed steady-state model for CO_2 absorption and desorption using single and promoted reactive absorbents, i.e. MEA, PZ, PZ/K_2CO_3, MDEA and CA/MDEA is presented in this section. The results presented here are pure predictions, i.e. none of the parameters were adjusted to fit the experiments. First, we compare the MEA model to experimental data and then we show the variability of some key parameters when using independent models. This analysis creates the basis for further comparison and evaluation of simulation results to other models and experiments respectively. Furthermore, we evaluate the model performance against absorption and desorption experimental data for PZ, PZ/K_2CO_3, MDEA and CA/MDEA. In addition, we show the impact of slurry formation on the CO_2 capacity of the PZ solvent in order to emphasize the importance of slurry formation when modeling solid precipitating solvents. Finally, we compare the closed-loop MEA model to pilot plant measurements with focus on the overall accuracy of the model. All of the used experimental data originates from the open literature and therefore only a short description will be given here.

3.8.1   Validation of the MEA CO_2 capture model

We show the performance of the CO_2 capture model using MEA for two datasets: the CASTOR test campaign (Knudsen et al., 2009) and data from Tobiesen et al. (2008, 2007). These datasets cover a broad range of conditions, relevant for a CO_2 capture plant operated in an energy market with increasing importance of renewables. The CASTOR campaign demonstrated the effect of essential process parameters, i.e. solvent flow, reboiler duty and reboiler pressure on the capture process performance. During this campaign, the lean CO_2 loading and solvent flow rate were modified in order to remove 90% of the inlet CO_2, i.e. the lean CO_2 loading varied between 0.17 and 0.28 and the solvent flow rate between 12 and 23 m^3/h. An almost constant rich loading of 0.47 mol/mol was obtained in all cases. Contrary, the Tobiesen data corresponds to operation at various CO_2 removals, from 20% to 90% CO_2 removal. Several parameters were changed during this campaign, such as lean flow rate, lean temperature, lean respectively rich CO_2 loading, etc. The lean loading changed between 0.18 to 0.41 and the rich loading between 0.21 and 0.45. A summary of the main operating conditions for both sources is presented in Table 3.3. More details can be found in the above sources.

Figure 3.3 presents the calculated CO_2 capture percentage versus experimental values for the CASTOR and Tobiesen data. It underlines that the model slightly under-predicts the CASTOR data and a little over-predicts the Tobiesen data, but the deviations between predictions and measurements are generally within ±10%. The mean absolute relative deviation (MARD) between the predictions and measurements is 4.25% and 5.06% for the CASTOR and for the Tobiesen data respectively. Note that the MARD between the experimentally determined gas side and liquid side removal is 9.48% and 4.48% for CASTOR and Tobiesen

data. Thus, the deviations between simulations and measurements are in the accuracy range of the experimental data.

Table 3.3. Main operating conditions and column specifications for CASTOR and Tobiesen data

| Column specification	CASTOR campaign	Tobiesen dataset
Absorber/Desorber diameter (m)	1.1/1.1	0.15/0.1
Absorber/Desorber height (m)	17.0/10.0	4.36/3.89
Packing type	IMTP 50	Mellapak 250Y
Operating conditions		
Gas flow rate (Nm^3/h)	4900 – 5000	140 – 150
Liquid flow rate (m^3/h)	12 – 23	0.18 – 0.54
Rich loading (mol /mol)	0.47 – 0.48	0.21 – 0.45
Lean loading (mol /mol)	0.21 – 0.45	0.18 – 0.41
MEA concentration (wt%)	30	30
Inlet Liquid temperature (K)	331 – 336	317 – 339
Stripper inlet temperature (K)	364 – 376	378 – 388
Pressure in absorber (kPa)	~ 101	99 – 104
Pressure in desorber (kPa)	123 – 219	≈ 200
Reboiler heat duty (kJ/kg CO_2)	4.0 – 4.7	3.6 – 11.0
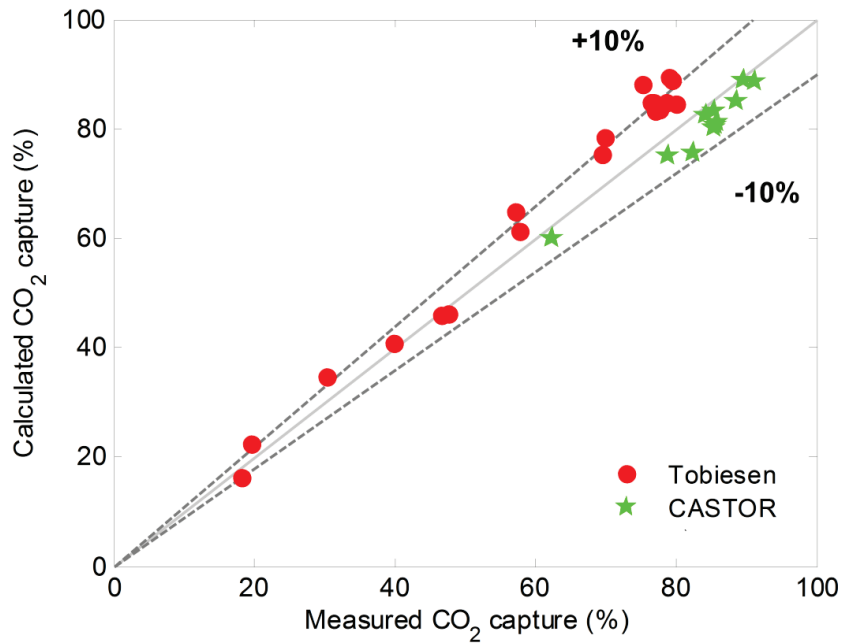
Figure 3.3. Comparison of calculated and measured CO_2 capture percentage for CASTOR and Tobiesen data

Figure 3.4 shows the comparison between calculated and measured reboiler lean loadings for the CASTOR and Tobiesen data. It underlines that the accuracy of the model at desorption conditions is comparable with the accuracy of the model at absorption conditions. The relative deviations between model and experiment are within ±10% with a MARD of 9.94% and 8.72% for the CASTOR and Tobiesen data. This figure shows that only 3 points are visibly outside of the ±10% accuracy range, corresponding to the highest solvent flow rates. Thus, it could be related to the accuracy of the Rocha et al. (1996) mass transfer model at high L/G ratios. The performance of the model is further illustrated by figure 3.5. This figure shows the calculated versus the measured specific reboiler duties. It shows that the agreement between model and the CASTOR data is good. The relative deviations for single runs are generally less than ±5%. The Tobiesen reboiler duty data is more scattered, ranging from 3.7 GJ/t CO_2 to 11 GJ/t CO_2. The highest values correspond to test cases with low loadings, below 0.3. The deviation between the Tobiesen data and the model is deemed satisfactory, within ±10% below 6 GJ/t CO_2 and the model systematically under-predicts the measurements at higher specific reboiler duties. Note that the reboiler is set-up as a specified temperature and pressure (TP) flash and heat loss to the surroundings is not accounted for in this work. This may result in under-predicted heat duties. As discussed below, the specific heat duty parameter is highly sensitive to temperature and small error in temperature measurement leads to high difference in the required energy input (Fosbøl et al., 2014) – Appendix B.
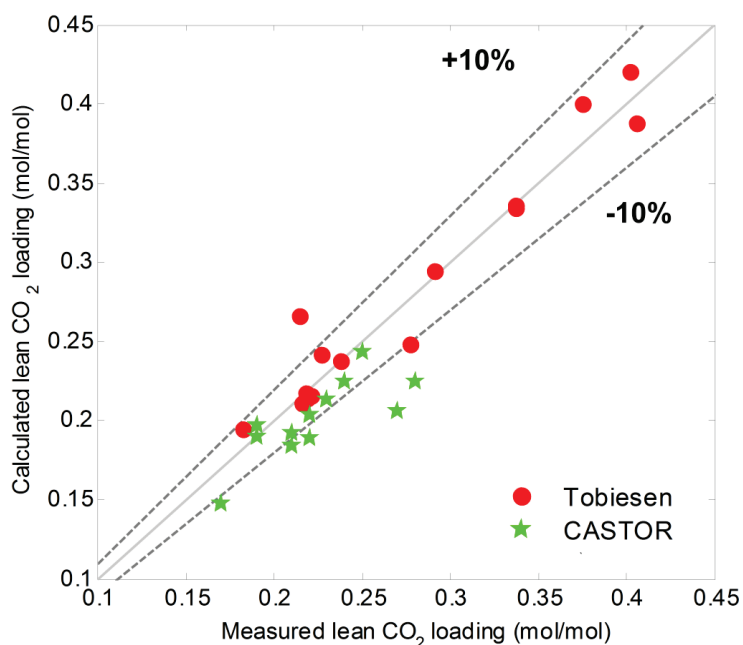

Figure 3.4. Comparison of calculated and measured reboiler lean loading for CASTOR and Tobiesen data
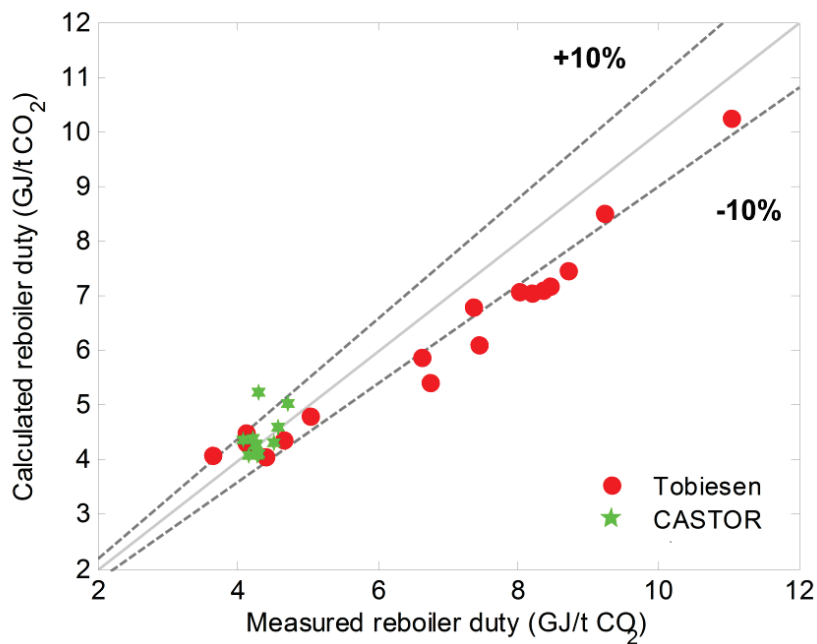
Figure 3.5. Comparison of calculated and measured specific reboiler duty for CASTOR and Tobiesen data

Benchmarking of the MEA model

In the Octavius FP7 EU project a benchmarking was performed, to investigate the accuracy and quality of the used modeling tools and to define the reproducibility of various calculated properties, e.g. lean/rich loading, CO_2 concentration/temperature profiles, specific heat duty, etc. As part of the benchmarking activities, the presented MEA CO_2 capture model has been compared to five independent models, developed by SINTEF (Norway), TUHH (Germany), IFPEN (France), EDF (France) and TNO (Netherlands). These models comprise anything from in-house models to Aspen Plus® units and combination of the two. A detailed description of the benchmarking procedure and simulation results is described in (Fosbøl et al., 2014), Appendix B. Here only the main conclusions are presented.

The OCTAVIUS benchmarking study demonstrated that there is a remarkably good agreement between the used models. Most of the deviations between the calculated key parameters range from 5% to 10% indicating that approximately this order of accuracy should be expected for a comparison to experimental data. The results indicate that in a benchmarking study, a 5-10% difference in calculation is therefore within the typical variability of the models. However, a few properties can be picked out which should be treated with care if they are to be used for comparison. This is the CO_2 concentration and temperature profiles as function of height, plus the reboiler temperature. Especially the reboiler temperature is critical. It is a property often used for design specification. The analysis shows that temperature and concentration profiles are less accurate in the mid sections of the column which is not critical to the simulation or comparison. Furthermore, this study

highlighted that at higher flooding, >70-80%, the specific reboiler duty (SRD), the flooding percent, the top CO_2 mole fraction, and the desorber top gas flow vary noticeably between simulations. The most important of these is the SRD which cannot be reliably compared to experimental data at high flooding velocities. An example for the expected accuracy of the SRD is shown in Figure 3.6. This figure shows the SRD as function of the reboiler operating temperature. It demonstrates the pronounced sensitivity of SRD with respect to reboiler temperature. The differences between the models are the greatest at low temperatures, <120 °C and at high temperatures, >122.5 °C. Low temperature corresponds to less CO_2 stripping and therefore to higher lean reboiler CO_2 loading, >0.25. High temperatures resemble low lean loadings, below 0.18 and higher flooding percentage, >70%. The results have shown that the models predict the specific reboiler duty within 5-10% which is 0.2-0.4 GJ/t CO_2 for the calculations performed. This is a significant contribution, and important to bear in mind, while doing a comparison to models and experimental data.
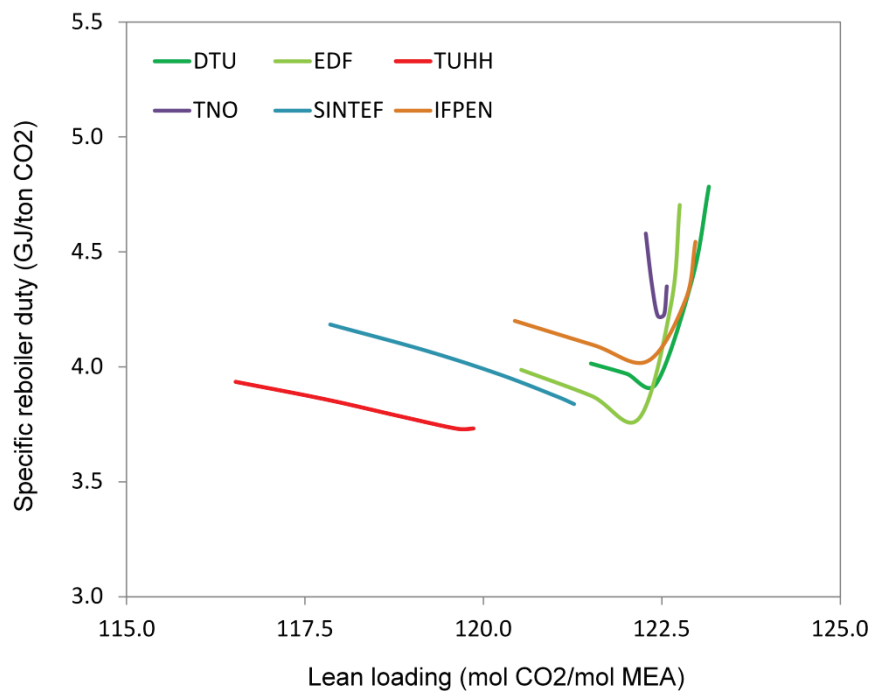

Figure 3.6. Specific reboiler duty versus reboiler temperature with various models

Composition and temperature profiles were also compared in the OCTAVIUS benchmarking study. This study outlined the differences between profiles from various models. For example, figure 3.7A illustrates that the majority of simulations for this specific problem gives linear concentration profiles. However, there is a well-visible difference in predicted concentrations, ±6%, in the mid column section. Note that the overall capture rate is the same. The conclusions on the temperature profile (figure 3.7B) are similar to the concentration profiles. The variation is greater in the mid-section. This is expected since temperature and composition are directly linked through the heat of absorption.

The differences between the models are related to the mass transfer, hydraulic and kinetic models as well as the underlying assumptions (Fosbøl et al., 2014). For example, the EDF calculations show that at 12 m there is decrease in the CO_2 concentration which results in an increase of temperature. These results are comparable with TNO indicating a high absorption efficiency in the top 8 m. The bottom section is not efficient. The trends from these two calculations are similar as the two partners use the same mass transfer correlation. DTU and SINTEF also use the same mass transfer correlation, but the temperature profile by SINTEF has a slightly different tendency in the range 0 to 2 m. This could be related to the thermodynamic model resulting in different water condensation rates. The importance of the mass and hydraulic parameters on the predictions has also been demonstrated by Cormos and Gaspar (2012).
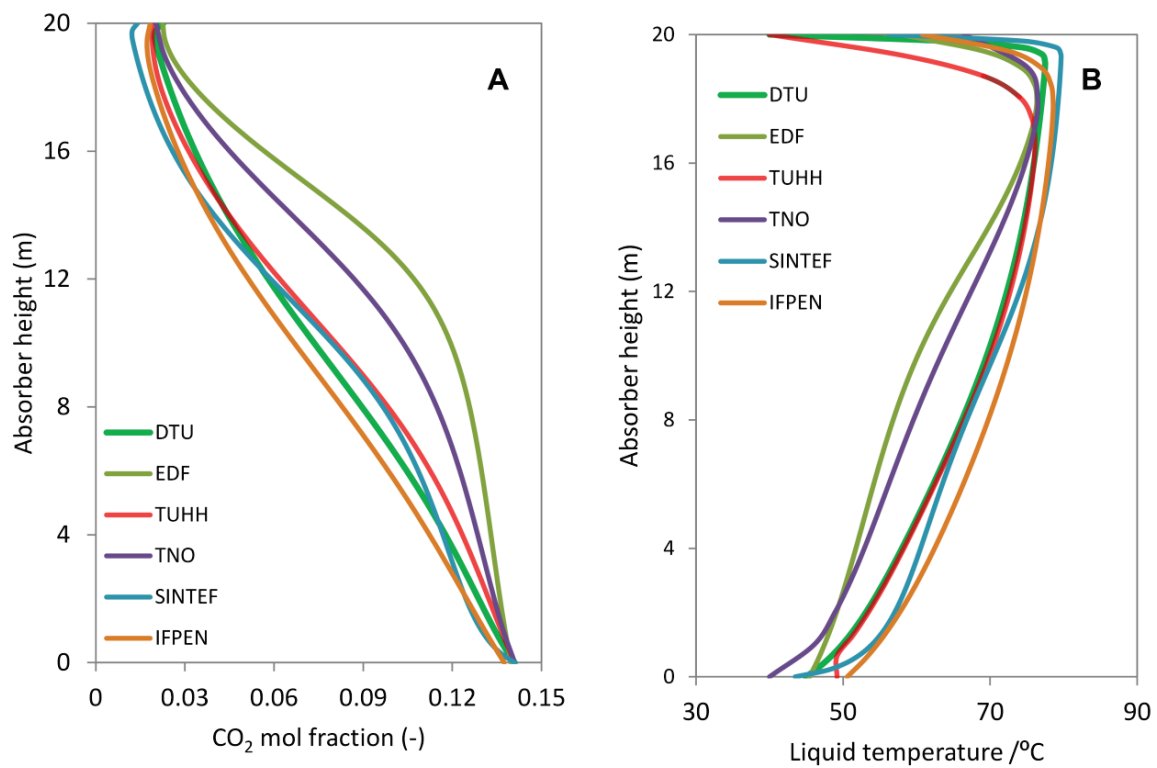
Figure 3.7. (A) CO_2 mol fraction and (B) temperature versus absorber height

A good practice in process simulation and pilot experiments would be to meticulously define all inputs and process variables, even the packing type, insulation thickness, etc. Neglecting this would open up for future interpretation which is not beneficial to accurate model development. The minimum requirement for information is outlined in Fosbøl et al. (2014), Appendix B. This benchmarking creates a basis for future rate based model developers and it may act as a baseline for modeling.

In summary, it was shown that the developed rate-based model for MEA accurately describes both, CO_2 absorption and desorption for a broad range of operating conditions and for pilot and industrial scale columns.

3.8.2 Validation of the PZ CO_2 capture model

The performance of the hybrid rate-based model for CO_2 absorption and desorption simulation using PZ is presented here. We show the model predictions against experimental measurements carried out at the J. J. Pickle Research Center, north of Austin, TX, USA for campaigns "Fall 2008" and "Fall 2010" (Plaza and Rochelle, 2011; Van Wagener, 2011). Both pilot campaigns were carried out with a synthetic flue gas of 12 mol% CO_2, not saturated with water at the inlet of the absorber. The pilot experiments were performed with approximately constant flue gas flow rate which was contacted with a 4 to 8 molal PZ solution ("Fall 2008" campaign) respectively 5 and 8 molal solution ("Fall 2010" campaign). The CO_2 loading of the lean solvent was varied between 0.2 and 0.37 mol CO_2/mol alkalinity. A summary of the experimental conditions and column specifications is presented in Table 3.4. More details regarding the pilot campaigns can be found in Plaza and Rochelle (2011) respectively Van Wagener (2011).

Table 3.4. Main operating conditions and column specifications

Column specifications	
Absorber/Desorber height (m)	6.1
Absorber/Desorber diameter (m)	0.43
Packing type	Mellapak 2X
Operating conditions	
Flue gas flow rate (kg/s)	0.16 – 0.22
Solvent flow rate (kg/s)	0.6 – 1.7
Inlet CO_2 mol %	12
PZ concentration (mol/kg water)	4,5,7,8
Lean CO_2 loading (mol/mol)	0.2 – 0.37
Rich CO_2 loading (mol/mol)	0.30 – 0.60
Lean temperature (°C)	37 – 47
Reboiler temperature (°C)	87 – 129
Reboiler pressure (kPa)	138 – 414

Figure 3.8 shows the calculated CO_2 capture percentage versus experimental values. It highlights that the hybrid CAPCO2 model and experiments are in good agreement for different piperazine concentrations, i.e. 4, 7 and 8 molal PZ. There is only one point much outside of the ± 10% accuracy range which is most probably

an outlier. The inlet temperature of the flue gas for this outlier was -5ºC, which represents the lower limit of the experimental temperature range. Furthermore, Plaza (2011) shows that the accuracy of the absorber titrations are within ± 10% and the liquid side removal matches the gas side results within ±15%. Thus, the model predictions are within the accuracy of the measurements.
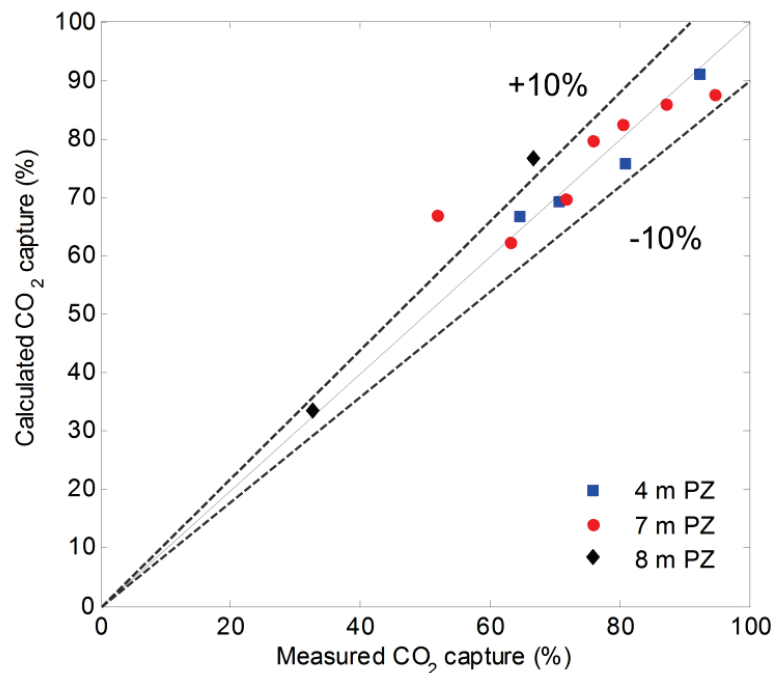

Figure 3.8. Predicted versus measured CO_2 capture percentage (campaign "Fall 2008")

Figures 3.9 and 3.10 present the model predictions against desorption measurements for campaigns "Fall 2008" and "Fall 2010". Figure 3.9 shows the calculated reboiler outlet lean loadings versus experimental values. It demonstrates the good agreement between the model and the pilot results. The deviations are generally within ±10% and the error in the prediction is not systematic.

The performance of the hybrid model for desorption calculation is also outlined in figure 3.10. This figure demonstrates the correspondingly good agreement between calculated and measured specific reboiler duties (SRD). Figure 3.10 shows that the deviations between model and experiment are greater above 5 GJ/t CO_2. It is worth noting that these points belong to the "Fall 2010" campaign when the reboiler pressure was above 350 kPa. High reboiler pressure corresponds to higher reboiler temperature, between 116 °C and 128 °C. Consequently, the heat loss to the surroundings may have been greater for these measurements. This would result in slightly higher calculated energy use. Additionally, figure 3.6 underlines the sensitivity of the SRD with respect to model input parameters, e.g. temperature, loading, etc. The certainty of the input parameters is especially important at greater and lower SRD values when small uncertainties in input parameters and design specifications lead to greater differences between the measured and calculated SRD values.
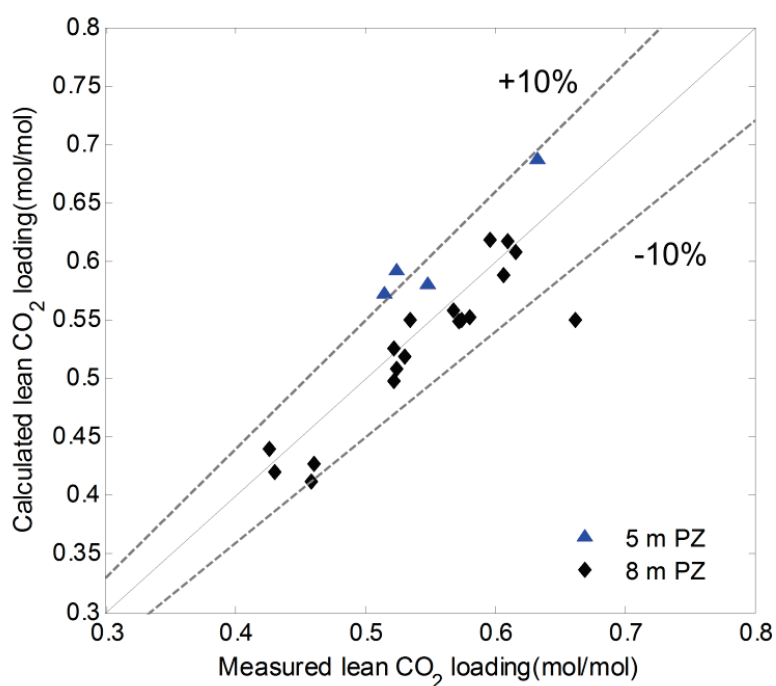
Figure 3.9. Predicted versus measured reboiler lean CO_2 loading (campaigns "Fall 2008" and "Fall 2010")
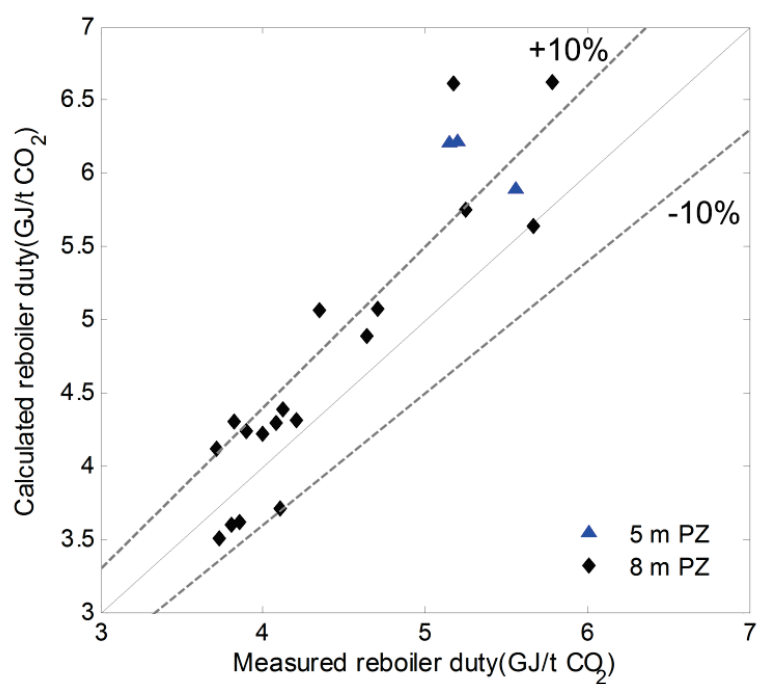

Figure 3.10. Predicted versus measured specific reboiler duty (campaigns "Fall 2008" and "Fall 2010")

The above results are pure predictions without fitting of the mass transfer and/or equilibrium models to the pilot results. Accordingly deviations of 5 – 10% should be expected when comparing model to experimental

data, as illustrated above and discussed in Fosbøl et al. (2014) – Appendix B. It can be concluded that the model predictions are generally in the expected range of accuracy for piperazine CO_2 capture simulation and the performance of the PZ model is similar with the performance of the MEA model.

The importance of solid formation on the rate-based modeling

The change in the PZ solvent capacity with respect to solid/slurry formation is investigated here. The absorption capacity of a 4.5 molal PZ solution is evaluated at two different CO_2 loadings and it is compared with the base case MEA solvent. Two larger scale scenarios, 100 tone CO_2/hr capacity absorber columns, are considered in the present simulation study. The flue gas is specific for a coal fired power plant with a capacity of 400MWe. We assume that the lean solution is available at 0.1 respectively 0.2 mol CO_2/mol PZ loading and at relatively low temperatures, approximately 25 °C. The equivalent loadings (mol CO_2/mol alkalinity) and the concentrations of the PZ and MEA solutions are set equal to keep the systems comparable. Low loading and temperature values are chosen to push the system to precipitate. The aim of the present work is to investigate the effect of solid formation on the absorption capacity rather than to reproduce a real industrial case. However, this simulation scenario might correspond to CO_2 absorption with a mixture of fresh solvent and lean solution.

Figures 3.11 and 3.12 show the simulation results for the two scenarios: 0.1 respectively 0.2 loading. In the present work, the CO_2 mol fraction along the column height, calculated with the hybrid CAPCO2 (hCAPCO2) and the traditional CAPCO2 model are given. The calculations for PZ and MEA are shown. The solid fraction of the liquid phase along the absorber height (red line) is also included in figure 3.11 and 3.12. The solid fraction is calculated with the hCAPCO2 model. Figure 3.11 emphasizes that the mol fraction of CO_2 calculated with the CAPCO2 and the hCAPCO2 model overlap for the 0.2 mol CO_2/mol PZ scenario. A small difference between the two can be noticed at the top of the column, where the loading respectively the temperature of the liquid are the lowest. Note in figure 3.11 that the solid fraction is decreasing exponentially from the top to the bottom of the column. The piperazine dissolves completely from the middle section of the column, when the loading reaches 0.27. As expected, MEA captures less CO_2 than PZ. The flue gas outlet CO_2 composition using PZ is 2.85 mol % while with MEA is 3.89%.

Figure 3.12 shows the behaviour of the model using 0.1 CO_2 loaded solution. It demonstrates that the solid-liquid phase change needs to be included in the absorber calculation. A solid fraction higher than 3% (mol solid/total mol) results in the decrease of the solvent capacity. The precipitated PZ behaves as an inert and the solvent captures less CO_2, as shown in figure 3.12. The outlet gas stream CO_2 composition is 1% lower considering precipitation than with CAPCO2. The hCAPCO2 model estimates an outlet CO_2 concentration of 4.8 mol% while the traditional two-phase model gives 3.68%. The drop in the capture rate with the increase of the solid fraction is expected since the solid PZ does not react with CO_2 and it leads to the

decrease of the driving force for absorption. Figure 3.12 captures a strange however rational phenomena. It shows that the 4.5 molal and 0.05 mol CO_2/mol MEA loaded solution dissolves 13% more CO_2 than PZ. Based on the results, it is recommended to include the solid-liquid phase change in the modeling of precipitating systems. It is not enough to correct the values of thermal properties and partial pressures to system with solids. The real concentrations and fluxes needs to be used for accurate description of precipitating systems.
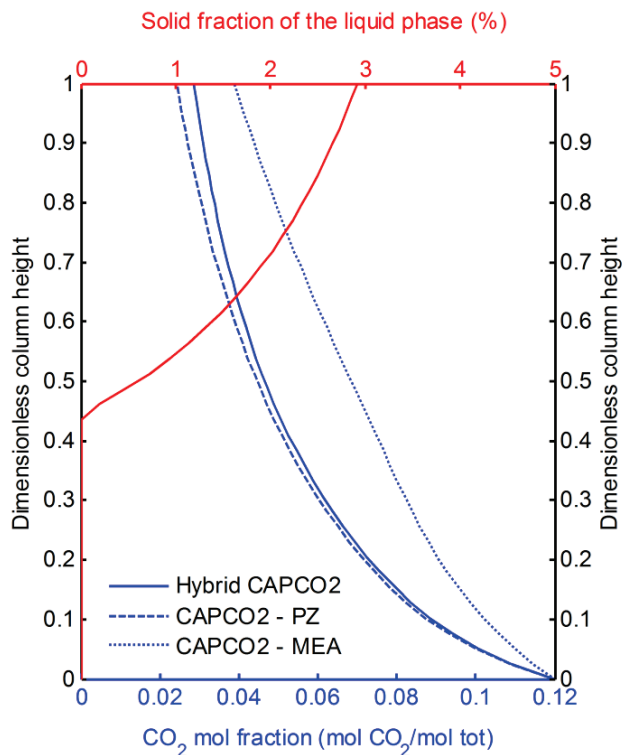

Figure 3.11. CO_2 mol fraction vs. height with CAPCO2 and hCAPCO2 for a lean loading of 0.2
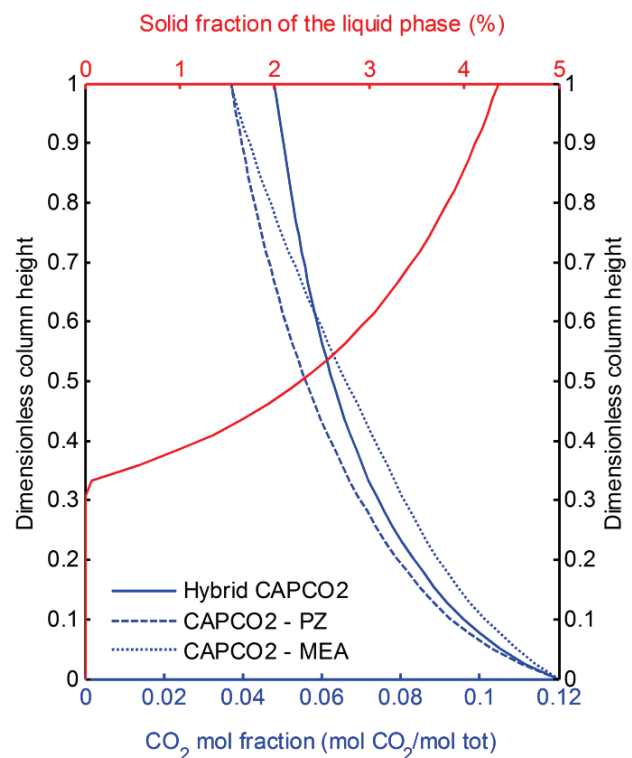
Figure 3.12. CO_2 mol fraction vs. height with CAPCO2 and hCAPCO2 for a lean loading of 0.1

This analysis reveals an unexpected change in the performance of the PZ solvent for the scenario when the solid fraction is higher than 4 % solid PZ in the liquid. It is expected that piperazine combined with organic bases are much more prone to precipitate and awareness should be taken when evaluating such systems. The hybrid model is a first step towards accurate modeling of absorption columns with solid formation. It does not describe the size of the crystals but estimates the conditions with risk of clogging of the capture units. The hybrid model is a first of its kind gas-liquid-solid packed column model for CO_2 absorption and desorption.

3.8.3 Validation of the PZ promoted K$_2$CO$_3$ capture model

The performance of the model for CO$_2$ absorption and desorption using PZ promoted K$_2$CO$_3$ solvent is presented in this section. We show the model predictions against experimental data from the J. J. Pickle Research Center, Austin, USA – the same pilot as the one used for the PZ campaign. The measurements for the PZ/ K$_2$CO$_3$ system were performed by Chen (2007) for two compositions: 1.6 m PZ/ 2.5 m K$_2$CO$_3$ and 2.5 m PZ/ 3.2 m K$_2$CO$_3$. Contrary to the other campaign, the CO$_2$ concentration of the synthetic flue gas was varied from 8% to 18 % and the lean loading of the solvent was changed between 0.07 – 0.30 mol CO$_2$/(2 mol PZ+mol K$_2$CO$_3$). The stripper pressure was also modified during this campaign: 160 kPa for the campaign with 1.6 m PZ/ 2.5 m K$_2$CO$_3$ solvent and the stripper was operated under vacuum conditions, between 34 kPa and 76 kPa when using the 2.5 m PZ/ 3.2 m K$_2$CO$_3$. The implemented mass transfer and physical property correlations have not been verified at vacuum conditions. Consequently, this dataset has been excluded from the desorber validation study. A summary of the main input parameters and column specifications for both absorber and desorber is given in Table 3.5. A detailed description of the experimental setup and operating conditions can be found in Chen (2007).

Table 3.5. Main operating conditions and column specifications for Chen data

Column specifications	
Absorber/Desorber height (m)	6.1
Absorber/Desorber diameter (m)	0.43
Packing type	Flexipac AQ 20
Operating conditions	
Flue gas flow rate (kg/s)	0.16 – 0.28
L/G ratio (kg/kg)	4.6 – 8
Inlet CO$_2$ mol %	8 – 18
PZ concentration (mol/kg water)	1.6 and 2.5
K$_2$CO$_3$ concentration (mol/kg water)	2.5 and 3.2
Lean CO$_2$ loading (mol/mol alk.)*	0.07 – 0.30
Rich CO$_2$ loading (mol/mol alk.)*	0.30 – 0.44
Gas temperature (°C)	40
Lean temperature (°C)	40 – 46
Reboiler temperature (°C)	117 – 118
Reboiler pressure (kPa)	160

mol alk. = 2 mol PZ + mol K$_2$CO$_3$

Figure 3.13 presents the calculated versus the measured CO_2 capture percentage using 1.6 m PZ/ 2.5 m K_2CO_3 and 2.5 m PZ/ 3.2 m K_2CO_3. It shows that the data are scattered but the agreement between model and measurements is deemed satisfactory good. The error between the model and experiment is not systematic. Some of the cases are a bit over- and others are a little under-predicted by the model. The results substantiate that the model is able to catch the effect of the PZ and K_2CO_3 concentration on the absorption rate. The absolute deviations for single runs are up to 20% for both solvents (generally within ±10%), even though the agreement between model and experiment seems to be better for the 1.6 m PZ/ 2.5 m K_2CO_3 solvent. This is confirmed by the MARD of 7.80% and 10.31% for the 1.6 m PZ/ 2.5 m K_2CO_3 respectively 2.5 m PZ/ 3.2 m K_2CO_3 solvents.
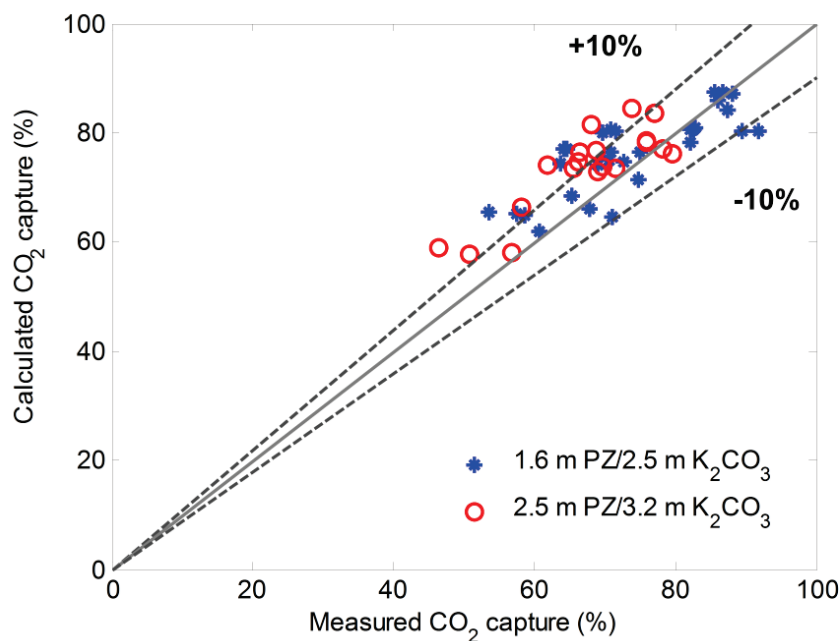

Figure 3.13. Predicted versus measured CO_2 capture percentage

Figures 3.14 and 3.15 show the model comparison against experimental data for CO_2 stripping using 1.6 m PZ/ 2.5 m K_2CO_3 solvent. The experimental CO_2 mass transfer flux is the average between the measured gas side and liquid side CO_2 mass transfer rates. For some cases the deviation between the gas and liquid side measurements was more than 20%. Consequently, deviations of the same magnitude are expected between model predictions and experimental values.

Figure 3.14 shows that the model calculates reasonably well the CO_2 stripping rate. The deviations between predictions and measurements are as expected, generally less than 15% and the absolute average deviation is 13.06%. Similar to the absorber results, some of the data are a bit under- and some are a bit over-predicted by the model. The error is not systematic. Figure 3.15 illustrates that, similar to the above presented results

on MEA and PZ, the agreement between the calculated and measured specific reboiler duty is fairly good, generally within ±10%. Some of the predictions are outside of this ±10% accuracy range at SRD between 8 and 14 GJ/t CO_2. A thorough analysis has been performed; however no correlations has been found between deviations and input parameters such as reboiler temperature/pressure, flow rate, rich CO_2 loading, etc. It suggests that the error is not systematic. A possible explanation is the sensitivity of SRD with respect to input parameters, as presented in figure 3.6, combined with significant uncertainties of measurements, as discussed by Chen (2007).
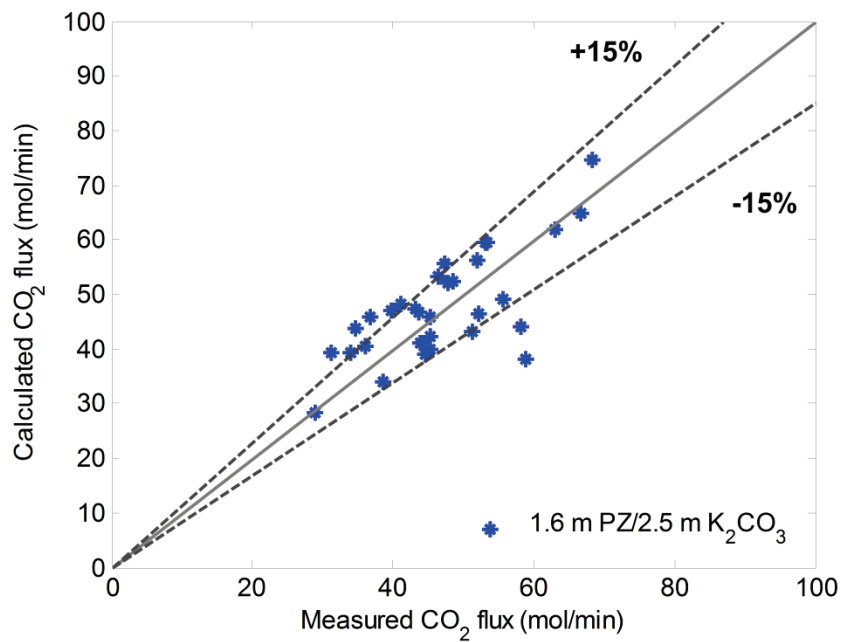

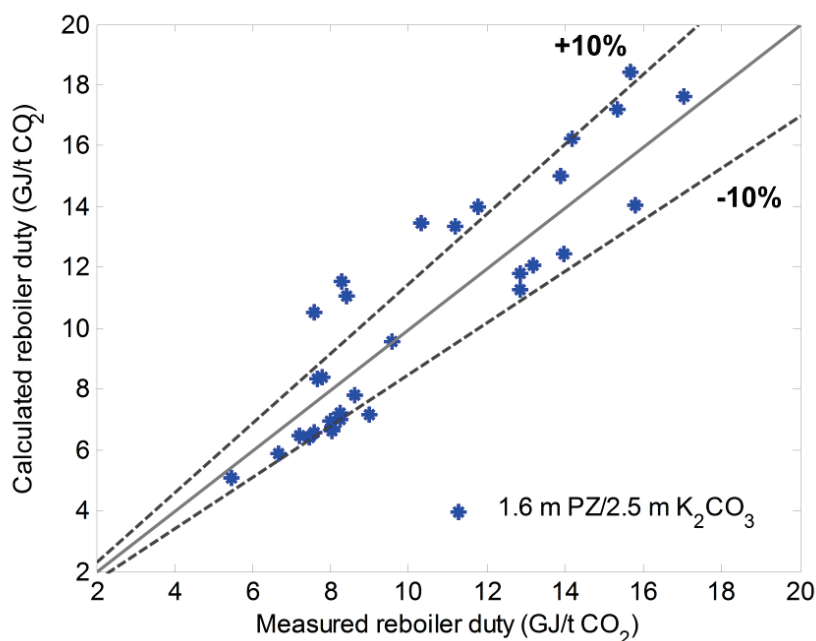Figure 3.14. Predicted versus measured CO_2 desorption rate

Figure 3.15. Predicted versus measured specific reboiler duty

Overall, the agreement between model and experiment is deemed satisfactory for both, CO_2 absorption and desorption simulation, considering the wide ranges of flue gas CO_2 concentrations, CO_2 loadings, L/G ratios and experimental error respectively.

3.8.4 Validation of the CA enhanced MDEA capture model

The validation of the model for CO_2 absorption using MDEA and CA enhanced MDEA (CA/MDEA) is presented in this section. We show model and experimental CO_2 loading and temperature profiles for two campaigns: (campaign 1) with MDEA and (campaign 2) with CA enhanced MDEA. Campaign 2 was divided in two: (campaign 2A) fixed packing height of 10 m and (campaign 2B) packing heights of 2, 4, 6, 8, and 10 m. Both of the campaigns were run with a synthetic flue gas, saturated at the absorber's inlet temperature. The synthetic saturated flue gas contained various CO_2 percent's from 3.6% to 13.6%. The low CO_2 content (3.6 – 5.3% CO_2) resembles a flue gas from a natural gas combined cycle power plant (NGCC) and the high CO_2 concentration (> 11% CO_2) corresponds to a flue gas from a coal fired power plant. The MDEA concentration was 30 wt.% for these campaigns and the CA/MDEA campaign was run with 0.05 mol/m^3 CA. These campaigns covered various liquid to gas (L/G) ratios and different inlet lean CO_2 loadings. Campaign 1 was run with fresh MDEA solvent and its inlet lean loading was between 0.01 and 0.09 mol/mol. Most of the experiments in campaign 2 were performed with a loaded solution of 0.2 – 0.25 mol CO_2/mol MDEA. These campaigns were carried out at Technical University of Denmark by Ph.D. student Arne Gladis. Table 3.6 summarizes the main design specifications and operating conditions. Further

details regarding the experimental setup and analysis can be found in Jensen (2015) and Sonderby et al. (2013).

Table 3.6. Main operating conditions and column specifications for MDEA

Column specifications		
Absorber packing height (m)	2 – 10	
Absorber diameter (m)	0.1	
Packing type	Mellapak 250Y	
Operating conditions	**Campaign 1**	**Campaign 2**
Flue gas flow rate (kg/h)	30	30
L/G ratio (kg/kg)	2.4 – 6.6	2.3 – 5.9
Inlet CO_2 mol %	4.3 – 13.1	3.6 – 13.5
MDEA concentration (wt.%)	30	30
CA concentration (mol/m^3)	-	0.05
Lean CO_2 loading (mol/mol)	0.01 – 0.09	0.19 – 0.34
Gas temperature (^{o}C)	25 – 30	25 – 30
Lean temperature (^{o}C)	30 – 43	25 – 42

Jensen (2015) in collaboration with Arne Gladis experimentally determined the liquid hold-up and the effective mass transfer area of the pilot absorber. They concluded that the effective mass transfer area of the absorber's packing, Mellapak 250Y is very small, around 100 m^2/m^3 with a liquid holdup of 3% to 8% for flow rates between 50 and 200 kg/h. These values are expected to hold for the MDEA and the CA/MDEA campaigns since the inlet conditions, i.e. flow rate, gas composition, pressure range were similar. Accordingly, first we evaluated the accuracy of the Rocha et al. (1996, 1993) respectively Billet and Schultes (1999) mass transfer models for simulation of the pilot absorber. The adjustable parameters of these models originate from Rocha et al. (1996, 1993) respectively Billet and Schultes (1999). This analysis showed that the Rocha model over-predicts both parameters, i.e. effective mass transfer area and liquid hold-up. The effective mass transfer area of the Rocha model can be adjusted by decreasing the surface enhancement factor (FSE) from the original value (0.35) to 0.17, but the calculated liquid hold-up remains double of the experimental value. The Billet and Schultes (1999) model gives reasonable fit for the liquid hold-up using the original parameters from Billet and Schultes (1999) and the calculated effective surface area can be corrected reasonably well by setting the theoretical surface area of the packing to 150 m^2/m^3. Note that both models have a strong dependency between effective surface area and L/G ratio. As a result, they over-predict the effective surface area with roughly 30% for L/G ratios above 4 kg/kg. Based on the above, we decided to use the Billet and Schultes (1999) model to simulate the pilot absorber.

Figure 3.16 shows the calculated versus measured rich CO_2 loading for campaigns 1 and 2. This figure illustrates that generally the agreement between model and experiment is good with both solvents (MDEA and CA/MDEA) nevertheless of the flue gas CO_2 concentration. Campaign 2B, performed with packing heights of 2, 4, 6, 8 and 10 m is a little over-predicted by the model. Two tests were performed for each height with constant flue gas flow rate and L/G ratios of 2.4 kg/kg and 5.6 kg/kg. The analysis revealed that the error is not systematic neither with respect to packing height nor L/G ratio; thus the model describes fairly well the effect of height on CO_2 absorption. The performance of the model is further illustrated in figures 3.17 and 3.18. These figures show the variation of CO_2 loading versus the column height using MDEA and CA/MDEA solvents. They outline that the model and experiment almost overlap for flue gas CO_2 concentrations of 3.6% to 5% and the model is less accurate at high CO_2 concertations, especially for CA/MDEA solvent (see figure 3.18). Figure 3.18 on CA/MDEA shows that the model over-predicts the CO_2 loading at the top and under-predicts at the bottom of the column at L/G ratio of 2.3 kg/kg. This behaviour may be related to the bicarbonate inhibition of the enzymatic effect, eq. (2.49). Note that the bicarbonate concertations decreases from bottom to top, proportional to CO_2 loading. An offset in this inhibition factor results in an offset in the calculated reaction rate and therefore it leads to an offset in CO_2 absorption rate respectively CO_2 loading. The simplified reaction mechanism, the kinetic parameters and the enhancement factor model strongly influences the shape of the concentration and temperature profiles, as shown in the benchmarking analysis using MEA, figures 3.7A and 3.7B (Fosbøl et al., 2014) – Appendix B .

Furthermore, the discrepancy between the model and experiment in figure 3.18 could be related to the hydraulic and mass transfer models. The benchmarking study on MEA showed that the mass transfer correlation significantly influences the concentration and temperature along the column height. Figure 3.7A shows that some of the models (DTU, TUHH, SINTEF and IFPEN) give linear concentration profiles other predicts a much steeper absorption at the top (EDF, TNO) with the greatest difference in the mid-section of the column. Note that similar agreement can be expected when comparing model to experiment. Additionally, Cormos and Gaspar (2012) and Gaspar and Cormos (2012) showed that the composition and temperature profiles, especially in the middle section of the column, strongly depend on the mass transfer and hydraulic model. The choice of model used to describe the liquid hold-up in the column exerts a significant influence on the mass transfer area and the mass transfer coefficients. Therefore, accurate prediction of the mid-section may require additional adjustment of the mass transfer model, reaction kinetics and re-evaluation of assumptions, e.g. liquid film reaction, equilibrium assumption at the interface, negligible heat loss to the surrounding, etc.
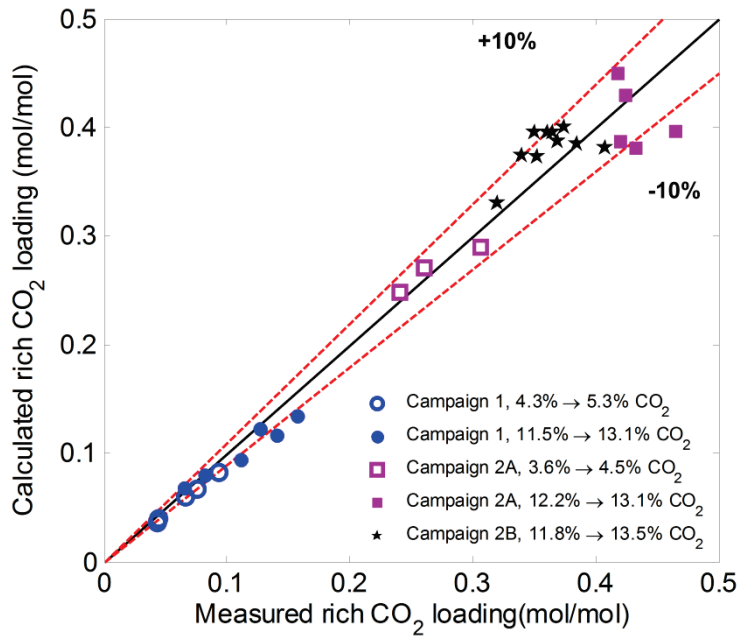
Figure 3.16. Calculated versus measured rich CO_2 loading using MDEA and CA/MDEA

Figures 3.19 and 3.20 shows the calculated and measured temperature profiles for campaign 2B at L/G ratios of 2.4 kg/kg respectively 5.6 kg/kg. These results corresponds to packing's heights of 2, 4, 6, 8 and 10 m using a flue gas with approximately 12.5% CO_2 and an inlet lean loading between 0.20 and 0.24 mol/mol. Note that CO_2 loading along the absorber's height were not measured during this campaign. Figure 3.19 on L/G =2.4 kg/kg shows that the model predicts very well the variation of temperature along short to tall columns, i.e. when using a packing height of 2, 4, 6, 8 and 10 m. Figure 3.20 on L/G=5.6 kg/kg shows that the model predicts a large and extended bulk over the height while the experiments suggest a 1 – 2°C increase in the temperature compared to the measured values for L/G=2.4 kg/kg (figure 3.19). Note that the calculated effective surface area for all of the runs in figure 3.19 is roughly 150 m^2/m^3 compared to the experimentally determined 100 m^2/m^3 (Jensen, 2015). Over-prediction of the mas transfer area results in higher absorption rate and therefore more heat of absorption; thus higher temperature. This is confirmed by the results in figure 3.16, campaign 2B.
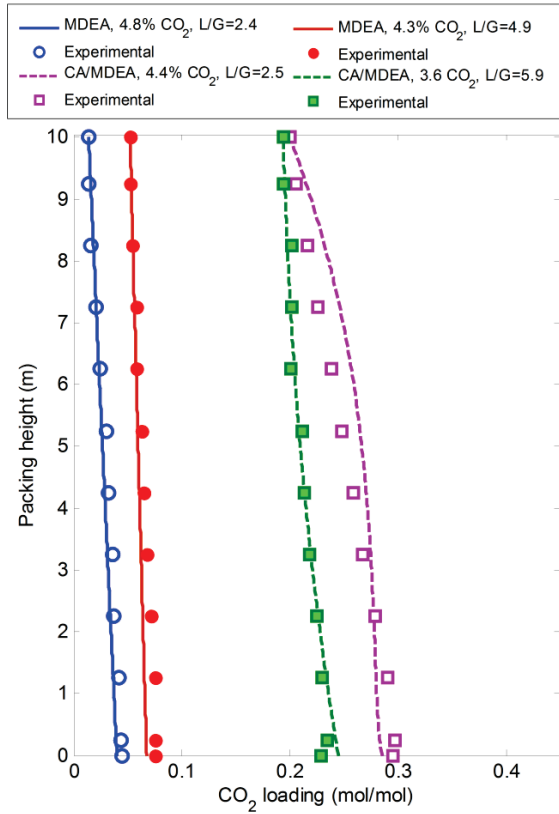
Figure 3.17. Measured and calculated CO_2 loading versus height using MDEA and CA/MDEA at low flue gas CO_2 concentrations
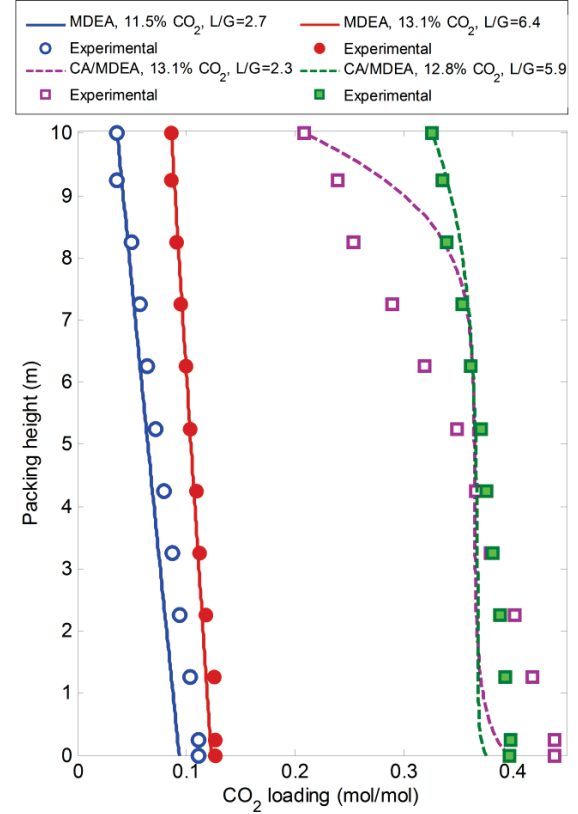
Figure 3.18. Measured and calculated CO_2 loading versus height using MDEA and CA/MDEA at high flue gas CO_2 concentrations
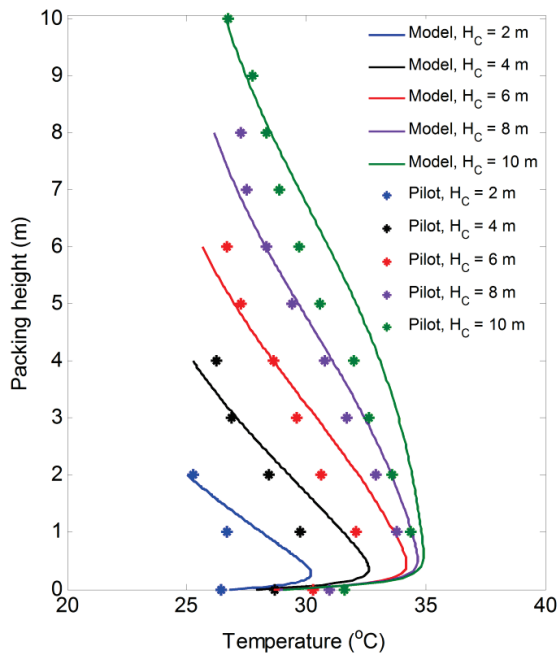

Figure 3.19. Measured and calculated temperature profiles for heights of 2, 4, 6, 8 and 10 m using CA/MDEA at L/G = 2.4 kg/kg (approx. 12.5% CO_2)
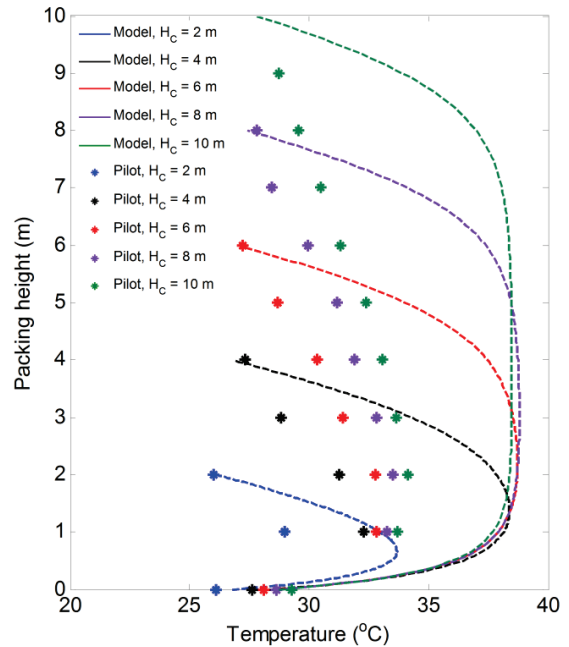

Figure 3.20. Measured and calculated temperature profiles for heights of 2, 4, 6, 8 and 10 m using CA/MDEA at L/G = 5.6 kg/kg (approx. 12.5% CO_2)

129

It can be concluded that the model generally predicts well the CO_2 mass transfer rate in the absorber using MDEA respectively CA enhanced MDEA. The relative deviations between calculated and measured lean outlet loadings are within ±10% for CO_2 flue gas concentrations of 3.6% to 13.5%. Thus, this model can be used to simulate flue gas cleaning of natural gas combined cycle and coal based power plants. However, awareness must be taken when using any model for column scale-up/design. These simulations showed that for some cases the model deviates from the measured composition and temperature profiles; thus it could lead to over- or under-predicted height required to capture a specified amount of CO_2. It is recommended to investigate the sensitivity of the composition and temperature profiles with respect to mass transfer, hydraulic, thermodynamic and kinetic sub-models for a wide range of operating conditions in order to increase confidence in model based designs.

3.9 Plant-wide simulation of post-combustion capture

The goal of this work goes beyond standalone simulation and validation of CO_2 absorption and desorption calculations. It aims to present the details of linking advanced models to process simulation packages and to evolve towards simulation of a power plant with integrated CO_2 capture. Power plant simulations, CO_2 capture estimations, and CO_2 transport calculations need to be connected for reliable process design, scale-up and techno-economic performance optimization. A tool connecting in-house models to process simulators and linking different process simulators has been demonstrated for integrated simulation of a power plant and CO_2 capture unit. This task was part of the EU FP7 OCTAVIUS project (Optimization of CO_2 Capture Technology Allowing Verification and Implementation at Utility Scale) which aims to demonstrate integrated concepts for zero emission power plants, covering all the components needed for power generation and CO_2 capture. A detailed description of the developed interface can be found in the publicly available OCTAVIUS deliverable 11.4. Here the focus being validation of the plant-wide CO_2 capture model.

To simulate the overall capture process using the CAPCO2 in-house model for CO_2 absorption and desorption, a generic communication protocol was implemented. The communication basis is CAPE-OPEN. CAPE-OPEN provides a set of common interfaces, which are currently available in most flowsheet software for unit operations and thermodynamic calculations. It is a tool which enables automatic transfer of calculation results between simulation engines, in-house unit operation models, and property packages. The methodology of the CAPE-OPEN interface implementation for the CAPCO2 model is described in Appendix C. In addition, the CAPCO2 model has been connected to Aspen Plus using the Aspen Custom Modeler (ACM) language. ACM enables incorporation of custom models into Aspen Plus, Aspen HYSYS and Aspen Dynamics. This requires that the user model (CAPCO2 model) is in accordance with the ACM specifications

and exposes all of the required functionalities. It is similar to CAPE-OPEN, but only implemented in the AspenTech software. The implementation of the column model in ACM is presented in Appendix D.

Both of the interfaces, CAPE-OPEN and ACM have been tested for post-combustion simulation in Aspen Plus using the CAPCO2 rate based model in conjunction with Aspen Plus built-in heat exchangers, mixers, boilers, and compressors. Both interfaces proved to work well, however the ACM implementation was more stable in Aspen Plus compared to the CAPE-OPEN implementation. Moreover, the CAPE-OPEN module failed to communicate with the extended UNIQUAC model in Aspen Plus, forcing us to use the electrolyte NRTL model for thermodynamic calculations. Consequently, we chose the ACM implementation of CAPCO2 in Aspen Plus with the extended UNIQUAC thermodynamic model for plant-wide simulation of CO_2 capture.

In this section, the developed ACM interface is demonstrated for closed-loop simulation of the pilot plant presented by Notz et al. (2012) to investigate the accuracy of the developed model for simulation of the complete post-combustion capture unit. This is an essential step towards reliable overall process scale-up, design and optimization.

3.9.1 Validation of the CO_2 post-combustion capture model

The closed-loop simulation of CO_2 post-combustion capture and comparison to pilot plant data is discussed here. The pilot data originates from Notz et al. (2012). This plant consists of interconnected absorber and stripper towers which are modelled using the CAPCO2 in-house rate-based model and the water-wash sections, represented by Aspen Plus flash units. Additional equipment for heat exchange, pressure change and mixing are represented by built-in units. The CAPCO2 model is incorporated with Aspen Plus units using the ACM interface.

Figure 3.21 shows the Aspen Plus flowsheet of the pilot plant and the main inlet parameters for experimental run 2. This test was performed using a flue gas with 11% CO_2, saturated with water at the inlet temperature of 48°C. The flue gas was cleaned with a 30 wt.% MEA solution with an inlet loading of 0.308 mol/mol. The solvent was regenerated at approximately 120°C and 2 bars. Both of the columns were equipped with Sulzer Mellapak 250Y structured packing. For more details we refer to the work of Notz et al. (2012).

Contrary to standalone simulation of an absorber or desorber column, only the flue gas stream has to be specified for closed-loop simulation. The lean inlet stream originates from the desorber. The MEA and water make-up flow rates are calculated by the Aspen Plus "Balance" flowsheeting option. In this work, the lean solvent flow rate initially was set to the measured value, 200 kg/h, then it was updated by Aspen Plus while converging the closed-loop simulation. In practice, the lean flow rate is controlled to achieve a specified CO_2

capture percentage, however in this work it is left as an independent variable and used for evaluation of the model's accuracy.
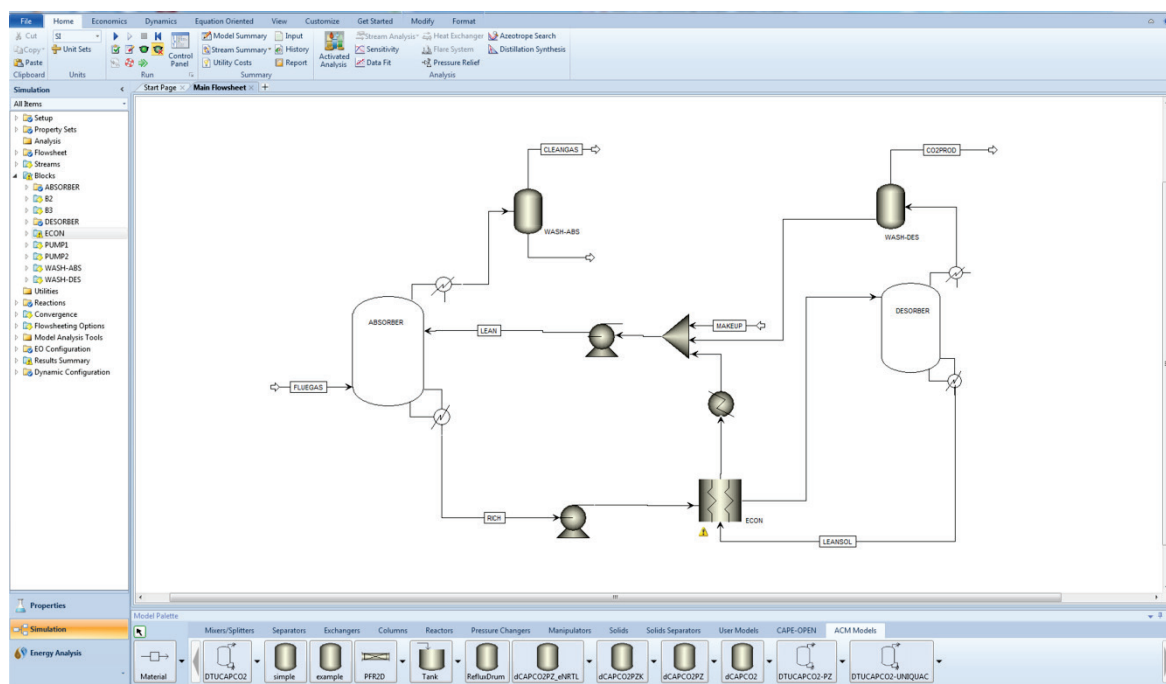
Figure 3.21. Aspen Plus flowsheet and main inlet parameters for run 2 (Notz et al., 2012).

Figures 3.22 and 3.23 show the measured and simulated concentrations and temperatures versus the height of the absorber respectively the height of the desorber. The experimental data corresponds to run 2 in Notz et al. (2012). These figures underline the fairly good agreement between measured and calculated concentrations and temperatures. They illustrate how the model describes well the characteristic shapes of the concentration respectively temperature curves. The model slightly over-predicts the CO_2 concentration of the liquid phase and a little under-predicts the temperature for absorption and desorption. The absolute relative deviations between the measured and calculated concentrations are less than 10% for all of the points. The maximum difference between the experimental and simulated temperatures is 5.6 ℃ and 3.6 ℃ for the absorption and desorption respectively. These results are consistent. Lower CO_2 absorption rate produces less heat and lower CO_2 desorption rate requires less heat for stripping.
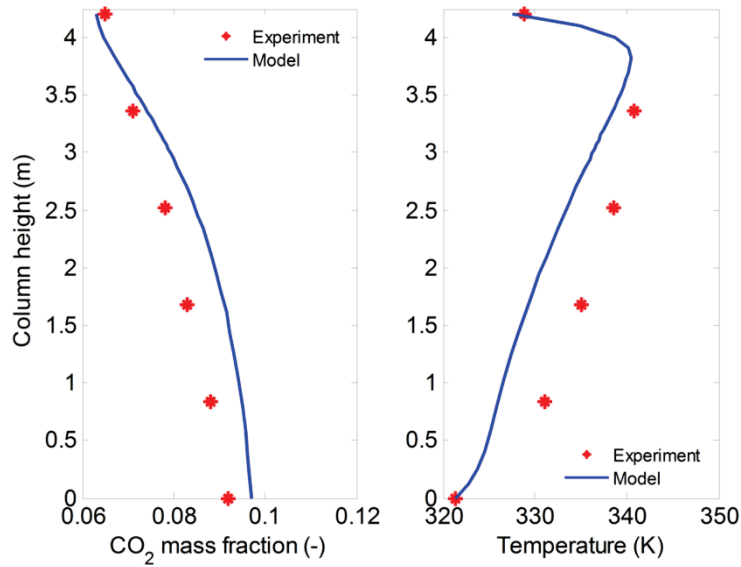
Figure 3.22. Absorber liquid phase CO_2 concentration and temperature versus height
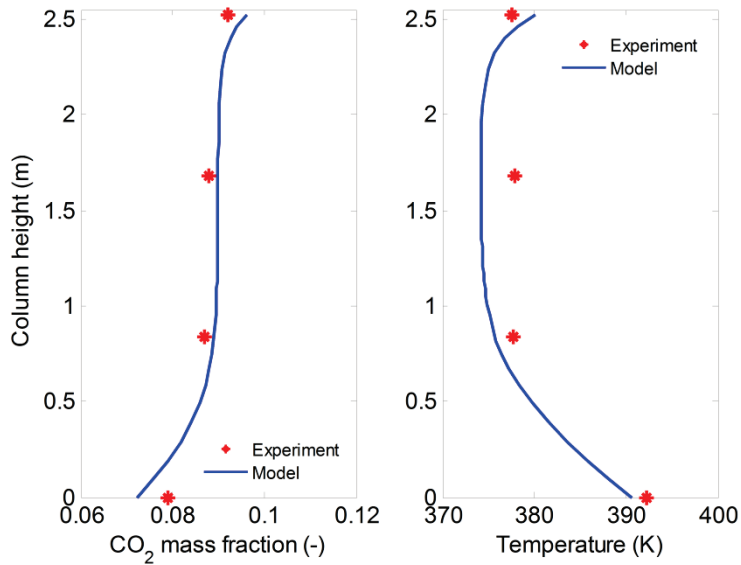
Figure 3.23. Desorber liquid phase CO_2 concentration and temperature versus height

Table 3.7 summarizes measured and calculated values for some key parameters used for confirming the agreement between the plant-wide model and experimental measurements. Parameters similar to the OCTAVIUS benchmarking activities are used for model evaluation. This table emphasizes the very good agreement between model and experiment. The relative deviation between the calculated and experimental solvent flow rate is -2.1%; the lean and rich loadings are also correctly predicted, within an accuracy of 5%. The good fit is further confirmed by the small deviations between calculated and experimentally determined

CO_2 removal rates, absorbed CO_2 flow rate and stripper overhead CO_2 composition. The pressure drop along the absorber height is under-predicted by 54%. It is calculated by the Rocha et al. (1993) model, eqs. (3.9) and (3.10). Note that various factors, such as packing, fan, preferential channels, etc. contribute to the pressure drop. In the present study, only the pressure drop caused by the packing is considered. This can result in large deviations between measurements and experiments.

Table 3.7. Overall process performance parameters

Parameter	Measured	Calculated	RD (%)*
Lean inlet solvent flow rate (kg/h)	200.00	195.80	-2.10
Lean loading (mol CO_2/mol MEA)	0.3075	0.3079	0.13
Rich loading (mol CO_2/mol MEA)	0.4655	0.4852	4.22
CO_2 removal rate (%)	51.32	54.65	6.50
Absorbed CO_2 flow rate (kg/h)	6.11	6.53	6.83
Stripper O/H CO_2 composition (mol %)	0.990	0.989	-0.09
Pressure drop in absorber (mbar)	8.03	3.70	-53.92
Reboiler heat duty (W)	7944.5	7735.75	-2.63
Specific reboiler duty (GJ/t CO_2)	3.98	3.82	-4.02
Heat duty of lean-rich heat exchanger (W)	15425.7	14789.4	-4.12

RD (%) = (Calculated-Measured)/Measured · 100

The specific reboiler duty (SRD) is very accurately estimated by the model. The deviation between model and experiment is -4.02%. Note that this value includes heat losses as calculated by Notz et al. (2012). The SRD is often used for performance evaluation and its accuracy is essential to increase confidence in simulation, design and optimization. The accuracy of heat duty calculations is further exemplified by the good agreement between experimental and simulated heat duty of the lean-rich cross heat exchanger. In conclusion, it has been shown that the developed plant-wide model is reliable for process simulation and it can be used for further design and optimization activities.

3.10 Conclusions

A general rate based model for CO_2 absorption and desorption using MEA, PZ, PZ promoted K_2CO_3 and enzyme promoted MDEA (CA/MDEA) has been developed and validated against experimental data. The model is built around differential mass and energy conservation equations coupled with algebraic equations for hydraulic and mass transfer characteristics and the extended UNIQUAC thermodynamic model. It uses the General Model (GM) to determine the CO_2 mass transfer rate across the gas-liquid interface. It also

implements the Rocha et al. (1993) equation to include pressure drop in the conservation equations. Furthermore, a CO_2 capture model for solid forming solvents has been introduced and applied to PZ. Compared to traditional CO_2 capture models, the developed model directly includes the solid-liquid phase change in the flow and transport equations. Finally, the CO_2 post-combustion process has been simulated in closed-loop and compared to experimental data using the CAPCO2 model in combination with Aspen Plus built-in units.

The agreement between model predictions and experimental measurements is good. The relative deviations between simulated and measured CO_2 capture percentage, lean reboiler loading and specific reboiler duty are generally within ±10% for all of the solvents. Also the agreement between experimental and simulated CO_2 concentration and temperature profiles through the column is good, in the expected range of variability of error (Fosbøl et al., 2014). The model catches well the specific shape of the profiles. In addition, key performance parameters for the closed-loop process, e.g. LG-ratio, heat duty, CO_2 loading, stripper overhead composition, etc. confirmed the very good agreement between plant-wide post-combustion capture model and pilot plant experiment. Furthermore, an analysis performed with the hybrid capture model revealed a surprising change in the performance of the PZ solvent: 5% solid formation reduces the CO_2 capture rate with 13%. Therefore, it demonstrates that an accurate description of the precipitation phenomenon is essential for realistic and accurate modeling of CO_2 absorption.

References

Aroonwilas, A., Veawab, A., 2004. Characterization and comparison of the CO2 absorption performance into single and blended alkanolamines in a packed column. Ind. Eng. Chem. Res. 43, 2228–2237. doi:10.1021/ie0306067

Billet, R., Schultes, M., 1999. Prediction of mass transfer columns with dumped and arranged packings - Updated summary of the calculation method of Billet and Schultes. Chem. Eng. Res. Des. 77, 498–504. doi:10.1205/026387699526520

Bishnoi, S., Rochelle, G.T., 2002. Absorption of carbon dioxide in aqueous piperazine/methyldiethanolamine. AIChE J. 48, 2788–2799. doi:10.1002/aic.690481208

Chen, E., 2007. Carbon dioxide absorption into piperazine promoted potassium carbonate using structured packing. ProQuest.

Cheng, S., Meisen, A., Chakma, A., 1996. Predict amine solution properties accurately. Hydrocarb. Process. Hydrocarb. Process 75, 81–84.

Cormos, A.-M., Gaspar, J., 2012. Assessment of mass transfer and hydraulic aspects of CO2 absorption in packed columns. Int. J. Greenh. Gas Control 6, 201–209. doi:http://dx.doi.org.globalproxy.cvt.dk/10.1016/j.ijggc.2011.11.013

Cullinane, J.T., Rochelle, G.T., 2006. Kinetics of carbon dioxide absorption into aqueous potassium carbonate and piperazine. Ind. Eng. Chem. Res. Ind.Eng.Chem.Res, Ind Eng Res, Ind Eng Chem Res, Ind. Eng. Chem. Res. 45, 2531–2545. doi:10.1021/ie050230s

Cullinane, J.T.T., Rochelle, G.T., 2004. Carbon dioxide absorption with aqueous potassium carbonate promoted by piperazine. Chem. Eng. Sci. 59, 3619–3630. doi:http://dx.doi.org/10.1016/j.ces.2004.03.029

Danckwerts, P. V, 1970. Gas-Liquid reactions. McGraw-Hill Chem. Eng. Ser.

Dang, H.Y., Rochelle, G.T., 2003. CO_2 absorption rate and solubility in monoethanolamine/piperazine/water. Sep. Sci. Technol. 38, 337–357. doi:10.1081/SS-12016678

Darde, V., Maribo-Mogensen, B., van Well, W.J.M., Stenby, E.H., Thomsen, K., 2012. Process simulation of CO_2 capture with aqueous ammonia using the Extended UNIQUAC model. Int. J. Greenh. Gas Control 10, 74–87. doi:10.1016/j.ijggc.2012.05.017

Dugas, R., Rochelle, G., 2009. Absorption and desorption rates of carbon dioxide with monoethanolamine and piperazine. Greenh. Gas Control Technol. 9 Proc. 9th Int. Conf. Greenh. Gas Control Technol. (GHGT-9), 16–20 Novemb. 2008, Washingt. DC, USA 1, 1163–1169. doi:http://dx.doi.org/10.1016/j.egypro.2009.01.153

Dugas, R.E., Rochelle, G.T., 2011a. CO_2 Absorption Rate into Concentrated Aqueous Monoethanolamine and Piperazine. J. Chem. Eng. Data 56, 2187–2195. doi:10.1021/je101234t

Dugas, R.E., Rochelle, G.T., 2011b. Modeling CO_2 absorption into concentrated aqueous monoethanolamine and piperazine. Chem. Eng. Sci. 66, 5212–5218. doi:10.1016/j.ces.2011.07.011

Faramarzi, L., Kontogeorgis, G.M., Michelsen, M.L., Thomsen, K., Stenby, E.H., 2010. Absorber Model for CO_2 Capture by Monoethanolamine. Ind. Eng. Chem. Res. 49, 3751–3759. doi:10.1021/ie901671f

Faramarzi, L., Kontogeorgis, G.M., Thomsen, K., Stenby, E.H., 2009. Extended UNIQUAC model for thermodynamic modeling of CO_2 absorption in aqueous alkanolamine solutions. Fluid Phase Equilib. 282, 121–132. doi:10.1016/j.fluid.2009.05.002

Fosbøl, P.L., Gaspar, J., Ehlers, S., Kather, A., Briot, P., Nienoord, M., Khakharia, P., Le Moullec, Y., Berglihn, O.T., Kvamsdal, H.M., 2014. Benchmarking and comparing first and second generation post combustion CO_2 capture technologies. Energy Procedia 63, 27–44. doi:10.1016/j.egypro.2014.11.004

Fosbøl, P.L., Maribo-Mogensen, B., Thomsen, K., 2013. Solids Modelling and Capture Simulation of Piperazine in Potassium Solvents. GHGT-11 37, 844–859. doi:http://dx.doi.org/10.1016/j.egypro.2013.05.177

Fosbøl, P.L., Thomsen, K., Stenby, E.H., 2009. Energy demand for CO_2 solvent regeneration Proceeding, 242–252.

Frailie, P., Plaza, J., Van Wagener, D., Rochelle, G.T., 2011. Modeling piperazine thermodynamics. Energy Procedia 4, 35–42. doi:10.1016/j.egypro.2011.01.020

Frailie, P.T., 2014. Modeling of carbon dioxide absorption/stripping by aqueous methyldiethanolamine/piperazine.

Freeman, S.A., Dugas, R., Van Wagener, D.H., Nguyen, T., Rochelle, G.T., 2010. Carbon dioxide capture with concentrated, aqueous piperazine. Int. J. Greenh. Gas Control 4, 119–124. doi:10.1016/j.ijggc.2009.10.008

Gabrielsen, J., 2007. CO_2 Capture from Coal Fired Power Plants. Book Partner, Nørhaven Digital, Copenhagen, Denmark.

Gabrielsen, J., Michelsen, M.L., Stenby, E.H., Kontogeorgis, G.M., 2006. Modeling of CO_2 absorber using an AMP solution. AIChE J. 52, 3443–3451. doi:10.1002/aic.10963

Gaspar, J., Cormos, A.-M., 2012. Dynamic modeling and absorption capacity assessment of CO_2 capture process. Int. J. Greenh. Gas Control 8, 45–55. doi:10.1016/j.ijggc.2012.01.016

Gaspar, J., Fosbøl, P.L., 2015. A general enhancement factor model for absorption and desorption systems: A CO2 capture case-study. Chem. Eng. Sci. 138, 203–215. doi:http://dx.doi.org.globalproxy.cvt.dk/10.1016/j.ces.2015.08.023

Gaspar, J., von Solms, N., Thomsen, K., Fosbøl, P.L., 2016. Multivariable Optimization of the Piperazine CO2 Post-Combustion Process. Energy Procedia 86, 229–238. doi:10.1016/j.egypro.2016.01.024

Gaspar, J., Waseem Arshad, M., Ask Blaker, E., Langseth, B., Hansen, T., Thomsen, K., von Solms, N., Fosbøl, P.L., 2014. A low energy aqueous ammonia CO2 capture process. Energy Procedia 63, 614–623. doi:10.1016/j.egypro.2014.11.066

Glibstrup, J., 2015. Enzymes promoted rate-based amine CO2 capture model development and simulation.

Higbie, R., 1935. The rate of absorption of a pure gas into a still liquid during short periods of exposure. Trans. Am. Inst. Chem. Eng. 31, 365–389.

Jensen, M.W., 2015. Pilot Scale Experimental Studies and Simulation of Dynamic Mode CO2 Capture.

Kenig, E.Y., Schneider, R., Górak, A., 2001. Reactive absorption: optimal process design via optimal modelling. Chem. Eng. Sci. 56, 343–350.

Khan, F.M., Krishnamoorthi, V., Mahmud, T., 2011. Modelling reactive absorption of CO2 in packed columns for post-combustion carbon capture applications. Chem. Eng. Res. Des. 89, 1600–1608. doi:10.1016/j.cherd.2010.09.020

Knudsen, J.N., Jensen, J.N., Vilhelmsen, P.-J., Biede, O., 2009. Experience with CO2 capture from coal flue gas in pilot-scale: Testing of different amine solvents. Energy Procedia 1, 783–790. doi:10.1016/j.egypro.2009.01.104

Koronaki, I.P., Prentza, L., Papaefthimiou, V., 2015. Modeling of CO2 capture via chemical absorption processes − An extensive literature review. Renew. Sustain. Energy Rev. 50, 547–566. doi:10.1016/j.rser.2015.04.124

Lawal, A., Wang, M., Stephenson, P., Yeung, H., 2009. Dynamic modelling of CO2 absorption for post combustion capture in coal-fired power plants. Fuel 88, 2455–2462. doi:10.1016/j.fuel.2008.11.009

LeVeque, R.J., 2007. Finite difference methods for ordinary and partial differential equations: steady-state and time-dependent problems. Siam.

Lu, Y., Ye, X., Zhang, Z., Khodayari, A., Djukadi, T., 2011. Development of a carbonate absorption-based process for post-combustion {CO2} capture: The role of biocatalyst to promote {CO2} absorption rate. Energy Procedia 4, 1286–1293. doi:http://dx.doi.org/10.1016/j.egypro.2011.01.185

Mason, 1958. Approximate formula for the thermal conductivity of gas mixtures. Phys. Fluids 1, 361 – 369.

Mores, P., Scenna, N., Mussati, S., 2011. Post-combustion CO2 capture process: Equilibrium stage mathematical model of the chemical absorption of CO2 into monoethanolamine (MEA) aqueous solution. Chem. Eng. Res. Des. 89, 1587–1599. doi:10.1016/j.cherd.2010.10.012

Nielsen, H.L., 2015. Rate based model development and simulation of CO2 absorption and desorption columns using piperazine promoted potassium carbonate.

Notz, R., Mangalapally, H.P., Hasse, H., 2012. Post combustion CO2 capture by reactive absorption: Pilot plant description and results of systematic studies with MEA. Int. J. Greenh. Gas Control 6, 84–112. doi:http://dx.doi.org/10.1016/j.ijggc.2011.11.004

Onda, K., TAKEUCHI, H., OKUMOTO, Y., 1968. MASS TRANSFER COEFFICIENTS BETWEEN GAS AND LIQUID PHASES IN PACKED COLUMNS. J. Chem. Eng. Japan 1, 56–62. doi:10.1252/jcej.1.56

Oyenekan, B.A., Rochelle, G.T., 2009. Rate modeling of CO2 stripping from potassium carbonate promoted by piperazine. Int. J. Greenh. Gas Control 3, 121–132. doi:http://dx.doi.org/10.1016/j.ijggc.2008.06.010

Pandya, J.D., 1983. Adiabatic gas absorption and stripping with chemical reaction in packed towers. Chem. Eng. Commun. 19, 343–361.

Pintola, T., Tontiwachwuthikul, P., Meisen, A., 1993. Simulation of pilot plant and industrial CO2-MEA absorbers. Gas Sep. Purif. 7, 47–52. doi:10.1016/0950-4214(93)85019-R

Plaza, J.M., 2011. Modeling of Carbon Dioxide Absorption using Aqueous Monoethanolamine, Piperazine and Promoted Potassium Carbonate. University of Texas.

Plaza, J.M., Rochelle, G.T., 2011. Modeling pilot plant results for CO2 capture by aqueous piperazine. Energy Procedia 4, 1593–1600. doi:10.1016/j.egypro.2011.02.029

Poulsen, N.S., 2014. Model development for promoted CO2 capture.

Reid, R.C., Prausnitz, J.M., Poling, B.E., 1987. The properties of gases & liquids. McGraw-Hill.

Rocha, J.A., Bravo, J.L., Fair, J.R., 1996. Distillation columns containing structured packings: A comprehensive model for their performance .2. Mass-transfer model. Ind. Eng. Chem. Res. 35, 1660–1667. doi:10.1021/ie940406i

Rocha, J.A., Bravo, J.L., Fair, J.R., 1993. Distillation-Columns Containing Structured Packings - a Comprehensive Model for their Performance .1. Hydraulic Models. Ind. Eng. Chem. Res. 32, 641–651. doi:10.1021/ie00016a010

Rochelle, G., Chen, E., Freeman, S., Van Wagener, D., Xu, Q., Voice, A., 2011. Aqueous piperazine as the new standard for CO2 capture technology. Chem. Eng. J. 171, 725–733. doi:10.1016/j.cej.2011.02.011

Sadegh, N., Stenby, E.H., Thomsen, K., 2015. Thermodynamic modeling of CO2 absorption in aqueous N-Methyldiethanolamine using Extended UNIQUAC model. Fuel 144, 295–306. doi:10.1016/j.fuel.2014.12.002

Snijder, E.D., te Riele, J.M., Versteeg, G.F., van Swaaji, W.P.M., 1993. Diffusion coefficients of several aqueous alkanolamine solutions. J. Chem. Eng. Data 38, 475–480.

Sonderby, T.L., Carlsen, K.B., Fosbol, P.L., Kiorboe, L.G., von Solms, N., 2013. A new pilot absorber for CO2 capture from flue gases: Measuring and modelling capture with MEA solution. Int. J. Greenh. Gas Control 12, 181–192. doi:10.1016/j.ijggc.2012.10.010

Thomsen, K., Rasmussen, P., 1999. Modeling of vapor–liquid–solid equilibrium in gas–aqueous electrolyte systems. Chem. Eng. Sci. 54, 1787–1802. doi:http://dx.doi.org/10.1016/S0009-2509(99)00019-6

Thomsen, K., Rasmussen, P., Gani, R., 1996. Correlation and prediction of thermal properties and phase behaviour for a class of aqueous electrolyte systems. Chem. Eng. Sci. 51, 3675–3683. doi:http://dx.doi.org/10.1016/0009-2509(95)00418-1

Tobiesen, F.A., 2006. Modelling and Experimental study of Carbon Dioxide Absorption and Desorption. Tapir Uttrykk, Dr. Thesis NTNU 2006, 236.

Tobiesen, F.A., Juliussen, O., Svendsen, H.F., 2008. Experimental validation of a rigorous desorber model for post-combustion capture. Chem. Eng. Sci. 63, 2641–2656. doi:http://dx.doi.org/10.1016/j.ces.2008.02.011

Tobiesen, F.A., Svendsen, H.F., Juliussen, O., 2007. Experimental validation of a rigorous absorber model for CO2 postcombustion capture. AIChE J. 53, 846–865. doi:10.1002/aic.11133

Tontiwachwuthikul, P., Meisen, A., Lim, C.J.J., 1992. CO2 absorption by NaOH, monoethanolamine and 2-amino-2-methyl-1-propanol solutions in a packed column. Chem. Eng. Sci. 47, 381–390. doi:10.1016/0009-2509(92)80028-B

Treybal, R.E., 1969. ADIABATIC GAS ABSORPTION AND STRIPPING IN PACKED TOWERS. Ind. Eng. Chem. 61, 36–41. doi:10.1021/ie50715a009

Van Wagener, D.H., 2011. Stripper Modeling for CO2 Removal Using Monoethanolamine and Piperazine Solvents. The University of Texas at Austin, Austin, Texas.

Van Wagener, D.H., Rochelle, G.T., Chen, E., 2013. Modeling of pilot stripper results for CO2 capture by aqueous piperazine. Int. J. Greenh. Gas Control 12, 280–287. doi:10.1016/j.ijggc.2012.11.018

Vazquez, G., Alvarez, E., Navaza, J.M., Rendo, R., Romero, E., 1997. Surface tension of binary mixtures of water plus monoethanolamine and water plus 2-amino-2-methyl-1-propanol and tertiary mixtures of these amines with water from 25 degrees C to 50 degrees C. J. Chem. Eng. Data, J.Chem.Eng.Data, J Chem En D, J Chem Eng Data 42, 57–59.

Versteeg, G.F., Van Dijck, L.A.J., Van Swaaij, W.P.M., 1996. On the kinetics between CO2 and alkanolamines both in aqueous and non-aqueous solutions. An overview. Chem. Eng. Commun. 144, 113–158. doi:10.1080/00986449608936450

Weiland, R.H., Dingman, J.C., Cronin, D.B., Browning, G.J., 1998. Density and viscosity of some partially carbonated aqueous alkanolamine solutions and their blends. J. Chem. Eng. Data 43, 378–382. doi:10.1021/je9702044

Wellek, R.M., Brunson, R.J., Law, F.H., 1978. Enhancement factors for gas-absorption with second-order irreversible chemical reaction. Can. J. Chem. Eng. 56, 181–186. doi:10.1002/cjce.5450560205

Chapter 4. Simulation and multivariable optimization of post-combustion capture using piperazine

Abstract

Piperazine presents a great potential to develop an energy efficient solvent based CO_2 post-combustion capture process. Recently 8 molal piperazine (PZ) has shown promising results, however it faces operational challenges due to limited solid solubility. The operating range can be extended by decreasing the concentration of PZ and/or increasing the lean loading. However, optimal process conditions must be determined accounting for heating and cooling demands plus solvent re-circulation.

In this paper, we identify and generalize trends of performance for a broad range of operating conditions: 1.8 to 9 mol PZ/kg water (molal) and 0.2 to 0.6 lean loading for absorption and desorption in both, open and closed-loop simulation. We pinpoint scenarios where intercooling significantly improves the performance of the post-combustion process. The energy penalty is minimized as part of the closed-loop multivariable optimization. The results are created in Aspen Plus using the hybrid CAPCO2 rate-based user model. This model includes precipitation when estimating the heat and mass transfer rates. The results show how the capture process needs to be operated up to 14% above the minimum achievable heat duty, to avoid clogging from solid formation. 5 molal PZ is the most promising trade-off between energy efficiency and solid-free operation with a specific reboiler duty of 3.22 GJ/t CO_2 at 0.34 lean loading. The performance of the process can be further improved by assuming a minimum temperature of 30 ºC which gives an optimal specific reboiler duty of 3.09 GJ/t CO_2 (8 m PZ, 0.334 lean loading) for conditions without advanced heat integration.

Keywords: *CO₂ capture, piperazine, rate-based close-loop simulation and optimization, solubility, reboiler and cooling duties.*

4.1   Introduction

The growing focus to reduce CO_2 emission imposes the need to implement CO_2 capture in fossil-fuel-fired power plants. Several alternatives are under development however post-combustion capture is the most promising short and mid-term solution to meet the requirements of a CO_2 neutral energy market. Post-combustion can be retrofitted to existing power plants and it is suitable for various processes in the steel industry, cement production, refining industry, and bio-chemical industry. The key obstacle in the industrial deployment is the process economics, primarily determined by the solvent.

Recent studies have shown that 8 m piperazine is a promising solvent for developing an energy efficient CO_2 capture process. Freeman et al. predicts a 10 to 20% improvement when using 8 m PZ compared to the reference case of 7 m (30wt %) MEA (Freeman et al., 2010). Furthermore, advanced process configurations, i.e. intercooling (IC), heat integration, etc. may further reduce the energy usage of the capture process by reducing the exergy loss (Chen, 2015).

A systematic evaluation of intercooling for various flue gas sources was conducted by Sachde& Rochelle (2014). They outlines how the performance of the absorber is greatly enhanced by intercooling when using 8 m PZ concluding that the benefits are especially significant at intermediate lean loadings. Moreover, Rochelle et al. introduces the two-stage flash stripper configuration with an advanced heat exchanger network using 8 m PZ (Rochelle et al., 2011). Later, a simulation study by Lin and Rochelle demonstrated that this flash-stripper configuration has 10% better energy performance compared to a traditional stripper (Lin& Rochelle, 2014). However, this improved energy usage comes at the price of a greater process complexity and larger capital cost. Furthermore, concentrated PZ has a limited operating range due to solubility issues. It precipitates at both lean and rich process conditions (Fosbøl, Maribo-Mogensen, & Thomsen, 2013). Precipitation may trigger the shut-down of the plant due to clogging of units. The risk of clogging is especially high in lean solutions, at process start-up and in the condensing reflux section of the stripper (Fosbøl et al., 2013; Gaspar et al., 2014).

Solid formation can be avoided by decreasing the piperazine concentration and/or by increasing its CO_2 loading. 5 molal PZ is a promising alternative to balance the high regeneration energy towards a moderate solvent flow rate. Chen et al. demonstrates how the absorption rate of 5 m PZ is approximately 30% higher than 8 m PZ but the absorber must be operated at a higher L/G ratio to achieve 90% CO_2 removal (Chen et al., 2014). On the other hand, Fosbøl et al. show how the precipitation-free operational range grows exponentially with CO_2 loading indifferent of piperazine composition (Fosbøl et al., 2013). They indicate that PZ precipitates at room temperature for high PZ concentrations, especially for lean loadings of 0.5 and below. Therefore, the optimum lean composition needs to be determined based on solvent re-circulation rate and energy demand, considering the solubility limit of PZ. It is worth noting that process conditions needs to

be sub-optimized for each PZ concentration to assure a consistent and fair comparison of the solvent capacity and energy demand. There is a lack of systematic experimental and/or modelling studies on this topic. An all-inclusive evaluation of mass transfer benefits and energy performance of the piperazine based CO_2 capture process has apparently not been conducted.

The objective of this study is to perform a systematic and comprehensive evaluation of the absorption capacity and energy performance of a 1.8, 3, 5, 7, 8 and 9 m PZ solution, for a flue gas from a coal based power plant (13.25 mol% CO_2). It aims at overcoming the lack of knowledge regarding the behavior and energy efficiency of various PZ solutions. This work shows a multivariable optimization, taking into account the reboiler duty, the cooling duties and the auxiliary electricity requirements. It presents optimum process conditions, e.g. L/G ratio, lean loading, column specifications, etc. Conclusions are given on solvent compositions resulting in low heat requirement and solid-free operation. The results are created by closed-loop simulation in Aspen Plus using the DTU in-house hybrid CAPCO2 rate-based model for CO_2 absorption and desorption. Hybrid CAPCO2 is a first-of-its-kind rate-based model which takes into account solid precipitation in the calculation of mass and heat transfer rate through the gas-liquid interface.

4.2 The piperazine CO_2 capture process model

This section presents the piperazine based CO_2 post-combustion capture model as implemented in Aspen Plus. It gives an overview of the hybrid CAPCO2 rate-based model and defines the boundaries of the capture process. The model is not based on existing rate based models in Aspen Plus.

4.2.1 CO_2 capture process configuration

Figure 4.1 shows the Aspen Plus flow-sheet of the CO_2 capture process. The design base of this simulation is the traditional process configuration with heat integration between the lean solution leaving the reboiler and the rich solution entering the stripper.

The capture plant is designed for a nominal 250 MWe capacity advanced supercritical pulverized coal power plant (ASC), producing 238 kg/s flue gas, with a CO_2 concentration of 13.25 mol% (150 t CO_2/h). We assume that the gas is subjected to De-NOx, an electrostatic precipitator, a wet limestone based desulphurization plant and direct contact coolers for control of the combustion products. Therefore, the flue gas contains mainly CO_2, inert gases and it is saturated with water at the absorber inlet temperature of 40 °C.

As shown in Figure 4.1, the saturated flue gas passes through a blower and enters the bottom of the absorber. The role of the blower is to increase the pressure of the gas flow to overcome the pressure drop in the absorber and water wash section. The flue gas contacts the lean piperazine solution in the absorber. The lean solution enters at the top of the column. In this study the concentration is varied between 1.8 and 9 mol

PZ/kg H$_2$O with a loading range of 0.2 to 0.6 mol CO$_2$/mol PZ, corresponding to an L/G ratio of 2 to 12 mol/mol. Table 4.1 summarizes the process design specifications.
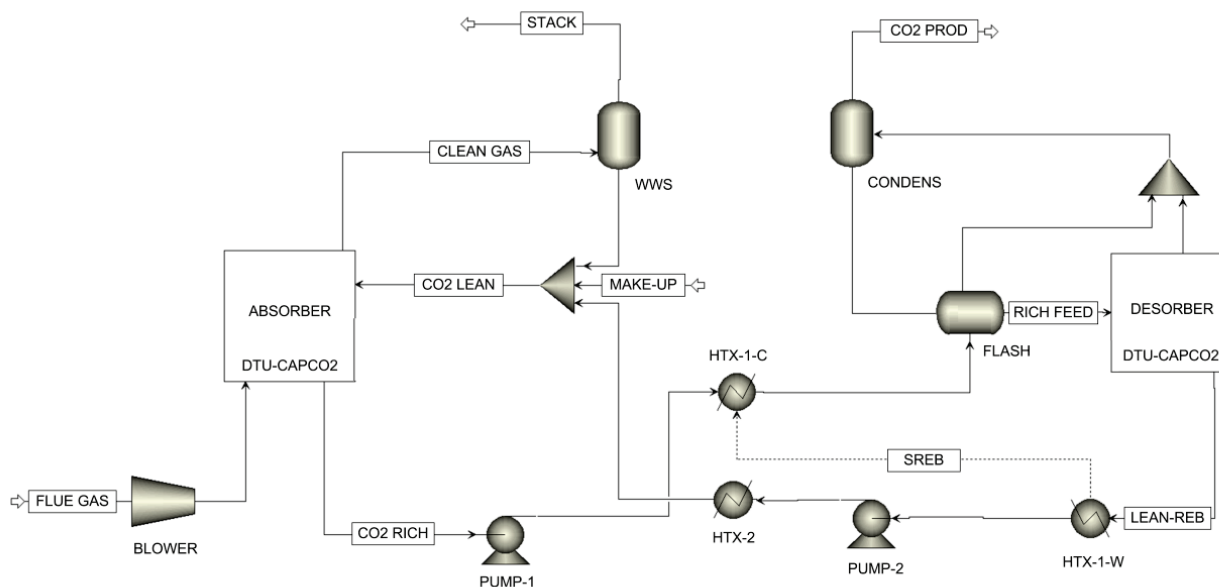

Figure 4.1. Flow-sheet of the CO$_2$ capture process

The gas phase exiting the top of the absorber is treated in a water wash column to remove the piperazine vapours before the cleaned exhaust gas is released to the atmosphere.

In the bottom of the absorber, the CO$_2$ rich PZ solution is pumped through the lean-rich heat exchanger. It recovers the heat of the lean stream from the reboiler by heating the stripper feed. The lean stream is cooled to 40 °C before entering the absorber. The rich stream enters the top of the stripper at approximately 100 – 110 °C.

The rich stream often contains two phases after the main cross-heat exchanger. To avoid convergence issues for the rate-based model, due to sudden evaporation in the top of the column, the stripper is simulated as a combination of two units: a flash and the CAPCO2 rate-based column (see figure 4.1). In the flash, the rich stream is isenthalpically decompressed to 190 kPa thereby pre-separating the feed into a liquid phase and gas phase. The liquid phase is sent to the top of the stripper while the vapor phase is mixed with the outlet gas stream of the column. This mix enters the condenser above the stripper. This approach eases the simulation of the stripper. CO$_2$ is released in the stripper by heat provided in the reboiler using low and mid pressure steam from the power plant.

Table 4.1. Design specifications for the post-combustion capture plant

Parameter	Unit	ASC
Flue gas flow rate	kg/s	238.46
Flue gas temperature	°C	40
Flue gas pressure	kPa	101.6
Flue gas CO_2 composition	mol%	13.25
Flue gas H_2O composition	mol%	12.11
Lean inlet temperature	°C	40
Lean loading	mol/mol	0.2 – 0.6
Piperazine concentration	mol/kg water	1.8 - 9
L/G ratio	mol/mol	2 – 12

The CO_2 product stream leaving the top condenser is washed to remove traces of piperazine. Water is retained by physical and/or chemical dehydration to avoid pipeline corrosion and hydrate formation. The dry CO_2 is compressed to 150 bar and stored underground. The energy required for compression is assumed constant and it is therefore not considered.

4.2.2 Process boundaries and design specifications

Design specifications for the absorber, stripper and utilities, e.g. pump, blower, heat exchanger are defined in table 4.2. The capture plant is designed for 90% CO_2 recovery which is achieved by adjusting the lean solvent flow for a given PZ concentration and lean loading. To achieve closed-loop convergence of the flow-sheet, the required lean loading out of the reboiler is reached by adjusting the reboiler duty. Apart from this, the water balance of the system is maintained by adjusting the water make-up flow. The lean loading and the operating temperature range are chosen in such a way to avoid the risk of solid formation in the equipment and pipelines. For this, we perform a thermodynamic analysis to determine the range at which solid appears. The approach is outlined in the following sections.

The absorber and the stripper are set up as packed columns equipped with structured Sulzer Mellapak 2X packing. It offers a low pressure drop and can be used for wide range of liquid loads. The diameter of the packed columns is calculated for an operating velocity of 70% flooding. Therefore, a typical diameter of 10 to 15 m and a height of 18 m are required for the range of operating conditions summarized in Table 4.1. In our study, a sensitivity study has shown that the CO_2 capture rate increases with the column height up to 18 m, where after it is unchanged. Based on the same approach the height of the stripper was set to 14 m. The rest of the design parameters such as condenser and intercooling temperature, efficiency factors and pump

head pressure are taken from the OCTAVIUS benchmarking project (Fosbøl et al., 2014) and the work of Plaza et al. (Plaza& Rochelle, 2011).

Table 4.2. Design specifications for the columns and utilities

Parameter	Unit	Value
CO_2 recovery	%	90
Operating velocity	% of flooding	70
Packing type	-	Mellapak 2X
Absorber/Desorber diameter	m	10 – 15
Absorber/Desorber height	m	18/14
Reboiler operating pressure	kPa	190
Water wash temperature	°C	40
Condenser temperature	°C	40
Intercooling temperature (at 9 m)	°C	40
Heat exchanger temperature approach	°C	5
Hydraulic efficiency of pumps/blower	%	80
Driver efficiency of pumps/blower	%	95
Pump head pressure	kPa	300

4.2.3 Rate-based simulation of precipitating CO_2 capture

In this work, the hybrid CAPCO2 in-house rate-based model is implemented to simulate CO_2 absorption and desorption combined with Aspen Plus built-in unit operations. The interface between Aspen Plus and CAPCO2 is CAPE-OPEN. It is worth noting that compared to traditional rate-based models, hybrid CAPCO2 includes the solid-liquid phase change when predicting the CO_2 mass and heat transfer rate between the gas phase and the liquid phase (Gaspar et al., 2014).

The hybrid rate-based model is built on the core of the original CAPCO2 model (Gabrielsen, 2007). It is formulated as a boundary value problem with specified inlet conditions. Profiles and outlet conditions are calculated. The liquid lean temperature, pressure, flow and composition are given at the top of the column, similar for the gas inlet at the bottom of the column. The mass and energy balances for the liquid phase and gas phase are solved simultaneously with algebraic equations for mass and hydraulic properties, mass and heat transfer fluxes, combined with the extended UNIQUAC thermodynamic model. Extended UNIQUAC is a rigorous model which is able to accurately predict solid precipitation (Fosbøl et al., 2013; Thomsen,

Rasmussen, & Gani, 1996; Thomsen& Rasmussen, 1999). The numerical approach and the equation system have been previously presented (Fosbøl, Thomsen, & Stenby, 2009; Gabrielsen, 2007; Gaspar et al., 2014).

In this work, the Rocha et al. model provides the mass transfer coefficients, the liquid hold-up and the interfacial area (Rocha, Bravo, & Fair, 1993; Rocha, Bravo, & Fair, 1996). The necessary physical property parameters, e.g. diffusivities, surface tension, viscosity, and density, entering this model originate from (Gaspar et al., 2015). These parameters were evaluated and validated against experimental data for a wide temperature and concentration range, for absorption and desorption conditions. The mass and heat transfer fluxes are determined in a film theory approach, using the General Method (GM) enhancement factor model (Gaspar& Fosbøl, 2015). The GM model connects the Onda's approximation for reversible reactions with the van Krevelen's approach for instantaneous irreversible reactions. Therefore, it is suitable to describe instantaneous, fast and intermediate reaction kinetics, such as the reaction between CO_2 and piperazine (Derks et al., 2006).

4.3 Parametric open-loop study of the piperazine capture process

We perform a parametric sensitivity study of the piperazine CO_2 capture process in order to reduce the degree of freedom for the design and optimization of the capture plant. First we study the absorber operation followed by the desorber. Later we perform a closed-loop analysis of the process to determine the optimal and solid–free operating conditions.

In this section, the absorber and the desorber are treated separately to identify trends of performance as function of L/G ratio, lean solvent composition, rich solvent composition, reboiler operating pressure and temperature. Other practical considerations, such as piperazine solubility window, minimum wetting of the column and flooding point are also taken into account in this analysis. The gained knowledge is used to narrow in the range of optimal process conditions and design parameters for the closed-loop sensitivity study shown below.

4.3.1 Thermodynamic analysis

We determine the domain of precipitation-free conditions using the extended UNIQUAC thermodynamic model (Fosbøl et al., 2013). We establish the transition temperature which shows the boundary where the first solid appears as function of CO_2 loading. This analysis gives the lower limit for the lean CO_2 loading.

Figure 4.2 shows the precipitation temperatures for 1.8, 3, 5, 7, 8 and 9 m PZ solutions. The constant concentration curves separate the operational window in two domains: a precipitation-free region above the curve and a precipitation-risk zone below the curve. In this work, we use two boundaries which determine the basis of our process conditions: 25 °C (bottom red line) and 30 °C (top green line). An intersection of

these lines with the solubility curves signifies the minimum CO_2 loading at which solid free operation is possible.

Figure 4.2 illustrates that the precipitation-free zone shrinks with the increase of the PZ concentration. For example, a 1.8 m PZ solution will not precipitate above 25 °C but a 5 m PZ solution forms solids at 0.34 loading and below. Moreover, this figure substantiates that precipitation does not occur above 0.43 loading and 25 °C, regardless of the piperazine concentrations in focus. Table 4.3 summarizes the lower limit for precipitation-free CO_2 loading for a lean solvent temperature of 25°C and 30°C. It highlights how higher loading needs to be used to prevent precipitation for concentrated PZ solutions.

Table 4.3. Lower limit for CO_2 loading for precipitation-free operation at 25 °C and 30 °C

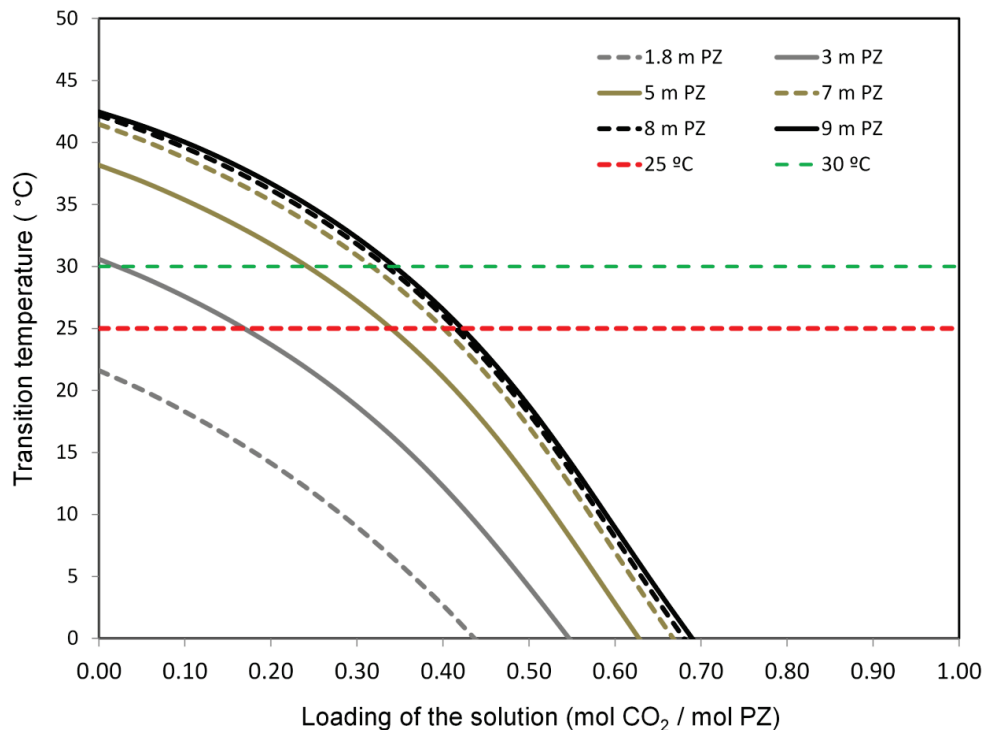| Solvent concentration (mol PZ/kg water)	1.8	3	5	7	8	9
Solvent concentration (wt. %)	13.4	20.5	30.1	37.6	40.8	43.7
Minimum CO_2 loading at 25 °C (mol/mol)	*	0.169	0.339	0.400	0.414	0.422
Minimum CO_2 loading at 30 °C (mol/mol)	*	0.023	0.242	0.317	0.334	0.344

no precipitation

Figure 4.2. Solid-liquid phase change transition temperature versus CO_2 loading for 1.8 to 9 m PZ

It can be concluded that the risk of clogging due to solid formation is higher in a lean solution compared to a rich solution. The results show that the minimum loading, to avoid solid formation above 25 °C, increases from 0 to 0.43 mol CO_2/mol PZ, when the concentration increases from 1.8 to 9 mol PZ/kg water.

4.3.2 Effect of lean composition on L/G ratio

The L/G ratio indicates the efficiency of the absorber and it is an important design and optimization parameter. A higher L/G corresponds to a less efficient solvent and results in expectedly higher reboiler duties. Therefore, the objective is to determine sets of CO_2 loadings and PZ concentrations which result in relatively low L/G ratios.

Figure 4.3 shows the variation of the L/G ratio at 90% CO_2 capture as function of lean compositions, using 1.8, 3, 5, 7, 8 and 9 m PZ. It emphasizes that the L/G ratio linearly increases up to 0.40 CO_2 loading, followed by an exponential increase up to 0.48. It indicates an irregular behavior for intermediate loadings, between 0.40 and 0.55, and above 5 molal PZ. This phenomenon is related to mass transfer pinch and it can be avoided by implementing intercooling, as discussed in the next section.
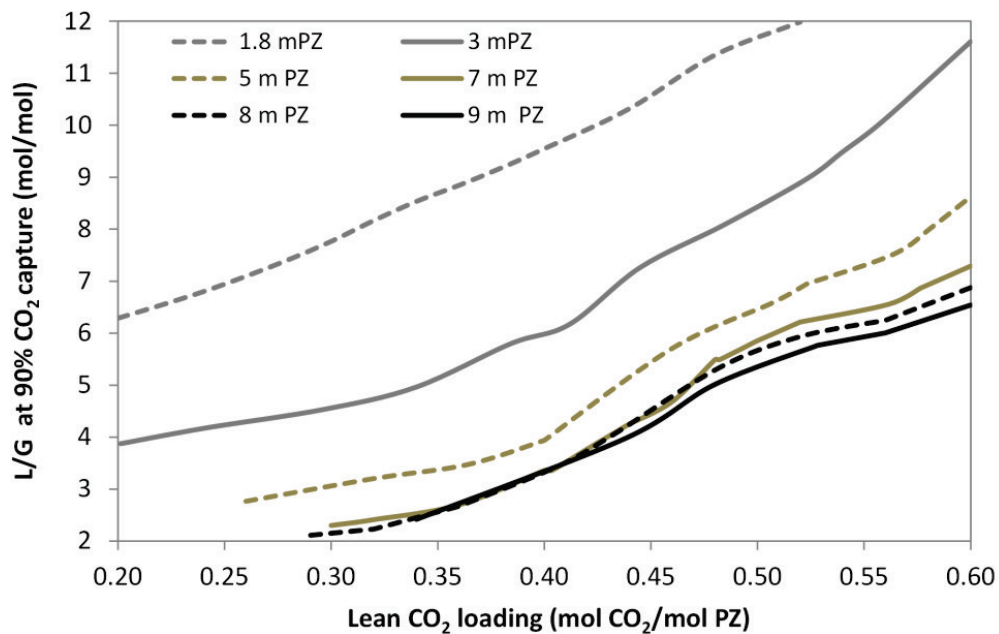

Figure 4.3. L/G ratio for 90 % CO_2 capture as function of lean loading for 1.8, 3, 5, 7, 8, and 9 m PZ

The simulation results are furthermore exemplified in Figure 4.4, which represents the L/G ratio as function of the piperazine concentration at various CO_2 loadings. It outlines how the L/G ratio exponentially reduces with concentration, up to approximately 8 molal. Further increase of the concentration has almost no impact

on the L/G ratio. This figure shows how the L/G curve has an exponential behaviour at low loading and approaches a linear behaviour at 0.60 lean CO_2 loading.
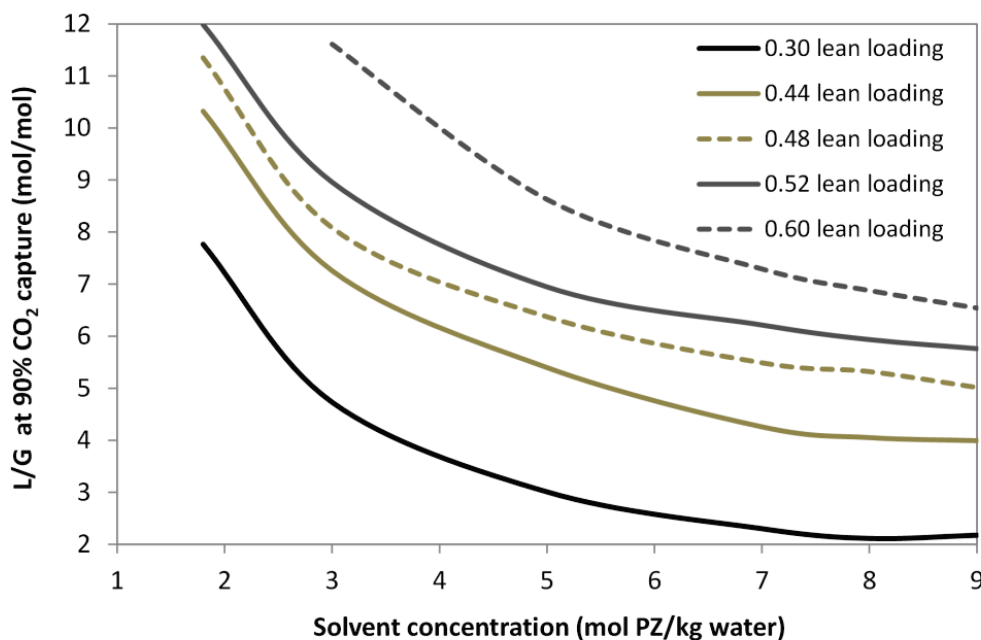

Figure 4.4. L/G ratio at 90% CO_2 capture as function of solvent concentration

It can be concluded, comparing figure 4.3 and 4.4, that the PZ concentration has a greater impact on the L/G ratio than the CO_2 lean loading. It indicates how the solvent circulation rate almost triple below 3 molal and it remains reasonably constant above 8 molal. Consequently, diluted and very concentrated PZ solutions have no practical importance for the CO_2 capture business from a coal-fired power plant. In summary, to reach a low solvent flow rate, a high PZ concentration and a low lean loading is needed.

4.3.3   Effect of lean composition on solvent capacity

The capacity of the solvent reflects the capability of PZ to remove CO_2 in the absorber. It is defined as the difference between the lean and the rich loading. A high solvent capacity is obtained when the lean loading is low and the rich loading is high. A high solvent capacity results in a lower solvent flow rate, equivalent to the above conclusions on the L/G ratio. It allows for a possible reduction of the heat duty.

In this section, we investigate two absorber designs which represent the outer boundaries of absorption conditions, to study the effect of solvent capacity: 1. an absorber without intercooling and 2. an isothermal absorber, operated at 50 ºC. In both cases, the flue gas flow rate and composition are kept constant. The lean solvent flow rate is adjusted to reach 90% CO_2 capture. The CO_2 loading and PZ concentration are varied. The isothermal case corresponds to an absorber with perfect intercooling.

Figure 4.5 presents the calculated rich loading for three representative lean loadings (0.30, 0.48 and 0.58 mol/mol) and for a wide PZ concentration range (1.8 to 9 mol PZ/kg water). The isothermal, 50 ºC, rich loading represents the upper limit of the solvent capacity. It resembles the conditions for which the maximum (equilibrium) rich loading is reached. Figure 4.5 shows that a plateau at 0.81 in the maximum rich loading is observed as function of PZ concentration. It decreases with respect to PZ concentration, being steeper at concentrations below 3 m PZ and above 8 m PZ, and insignificant in the intermediate region.

The calculated rich loading varies as function of the lean loading. Figure 4.5 substantiate how a low lean loading (0.30 mol/mol) results in a rich loading close to the maximum rich loading and the absorber operates near equilibrium conditions. At 0.48 lean loading, the rich loading is 3 to 15% less than at 0.30 lean load. However, further increase of the lean loading (from 0.48 to 0.58 mol CO_2/mol PZ) improves the absorber performance. The observed behaviour is related to temperature induced equilibrium constraints, as explained by Plaza et al. (Plaza, 2011) and Sachde and Rochelle (Sachde& Rochelle, 2014). They show how mass transfer approaches pinch condition at the location of the temperature bulge for intermediate lean loadings. This results in capture capacity penalties. At low lean loadings, the temperature bulge is located near to the top of the column and at high lean loadings, the L/G ratio is sufficiently large to reduce the magnitude of the temperature bulge. Therefore, temperature related mass transfer limitations are avoided at low and high loadings.
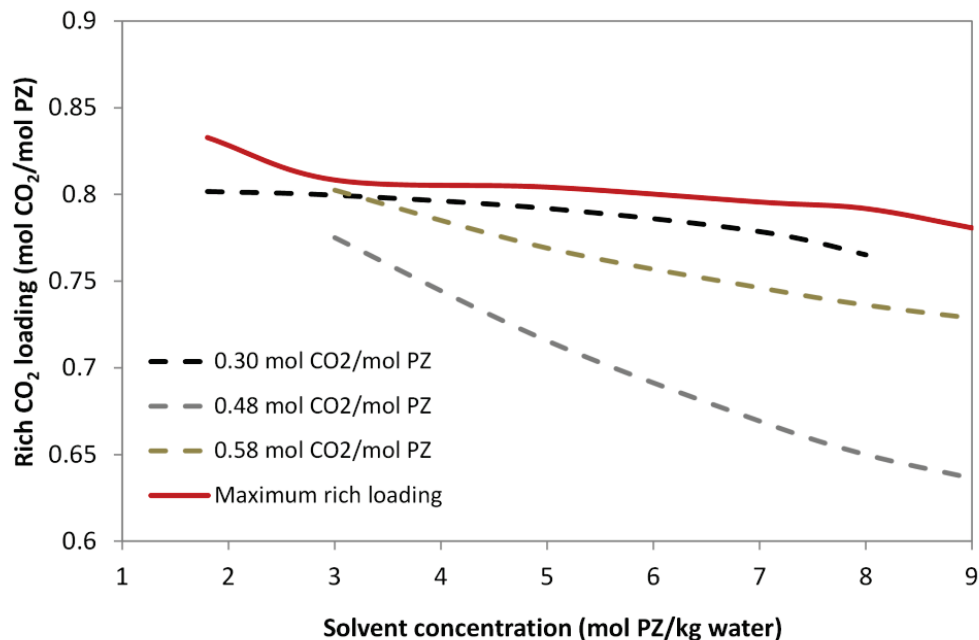

Figure 4.5. Rich loading as function of PZ concentration at 90% CO_2 capture for 0.30, 0.48 and 0.58 lean loading

It can be concluded that intercooling would offer large solvent capacity benefits, up to 20%, at intermediate lean loadings by reducing the magnitude of the temperature bulge and thereby breaking the mass transfer pinch. Intercooling leads to improvements of the absorber by decreasing the L/G ratio required for 90% CO_2 capture. Consequently, it leads to a greater rich CO_2 loading. Intercooling has much less impact on the absorber's performance for low and high lean loadings and tend to be insignificant to the capture capacity for these conditions.

4.3.4 Effect of rich loading on energy demand

This section describes the impact of rich loading on the energy performance of the stripper. The approach of this analysis is to vary the steam input to the reboiler at constant stripper feed composition and temperature. In this analysis, parameters which influence the energy performance of the system, e.g. pressure, height, and diameter, are kept constant to isolate the effect of rich loading on the energy performance. The energy performance is expressed in terms of specific reboiler duty (SRD) which gives the heat required to regenerate 1 tonne of CO_2.

Figure 4.6 illustrates the SRD as function of PZ concentration for 0.70 and 0.80 rich loading. Results for low, middle and high lean loadings are shown. Note, 0.80 rich loading corresponds to an absorber with perfect intercooling close to equilibrium, see figure 4.5, while 0.70 loading resembles an arbitrary less efficient absorber. This figure exemplifies how the energy demand reduces when rich loading increases. Furthermore, it illustrates how the SRD decreases exponentially up to 7 molal PZ, at which the SRD flattens. Further increase of the PZ concentration only slightly improves the performance of the stripper. Figure 4.6 underlines that the effect of PZ concentration on the energy demand is more noticeable at 0.70 rich loading compared to 0.80.
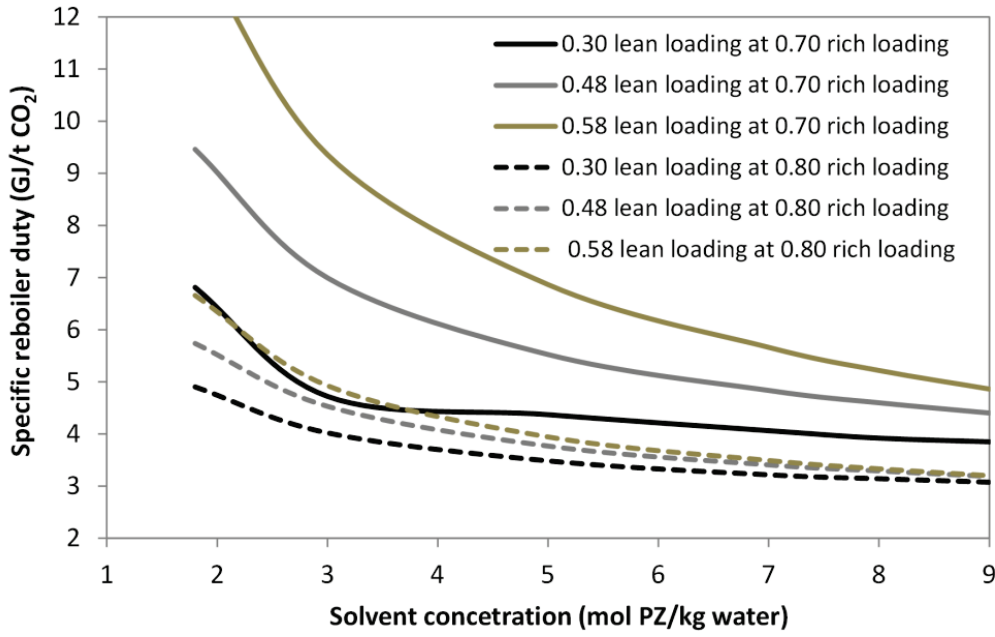
Figure 4.6. Specific reboiler duty as function of solvent concentration for rich loading of 0.7 and 0.8

In conclusion, it is beneficial to design a process with high rich loading and low lean loading which results in significantly less energy consumption. It can be concluded, comparing figure 4.4 and 4.6, that it is desirable to choose a solvent with PZ concentration above 5 molal, to avoid high solvent circulation rate and high steam demands.

4.3.5   Effect of pressure on energy demand

The energy performance is evaluated with respect to reboiler pressure in this section. This analysis is performed equivalent to the above described approach on the impact of rich loading. The feed stream and the column specifications are the same while the reboiler pressure is varied. The energy performance is shown in terms of equivalent work. This is a convenient way to quantify and combine the work lost from the turbine upstream of the power plant and the work needed to compress the pure CO_2 gas stream (Madan et al., 2013).

The equivalent work is calculated by eq. (4.1) with an assumed turbine efficiency of $\eta = 75\%$, a temperature difference of $\Delta T = 5K$ and a sink temperature of $T_{sink} = 313$ K. The compression work, $W_{compression}$, is estimated using the correlation from Madan et al. (Madan et al., 2013). In this work, results for 0.80 rich loading are examined at 190 kPa and 250 kPa for a lean loading of 0.30, 0.48 and 0.58 mol CO_2/mol PZ.

$$W_{eq} = \eta \left(\frac{T_{source} + \Delta T - T_{sink}}{T_{source} + \Delta T} \right) Q_{reboiler} + W_{compression} \qquad (4.1)$$

Figure 4.7 shows the effect of CO_2 content and PZ concentration on the equivalent work for the two pressures. It shows how the equivalent work reduces exponentially when increasing the solvent concentration, regardless of pressure. Furthermore, it outlines a 4 to 20% less work at 190 kPa compared to 250 kPa. The same behavior was shown experimentally by van Wagener et al. for 8 molal PZ (Van Wagener, Rochelle, & Chen, 2013). This is due to the relation between the boiling temperature and pressure. The boiling point temperature increases with pressure which results in greater reboiler temperature at 250 kPa compared to 190 kPa. Therefore, the first term in eq. (4.1) increases due to the source temperature increase. It results in greater equivalent work. In addition, a small increase of the pressure gives only a minor decrease of the work needed for CO_2 compression.
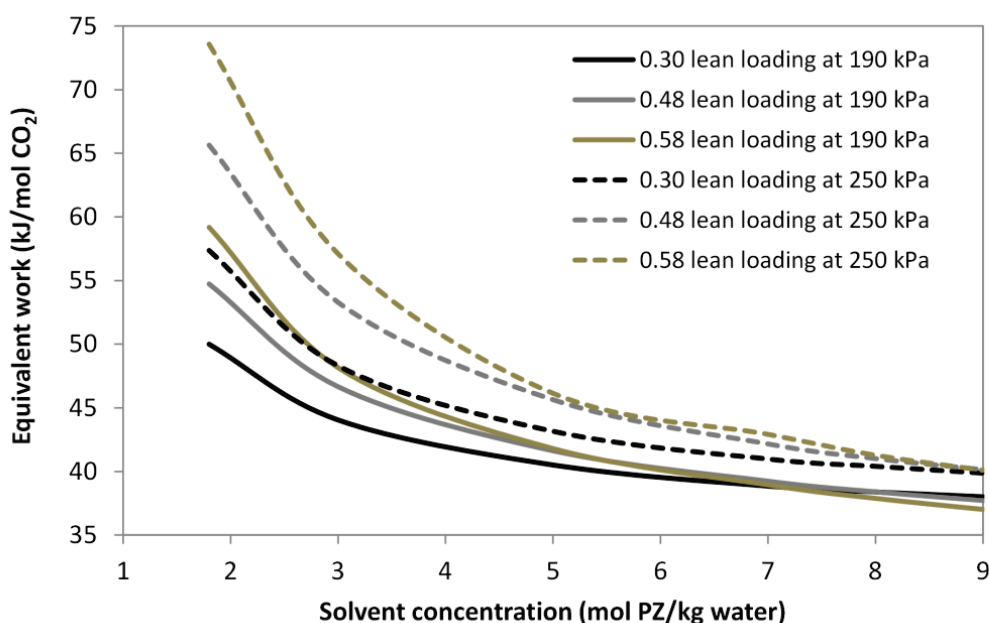

Figure 4.7. Equivalent work as function of lean concentration at 190 and 250 kPa for 0.8 rich loading

The results demonstrate that it is more beneficial to run the stripper at 190 kPa than at 250 kPa. The analysis substantiates the positive effect of increasing the solvent concentration on the energy demand of the stripper and compression stages. It is generally a good practice to choose a solvent with a PZ concentration above 5 molal and an intermediate to low CO_2 lean loading. Above 5 molal PZ the work for CO_2 stripping and compression is below 50 kJ/mol and the equivalent work only weakly depends on the lean CO_2 loading.

4.3.6 Effect of lean loading and solid formation on energy demand

In this section we show how the energy demand of the stripping process varies with respect to lean CO_2 loading. The value of the lean loading is determined by the heat input to the reboiler, e.g. a greater steam flow to the reboiler results in a larger CO_2 boil-up and a leaner solution. Moreover, we show for which

conditions the solvent forms solid PZ and we demonstrate that the solubility limit needs to be considered when designing the post-combustion capture plant. In this analysis, the reboiler pressure is set to 190 kPa.

Figure 4.8 and 4.9 show the specific reboiler duty (SRD) for 0.80 and 0.65 CO_2 rich load, at several piperazine concentrations. 0.80 CO_2 load (Figure 4.8) can be reached when equilibrium is almost achieved in the absorber while 0.65 CO_2 load (Figure 4.9) corresponds to a relatively inefficient absorber. These figures exemplify how the energy demand exponentially decreases with the lean loading until it reaches a minimum value between 0.20 and 0.27 in loading. The optimum SRD is reached when the heat of water condensation in the column is balanced by the heat of CO_2 stripping. Below this loading point, the steam flow to the reboiler is too high and it is mostly consumed by evaporation of water. Above the optimal loading point, the steam flow is insufficient and the SRD increases due to lower CO_2 recovery rate. It corresponds to a low energy input system.
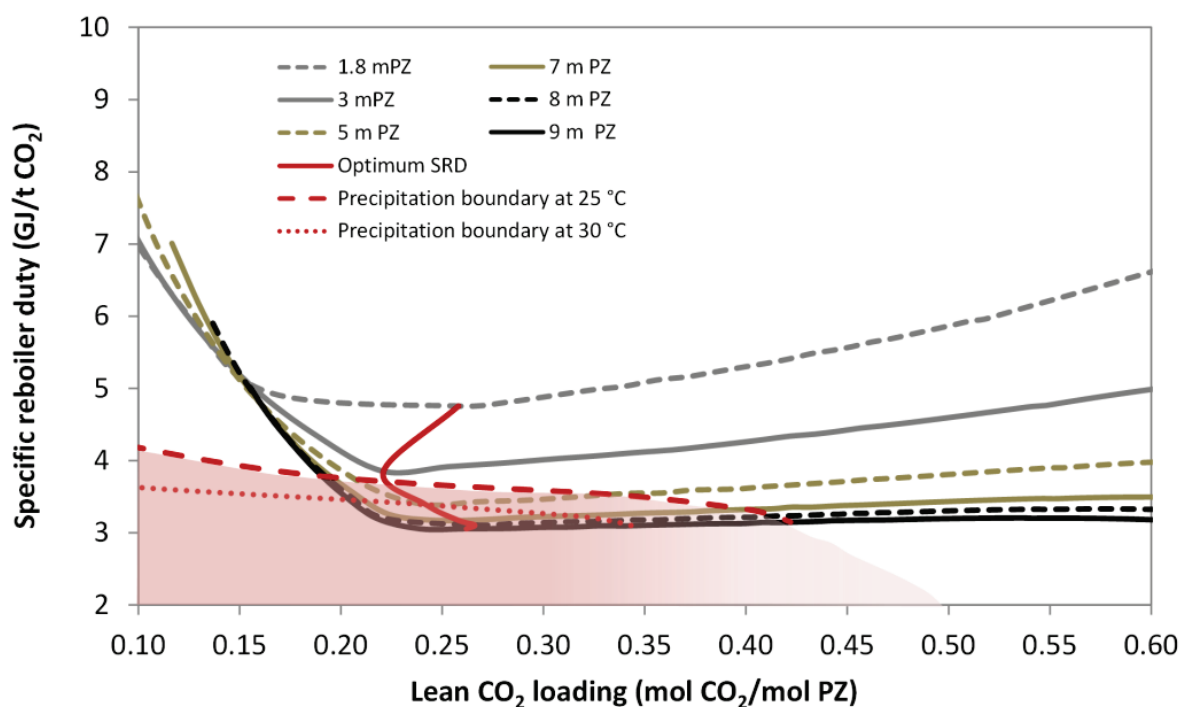
Figure 4.8. Specific reboiler duty as function of lean loading for 0.80 rich CO_2 load

The results show that the SRD at 0.80 rich loading (figure 4.8) is less compared to 0.65 rich loading (figure 4.9) independent of the piperazine and CO_2 concentrations. For example, the lowest SRD of a 5 molal solution is 3.39 GJ/t CO_2 at 0.80 rich loading and it is 4.44 GJ/t CO_2 at 0.65 rich loading. Similar differences in the SRD can be seen at other concentrations also.

It can be concluded that greater rich CO_2 loading of the stripper's feed assures cheaper solvent regeneration. Furthermore, Figure 4.8 (0.80 rich loading) highlights that the SRD increases only slowly above 0.25 lean loadings while the change in the SRD is much more significant at lower rich loadings, see Figure 4.9. In this connection it is preferable to run the absorber at higher rich CO_2 loading to secure a wider solid-free operating range and a low reboiler duty.
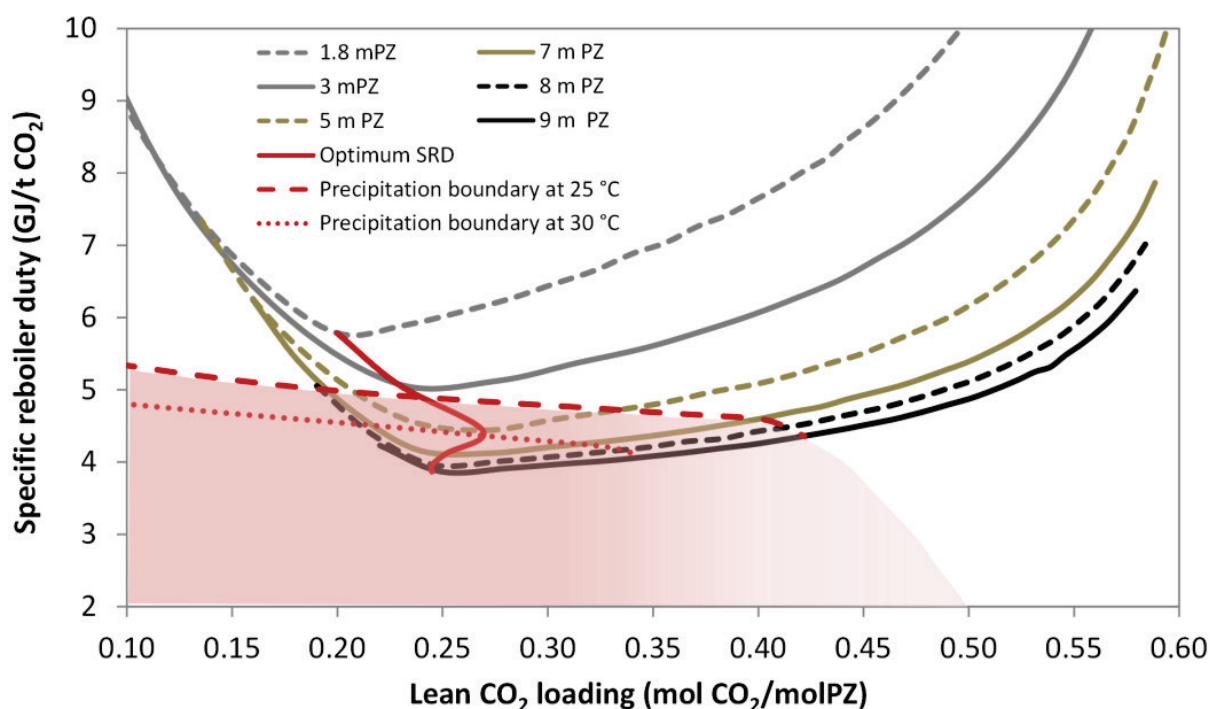

Figure 4.9. Specific reboiler duty as function of lean loading for 0.65 rich CO_2 load

Figure 4.8 and 4.9 show the importance of the precipitation boundary at 25 °C and 30 °C. Below the precipitation boundary, solid formation occurs. These figures outline how the minimum of the SRD is located inside the precipitation-risk (red) area. Precipitation will occur in concentrated lean PZ solutions above 3 molal, assuming a minimum temperature of 25 °C. This is true for 0.80 as well as for 0.65 rich loading.

It is necessary to run the stripper at non-optimal conditions (greater lean loadings) in order to prevent solid formation. For example, figure 4.8 and 4.9 show that the 5 molal solvent has to be operated at 0.34 lean loading (3.52 GJ/t CO_2), which is above the optimal loading of 0.25 (3.39 GJ/t CO_2). The additional energy needed to run the process outside of the precipitation zone is 5 % (0.80 rich loading) to 12% (0.65 rich loading) higher. The precipitation-free area can be extended by keeping the lean solvent at higher temperature, e.g. 30 °C. This allows for use of the 5 m solvent without solid formation, but precipitation problems still occur in the 7 to 9 molal solvents. It has to be mentioned that at 30 °C, heating of units, e.g.

storage and buffer tanks, water wash column, intermediate piping, etc. may require active heating during winter or night conditions, especially during shut down to prevent clogging.

4.4   Multivariable closed-loop optimization of the piperazine CO_2 capture process

In this section we perform a closed-loop optimization of the piperazine CO_2 capture process. This study aims at minimizing the sum of heating duties, cooling duties and auxiliary power demands (pumps and blower) as function of piperazine concentration and CO_2 loading of the lean solvent. We determine optimal operation points which are above the solubility limit of piperazine. Therefore, these conditions correspond to solid free and low energy systems. The input and design specifications for this study are given in table 2.B.2 and 4.2.

Two conflicting and competing criteria need to be considered when designing an energy-efficient and solid-free CO_2 capture plant using piperazine: 1. It is desirable to have an intermediate PZ concentration with an intermediate to high CO_2 lean loading to avoid precipitation in the absorber. 2. It is less energy intensive to operate the stripper at low to intermediate lean loadings and higher piperazine concentrations. These criteria are emphasized by Figure 4.8 and Figure 4.9. A balance between minimum stripping heat and precipitation-free conditions, in between criteria 1 and 2, needs to be found. This will resemble a technically feasible and optimal condition.

Figure 4.10 and 4.11 show the heating and the cooling duties as function of lean loading and PZ concentration. The auxiliary power demand is not shown here since it plays a minor role in the optimization. These figures show the results for 3, 5 and 8 molal PZ solutions. We do not treat more diluted or more concentrated solutions, e.g. 1.8 and 9 molal PZ. The reason being that the above study revealed a tripled solvent circulation rate below 3 molal and little effect was seen by increasing the PZ concentration above 7 molal. Here we included the results for the 8 molal solution since it is previously was considered a standard concentration for the piperazine CO_2 capture process (Rochelle et al., 2011).

Figure 4.10 shows the results for two process configurations: (1) a simple absorber without intercooling and (2) an absorber with intercooling in the middle of the column. This figure illustrates that the minimum reboiler duty for configuration 1 (~3.1 GJ/ton CO_2) can be reached using a 5 or 8 molal PZ solutions at approximately 0.30 loading. However, precipitate forms at these conditions. To avoid solid formation, the stripper must be operated at higher lean loadings: 0.34 and 0.41 for 5 molal respectively 8 molal solvents. These lean loadings correspond to an SRD of 3.22 GJ/ton CO_2 (5 molal) respectively 3.44 GJ/ton CO_2 (8 molal). Precipitation can also be avoided by decreasing the piperazine concertation, for example to 3 molal which has an SRD of 3.54 GJ/ton CO_2 at 0.28 lean loading.
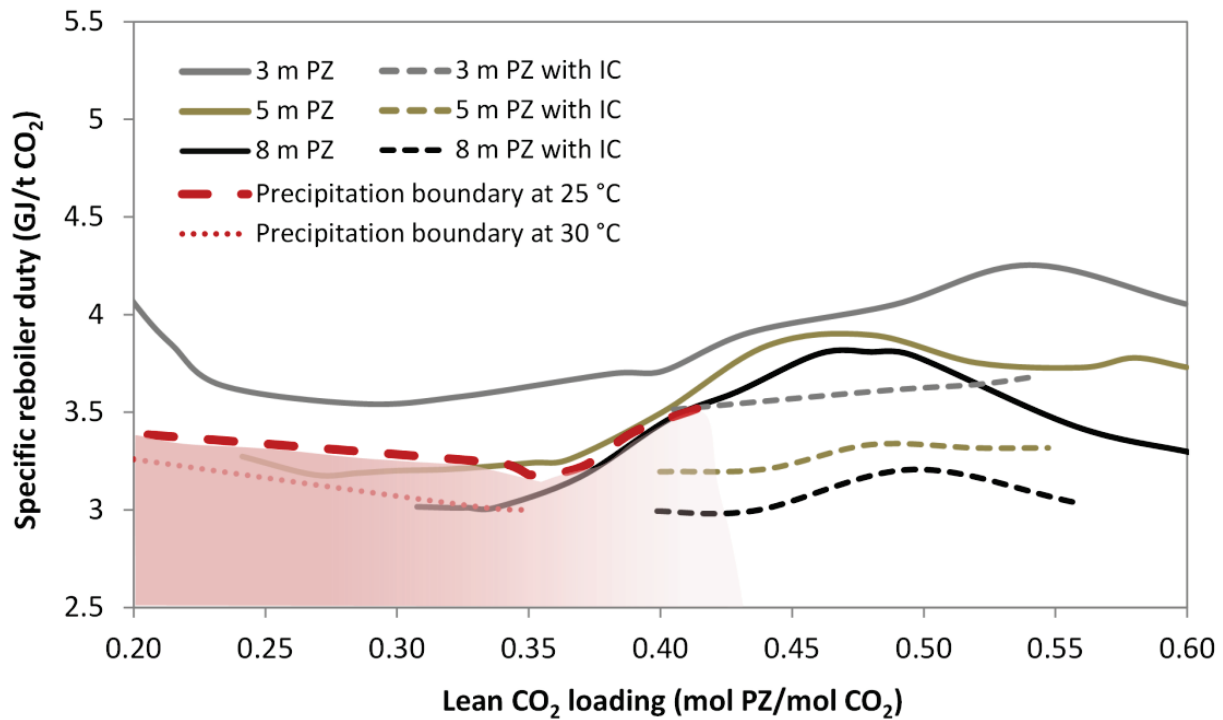
Figure 4.10. Specific reboiler duty (SRD) as function of lean loading for 3, 5 and 8 m PZ with and without intercooling (IC)

In case of configuration 2 (absorber with IC), the SRD reduces to 3.02 GJ/t CO_2 at around 0.42 lean loading and 8 molal solution. Generally, the SRD for configuration 2 is 5 to 17% (approximately 0.22 GJ/t CO_2) less compared to configuration 1. This is shown in Figure 4.10. Therefore, intercooling reduces the heat at the cost of higher process complexity. Note that intercooling does not enhance the performance of the absorber for low and high lean loadings, and we limited the investigated CO_2 loading range to 0.40 to 0.55.

Another approach to lower the SRD is to shift the minimum lean solvent temperature to 30 °C. It results in a reboiler duty of 3.09 GJ/t CO_2 (8 molal PZ, 0.33 lean loading) as shown in Figure 4.10. In practice, it resembles a case where the lean solvent is kept above 30 °C in all the units, such as coolers, absorber, storage tanks, etc. This design may require active heating during winter and night conditions.
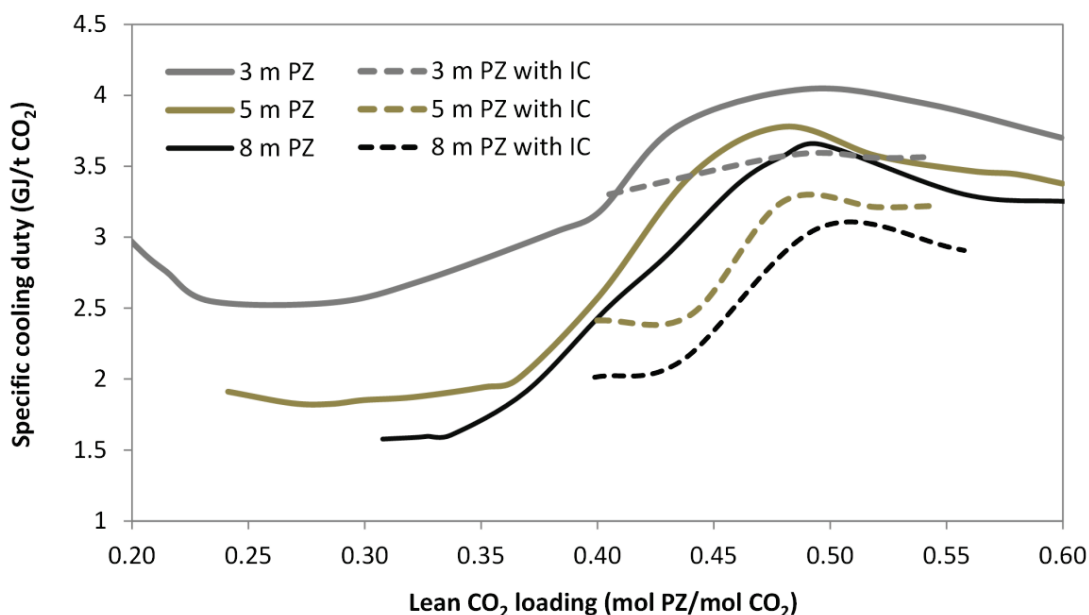
Figure 4.11. Specific cooling duty (SCD) as function of lean loading for 3, 5 and 7 m PZ with and without intercooling

Figure 4.11 shows the specific cooling duty versus lean loading and PZ concentrations for an absorber with and without IC. In this study we account for the heat removed in the lean-rich cross heat exchanger, the heat removed in the condenser of the stripper and the heat removed by the IC. This value corresponds to the unrecoverable lost heat from the process.

It can be seen, comparing Figure 4.10 and Figure 4.11, that the specific cooling and heating duties follow similar trends. Generally, the specific cooling duty reaches a minimum between 0.25 and 0.34 lean loading followed by an exponential increase with respect to lean loading. The simulation results reveal that the condenser's duty is relatively constant for the studied loading range. However, the duty of the cross lean-rich heat exchanger varies significantly with respect to lean loading due to variation of the solvent flow. This is outlined by Figure 4.3 which shows that the L/G ratio doubles or even triples at 0.6 lean loading compared to 0.3. It is worth noting in figure 4.11 that the specific cooling duty for configuration 2 (IC) is lower compared to configuration 1. In case of configuration 2, the absorber is operated close to the maximum (equilibrium) rich loadings and it gives a lower L/G ratio. As a result, the cooling duty of the cross heat exchanger reduces significantly compared to the additional cooling required by the IC.

The closed-loop optimization study illustrates that the piperazine CO_2 capture process must be operated above the optimal total energy demand, i.e. sum of heating, cooling and auxiliary energy demand in order to avoid precipitation of PZ in the lean solvent. The 5 molal piperazine solvent gives the lowest precipitation-free total energy of 5.14 GJ/t CO_2 at 0.34 lean loading. This value is 1.3% higher compared to the minimum

total energy. This value is close to the IC process configuration. The total energy demand can be further lowered to 4.86 GJ/t CO_2 (0.33 CO_2 lean loading and 8 molal PZ) by assuming a greater minimum process temperature of 30 °C.

Several aspects: such as climate, availability of cooling water, balance between capital and operational cost, etc. must be considered when designing and optimizing a piperazine based CO_2 capture process.

We have shown that the 3 molal PZ solution has the advantage of a large precipitation-free operational range which makes it attractive to cold countries. We have also seen that this solvent has a significantly greater energy demand compared to solutions of 5 molal PZ and above. The 5 molal solution balances between solid-free operational window and energy requirement while the 8 molal solvent gives the lowest energy demand if the process temperature in all the units, e.g. columns, storage tanks, pipes, etc. can be kept above 30°C. We concluded that it is beneficial to design and operate the absorber close to the maximum (equilibrium) rich CO_2 loading at the expense of higher capital cost, e.g. IC or greater pump work. We also concluded that it is beneficial to design the stripper for lower pressure. High pressure indeed results in less CO_2 compression, but requires higher reboiler temperatures. The closed loop simulation has a clear benefit compared to the open loop simulation. It gives a more realistic prediction of the capture plant performance by accounting for the interactions between units. This study shows that open-loop simulations are useful to identify trends of performance for key process parameters but closed-loop simulations are essential to identify the global optimal set of operating parameters.

4.5   Conclusions

This work showed a systematic analysis and optimization of a CO_2 post-combustion capture process for 1.8, 3, 5, 7, 8, and 9 molal piperazine solutions at a nominal 250 MWe capacity advanced supercritical pulverized coal power plant (ASC) with 13.25% CO_2. It presents the effect of the most important process parameters, such as solvent concentration, L/G ratio, lean and rich loading, reboiler pressure and temperature on the absorber efficiency as well as the energy requirement of the capture process. Additionally, in closed-loop we optimized the piperazine concentration and the lean CO_2 loading to secure a minimum energy demand without precipitation. This study was performed using the hybrid CAPCO2 in-house rate-based model (Gaspar et al., 2014) for absorption and desorption in combination with Aspen Plus' built-in units. The Hybrid CAPCO2 model actively includes solid precipitation. The mass and heat transfer fluxes are calculated using the concentration of the dissolved species since piperazine is deactivated when present as solid. It uses the extended UNIQUAC model for phase equilibria and thermal properties calculation. The GM enhancement factor model accurately predicts the mass transfer enhancement through the gas-liquid interface (Gaspar& Fosbøl, 2015).

The important issue of precipitation is in the focus of this work when determining optimal operating conditions. A thermodynamic analysis revealed how piperazine precipitates at conditions of interest for a CO_2 capture process. Any solution between 3 molal and 9 molal PZ precipitates above 0.2 CO_2 loading and ambient conditions, 25°C. Even at a higher solvent temperature of 30°C, precipitation problems still occur above 5 molal and 0.30 lean loading. Thus, the optimal operational window is limited due to precipitation constraints. It is recommended to use a moderate PZ concentration and to increase the CO_2 loading at the expense of greater heat demand, to avoid clogging of units, e.g. absorber, pipe, tanks, etc. due to solid formation.

A sensitivity study has demonstrated that the required L/G ratio for 90% CO_2 capture as well as the heat duty strongly depends on the piperazine concentration and the lean CO_2 loading. The highest impact is observed up to 7 molal. Further increase of the piperazine concentration results only in minor decrease of the L/G ratio and energy demand. This study emphasizes how the rich loading influences the performance and the stripper design. A rich loading of 0.70 gives at least 0.8 GJ/t CO_2 higher energy demand compared to a 0.80 rich loading. The greatest difference is seen at high lean CO_2 loadings. Furthermore, we have shown how greater reboiler pressure results in higher equivalent work. The energy for regeneration and compression is up to 15 kJ/mol (20%) greater at 250 kPa compared to 190 kPa. Furthermore, this sensitivity analysis shows that the minimum SRD (approximately 3.1 GJ/t CO_2) is obtained at lean loadings between 0.20 and 0.30. However these values fall in the precipitation-risk zone and the capture process needs to be operated 13% above the minimum duty to avoid risk of clogging.

The closed-loop sensitivity study shows that the lowest feasible solid-free specific reboiler duty, 3.22 GJ/t CO_2, can be reached at 0.34 lean CO_2 loading and 5 molal PZ. At this condition, the total energy demand, i.e. sum of heating, cooling and auxiliary energy is 5.14 GJ/t CO_2, a value which is close to the energy demand of the IC process configuration. It can be further lowered by assuming a greater minimum process temperature of 30 °C, which gives 3.09 GJ/t CO_2 at 0.33 CO_2 lean loading and 8 molal solution.

Our study demonstrates that intercooling is a promising process configuration alternative when operating the capture plant at intermediate lean loadings (between 0.40 and 0.50). Intercooling assures solid free operation and a low SRD of 3.02 GJ/t CO_2 (0.42 lean loading and 8 molal PZ). However, intercooling comes at a price of greater process complexity and additional capital cost for pumps, heat exchangers, and solvent redistributors.

It can be concluded that various factors such as geographical location, process complexity, availability of cooling water, etc. determine the feasible and optimal solvent for the design of a piperazine CO_2 capture process. The 3 molal solvent is a reasonable choice for plants operating at very low to ambient temperatures. In this case the optimal SRD is 3.54 GJ/ton CO_2 at 0.28 lean loading. The 8 molal solvent is the most

promising solvent when cooling is expensive and the solvent can be kept above 30 °C, without additional heating. The optimal SRD for this solvent is 3.09 GJ/t CO_2 at 0.33 CO_2 loading. The 5 molal solvent will be the optimal solvent concentration for most capture plants which are exposed to temperature fluctuations between summer and winter conditions. The 5 molal PZ solvent is the safe choice: it assures low heat duty (3.22 GJ/t CO_2 at 0.34 lean loading) and it does not form solids at ambient conditions (above 25 °C).

Based on the preliminary study by (Gaspar et al., 2015) – Appendix E, we expect that the optimal and feasible operating points found in this work for the coal fired plant (ASC) will be similar for a natural gas combined cycle (NGCC) plant. However, higher heating duties are expected due to lower partial pressure of CO_2 in the flue gas.

Since implementation of CO_2 capture will introduce significant capital and operating cost, other process configurations as well as dynamic-optimal scheduling of the capture process should also be studied. The SRD calculations performed in this work are based on process calculations without any particular optimization of the process configuration or advanced heat integration. This sensitivity is set up with the strategy to determine trends of process performance, without too much interference from other types of optimization. There is still a great potential for further decreasing the SRD by more advanced process configurations, such as split flow arrangement, lean-vapor-recompression, rich split flow, network of heat exchangers, etc. However, the cost of implementing and operating more advanced process configurations should be included in these kinds of studies. The local design optima found in this work will most likely remain for more advanced process configurations but will have a possibly lower SRD.

Acknowledgments

References

Chen, E. (2015). Pilot Plant Results for 5 M Piperazine with the Advanced Flash Stripper. Abstract from 3nd Post Combustion Capture Conference, Regina, Canada, http://ieaghg.org/docs/General_Docs/PCCC3_PDF/5_PCCC3_6_Chen.pdf.

Chen, E., Fulk, S., Sache, D., Lin, Y., & Rochelle, G. T. (2014). Pilot Plant Activities with Concentrated Piperazine. Energy Procedia, 63, 1376-1391.

Derks, P. W. J., Kleingeld, T., van Aken, C., Hogendoom, J. A., & Versteeg, G. F. (2006). Kinetics of absorption of carbon dioxide in aqueous piperazine solutions. Chemical Engineering Science, 61, 6837-6854.

Fosbøl, P. L., Gaspar, J., Ehlers, S., Kather, A., Briot, P., Nienoord, M., Khakharia, P., Le Moullec, Y., Berglihn, O., & Kvamsdal, H. M. (2014). Benchmarking and comparing first and second generation post combustion CO2 capture technologies. Energy Procedia.

Fosbøl, P. L., Thomsen, K., & Stenby, E. H. (2009). Energy demand for CO2 solvent regeneration. , Proceedings, 242-252.

Fosbøl, P. L., Maribo-Mogensen, B., & Thomsen, K. (2013). Solids Modelling and Capture Simulation of Piperazine in Potassium Solvents. Energy Procedia, 37, 844-859.

Freeman, S. A., Dugas, R., Van Wagener, D. H., Nguyen, T., & Rochelle, G. T. (2010). Carbon dioxide capture with concentrated, aqueous piperazine. International Journal of Greenhouse Gas Control, 4, 119-124.

Gabrielsen, J. (2007). CO2 Capture from Coal Fired Power Plants.

Gaspar, J., & Fosbøl, P. L. (2015). A general enhancement factor model for absorption and desorption systems: A CO2 capture case-study. Chemical Engineering Science, 138, 203-215.

Gaspar, J., Thomsen, K., von Solms, N., & Fosbøl, P. L. (2014). Solid Formation in Piperazine Rate-based Simulation. Energy Procedia, 63, 1074-1083.

Gaspar, J., von Solms, N., Thomsen, K., & Fosbøl, P. L. (2015). Multivariable Optimization of the Piperazine CO2 Post-Combustion Capture Process. Energy Procedia, Procecddings of the 8th Trondheim Conference on Capture, Transport and Storage (TCCS8).

Lin, Y., & Rochelle, G. T. (2014). Optimization of Advanced Flash Stripper for CO2 Capture using Piperazine. Energy Procedia, 63, 1504-1513.

Madan, T., Van Wagener, D. H., Chen, E., & Rochelle, G. T. (2013). Modeling pilot plant results for CO2 stripping using piperazine in two stage flash. Ghgt-11, 37, 386-399.

Plaza, J. M. (2011). Modeling of Carbon Dioxide Absorption using Aqueous Monoethanolamine, Piperazine and Promoted Potassium Carbonate.

Plaza, J. M., & Rochelle, G. T. (2011). Modeling pilot plant results for CO2 capture by aqueous piperazine. 10th International Conference on Greenhouse Gas Control Technologies, 4, 1593-1600.

Rocha, J. A., Bravo, J. L., & Fair, J. R. (1996). Distillation columns containing structured packings: A comprehensive model for their performance .2. Mass-transfer model. Industrial & Engineering Chemistry Research, 35, 1660-1667.

Rocha, J. A., Bravo, J. L., & Fair, J. R. (1993). Distillation-Columns Containing Structured Packings - a Comprehensive Model for their Performance .1. Hydraulic Models. Industrial & Engineering Chemistry Research, 32, 641-651.

Rochelle, G., Chen, E., Freeman, S., Van Wagener, D., Xu, Q., & Voice, A. (2011). Aqueous piperazine as the new standard for CO2 capture technology. Chemical Engineering Journal, 171, 725-733.

Sachde, D., & Rochelle, G. T. (2014). Absorber Intercooling Configurations using Aqueous Piperazine for Capture from Sources with 4 to 27% CO2. Energy Procedia, 63, 1637-1656.

Thomsen, K., & Rasmussen, P. (1999). Modeling of vapor–liquid–solid equilibrium in gas–aqueous electrolyte systems. Chemical Engineering Science, 54, 1787-1802.

Thomsen, K., Rasmussen, P., & Gani, R. (1996). Correlation and prediction of thermal properties and phase behaviour for a class of aqueous electrolyte systems. Chemical Engineering Science, 51, 3675-3683.

Van Wagener, D. H., Rochelle, G. T., & Chen, E. (2013). Modeling of pilot stripper results for CO2 capture by aqueous piperazine. International Journal of Greenhouse Gas Control, 12, 280-287.

Chapter 5. Dynamic modelling and validation of CO_2 post-combustion capture using piperazine (PZ) and MEA

5.1 Introduction

During the last decades, several research groups developed steady-state models for simulation of CO_2 post-combustion capture. These models have been used for process design and optimization. However, it has been recognized that dynamic models are required in order to understand the transient behaviour of the capture process, to identify process bottlenecks and to observe the effect of interactions between the units of a power plant with integrated CO_2 capture (Lawal et al., 2010). Accordingly, dynamic simulations, controllability and flexibility evaluations receive increasing attention as post-combustion capture reaches industrial deployment. A comprehensive overview of the current status on dynamic modelling of CO_2 post-combustion capture is presented by Bui et al. (2014). Some of the recent contributors are particularly noteworthy in the context of dynamic modelling, such as Biliyok et al. (2012); Enaasen Flø et al. (2015); Harun et al. (2012); Jayarathna et al. (2013); Karimi et al. (2012); Lawal et al. (2012) and Mac Dowell et al. (2013). They presented plant-wide dynamic models for post-combustion capture plants and investigated the response of the capture plant for changes in key process parameters, e.g. flue gas flow, lean solvent flow, make-up water flow, reboiler duty, etc. These studies represent a first insight into the dynamics of a capture process and represent the basis for controllability and flexibility studies.

Validation of post-combustion capture process models against dynamic experimental data is needed to prove the reliability of transient simulation results. There are only a few dynamic validation studies that we are aware of, mainly due to the lack of experimental data. Validation of an absorber model against dynamic pilot plant data was first performed by Kvamsdal et al. (2011). Later, Biliyok et al. (2012) validated the model of a post-combustion capture plant using plant log-data. These data were not collected from specifically designed dynamic campaigns, and therefore it is not certain if it captures the relevant dynamics of the system. Absorber and desorber temperature profiles collected in a dynamic campaign were used for model validation by Bui et al. (2013). They compared calculated and measured data for step-changes in the flue gas flow rate

and the lean solvent flow rate. In recent papers, Enaasen et al. (2014) and Enaasen et al. (2015) presented a dynamic process model of a post-combustion CO_2 capture plant implemented in K-Spice respectively Matlab. They compared model predictions to experimental data, collected from the Brindhisi and Gløshaugen plant. Both of the campaigns targeted industrially relevant operational scenarios, e.g. step changes in the flue gas respectively steam flow rate. These studies used monoethanolamine (MEA) as solvent. To our knowledge, only a few studies present dynamic models for CO_2 post-combustion capture using other solvents than MEA. Gaspar and Cormos (2012) presented a dynamic absorber model for MEA, diethanolamine (DEA), 2-amino-methylpropanol (AMP) and methyl-diethanloamine (MDEA). They demonstrate that kinetics play a key role in the dynamic behaviour of the capture process. Thus, it is essential to validate and investigate the transient behaviour of post-combustion capture plants using novel solvents. Furthermore, Dietl et al. (2012) investigated the dynamic behaviour of a CO_2 capture plant using an amino acid solvent. They presented the dynamics of a capture process for a decrease in heat duty at constant flue gas flow rate. They showed the differences between the dynamics of standalone and coupled simulation of an absorber and a desorber. This study underlined that it is important to study the dynamics of post-combustion as a whole and not as separated process units.

This chapter presents a mechanistic dynamic rate-based model for CO_2 post-combustion capture and it applies to the innovative piperazine (PZ) and the benchmark monoethanolamine (MEA) solvents. The model of the plant consists of an absorber, a desorber and auxiliary units, i.e. sump, the buffer tank, the reboiler and the heat exchanger. The developed mathematical model takes into account the accumulation of mass and energy in both the gas and the liquid phase and it uses the general model (GM) enhancement factor to account for the simultaneous reactions and mass transfer phenomena. The kinetic model includes two parallel reactions to describe the CO_2-PZ system and one single reaction to characterize the CO_2-MEA system. It is essential to include both of the reactions for the PZ solvent since the contribution of the bicarbamate forming reaction is greater than 30% at high CO_2 loading (Gaspar and Fosbol, 2016). Furthermore, the dynamic model uses the extended UNIQUAC thermodynamic model to calculate vapour-liquid equilibrium, thermal properties and speciation in the electrolyte systems. The model of the complete post-combustion plant is implemented in Matlab in combination with FORTRAN subroutines for mass transfer, hydraulic and thermodynamic model calculations. The developed CO_2 capture model is compared to dynamic experimental data using MEA for step changes in the flue gas flow rate and the reboiler heat duty and the model is compared to steady-state pilot plant data using PZ for various lean CO_2 loadings and a broad range of L/G ratios as well as reboiler operating pressures. Additionally, the transient response of an absorber and a desorber for step changes of key process parameters, e.g. flue gas flow and composition, lean and rich CO_2 loading, etc. is investigated here for both amines. To the author's knowledge, this is the first study that presents a dynamic packed column in Matlab for PZ CO_2 capture process. The outcome of this

study is essential for further simulation, development, and understanding of the dynamic behaviour of post-combustion capture units using novel solvents.

5.2 Dynamic model for CO_2 absorption and desorption

This section presents the mechanistic first-principles dynamic model for CO_2 absorption and desorption. It introduces the basic assumptions and presents the mass and energy balance equations for the gas phase and for the liquid phase. The implementation methodology is discussed at the end of this section.

The developed model classifies in the second highest level of model complexity for packed columns according to Kenig et al. (2001). It is a dynamic rate-based model which includes an enhancement factor to estimate the real CO_2 mass transfer rate using correlations for mass transfer and hydraulic properties. It uses electrolyte thermodynamics to predict the concentration of species in the liquid phase and to calculate thermal properties such as heat capacities, equilibrium partial pressure, solubility coefficient, etc.

5.2.1 Modeling assumptions

A common approach to represent packed columns, e.g. absorber and desorber, is as a cascade of dynamic, non-equilibrium segments where an interface divides each segment into a gas side and a liquid side. The mass and heat transfer takes place through this gas-liquid interface. The equations for the segments are identical with the exception of the column boundaries, i.e. the first and the last segments. The solvent temperature, composition and flow rate are specified for the N-th segment at the top of the column. The gas temperature, composition and flow rate are specified at the bottom of the column, the first control element. In the development of the dynamic model, we apply the following assumptions:

- Radial distribution of temperature, composition and fluxes are neglected.
- Accumulation in the gas phase and in the liquid phase is much slower compared to changes in composition and temperature, i.e. $\partial C_g / \partial t = 0$ and $\partial C_l / \partial t = 0$.
- Gas phase is ideal due to low pressure.
- The amine is non-volatile.
- Amine degradation rate is much slower compared to the investigated time interval.
- Reaction takes place only in the liquid film.
- Phase equilibrium prevails at the gas-liquid interface.
- Heat loss to the surroundings is negligible.

In addition, we consider that mass and heat transfer between the phases is bi-directional. Positive sign shows mass transfer from the gas phase to the liquid phase, i.e. absorption and condensation. Negative sign refers to desorption and evaporation.

5.2.2 Mass and energy conservation for the gas phase and the liquid phase

The developed rate-based model (dCAPCO2) consists of partial differential equations to describe the variation of process parameters in time and space. The absorber and the desorber model are identical with the exception that the desorber requires a reboiler. Table 5.1 shows these conservation equations for a segment of height dz. For more details we refer to Gaspar et al. (2015b), Appendix F.

Table 5.1. Equations system of the dCAPCO2 rate-based model

Gas phase equations

Total material balance	$0 = -\dfrac{\partial N_g}{\partial z} - a_{eff}\left(J_{CO_2,gl} + J_{H_2O,gl}\right)$	(5.1)
Component material balance	$\varepsilon\left(1 - h_l\right)C_g\dfrac{\partial y_{i,g}}{\partial t} = -N_g\dfrac{\partial y_{i,g}}{\partial z} + y_{i,g}\dfrac{\partial N_g}{\partial z} - a_{eff}J_{i,gl}$	(5.2)
Energy balance	$\varepsilon C_{p,g}C_g\dfrac{\partial T_g}{\partial t} = -C_{p,g}N_g\dfrac{\partial T_g}{\partial z}C_{p,g}T_g\dfrac{\partial N_g}{\partial z} - a_{eff}q_{cond}$	(5.3)

Liquid phase equations

Total material balance	$0 = \dfrac{\partial N_l}{\partial z} + a_{eff}J_{H_2O,gl}$	(5.4)
Component material balance	$\varepsilon h_l C_l\dfrac{\partial X_{i,l}}{\partial t} = N_l\dfrac{\partial X_{i,l}}{\partial z} + X_{i,l}\dfrac{\partial N_l}{\partial z} + a_{eff}J_{i,gl}$	(5.5)
Energy balance	$\varepsilon C_{p,l}C_l\dfrac{\partial T_l}{\partial t} = C_{p,l}N_l\dfrac{\partial T_l}{\partial z} + C_{p,l}T_l\dfrac{\partial N_l}{\partial z} + a_{eff}\left(q_{cond} + q_{conv} + q_{gen}\right)$	(5.6)

In equations (5.1) to (5.6), N_g represents the total gas flux (mol/m²s); N_l is the apparent solvent flux, expressed on a CO_2-free basis (mol/m²s); C_g respectively C_l refer to the mol-density of the gas respectively liquid phase (mol/m³). The parameters ε refer to the void fraction, h_l is the liquid holdup, a_{eff} is the effective mass transfer area and $C_{p,g}$ respectively $C_{p,l}$ show the specific heat capacity of the gas respectively liquid phase. Similar to the liquid flux, the composition of the liquid phase, eq. (5.5) is defined on a CO_2-free basis. Thus, X_i represents the amount of component i (CO_2 and H_2O) per moles of water plus amine (MEA and PZ). This approach ensures to overcome the uncertainties related to physical property correlations, e.g. viscosity,

diffusivity, etc. of CO_2 loaded solutions. The composition of the gas phase is represented by y_i, where i is CO_2 and H_2O; T_g and T_l denote the temperature of the gas and liquid phase respectively.

The dCAPCO2 model uses the General Method (GM) enhancement factor model to determine the CO_2 mass transfer flux, $J_{CO2,gl}$, through the gas-liquid interface (Gaspar and Fosbøl, 2015). The GM model for the investigated amines is presented in Chapter 2. The dynamic capture model uses the extended UNIQUAC thermodynamic model for vapour-liquid and thermal properties calculation. Faramarzi et al. (2009), Fosbøl et al. (2013) and Sadegh et al. (2015) demonstrated the very good agreement between the extended UNIQUAC thermodynamic model and several experimental dataset. The mass transfer and hydraulic parameters, i.e. mass transfer area, hold-up, pressure drop and mass transfer resistance are calculated with the Rocha model (Rocha et al., 1996, 1993). The physical properties correlations entering this model are presented in Table 3.2. These were verified to experimental data for absorption and desorption conditions. Similar to previous works, the energy conservation equations (5.3) and (5.6), include a conductive heat transfer term (q_{cond}), a heat source term (q_{gen}) and a convective term (Enaasen et al., 2015; Gáspár and Cormoş, 2011; Nittaya et al., 2014). The source term represents the heat produced by CO_2 and H_2O evaporation respectively condensation. The convective term accounts for interphase mass transport. Thermal properties entering these equations are obtained from the extended UNIQUAC thermodynamic model. Conductive heat transfer is a result of temperature gradient between the gas phase and the liquid phases. The Chilton-Colburn analogy gives the heat transfer coefficient entering the conductive heat transfer term (Bird et al., 2007).

The models of the absorber sump and of the reboiler are simplified in this study. A dynamic continuous stirred-tank model is used for simulation of the absorber sump (Harun et al., 2012). The reboiler and heat exchanger is modelled as a flash tank with instantaneous heat exchange between the heating medium and solvent assuming perfect level control, similar to (Enaasen Flø et al., 2015).

5.2.3 Interfacing Matlab and FORTRAN

The dynamic model and the steady-state model shares the GM enhancement factor model, the extended UNIQUAC thermodynamic model, and the mass and hydraulic characteristics model. Essentially, all the independent variables entering the partial differential equation system of the dynamic model are calculated using the same sub-modules as the steady-state model presented in Chapter 3. These are implemented in FORTRAN and they are interfaced with Matlab using binary MEX files. This approach eases code maintenance and assures consistency between the dynamic and the steady-state model.

A simple solution to connect the FORTRAN modules to Matlab, is to migrate the source code together with its dependencies using the Dynamic Link Libraries (DLL) technology. This technology gives access to the functionalities of the rate-based model. Then, this DLL is called in Matlab by the use of MEX files.

5.2.4 Solution strategy

The material and energy conservation equations presented in table 5.1 are discretized in the axial domain using the finite differences method (FDM). FDM represents the spatial derivatives in discrete grid points. Therefore, the partial differential equations system (PDE) reduces to a system of ordinary differential and algebraic equations (DAE), with time as the independent variable. This set of DAE is integrated using the ODE15s Matlab solver with the boundary conditions at the top for the liquid phase and at the bottom for the gas phase. This approach provides a simple way to solve the model. However, realistic initial conditions have to be provided to obtain convergence. To assure fast convergence and robustness, the dynamic model is initialized using steady-state values, determined by the CAPCO2 steady-state model.

5.3 Validation of the Dynamic Model

The dynamics of a post-combustion capture plant is mainly influenced by the absorber and the desorber. Consequently, we focus on the transient response of these columns using the baseline MEA and the promising PZ solvents. We compare the transient behaviour of the columns using MEA to dynamic pilot plant measurements for two scenarios: flue gas ramp-up respectively ramp down (test 1) and steam flow rate ramp up and ramp down (test 2). We present CO_2 absorption and desorption rates and temperature profiles. Furthermore, we validate the model for PZ CO_2 capture simulation against pilot plant steady-state experiments. We show absorption and desorption efficiencies, temperatures and reboiler heat duties.

5.3.1 Model validation using MEA

5.3.1.1 The MEA pilot campaign

The MEA dynamic campaign was carried out using an approximately 13.5 dry mol% CO_2 flue gas which was saturated with water before entering the absorber. The composition of the flue gas stream from the power plant fluctuated ±1.5%. This gas flow was contacted with a 30 wt.% MEA solution with a loading of approximately 0.21 mol CO_2/mol MEA. Before the step change, the capture plant was operated at nominal 90% CO_2 capture. Both of the columns, absorber and stripper, have a diameter of 1.1 m. The height of the absorber is 17 m and the height of the stripper is 10 m. The absorber was equipped with Mellapak 2X structured packing and the desorber with IMTP50 dumped packing. The heat to the reboiler was supplied by utility steam from the power plant at 2.5 barg. The capacity of the pilot is 1 t/h CO_2.

We simulate the capture process in open control loop, identical to the pilot plant operation. The focus is on the dynamic behaviour of the absorber and the desorber. In this analysis, we specify the flue gas flow and the steam input to the reboiler and we keep the levels in the absorber sump and the reboiler drum according to the experimental values. In addition, we specify the temperature of the stripper feed to minimize the influence of the absorber on the desorber and vice-versa. This approach aims at eliminating uncertainties related to additional units, such as the network of heat exchangers.

Minor initial state discrepancies will increase over time due to the recycle lean stream. One can see that a small initial over-prediction of the lean CO_2 loading results in lower CO_2 capture rate. Consequently, the stream entering the stripper will contains less CO_2. This difference will iterate and potentially increase in time. Moreover, the initial steady-state of the capture plant is another source of error. It is hard to ensure full steady-state, especially when the capture unit is connected to a power plant since fluctuations of the power plant perturb the capture unit. To minimize these uncertainties, first we close the lean-recycle loop and we use these steady-state conditions as starting point for the dynamic simulation. Essentially, this approach translates to minor adjustments (up to 5%) of the lean flow entering the absorber and the steam flow to the reboiler. Similar approach was adopted by Biliyok et al. (2012) and Kvamsdal et al. (2011).

5.3.1.2 Capture plant load change scenario

Part load operation of power plants is a common scenario observed during flexible operation. It results in sudden changes of the flue gas flow rate and the quality of the steam. Consequently, we compare the observed dynamics of the absorber and of the desorber to model predictions for: (test 1a) flue gas flow ramp down from 5000 Nm^3/h to 3500 Nm^3/h and (test 1b) flue gas flow rate ramp up from 4100 Nm^3/h to 5000 Nm^3/h. The step change is applied after 30 min respectively 17 min of steady-state operation. Figure 5.2A shows the measured flue gas flow rate versus time for these scenarios. Test 1 results in modified contact time between the gas and the liquid phase and therefore in varying CO_2 removal efficiency.

Figure 5.2B shows the change in the absorber outlet CO_2 composition as function of time for test 1a and 1b. It illustrates how the model and the experiment agree well for both, ramp up and ramp down scenarios. The deviations are within 10%, in the expected accuracy range of any model (Fosbøl et al., 2014). This figure illustrates how the model captures well the dynamics of the absorber. It predicts the fast responses in the CO_2 concentration occurring after the change in the flue gas flow rate. It also predicts the slower, transient evolution of the capture plant as well. It can be observed for test 1b that the CO_2 composition of the outlet gas stream increases suddenly after the step change (17 min) and there is a second increase after 33 min. This is well-captured by the model. The second jump in the CO_2 content is due to the interaction between the absorber and the desorber. Higher flue gas flow (test 1b) produces an increase in the CO_2 loading of the rich stream. As a consequence, CO_2 accumulates in the sump of the absorber and drifts the CO_2 loading of the

stripper's feed. However, the heat input to the reboiler is kept constant and as a consequence the outlet lean CO_2 loading of the reboiler increases. Thus, as shown in figure 5.2B that the model describes well the interaction between the absorber and desorber.
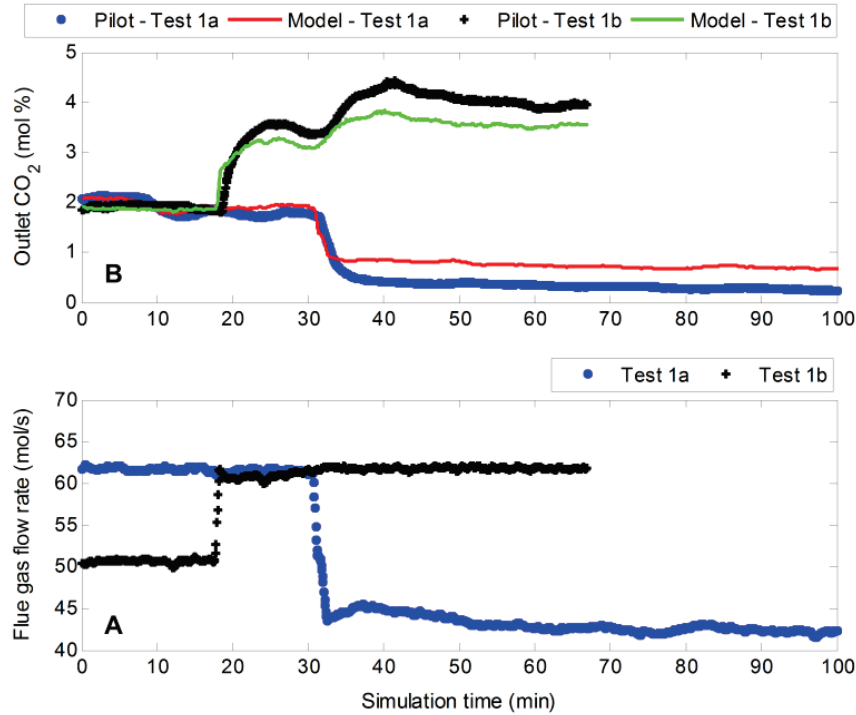

Figure 5.2. (A) Pilot flue gas flow rate and (B) predicted CO_2 composition.

To provide further insight, figure 5.3 and 5.4 show the changes in the CO_2 absorption and desorption rates for test 1a and 1b. These figures illustrate how the model follows the transient evolution of the pilot plant. The model captures how the CO_2 absorption rate changes fast and it reaches a new steady-state in approximately 10 min. The response in the CO_2 desorption rate is delayed with $10 - 15$ min which is caused by the sump, as explained above. Furthermore, the results reveal that a decrease of the flue gas flow (figure 5.3) has a greater impact on the CO_2 removal efficiency than an increase (figure 5.4). The settling time for test 1a is 70 min compared to 30 min for test 1b. Figure 5.3 on test 1a shows that the CO_2 absorption respectively desorption rate reduces roughly 15% after the step change.
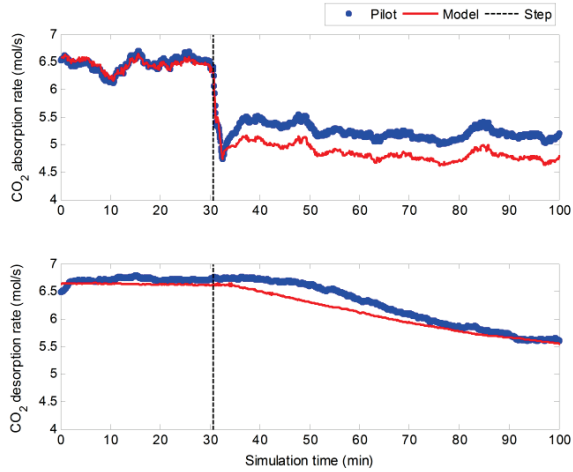
171

Figure 5.3. CO$_2$ absorption and desorption rate for test 1a – flue gas ramp-down
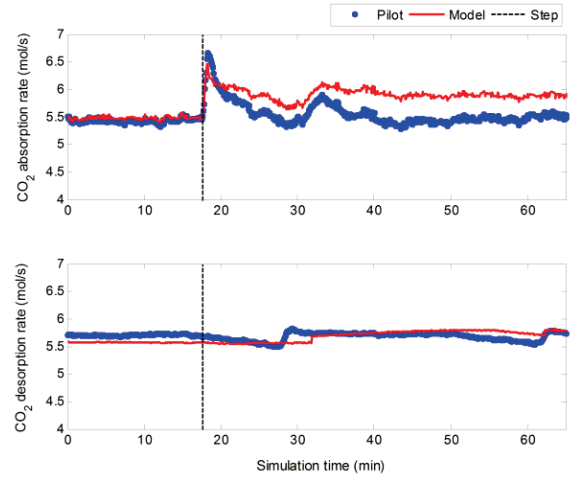

Figure 5.4. CO$_2$ absorption and desorption rate for test 1b – flue gas ramp-up

Figure 5.5 presents the absorber temperature profile at different time intervals. Generally, the model and the experiments are in good agreement. Figure 5.5A demonstrates how the temperature-bulge moves towards the middle of the column when the flue gas flow rate decreases. On the other hand, figure 5.5B shows that the temperature remains relatively constant when the flue gas flow rate increases. This is expected, since the CO$_2$ absorption rate is almost constant. This figure outlines the presence of a systemic deviation between the model and the experiment, but the deviations are in the expected range (up to 10%). This discrepancy may be related to the mass transfer model as shown by Cormos and Gaspar (2012). Moreover, here we show the liquid phase temperature, but in practice the gas and liquid temperature cannot be measured separately. Note, we do not show the temperature profiles for the desorber since the changes in temperature are insignificant.
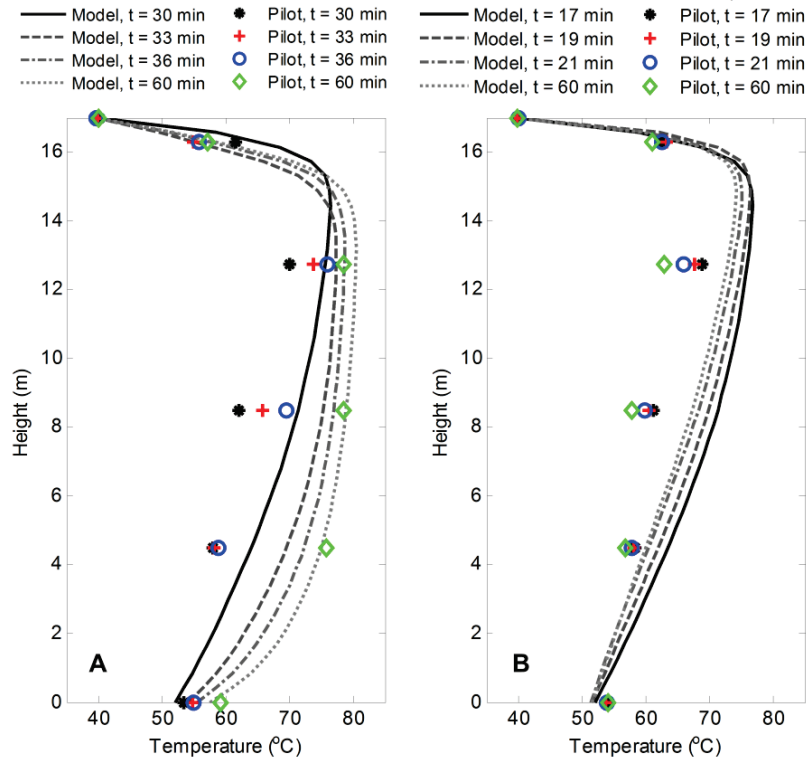
Figure 5.5. Absorber temperature profile for (A) test 1a and (B) test 1b at different times

This analysis reveals how the response of the absorber is fast for changes in the flue gas flow rate and the effect of flue gas flow on the stripper is damped by the sump and consequently there is a time-delay between the step change and the response of the stripper. Furthermore, the results reveal that the model predicts well CO_2 absorption and desorption as well as the trend of the temperature variation.

5.3.1.3 Steam flow change scenario

Excess or shortage of steam supply is another common flexible operation scenario. Consequently, we compare the dynamics of the capture plant to pilot plant dynamic data for: (test 2a) reduction of the steam flow rate by 25% and (test 2b) increase of the steam flow by 15%. The step change is applied after 28 min respectively 25 min of steady-state operation.

The transient responses in the absorption respectively desorption rates for test 2a and 2b are presented in figure 5.6 and 5.7. These figures show how the CO_2 stripping efficiency decreases rapidly when the reboiler duty reduces and vice-versa. There is a time-delay of 10-15 min in the response of the absorber, due to the buffer mixing tank. The role of this tank, similar to the absorber sump, is to smoothen the changes in the lean feed.

Figure 5.6 on reboiler duty shortage shows that the model predicts fairly well the transient behaviour of the capture plant. It describes well the time delay in the response of the absorber as well as the sudden drop in stripping efficiency. The measured and calculated absorption rates almost overlap but the model under-predicts the desorption rate with approximately 0.6 mol/s. This corresponds to a systematic relative deviation of approximately 10%. The reason for under-prediction of the measured values may be related to changes in the heat-loss through the reboiler as well as the assumption of a flash tank reboiler with instantaneous heat exchange between the heating medium and the solvent.
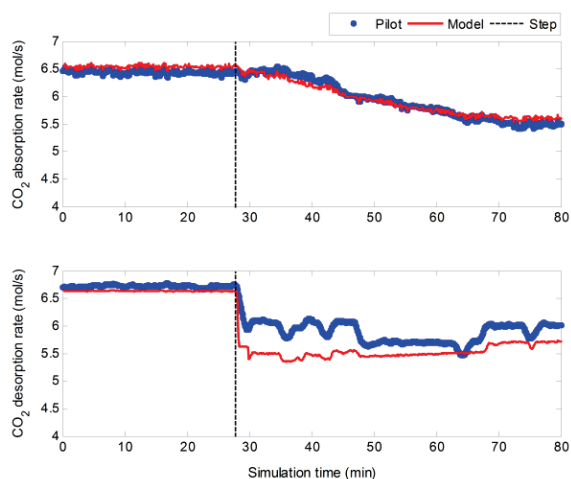

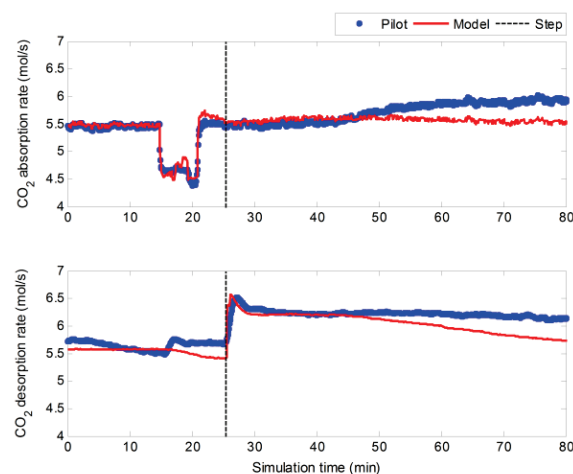Figure 5.6. CO_2 absorption and desorption rate for test 2a – steam shortage

Figure 5.7. CO_2 absorption and desorption rate for test 2b – steam excess

Figure 5.7 shows the dynamics of the capture plant for excess of steam. It demonstrates that the model predicts a similar trajectory as observed in the pilot plant: a 15% increase of the reboiler duty produces a 0.5 mol/s higher CO_2 desorption rate. The settling time for the stripper is around 10 min and there is a delay of 20 min in the response of the absorber. It has to be mentioned that unexpected sudden changes were recorded during test 2b. For example, the CO_2 absorption rate reduced from 5.5 mol/s to 4.5 mol/s between 16 and 20 min, due to a drop in the flue gas flow rate but the CO_2 outlet mol fraction remained constant. Thus, it suggests that the flow rate or concentration probes failed and the reliability of this dataset is questionable. Nevertheless, we show the results for this run with the purpose of discussing the dynamics of steam excess scenario and to emphasize the importance of reliable measurements for validation of process dynamics.

Figure 5.7 emphasizes how sensitive is a dynamic simulation to small discrepancies between model and measurement. After 47 min of operation, the model under-predicts the CO_2 desorption rate; thus the CO_2 loading of the absorber feed increases. As a consequence of higher lean loading, the CO_2 absorption rate decreases (see Figure 5.7A). The interaction of the absorber and desorber makes dynamic validation a laborious task: even a small deviation from the pilot plant over time may result in large discrepancies.

Figure 5.8 presents the calculated and measured temperature profiles for test 2a and 2b at different time intervals. The pilot and simulation results emphasize that steam shortage produces temperature decrease (figure 5.8A) and steam excess results in higher temperature values (figure 5.8B). Figure 5.8B illustrates how the measured and simulation values agree well. The deviations between model and pilot data are less than 2.2 K at the bottom, middle and top. On the other hand, the model predicts greater temperature change compared to experimental values for steam shortage (test 2a). The deviations are between -3.6 K and 6.6 K in the middle section and they are less than 2.5 K at the top and bottom. This may be related to the lower stripping rate, shown in figure 5.6. Figure 5.8 demonstrates that the measured and calculated reboiler temperatures almost overlap. The difference between model and pilot plant data is less than 0.7 K.
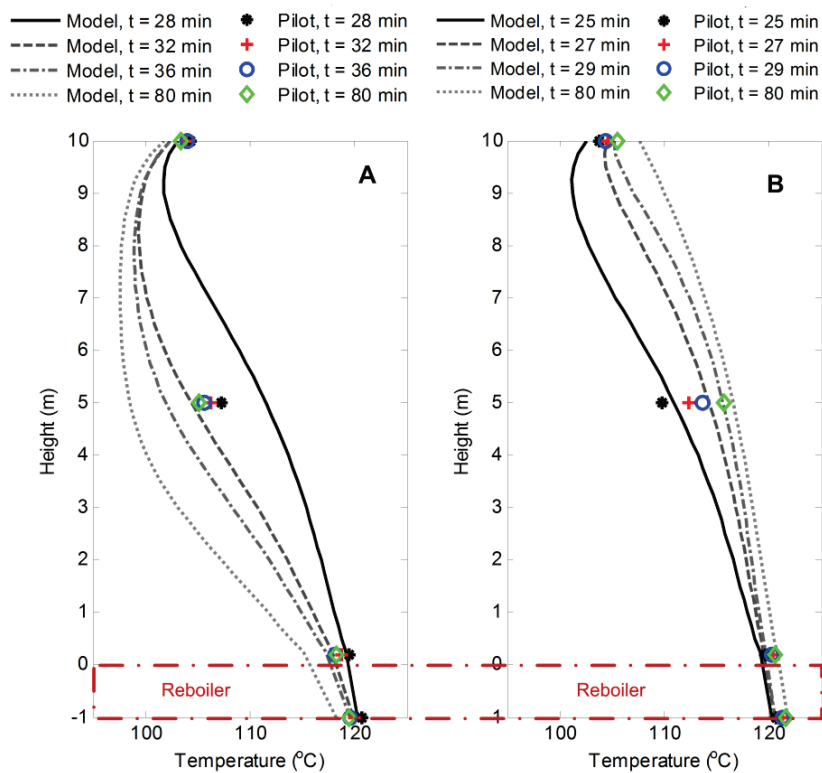

Figure 5.8. Desorber temperature profile for (A) test 2a and (B) test 2b at different times

Fosbøl et al. (2014) showed that a 5 – 10% deviation should be expected when comparing model to experimental data. Some properties, such as outlet temperature (top respectively bottom), solvent temperature to reboiler are more trustworthy than other properties such as stripper top CO_2 flow, reboiler temperature, temperature in the mid sections of a column, etc. Conclusively, the dynamic model predictions are in the expected accuracy range and the model estimates similar transient trajectory as observed in the pilot plant: it catches the fast responses as well as the slower responses with time-delays.

5.3.2 Model validation using PZ

We compare the model predictions for CO_2 absorption and desorption to experimental measurements carried out at the J. J. Pickle Research Center, north of Austin, TX, USA. Here, we include results for campaigns "Fall 2008" and "Fall 2010" (Frailie et al., 2011; Plaza and Rochelle, 2011). To our knowledge, open-source dynamic data for PZ are not available, and the accuracy of the model is evaluated at steady-state conditions.

5.3.2.1 The PZ pilot campaign

The "Fall 2008" and "Fall 2010" pilot campaigns with PZ were carried out with a synthetic flue gas of 12 mol% CO_2, not saturated with water at the inlet of the absorber. The pilot experiments were performed with approximately constant flue gas flow rate which was contacted with a 4 to 8 molal PZ solution ("Fall 2008" campaign) respectively 8 molal solution ("Fall 2010" campaign). The CO_2 loading of the lean solvent varied between 0.2 and 0.37 mol CO_2/mol alkalinity. More details regarding the pilot campaigns can be found in (Frailie et al., 2011; Plaza and Rochelle, 2011).

5.3.2.2 Validation at absorber conditions

We compare the model predictions to the results of "Fall 2008" campaign. During this campaign, the absorber was operated with different L/G ratios and lean CO_2 loadings. Thus, these data are useful to investigate the accuracy of the model at full-load and part-load operation of the plant. We eliminated the "Fall 2010" campaign from this analysis since it was run with an absorber with intercooling.

The model predictions against the measured values are shown in figure 5.9 and 5.10. Figure 5.9 highlights that the calculated and measured CO_2 absorption rates are in good agreement for different piperazine concentrations, i.e. 4, 7 and 8 molal PZ. There is only one point much outside of the $\pm$ 10% accuracy range which is most probably an outlier. The inlet temperature of the flue gas for this outlier is -5ºC, which represents the lower limit of the experimental temperature range. Furthermore, (Plaza, 2011) shows that the accuracy of the absorber titrations are within $\pm$ 10% and the liquid side removal matches the gas side results within $\pm$15%. Thus, the model predictions are within the accuracy of the measurements. Figure 5.10 shows the calculated rich outlet solvent temperature as function of the measured values. The deviations between model and pilot results are between -2.9 K and 3.4 K, within $\pm$ 10%.
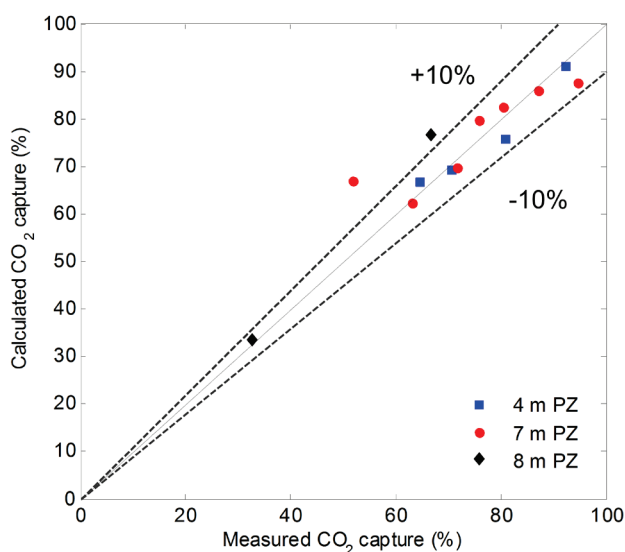
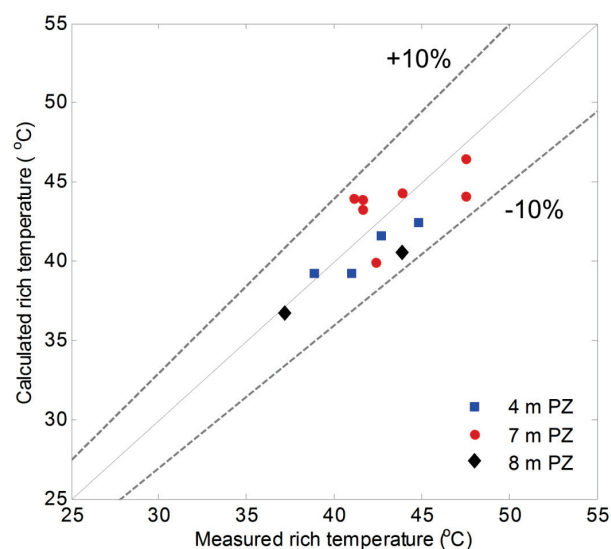Figure 5.9. Predicted versus measured CO_2 absorption rates

Figure 5.10. Predicted versus measured absorber rich temperature

It can be concluded that the developed model is in good agreement with the experimental data and it can be used for piperazine CO_2 absorption simulation at different PZ concentrations and L/G ratios.

5.3.2.3 Validation at desorber conditions

Here, we compare the model predictions to measurements of the "Fall 2008" and "Fall 2010" campaign using 8 molal PZ solution. The main difference between the two campaigns relies in the reboiler operating pressure. The "Fall 2008" tests were run at relatively low (137 kPa) and high pressures (between 350 and 413 kPa) while the reboiler pressure was moderate, between 200 kPa and 270 kPa during the "Fall 2010" campaign. Thus, these tests resemble scenarios with different steam supply.

Figure 5.11 shows calculated lean loadings versus experimental values. The agreement between the model and the pilot results is good. The predictions generally are in the ±10% range and the error in the prediction is not systematic.

Figure 5.12 shows a correspondingly good agreement between calculated and measured specific reboiler duties. The deviations generally fall within ±10%. The data is more scattered above 5 GJ/t CO_2 and some of the predictions deviate more than 20 % from the measured value. It is worth noting that these points belong to the "Fall 2010" campaign when the reboiler pressure was above 350 kPa. High reboiler pressure means higher temperatures, between 116 °C and 128 °C, and therefore the heat loss may be altered for the mentioned points.
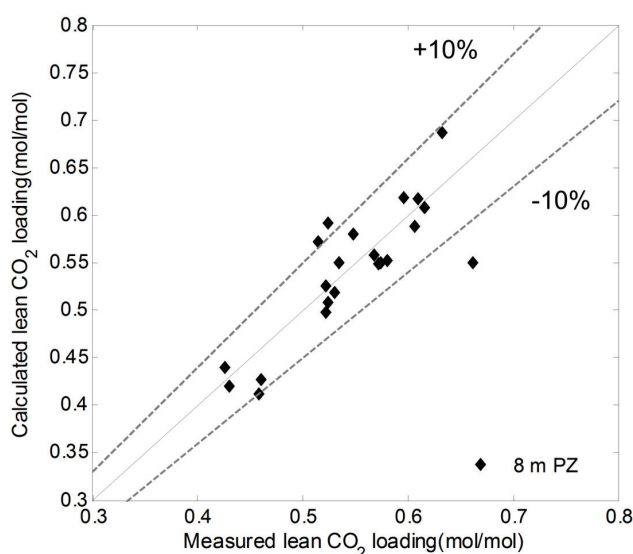
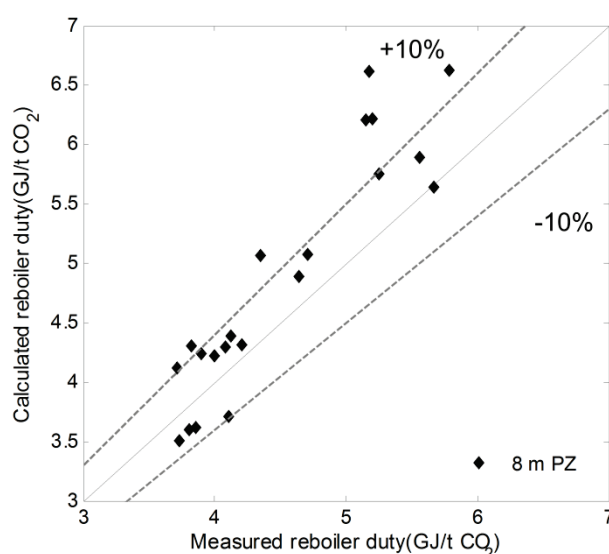Figure 5.11. Predicted versus measured stripper lean loading (mol/mol)

Figure 5.12. Predicted versus measured specific reboiler duty

It can be concluded that the model and the experimental measurements generally agrees well for absorption and desorption. The deviations are in the expected range, taking into account uncertainties and variations of some calculated simulation properties and accuracy of the measurements.

5.4 Dynamic simulation and analysis

One of the major costs associated with the operation of a CO_2 post-combustion capture plant is the circulation and regeneration of the solvent. They are mainly influenced by the performance of the absorber and the desorber units. Accordingly, we focus first on the transient response of the absorber for step changes in the flue gas flow rate, flue gas composition and lean CO_2 loading. Afterwards, we analyse the dynamics of the stripper for variation of the CO_2 loading and temperature of the feed stream. This study represents the first step towards the development of suitable control strategies for the piperazine-based CO_2 capture plant.

The base case operating conditions correspond to a 1 t/hr CO_2 capacity post-combustion capture plant using 30 wt% MEA (7 molal) and 30 wt% PZ (5 molal) solutions, respectively. The loading of the lean solution entering the absorber is approximately 0.20 mol CO_2/mol alkalinity at 40°C. The flue gas coming from a coal-fired power plant contains 12.4 mol% of CO_2 and it is saturated with water before entering the absorber. Table 5.2 summarizes the main design specifications and process parameters for the post-combustion CO_2 capture plant (Faber et al., 2011).

Table 5.2. Design specifications for the absorber and the stripper

Flue gas flow rate (mol/s)	61.5
Flue gas temperature (°C)	40
Flue gas pressure (kPa)	101.32
Flue gas CO_2 composition (mol%)	12.4
Flue gas H_2O composition (mol%)	10.9
Lean inlet temperature (°C)	40
PZ/MEA lean loading (mol/mol alk.)	0.18/0.2
Amine concentration (wt%)	30
L/G ratio for PZ/MEA (mol/mol)	3.5/3
CO_2 recovery (%)	90
Column diameter (m)	1.1
Absorber/Desorber height (m)	17/10
Reboiler operating pressure (kPa)	185

5.4.1   Absorber Simulation

This section shows the dynamic behaviour of the absorber for three scenarios: ±10% step change in the flue gas CO_2 concentration (case 1), ±10% step change in the lean CO_2 loading (case 2) and ±10% step change in the flue gas flow rate (case 3). These steps are applied to the base case after 10 min of steady-state operation. Here, we show the results for both solvents: PZ and MEA.

In practice, case 1 resembles operational conditions when the output of the power plant changes due to the heterogeneity of the fuel. This case is common, especially for biomass co-fired power plants. Case 2 resembles a scenario when a disturbance occurs in the operation of the stripper, e.g. steam supply shortage. Case 3 corresponds to part load operation of the power plant and represents one of the most common scenarios observed during flexible operation. Case 1 and case 2 result in changes of the CO_2 concentration gradient between the gas phase and the liquid phase. This gradient represents the driving force for absorption. Case 3 results in varying contact time inside the column, which changes the L/G ratio between the gas and the liquid phases.

Figure 5.13 shows the dynamic performance of the absorber for each case study using MEA and PZ. This figure illustrates how an increase of the flue gas CO_2 content, lean CO_2 loading, or the flue gas flow rate results in a reduction of the CO_2 capture efficiency and vice-versa (case 1 to 3). Furthermore, it highlights that the effect of a step change is greater using PZ compared to MEA. A 10% decrease of the shown

variables results in a CO_2 capture percentage of approximately 92% and 96% for MEA and PZ, respectively. For a 10% increase, the CO_2 capture percentage reduces to 86% and 83% for MEA and PZ, respectively.

Figure 5.13 also indicates that, for all the cases, the MEA system reaches steady-state faster than PZ. The CO_2 capture percentage stabilizes in about 10-15 minutes using MEA and using PZ stabilizes in roughly 40 min for a 10% step increase and in about 1 hour for a -10% step change. This is contrary to expected since PZ has a faster kinetics than MEA (Dugas and Rochelle, 2011b).
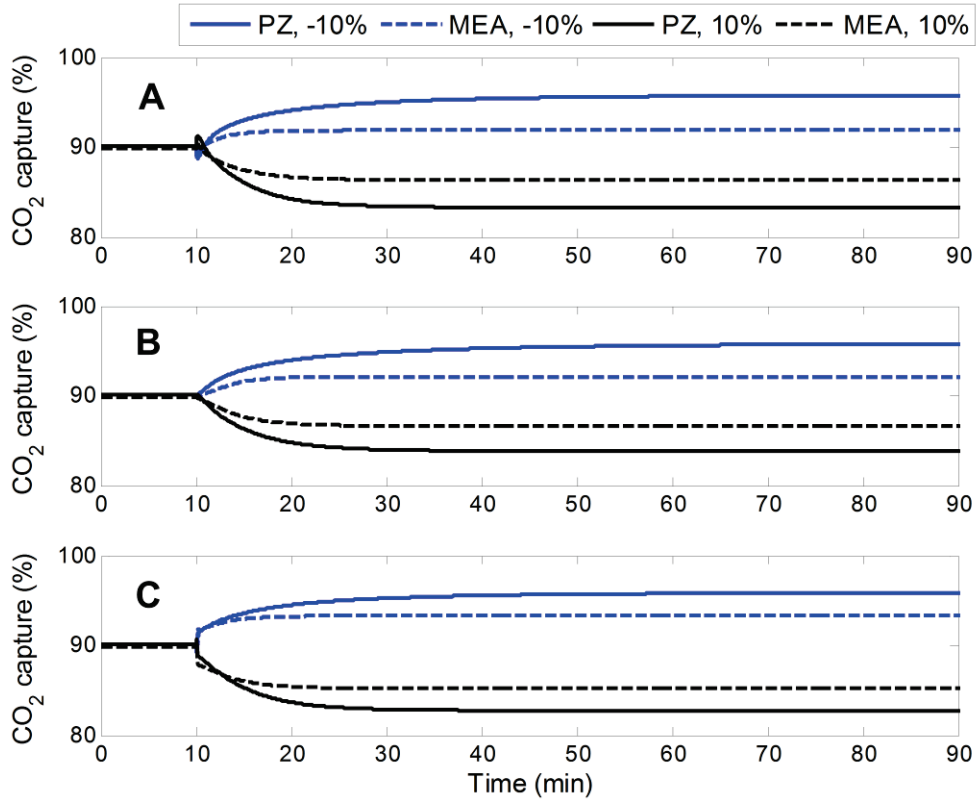
Figure 5.13. CO_2 capture percentage versus time using MEA and PZ for (A) case 1 – CO_2 composition, (B) case 2 – Lean loading and (C) case 3 – flue gas flow.

It was shown by Gaspar and Cormos (2012) that solvents with fast kinetics respond faster than those with slower kinetics. To understand this behaviour, the dynamics of the absorber for -10% step change in the flue gas CO_2 content is discussed in detail (figure 5.13A). Detailed analysis of case 2 and case 3 are not shown here for brevity; however, the dynamics of the system is similar to case 1. We chose the -10% step scenario since the difference between PZ and MEA is the most visible compared to the other cases.

Case 1: Decrease of the flue gas CO₂ composition

The case study presented here is equivalent to reducing the amount of CO_2 available for capture and it consists in lowering the driving force for absorption. The focus is on defining the differences between PZ and MEA and describing the dynamic coupling between temperature, gas phase composition, and liquid phase composition. These results are shown in figures 5.14 to 5.16.

Figure 5.14 presents how the gas phase CO_2 concentration decreases as function of time at several locations in the column for both MEA and PZ solvents. Figure 5.13A also shows how the CO_2 capture percentage increases. This is expected, since the free-amine to CO_2 gas ratio increases when the CO_2 composition is reduced. Furthermore, figure 5.14 illustrates that the MEA system responds faster since it reaches steady-state within 10 minutes. Contrary to MEA, PZ responds much slower. The settling time for the outlet top CO_2 concentration ($H_c=17\ m$) is roughly 30 min; however, the CO_2 concentration in the middle section of the absorber reaches steady state much slower, in approximately 2 hours. Nevertheless, both solvents present an initial fast response followed by a slow transient period as the system approaches the new steady-state.

Gáspár and Cormoş (2011) and Mac Dowell et al. (2013) showed that, for the MEA, the dynamics of mass transfer is tightly coupled to temperature changes and vice-versa. This is expected since additional CO_2 absorption by MEA produces more heat. On the other hand, higher temperature results in greater evaporation rate and it is favourable from a kinetic point of view. This coupling is obvious by comparing figures 5.14 to 5.16 as discussed below.

Figure 5.15 presents the CO_2 absorption rate as function of the column's height. Figure 5.15A on MEA outlines the presence of a small bulge in the absorption rate, but the efficiency of the column is well-balanced, between 0.1 and 0.2 mol CO_2/s alongside the height of the column. Contrary to MEA, there is a visible peak in figure 5.15B on PZ. This peak results in: (1) a more efficient section (4-7 m long, with an average absorption rate of 0.4 mol CO_2/s) where most of the CO_2 absorption takes place and (2) two less efficient sections above and below the mass transfer bulge (absorption rate below 0.15 mol CO_2/s). Figure 5.15B shows that this bulge moves downwards as a consequence of the 10% step decrease in the CO_2 content.

To provide further insight on the dynamics of mass transfer, we present the temperature profile inside the column at selected time snapshots in Figure 5.16. This figure reveals how the temperature profile is almost constant for MEA and it stabilizes in less than 10 min, similar to the gas phase composition in figure 5.14. The PZ temperature changes more slowly than the corresponding MEA temperature profiles. Figure 6B shows that the PZ temperature bulge gradually expands over the middle section of the absorber.
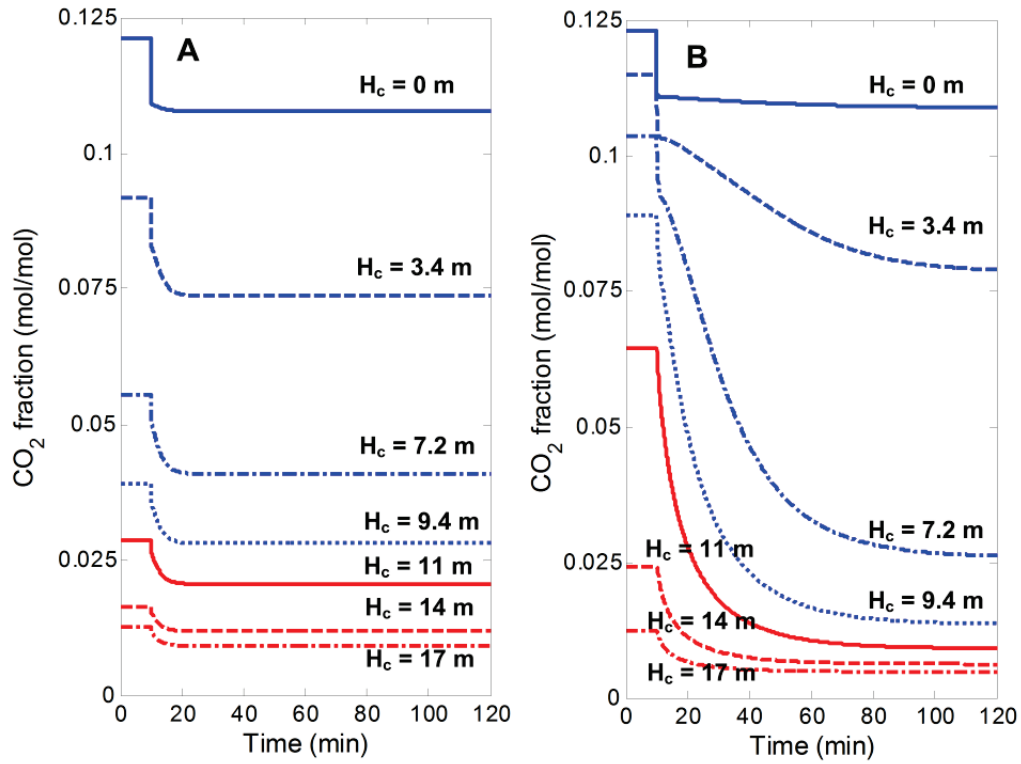
Figure 5.14. Gas phase CO_2 composition versus time using (A) MEA and (B) PZ.

By inspecting figure 5.15B and 5.16B on PZ, one can observe that the shift of the temperature bulge produces a change in the CO_2 absorption rate. Before the step change ($t=10$ min), the location of the peak is at 11.5 m while the temperature bulge is located around 14 m. As the system evolves, the mass transfer peak gradually moves to $H_c=5$ m, while the bulge expands over 7 m of height.

The results from this analysis show that the slow change of the temperature is synchronized with the shift of the mass transfer peak from the top to the bottom of the column. The absorption rate strongly depends on the temperature and it may result in a mass transfer pinch, as reported for steady-state conditions by Sachde and Rochelle (2014).

This analysis reveals that piperazine responds slower to disturbances than MEA and the inlet parameters have a significant effect on the PZ process. Accordingly, feedback controllers with high gains and short time-integrals may be required in the case of PZ to maintain the dynamic operation of the absorber column within reasonable short closed-loop settling times in the presence of these disturbances.
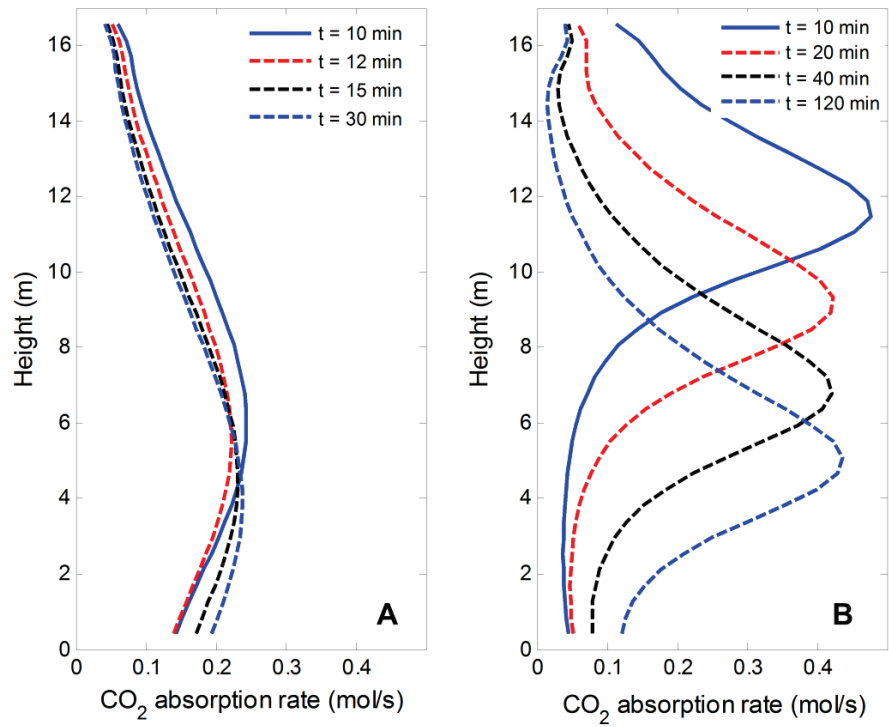
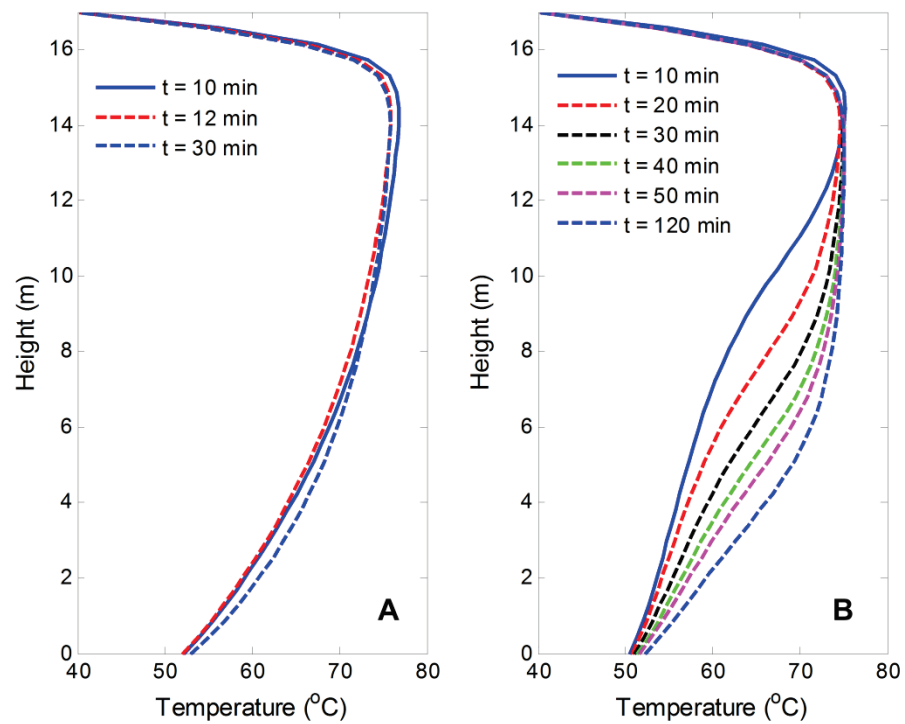Figure 5.15. CO_2 absorption rate versus height using (A) MEA and (B) PZ

Figure 5.16. Temperature versus absorber's height using (A) MEA and (B) PZ.

5.4.2 Desorber Simulation

We analyse the transient behaviour of the stripper using MEA and PZ for two scenarios: ±0.02 mol/mol alk. step change in the CO_2 loading of the rich feed (case 4) and ± 1°C step change in the temperature of the rich feed (case 5). The reboiler heat duty is kept constant during this analysis and the step is applied after 10 min of steady-state operation. Case 4 corresponds to small disturbances in the operation of the absorber. It may result from changes in the flue gas stream, as demonstrated above in cases 1 to 3. Case 5 resembles a disturbance in the operation of the absorber or the lean-rich cross-heat exchanger.

Figure 5.17 shows the dynamic response of the stripper for cases 4 and 5. It outlines that a step change response of the stripper is to some extent similar between MEA and PZ. Generally, the transient behaviour is a sudden decrease of the lean loading followed by an increase towards steady state. However, some differences between the cases are noteworthy: (1) Steady-state is reached within 10–15 min when rich loading decreases respectively rich temperature reduces, except for the +1°C step change using PZ, then steady-state is reached within 30 min (figure 5.17B). (2) A greater rich loading respectively lower rich temperature reduces the performance of the stripper using PZ and improves the stripping efficiency using MEA. The settling time is around 30-40 min. The simulation results (not shown here) demonstrate that the same behaviour is observed for slightly larger step changes of ±0.03 in loading and ±4°C in the temperature of the rich feed.
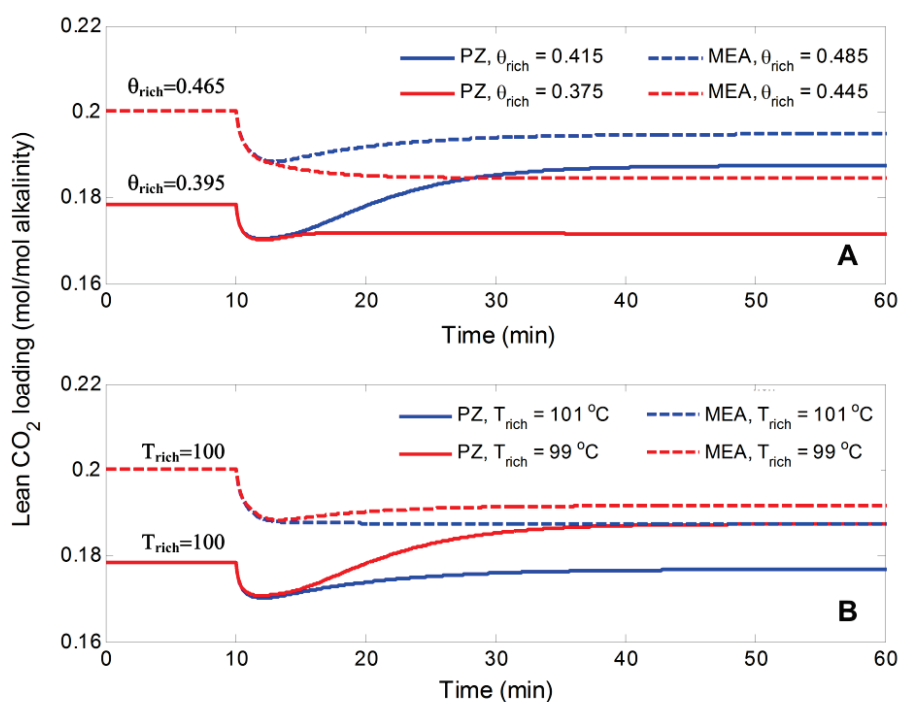

Figure 5.17. Lean CO_2 loading for (A) case 4 – rich loading and (B) case 5 – feed temperature

Figure 5.17 demonstrates the phenomenon of inverse response of the stripper for the PZ solvent when: (case 4a) rich loading increases (figure 5.17A, blue line) and (case 5b) feed temperature decreases (figure 5.17B, red line). Inverse response of a unit arises from competing dynamic effects that operate on two different time scales. The temperature of the liquid flowing into the surge tank (reboiler) is already below boiling point and a decrease of this temperature results in increased condensation in the tank. This cause the drum level to temporary increase but the temperature in the surge tank temporary decreases. This results in lower CO_2 stripping rate. However, this effect is only temporary and after a while the temperature of the surge tank increases. This results in higher CO_2 evaporation.

We exemplify in figure 5.18 the two competing effects resulting in inverse response of the stripper for cases 4a and 5b. Figure 5.18A shows that the solvent flow rate to the reboiler increases instantaneously from 188.3 mol/s to 189.3 mol/s for cases 4a and 5b, respectively. As a consequence of the greater solvent hold-up, the reboiler outlet vapour flow increases 0.3 mol/s in 1 min (see figure 5.18B). The increased boiling produces a leaner reboiler stream, which corresponds to more efficient stripping (figure 5.17). However, the initial efficiency improvement is followed by a slow transient decrease. Figure 5.18 shows that the solvent flow to the reboiler, and consequently the reboiler boil-up, reduces below their initial values within 8-15 min. Lower boil-up rate produces lower CO_2 desorption rate.

It can be concluded that the transient behaviour of the MEA system cannot be extrapolated to other solvents. Dynamic models are necessary to fully understand the transient behaviour of a capture plant and to design robust control structures.
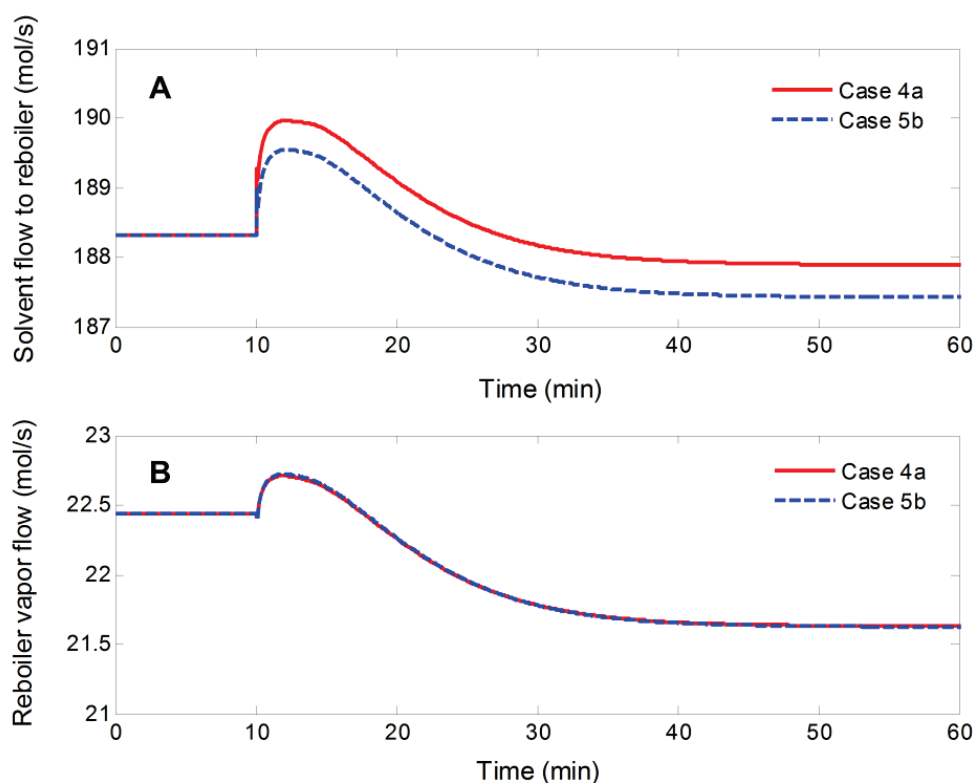
Figure 5.18. (A) Stripper outlet solvent flow and (B) Reboiler boil-up for cases 4a and 5b using PZ.

5.5 Conclusions

A mechanistic dynamic rate-based model for CO_2 post-combustion capture simulation using piperazine (PZ) and monoethanolamine (MEA) has been developed. The capture plant model includes a rate-based dynamic absorber, desorber, heat exchangers and buffer tanks. The developed mathematical model takes into account the accumulation of mass and energy in both the gas and the liquid phase and it uses the GM enhancement factor model for CO_2 mass transfer rate calculation respectively the extended UNIQUAC thermodynamic model to predict phase equilibrium and thermal properties. Furthermore, the mass and hydraulic characteristics are obtained by the Rocha mass transfer and hydraulic model (Rocha et al., 1996, 1993). The kinetic model includes two parallel reactions for the PZ system and one reaction for the MEA solvent. The importance of the bicarbamate forming reaction for the PZ system is especially important at high CO_2 loadings when its contribution to the overall CO_2 mass transfer rate is above 30%. The developed model has been compared to dynamic experimental pilot plant data using MEA and it has been compared to steady-state pilot plant measurements using PZ. This validation showed the good agreement between experimental data and model predictions. The model predicts the transient evolution of the pilot plant for industrially relevant scenarios, e.g. changes in the lean solvent and steam flow rate. It catches the fast responses of

columns as well as the slow transient evolution with time delays. The model also compares well to measurements for a broad range of L/G ratios, lean loadings and reboiler pressures.

Additionally, the dynamic response of the absorber and of the desorber using PZ and MEA for changes in key process parameters, e.g. flue gas composition, lean solvent flow rate, temperature and CO_2 loading of the stripper's feed, etc. has been investigated. This study showed that step changes in the flue gas and the lean flow rate have a significant impact on the absorber. The settling time is approximately 2–3 times slower in case of PZ compared to MEA. This behaviour is related to the coupling between temperature and mass transfer rate. The analysis of the desorber revealed a strong influence of the rich loading and feed's temperature on the lean CO_2 loading. The results outlined that a step change in the composition or the temperature of the stripper's feed produces a sudden decrease of the lean loading followed by a slower transient period when approaching steady-state, for both solvents (MEA and PZ). Thus, the desorber evolves on a fast and a slow time-scale. The simulation results revealed the presence of inverse response for increased rich loading or decreased feed temperature. The observed initial decrease in the outlet lean loading is later overcome by a decrease in the vapour boil-up.

This study demonstrates that the implemented model and its numerical implementation enables transient simulation of a pilot-scale post-combustion capture plant and is therefore considered adequate for dynamic optimization and control strategies development. However, comparison to large scale plant-data covering a wide range of operating conditions is needed to ensure general dynamic validity of the model. It is especially important to compare the model to large scale experiments since post-combustion capture reached industrial deployment-stage. Therefore, great effort is invested in plant-wide dynamic simulation and control using efficient solvents such as PZ in addition to investigation of the effect of design variables on process dynamics, e.g. size of storage tanks and sumps, dimensions of the absorption and desorption towers and heat exchangers.

References

Biliyok, C., Lawal, A., Wang, M., Seibert, F., 2012. Dynamic modelling, validation and analysis of post-combustion chemical absorption CO2 capture plant. Int. J. Greenh. Gas Control 9, 428–445. doi:10.1016/j.ijggc.2012.05.001

Bird, R.B., Stewart, W.E., Lightfoot, E.N., 2007. Transport phenomena. J. Wiley.

Bui, M., Gunawan, I., Verheyen, V., Artanto, Y., Meuleman, E., Feron, P., 2013. Dynamic Modeling and Validation of Post-combustion CO2 Capture Plants in Australian Coal-fired Power Stations. GHGT-11 37, 2694–2702. doi:http://dx.doi.org/10.1016/j.egypro.2013.06.154

Bui, M., Gunawan, I., Verheyen, V., Feron, P., Meuleman, E., Adeloju, S., 2014. Dynamic modelling and optimisation of flexible operation in post-combustion CO2 capture plants-A review. Comput. Chem. Eng. 61, 245–265. doi:10.1016/j.compchemeng.2013.11.015

Cormos, A.-M., Gaspar, J., 2012. Assessment of mass transfer and hydraulic aspects of CO2 absorption in packed columns. Int. J. Greenh. Gas Control 6, 201–209. doi:http://dx.doi.org.globalproxy.cvt.dk/10.1016/j.ijggc.2011.11.013

Dietl, K., Joos, A., Schmitz, G., 2012. Dynamic analysis of the absorption/desorption loop of a carbon capture plant using an object-oriented approach. Chem. Eng. Process. Process Intensif. 52, 132–139. doi:http://dx.doi.org.globalproxy.cvt.dk/10.1016/j.cep.2011.11.002

Dugas, R.E., Rochelle, G.T., 2011. Modeling CO2 absorption into concentrated aqueous monoethanolamine and piperazine. Chem. Eng. Sci. 66, 5212–5218. doi:10.1016/j.ces.2011.07.011

Enaasen Flø, N., Knuutila, H., Kvamsdal, H.M., Hillestad, M., 2015. Dynamic model validation of the post-combustion CO2 absorption process. Int. J. Greenh. Gas Control 41, 127–141. doi:http://dx.doi.org.globalproxy.cvt.dk/10.1016/j.ijggc.2015.07.003

Enaasen, N., Zangrilli, L., Mangiaracina, A., Mejdell, T., Kvamsdal, H.M., Hillestad, M., 2014. Validation of a Dynamic Model of the Brindisi Pilot Plant. 12th Int. Conf. Greenh. Gas Control Technol. GHGT-12 63, 1040–1054. doi:http://dx.doi.org/10.1016/j.egypro.2014.11.111

Faramarzi, L., Kontogeorgis, G.M., Thomsen, K., Stenby, E.H., 2009. Extended UNIQUAC model for thermodynamic modeling of CO2 absorption in aqueous alkanolamine solutions. Fluid Phase Equilib. 282, 121–132. doi:10.1016/j.fluid.2009.05.002

Fosbøl, P.L., Gaspar, J., Ehlers, S., Kather, A., Briot, P., Nienoord, M., Khakharia, P., Le Moullec, Y., Berglihn, O.T., Kvamsdal, H.M., 2014. Benchmarking and comparing first and second generation post combustion CO2 capture technologies. Energy Procedia 63, 27–44. doi:10.1016/j.egypro.2014.11.004

Fosbøl, P.L., Maribo-Mogensen, B., Thomsen, K., 2013. Solids Modelling and Capture Simulation of Piperazine in Potassium Solvents. GHGT-11 37, 844–859. doi:http://dx.doi.org/10.1016/j.egypro.2013.05.177

Frailie, P., Plaza, J., Van Wagener, D., Rochelle, G.T., 2011. Modeling piperazine thermodynamics. Energy Procedia 4, 35–42. doi:10.1016/j.egypro.2011.01.020

Gaspar, J., Cormos, A.-M., 2012. Dynamic modeling and absorption capacity assessment of CO2 capture process. Int. J. Greenh. Gas Control 8, 45–55. doi:10.1016/j.ijggc.2012.01.016

Gáspár, J., Cormoş, A.M., 2011. Dynamic modeling and validation of absorber and desorber columns for post-combustion CO2 capture. Comput. Chem. Eng. 35, 2044–2052.

Gaspar, J., Fosbol, P.L., 2016. General enhancement factor model (GM) for multiple parallel reactions: Piperazine (PZ) CO2 capture. Chem. Eng. Sci.

Gaspar, J., Fosbøl, P.L., 2015. A general enhancement factor model for absorption and desorption systems: A CO2 capture case-study. Chem. Eng. Sci. 138, 203–215. doi:http://dx.doi.org.globalproxy.cvt.dk/10.1016/j.ces.2015.08.023

Gaspar, J., Jørgensen, J.B., Fosbøl, P.L., 2015. A Dynamic Mathematical Model for Packed Columns in Carbon Capture Plants, in: Proceedings of ECC Conference. IFAC, http://www.ifac-papersonline.net/, pp. 2743–2748. doi:10.1109/ECC.2015.7330952

Harun, N., Nittaya, T., Douglas, P.L., Croiset, E., Ricardez-Sandoval, L.A., 2012. Dynamic simulation of MEA absorption process for CO2 capture from power plants. Int. J. Greenh. Gas Control 10, 295–309. doi:10.1016/j.ijggc.2012.06.017

Jayarathna, S.A., Lie, B., Melaaen, M.C., 2013. Amine based CO2 capture plant: Dynamic modeling and simulations. Int. J. Greenh. Gas Control 14, 282–290. doi:http://dx.doi.org/10.1016/j.ijggc.2013.01.028

Karimi, M., Hillestad, M., Svendsen, H.F., 2012. Investigation of the dynamic behavior of different stripper configurations for post-combustion CO2 capture. Int. J. Greenh. Gas Control 7, 230–239. doi:10.1016/j.ijggc.2011.10.008

Kenig, E.Y., Schneider, R., Górak, A., 2001. Reactive absorption: optimal process design via optimal modelling. Chem. Eng. Sci. 56, 343–350.

Kvamsdal, H.M., Chikukwa, A., Hillestad, M., Zakeri, A., Einbu, A., 2011. A comparison of different parameter correlation models and the validation of an MEA-based absorber model. 10th Int. Conf. Greenh. Gas Control Technol. 4, 1526–1533. doi:http://dx.doi.org.globalproxy.cvt.dk/10.1016/j.egypro.2011.02.021

Lawal, A., Wang, M., Stephenson, P., Koumpouras, G., Yeung, H., 2010. Dynamic modelling and analysis of post-combustion CO2 chemical absorption process for coal-fired power plants. Fuel 89, 2791–2801. doi:10.1016/j.fuel.2010.05.030

Lawal, A., Wang, M., Stephenson, P., Obi, O., 2012. Demonstrating full-scale post-combustion CO2 capture for coal-fired power plants through dynamic modelling and simulation. Fuel 101, 115–128. doi:10.1016/j.fuel.2010.10.056

Mac Dowell, N., Samsatli, N.J., Shah, N., 2013. Dynamic modelling and analysis of an amine-based post-combustion CO2 capture absorption column. Int. J. Greenh. Gas Control 12, 247–258. doi:http://dx.doi.org/10.1016/j.ijggc.2012.10.013

Nittaya, T., Douglas, P.L., Croiset, E., Ricardez-Sandoval, L.A., 2014. Dynamic modelling and control of MEA absorption processes for CO2 capture from power plants. Fuel 116, 672–691. doi:10.1016/j.fuel.2013.08.031

Plaza, J.M., 2011. Modeling of Carbon Dioxide Absorption using Aqueous Monoethanolamine, Piperazine and Promoted Potassium Carbonate. University of Texas.

Plaza, J.M., Rochelle, G.T., 2011. Modeling pilot plant results for CO2 capture by aqueous piperazine. Energy Procedia 4, 1593–1600. doi:10.1016/j.egypro.2011.02.029

Rocha, J.A., Bravo, J.L., Fair, J.R., 1996. Distillation columns containing structured packings: A comprehensive model for their performance .2. Mass-transfer model. Ind. Eng. Chem. Res. 35, 1660–1667. doi:10.1021/ie940406i

Rocha, J.A., Bravo, J.L., Fair, J.R., 1993. Distillation-Columns Containing Structured Packings - a Comprehensive Model for their Performance .1. Hydraulic Models. Ind. Eng. Chem. Res. 32, 641–651. doi:10.1021/ie00016a010

Sachde, D., Rochelle, G.T., 2014. Absorber Intercooling Configurations using Aqueous Piperazine for Capture from Sources with 4 to 27% CO2. 12th Int. Conf. Greenh. Gas Control Technol. GHGT-12 63, 1637–1656. doi:http://dx.doi.org/10.1016/j.egypro.2014.11.174

Sadegh, N., Stenby, E.H., Thomsen, K., 2015. Thermodynamic modeling of CO2 absorption in aqueous N-Methyldiethanolamine using Extended UNIQUAC model. Fuel 144, 295–306. doi:10.1016/j.fuel.2014.12.002

Chapter 6. Controllability and flexibility analysis of CO_2 post-combustion capture using piperazine and MEA

Abstract

In this study, we developed a decentralized control scheme and investigate the performance of the piperazine (PZ) and monoethanolamine (MEA) CO_2 capture process for industrially-relevant operation scenarios. The base for the design of the control schemes is Relative Gain Array (RGA) analysis combined with open-loop dynamic sensitivity analysis.

This study suggests that controllers with smaller time integrals and larger gains are required to maintain the PZ plant within reasonable short closed-loop settling times when compared to MEA. It also shows that the offset from the designated set-points in the presence of disturbances in the flue gas flow and heat duty is larger using PZ compared to MEA. The settling time for the PZ plant is generally larger than for MEA. However, the PZ plant rejects the disturbances faster and with less variability in the load of the power plant. Furthermore, this study indicates that the proposed PI-based control structure can handle large changes in the load provided that the manipulated variables, i.e. lean solvent flow or reboiler duty, do not reach their saturation limit. Additionally, we observed that shortage in the steam supply (reboiler duty) may represent a critical operational bottleneck, especially when PZ is being used. The MEA plant controllers drive the system towards drying out/flooding while the CO_2 capture rate performance of the PZ plant reduces drastically in the presence of constraints in the availability of steam. These findings suggest the need for advanced control structures, e.g. MPC, which can explicitly account for constraints in the process variables.

Keywords: *Controllability; flexible operation; dynamic CO_2 capture rate-based model; piperazine; sensitivity study*.

6.1   Introduction

Climate change as a result of anthropogenic activities is a key concern of our society. One of the main causes is the accelerated build-up of greenhouse gases in the atmosphere, such as carbon dioxide (CO_2), methane and water. The main greenhouse gas pollutant is CO_2, accounting for nearly three-quarters of the total amount of greenhouse gases (Pachauri et al., 2008). Although the use of non-fossil energies such as nuclear power, hydroelectricity, and renewables has increased by 50% in the last decades, their combined share in the overall energy consumption has remained essentially flat, around 12% (Yamaguchi, 2012). On the other hand, the global amount of energy-related CO_2 emission has increased almost 47% since 1990. Thus, this increase of CO_2 in the atmosphere directly ties to the global fossil energy consumption (Yamaguchi, 2012). Consequently, immediate and large mitigation of CO_2 can be achieved by integrating CO_2 capture technologies with fossil-fired power plants.

CO_2 post-combustion capture is the most mature capture process that can be retrofitted to existing power plants. Although several experimental and simulation studies performed at steady-state have demonstrated its technology readiness (Wang et al., 2011), it has been recognized that dynamic studies are required to gain insight on the transient behaviour of this capture process and to design practical operational strategies through testing and implementation of efficient control strategies. Dynamic studies can identify potential bottlenecks during operation and to ensure feasible dynamic operability of power plants with integrated CO_2 capture in a dynamic energy market environment (Lawal et al., 2010).

Various control studies have been developed for post-combustion capture. Most of them suggest that important controlled variables (CVs) for this process are the CO_2 removal efficiency and the reboiler lean loading. These variables can be modified by adjusting the lean solvent flow rate and the reboiler duty, respectively (Harun et al., 2012; Lin et al., 2012, 2011). Lawal et al. (2010) presented a dynamic model of a complete CO_2 capture process using gRPOMS and presented the performance of a decentralized control structure under various disturbances. That study demonstrated the importance of the make-up water flow control for a stable closed-loop operation of the capture plant. This analysis also revealed that the performance of the absorber is more sensitive to the L/G ratio (i.e. the ratio of the lean amine flow rate to the flue gas flow rate entering the absorber) compared to the flue gas flow rate itself. Similar observations were made by Lin et al. (2011) and Posch and Haider (2013). Lin et al. (2011) suggested that the lean solvent flow rate and the lean solvent CO_2 loading are also critical to achieve a suitable closed-loop process performance, i.e. maintain the controlled variables as close as possible to their set-points. That study proposed to control CO_2 removal efficiency by the lean solvent flow rate entering the absorber and the reboiler outlet lean loading by the steam flow to the reboiler. Furthermore, Posch and Haider (2013) showed that the L/G ratio should be maintained at a specified value to achieve a desired capture rate. However, Gaspar et al. (2015a)

showed that using a L/G ratio controller results in longer plant settling times, i.e. time needed to reach the desired set point in CO_2 capture efficiency. In general settling times represents the time required for the process outputs to deviate less than 5% from the set-points for a long period (Seborg et al., 1989).

Nittaya et al. (2014) proposed three decentralized control strategies for this process based on relative gain array (RGA) and heuristic analyses. This study employed a mechanistic rate-based model validated against steady-state plant data. The RGA analysis (control A) suggested to pair the sump and reboiler surge tank level with the rich amine flow leaving the sump respectively the lean flow exiting the reboiler. The RGA analysis also showed that the CO_2 removal efficiency should be paired with the reboiler steam flow and the reboiler temperature should be paired with the lean solvent flow rate to the absorber. A heuristic approach (control B) based on the insight gained from the process dynamics showed that CO_2 removal efficiency should be paired with lean solvent flow to the absorber and the reboiler's temperature with the steam flow rate. Other promising pairing to keep the reboiler temperature under tight control (control C) is to pair the reboiler temperature with the rich flow leaving the sump. All of the proposed control structures were able to achieve the control objectives. Heuristic approach, control B, yielded in faster disturbance rejection and set point tracking but may fail if an error arises in that control loop, e.g., malfunctioning of V1 and/or saturation of reboiler steam valve. Control C has similar performance with control A but lower energy demand for regeneration. Panahi and Skogestad (2011) and Panahi and Skogestad (2012) developed different control structures using a self-optimizing method for three regions of the flue gas flow rates. In that study, they compared the performance of the decentralized control strategies to a 2x2 Model Predictive Control (MPC) for different changes in the flue gas flow rate. Similar to Nittaya et al. (2014), that study suggested that pairing the reboiler duty with the CO_2 removal efficiency and the lean inlet flow rate with the absorber sump level improves process operation, i.e. the plant reaches steady-state faster and requires less steam for solvent regeneration. Conclusively, this control configuration has a dynamic performance comparable to an MPC. Sahraei and Ricardez-Sandoval (2014a) also compared a decentralized multi-loop control structure based on RGA analysis to a full 6x6 MPC. The responses to step changes in the feed, CO_2 capture set-point and constrained heat supply were studied. The RGA analysis showed that the optimal pairing to minimize interaction between the control loops at steady-state is to control the CO_2 capture rate by the lean solvent flow rate and the reboiler temperature with the reboiler duty. However, that study showed that the MPC performs significantly better in terms of close-loop settling time, integral squared error and it maintains the manipulated variables within their saturation limits in the presence of changes in the flue gas flow rate and during set-point tracking.

A different set of control variables were chosen by Luu et al. (2015) and Abdul Manaf et al. (2016). They selected as control variables the CO_2 capture efficiency, the specific reboiler heat duty and reboiler temperature. The specific reboiler duty is a commonly used performance indicator for post-combustion

capture plants. Luu et al. (2015) implemented a mechanistic rate-based model in gPROMS and compared a standard PID feedback control scheme, a cascade PID scheme and an MPC based control structure for stepwise set-point tracking and capture plant load change scenarios. This study also confirmed that MPC strategy has a better control performance than PID based control schemes and it is able to keep the plant at the desired set-points without violating operational, economic and environmental constraints. Later, Abdul Manaf et al. (2016) identified a black box model based on pilot scale capture plant data. This model consists of an absorber, desorber and lean-rich heat exchanger. Based on an RGA analysis, they proposed to control the CO_2 capture efficiency and specific reboiler duty by manipulating the lean solvent flow rate and the reboiler duty. The proposed control structure was able to reduce the reboiler heat duty while maintaining the set point for the CO_2 capture rate.

In a recent study, He et al. (2015) presented a flexibility analysis study of a post-combustion capture process using MPC. They investigated the closed-loop behaviour of the plant for high frequency oscillatory changes in the load and identified optimal operating scenarios. In addition, that study reveals that simultaneous scheduling and control is economically more appealing than a sequential approach. Zhang et al. (2016) simulated a post-combustion capture plant able to remove 90% of CO_2 from the flue gas of a supercritical 550 MWe power plant in Aspen Plus (steady-state simulation) and Aspen Plus Dynamics (dynamic simulation). This study showed that three and six parallel trains may be needed to capture 90% of CO_2 from a 550 MWe supercritical power plant. They implemented the conventional PID control structure by pairing the CO_2 capture rate with the lean solvent flow rate and the reboiler temperature with the steam rate. Then, to improve the control performance, a linear MPC was applied to control the CO_2 capture efficiency and the reboiler temperature while the other process variables were regulated by PID control. They evaluated the performance of a PID and a linear MPC controller for typical scenarios, e.g. 5% ramp changes in the flow rate respectively CO_2 composition of the flue gas, 50% decrease in power plant load, random changes in the power plant load. Moreover, this study investigated the controllability of the plant for scenarios when different parallel trains have difference removal efficiencies in order to resemble real industrial conditions. In all cases, the MPC showed superior performance to the PID control structure by reducing the large overshoot and long settling time. In addition, they showed that a bypass valve to shunt the excessive flue gas around the absorber is a viable approach to avoid absorber flooding in presence of excessive flue gas flow rate. All of these studies were performed using the baseline MEA solvent.

Recently, new efficient solvents with higher CO_2 capacity and lower solvent regeneration energy demand have been suggested (Puxty et al., 2009; Valencia-Marquez et al., 2015). Only little knowledge is available on dynamics and controllability of plants with these novel solvents. An example of a promising solvent is the 5 molal piperazine solution which offers higher CO_2 capacity and an energy improvement of approximately 20% compared to MEA (Chen, 2015). To the authors' knowledge, there is a very limited knowledge about

the dynamic behaviour of this solvent in the context of CO_2 capture. Gaspar et al. (2015b) implemented a dynamic rate-based model using MEA and PZ and compared the transient behaviour of the two solvents for ramp changes in the L/G ratio and step changes in the reboiler temperature. Walters et al. (2013) presented a first-principle based dynamic model for the alternative two-stage flash stripper configuration with piperazine (PZ) assuming equilibrium stage process and validated it against steady-state experiments. Accordingly, there is a need to develop dynamic models and perform controllability studies that provide insight on the dynamic feasibility and operability of these plants while using solvents other than MEA.

This work provides insight on the open-loop dynamics of the CO_2 capture process and addresses the controllability of a CO_2 capture plant using both PZ and MEA solvents. To achieve these goals, a decentralized control structure (PI-control) is developed based on Relative Gain Array (RGA) analysis. The performance of the post-combustion plant is investigated in the presence of disturbances in key process variables, e.g. solvent flow rate, steam flow rate, flue gas flow rate, etc. Insight from this comparison will help to understand similarities and differences in the operation of the benchmark MEA plant and the novel PZ plant. Additionally, this study pinpoints possible challenges which may emerge when using PZ as solvent. The present sensitivity analysis and controllability study was carried out using the dCAPCO2 in-house rate-based model implemented in Matlab (Gaspar et al., 2016a, 2015b). This model uses the extended UNIQUAC thermodynamic model (Faramarzi et al., 2009) and the GM enhancement factor model (Gaspar and Fosbøl, 2015).

The structure of the work is as follows: First the CO_2 capture model is presented in Section 2. Then the design of a decentralized PI-control layer for both solvents, i.e. PZ and MEA, as well as the dynamic sensitivity analysis of the plant is shown in Section 3. In Section 4, the performance is compared between the PZ and MEA plants for industrially-relevant operational scenarios, i.e. multiple ramp changes in the flue gas flow rate, limited availability of steam supply and effect of valve stiction scenarios. Concluding remarks are presented at the end.

6.2 Post-combustion CO_2 capture model development

This section presents the CO_2 post-combustion capture process model used to perform the controllability and flexibility analysis of a capture plant with 5 molal (30wt%) piperazine (PZ) and 30 wt% monoethanolamine (MEA), respectively The design base of the plant is the traditional process configuration with heat integration between the lean solution leaving the reboiler and the rich solution entering the stripper. It resembles the pilot plant topology and design specifications presented by Faber et al. (2011). The solvent characteristics for the PZ plant were adopted from previous studies (Gaspar et al., 2016b; Van Wagener, 2011). The main input parameters and design specifications for the absorber, stripper and utilities for the PZ and MEA solvents are summarized in Table 6.1.

The capture plant is designed to remove 1 t/h CO_2 from the exhaust of a coal fired power plant. Subsequently, the flue gas contains 12.4 mol% CO_2 and it is saturated with water at the absorber inlet temperature of 40°C. Moreover, we assume that the flue gas is treated for control of post-combustion products and therefore it consists of inert gases (mixture of N_2 and O_2), CO_2 and H_2O. It is assumed that the inert gas has the same characteristics as air. These conditions resemble the experimental values reported by Faber et al. (2011).

Table 6.1. Nominal input operating parameters and design specifications for the CO_2 capture plant

Input parameters	Unit	PZ	MEA
Flue gas flow rate	mol/s	61.5	61.5
Flue gas temperature	°C	40	40
Flue gas pressure	kPa	101	101
Flue gas CO_2 composition	mol%	12.4	12.4
Flue gas H_2O composition	mol%	10.9	10.9
Flue gas inert composition (N_2+O_2)	mol%	76.7	76.7
Lean solvent flow rate	mol/s	195	251
Lean inlet temperature	°C	40	40
PZ/MEA lean loading	mol/mol alk.*	0.17	0.19
Amine concentration	wt.%	30	30
Reboiler operating pressure	kPa	185	185
Heat exchanger temperature approach	°C	10	10
Column diameter	m	1.1	1.1
Height of packing in absorber/desorber	m	17/10	17/10
Buffer tank diameter	m	4	4
Absorber/Desorber sump diameter	m	1.1	1.1

mol/mol alk. = mol CO_2/2 mol PZ

Figure 6.1 shows the flowsheet of the capture process used in this work. As shown in this figure, the CO_2 rich flue gas is washed in counter-current with a solvent, i.e. PZ or MEA. The lean amine solution enters at the top of the absorber with a temperature of 40°C. The lean CO_2 loading of the PZ solvent is 0.17 mol/mol alkalinity to ensure precipitation-free operation of the capture plant at low reboiler duty (3.4 GJ/t CO_2) (Gaspar and Fosbøl, 2016; Gaspar et al., 2016b). The lean loading of the MEA solvent is 0.19 mol/mol. The CO_2 loading of the MEA solvent is below its typical value (0.21 mol CO_2/mol MEA), i.e. the loading at which the reboiler duty is the smallest. The slower lean CO_2 loading for the MEA system was preferred in order to maintain the solvent hold-up of the system at comparable levels between the PZ and the MEA plant

and to keep the two plants comparable from a control point of view. Subsequently, the lean solvent flow rate is 195 mol/s and 251 mol/s for the PZ and MEA plants, respectively. As expected, a greater CO_2 loading results in higher MEA lean solvent flow rate which can lead to slower response of the plant. Note that the lean solvent removes 90% of the inlet CO_2 at the nominal operating point. This capture efficiency was set according to the European best practice guidelines for assessment of CO_2 capture technologies (Ennio et al., 2011). The CO_2 rich amine solution exits at the bottom of the absorber and it is collected in the sump of the absorber before it is pumped through the lean-rich heat exchanger. The role of this heat exchanger is to recover the heat of the lean stream from the reboiler by heating the CO_2 rich feed of the stripper. Thus, the hot rich stream enters the top of the stripper at approximately 100 – 110 °C. In the stripper tower, the CO_2 is released by heat provided in the reboiler using utility steam from the power plant. Further, the regenerated lean solvent is recycled to the buffer tank through the lean-rich heat exchanger.
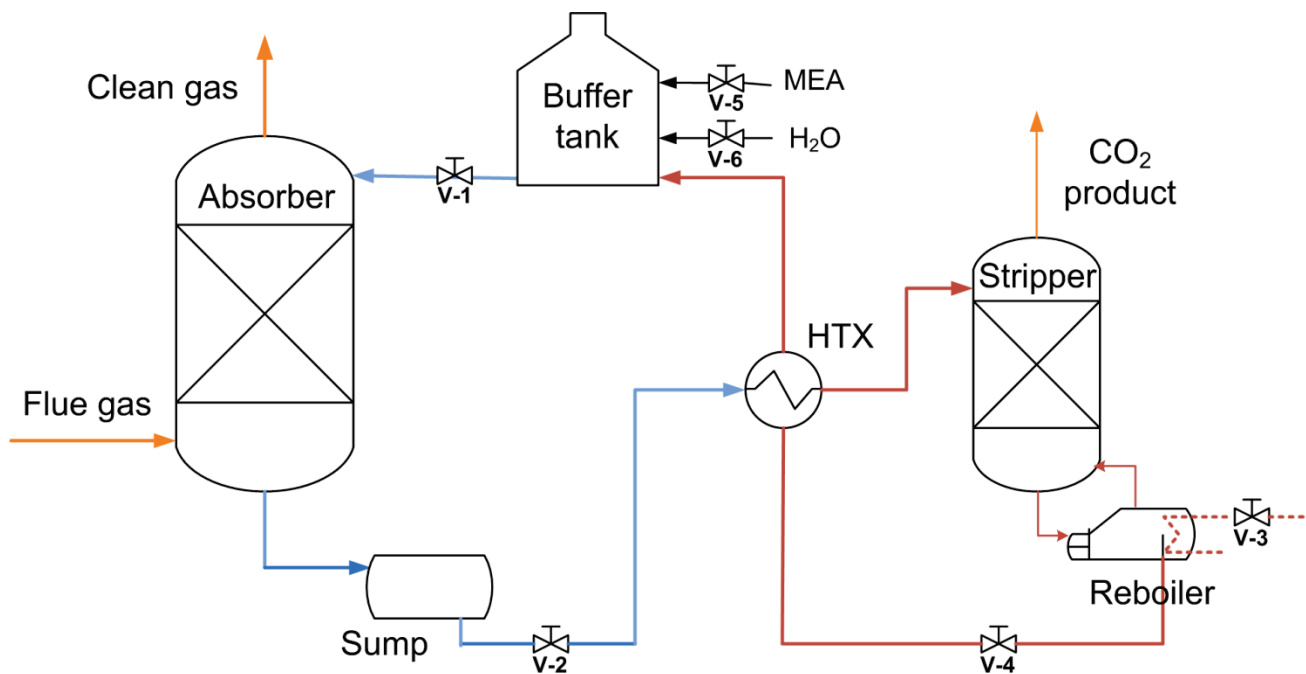

Figure 6.1. Post-combustion CO_2 capture process flowsheet

The design specifications for the packed columns and additional units are in accordance with the characteristics of the pilot plant data used in this work to validate the CO_2 capture plant model (Faber et al., 2011). The absorber and the stripper are packed columns equipped with Mellapak 2X structured packing and IMTP50 dumped packing, respectively. The design specifications for the packed columns and additional units are shown in Table 6.1. Note that the buffer tank is designed to allow large solvent flow rate changes during flexible operation of the capture plant. A similar approach was adopted by Nittaya et al. (2014) and Sahraei and Ricardez-Sandoval (2014a). The heat exchanger operates with a lean-rich temperature difference of 10°C.

As shown in Figure 6.1, the process consists of various unit models for the columns and the additional units, i.e. sump, the buffer tank, the reboiler and the heat exchanger. These models were developed from first principle mass and energy conservation equations coupled with algebraic equations, i.e. physical property correlations, mass transfer model, hydraulic model and the extended UNIQUAC thermodynamic model. The resulting set of conservation equations have been implemented in Matlab. Detailed description and validation of the dynamic model is presented in Chapter 5.

6.3   Dynamic analysis and control design

The transient evolution of a CO_2 capture plant using PZ and MEA in the presence of process disturbances and changes in operational conditions is essential to design suitable control structures. (Gaspar and Cormos, 2012) have shown the key role of reaction kinetics in the dynamics of a capture plant. In addition, differences in the physical properties of amines influence the mass transfer and hydraulic characteristics and therefore the dynamic behaviour of a capture plant. For example Bui et al. (2016) reported that as MEA degrades, significant changes occur in their physical properties, e.g. viscosity which lead to poor liquid distribution. This is why PZ and MEA may respond differently to changes in the load and process operating conditions.

Initially, an open-loop parametric sensitivity analysis was performed exploring the effect of key variables on the process dynamics and identifying their effect on the process efficiency and the control objectives. Then, the most promising pairings between the controlled variables (CV) and manipulated variables (MV) were identified to minimize the interaction (at steady-state) between multiple feedback control loops. Based on these insights, a decentralized control structure is developed and used to evaluate the performance of the plant in closed-loop in the presence of industrially-relevant operational scenarios, e.g. changes in the power plant's load, valve stiction in the lean solvent stream and shortage of heat supply. The procedure to identify the control strategies employed in this study is described below.

6.3.1   Control objectives and process variables

The performance of the control structure reflects its ability to maintain the capture process at the desired 90% CO_2 removal efficiency (Ennio et al., 2011). In addition, the liquid inventory of the system has to be regulated to maintain a stable closed-loop operation of the plant. The gas inventory is not considered since it was assumed a linear pressure drop in the packed columns. The required purity of the CO_2 product stream (>99%) is ensured by the use of physical and/or chemical dehydration performed after the capture process to avoid down-stream corrosion and hydrate formation. Thus, this purification step can be partially de-linked from the main capture units and is not considered here for brevity. Previous studies have shown that the amine and the water balance are critical to keep the CO_2 capture plant at the desired set-points (Lin et al.,

2011). In this work, both the water and amine make-up flow rates are controlled by adjusting their flowrates based on overall water and amine material balance, i.e. the water and amine from the wash sections are recycled to the buffer tank. Note the make-up flow rates are negligible compared to the overall liquid hold-ups of the system. This approach has also been adopted in previous controllability studies (He et al., 2015; Nittaya et al., 2014; Sahraei and Ricardez-Sandoval, 2014a).

As shown in Figure 6.1, there are six manipulated variables (MVs) that can be potentially used to maintain the capture process at specified set points. These variables adjust the lean absorber inlet flow rate (V1), the rich feed flow rate (V2), the steam flow rate (V3), the recycle flow rate (V4) and the water and amine make-up flow rates (V5 and V6). As discussed above, V5 and V6 are already assigned to manual control and therefore were not considered as manipulated variables in this study. In this work, the CO_2 capture efficiency (CV1) and the reboiler lean CO_2 loading (CV3) are considered as controlled variables given that they determine the performance of the capture process. In addition, the levels in the absorber's sump (CV2) and the reboiler's tank (CV4) are also considered as controlled variables since they can be potentially used to regulate the solvent inventory, i.e. to avoid drying out and over-flooding of the tanks. Upper and lower bounds are considered for the MVs and CVs to mimic the plant physical limitations such as saturation limits of the valves and operational constraints, e.g. overflowing and drying out of the tanks, relatively constant flow regime in packed columns, etc.

Table 6.2. Nominal steady-state values and physical limitations for the MVs and the CVs

Manipulated variables (MVs)			Nominal Condition		Operational constraints	
			PZ	MEA	PZ	MEA
MV1	F_{Lean}	Lean solvent flow rate (mol/s)	195.6	251.1	195.6 ± 97.6	251.1 ± 125.5
MV2	F_{Rich}	Sump outlet flow rate (mol/s)	190.0	247.2	190.0 ± 95.0	247.2 ± 123.6
MV3	Q_{Reb}	Reboiler duty (MW)	1.042	1.490	1.042 ± 0.521	1.490 ± 0.745
MV4	F_{Reb}	Surge tank flow rate (mol/s)	182.6	236.9	182.6 ± 91.3	236.9 ± 118.5
Controlled variables (CVs)			Nominal Condition		Operational constraints	
			PZ	MEA	Lower	Upper
CV1	$CC_{\%}$	CO_2 capture efficiency (%)	89.9	89.9	60%	100%
CV2	L_{Sump}	Sump solvent level (m)	0.90	1.52	0.2	3.0
CV3	θ_{Reb}	Reboiler loading (mol/mol alk.)	0.17	0.19	0.1	0.3
CV4	L_{Reb}	Reboiler's tank level	1.04	1.82	0.2	3.0

Table 6.2 lists the nominal values for the control and manipulated variables considered for this analysis. The nominal values correspond to stable steady-state operation of the capture plant, which were determined using the input parameters and design specifications from Table 6.1. Table 6.2 also summarizes the operational constraints considered for the MVs and CVs.

6.3.2 Dynamic sensitivity analysis of the capture plant

To select suitable feedback control loops, a dynamic sensitivity analysis on the MVs, and its effect on the CVs, was performed using PZ and MEA as solvents. Step changes of ±10% on all of the manipulated variables were performed in order to determine the steady-state gains (K_p) and the process time constants (τ_p) for each MV-CV pairing loop. This analysis is required to design and tune the controllers using model-based control techniques. The resulting process model parameters between each manipulated variables and all controlled variables are presented in Table 6.3. In addition, this work details the dynamic behaviour of the open-loop capture plant using PZ and MEA for step changes in the two main MVs: the lean solvent flow rate and the reboiler duty. The focus is on revealing the effect of these MVs on the efficiency of the absorption-regeneration process.

Table 6.3. Process gains and time constants for the PZ and MEA plant

Capture plant		F_{Lean}		Q_{Reb}		F_{Rich}		F_{Reb}	
		K_p	τ_p (min)	K_p	τ_p (min)	K_p	τ_p (min)	K_p	τ_p (min)
PZ									
	$CC_\%$	5.854	71.2, 23.9	5.6E-5	147.6	-0.261	42.1	-0.252	39.3
	θ_{Reb}	0.003	44.6	-5.9E-7	41.8	-0.001	96.8, 99.2	-0.006	346.6, 523.0
	L_{Sump}	0.010	6.5	-1.7E-7	134.2	-0.154	103.9	0.009	86.9
	L_{Reb}	0.010	12.5	1.3E-7	4.0	0.010	6.6	-0.156	97.2
MEA									
	$CC_\%$	0.073	80.5, 21.3	1.26E-5	114.9	0.045	116.8	1.269	192.6, 84.1
	θ_{Reb}	0.001	35.4	-1.0E-7	13.4	-0.001	83.7, 90.0	-0.008	824
	L_{Sump}	0.013	8.2	-2.5E-8	49.2	-0.203	128.3	0.076	135.3
	L_{Reb}	0.014	13.7	8.85E-8	2.8, 2.6	0.0143	8.3	-1.231	144.4

6.3.2.1 Step change in the lean solvent flow rate

The performance of the absorber and the desorber strongly depends on the solvent lean flow rate. Figures 2A and 2B show the effect of ±10% step changes in the lean solvent flow rate on CO_2 capture percentage and the specific reboiler duty (SRD). The SRD at time i shows the heat used for reboiler duty required to regenerate 1 tonne of CO_2. It is a common metric used to quantify the energy performance of a capture plant. The step disturbance is applied after 10 min of steady-state operation.

Figure 6.2A illustrates how the CO_2 capture percentage reduces when the lean solvent flow rate decreases and vice-versa. As shown in this figure, the change in the solvent flow has a larger effect on the PZ process than on the MEA system. A 10% decrease of the solvent flow rate results in a CO_2 capture percentage of 85% and 88% when using PZ and MEA as solvents, respectively. Thus, controllers with higher gains may be required to maintain the PZ CO_2 capture plant at the desired 90% capture efficiency. Furthermore, Figure 6.2A shows that the response of the absorber consists of an initial fast change (approximately 30 min), followed by a slow evolution towards the new steady-state (5 to 7 hours) for both solvents. However, the dominant time constant of the PZ plant is 197 min compared to 67 min for the MEA plant. Thus, controllers with short time integrals may be required to maintain the PZ plant within reasonable short closed-loop settling times. Settling time refers to the time needed to reach the desired set points.

Figure 6.2B shows the relative SRD, Δ_{SRD} as function of simulation time. Δ_{SRD} is the difference between the SRD at time i and the steady-state SRD at $t=0$. The nominal SRD is 3.4 GJ/t CO_2 and 4.9 GJ/t CO_2 for the PZ and MEA solvents. The SRD of the MEA process is slightly higher than the commonly reported value (4.0 – 4.5 GJ/t CO_2) (Fosbøl et al., 2014). This is due to the use of a leaner CO_2 solution in this study: 0.19 mol CO_2 /mol MEA compared to the commonly used 0.21 mol/mol. As mentioned above, the reason for a leaner solution is to have similar solvent hold-ups between the MEA and PZ plants. Moreover, the use of a leaner MEA solution influences only the energy demand of regeneration and it does not impact the dynamics of the system.

Figure 6.2B shows that a higher solvent flow produces a sudden increase in the SRD, followed by a slow decrease towards the initial, nominal SRD value. On the other hand, a lower solvent flow results in a rapid decrease, followed by an increase of the SRD. The system shows inverse response in the SRD with respect to changes in the solvent flow rate. This is related to the slow drift in the CO_2 loading of the "Buffer tank" in Figure 6.1. The settling time for both solvents is approximately 6 hours.

The results from this analysis indicate that the degree of nonlinearity is higher for the piperazine plant. While a 0.5% change in the CO_2 capture percentage was observed for a 10% step increase in the lean flow rate for

both solvents, a 5% and 2% change in the same process variable was observed for 10% step decrease of the lean flow rate using PZ and MEA solvents. Furthermore, Figures 6.2A and 6.2B outlines that, regardless of the solvent, a poor control on the CO_2 absorption efficiency may result in additional energy penalties. This undesirable effect is more significant for the PZ solvent, up to 0.2 GJ/t CO_2 compared to 0.1 GJ/t CO_2 for MEA, even though both values are still low compared to the nominal value for energy consumption.
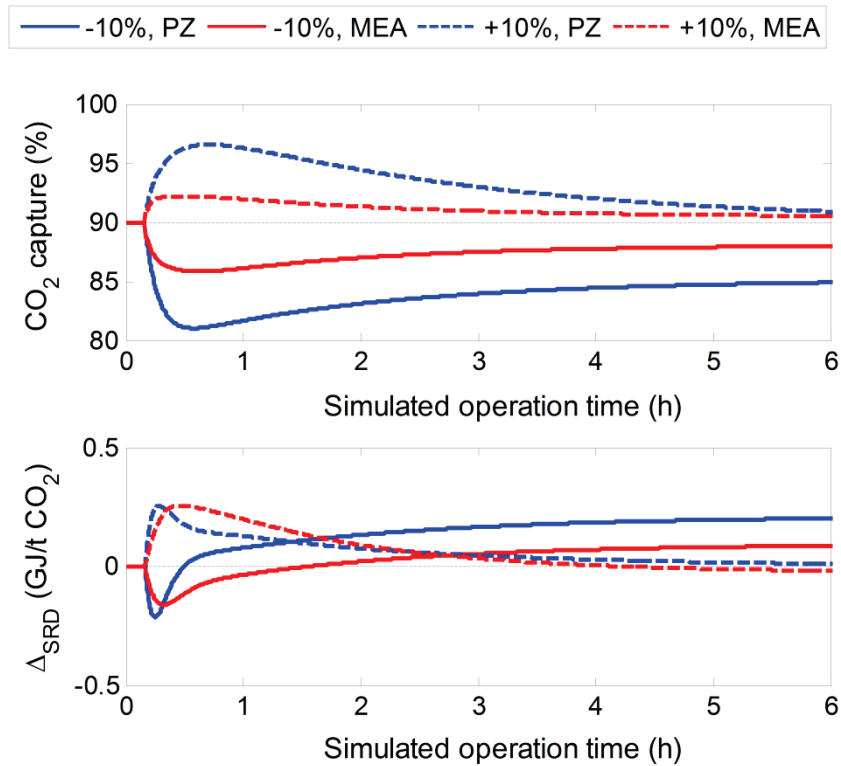
Figure 6.2. (A) CO_2 capture efficiency and (B) relative specific reboiler duty (Δ_{SRD}) for a ±10% step in the lean solvent flow rate.

6.3.2.2 Step change in the reboiler duty

The availability and quality of the steam used for solvent regeneration is a key variable in the operation of a CO_2 capture plant. Thus, understanding the effect of a change in the reboiler duty on the performance of the absorber and the desorber is essential when operating a post-combustion CO_2 capture plant. Figures 6.3A and 6.3B show the response of the process to ±10% step change in the reboiler duty, after 10 min of steady-state operation. Figure 6.3A shows that, regardless of the solvent being used, shortage of steam results in lower CO_2 capture percentage. This expected observation is due to the accumulation of CO_2 in the buffer tank, since less CO_2 is stripped out in the desorber section. On the other hand, an excess of steam leads to leaner recycle stream to the buffer tank since more CO_2 is stripped out in the desorber. Figure 6.3A suggests that the steady-state gain of the PZ CO_2 capture process is roughly double the MEA system. Thus, a change in the steam supply (reboiler duty) has a more pronounced impact on the PZ plant than on the MEA plant.

Furthermore, the time constant of the PZ plant between the reboiler duty and the CO_2 capture rate (%) is 146 min compared to 115 min for the MEA plant. Thus, controllers with shorter time integrals may be required to maintain the 90% CO_2 capture set-point of the PZ plant by manipulating the reboiler duty. Figure 6.3B shows the Δ_{SRD}, for ±10% step change in the reboiler duty for the PZ and MEA plants. This figure shows that the steady-state gain of the PZ process is 0.05 for a 10% decrease of the reboiler duty while it is 0.2 for a 10% increase on the same manipulated variable. Contrary to PZ, the gain for the MEA system is approximately 0.38 for ±10% step change in the reboiler duty variable. Thus, the PZ plant has a higher degree of non-linearity. It is important to note that a 10% reduction in the reboiler duty using PZ results in lower CO_2 capture efficiency whereas the SRD remained relatively constant for this change. However, a 10% increase in the steam supply induces an additional 0.2 GJ/t CO_2 energy penalty in case of PZ. On the other hand, the response of the MEA process is approximately first-order: a 10% increase of the reboiler duty leads to an increase in the SRD of 0.4 GJ/t CO_2 and a 10% decrease results in 0.4 GJ/t CO_2 reduction of the SRD. This analysis suggests that the lean solvent flow rate and the reboiler duty have a larger influence on the PZ capture process CO_2 removal efficiency, compared to the MEA process. However, a change in the steam supply (reboiler duty) has more significant effect in the SRD of the MEA process compared to PZ.
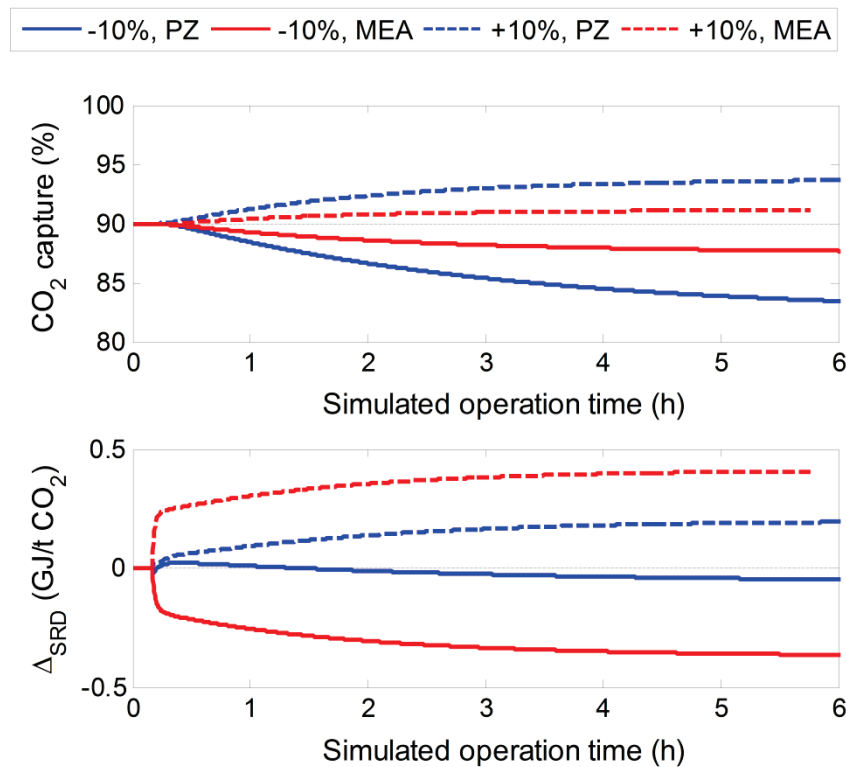

Figure 6.3. (A) CO_2 capture efficiency and (B) relative specific reboiler duty (Δ_{SRD}) for a ±10% step in the reboiler duty.

6.3.3 Design of a decentralized control structure

This section presents the design of a decentralized multi-loop control structure based on RGA analysis and process insights. The RGA method determines the best paring between manipulated variables and control variables that minimizes the interaction between multiple control loops. The RGA matrix of a process, Λ_{RGA}, is defined as follows:

$$\Lambda_{RGA} = G \otimes \left(G^{-1}\right)^T \tag{6.1}$$

where G is the process steady-state gain matrix. Equation (6.1) shows that Λ_{RGA} is based on the process steady-state gains; therefore, the RGA method may return ill-posed control schemes for highly non-linear and interactive systems. Accordingly, it is important to consider the RGA analysis together with a heuristic approach to ensure the suitability of the control structure selected. Substituting the values of the steady-state gains from Table 6.3 into eq. (6.1), the RGA matrices for the PZ and MEA CO_2 capture processes are as follows:

$$\Lambda_{RGA}^{PZ} = \begin{array}{c} \\ CC_\% \\ L_{Sump} \\ L_{Reb} \\ \theta_{Reb} \end{array} \begin{array}{cccc} F_{Lean} & Q_{Reb} & F_{Rich} & F_{Reb} \\ \begin{bmatrix} 0.366 & 0.725 & -0.036 & -0.055 \\ -0.058 & 0.003 & 1.0646 & -0.009 \\ -0.065 & -0.003 & -0.009 & 1.0775 \\ 0.758 & 0.2747 & -0.019 & -0.013 \end{bmatrix} \end{array} \tag{6.2}$$

$$\Lambda_{RGA}^{MEA} = \begin{array}{c} \\ CC_\% \\ L_{Sump} \\ L_{Reb} \\ \theta_{Reb} \end{array} \begin{array}{cccc} F_{Lean} & Q_{Reb} & F_{Rich} & F_{Reb} \\ \begin{bmatrix} 0.568 & 0.3329 & 0.023 & 0.075 \\ 0.015 & -0.0005 & 0.989 & -0.003 \\ 0.047 & 0.0032 & -0.001 & 0.959 \\ 0.369 & 0.6643 & -0.012 & -0.022 \end{bmatrix} \end{array} \tag{6.3}$$

As shown in the above equations, the RGA analysis suggests that, regardless of the solvent being used, the liquid level in the absorber's sump, L_{Sump}, and the liquid level in the reboiler's tank, L_{Reb}, need to be controlled using the rich amine flow rate leaving the sump, F_{Rich}, and the lean amine flow rate leaving the reboiler, F_{Reb}. Furthermore, the RGA matrix for the PZ CO_2 capture process, Λ_{RGA}^{PZ}, indicates that the CO_2 capture percentage, $CC_\%$ needs to be controlled with the reboiler duty, Q_{Reb}, whereas the reboiler lean loading, θ_{Reb} is controlled by the lean solvent flow rate to the absorber, F_{Lean}. The opposite pairing was specified for the MEA plant, i.e. $CC_\%$ is controlled using F_{Lean} whereas θ_{Reb} is controlled using Q_{Reb}. The definition and nominal values for the CVs and MVs are presented in Table 6.2.

Each control-loop consists of proportional-integral (PI) controllers. The implemented PI-controllers were initially tuned using internal model control (IMC) (Seborg et al., 1989). Then, they were manually fine-tuned such that the closed-loop system can recover quickly and smoothly from different changes in load and in the process operating conditions. These fine adjustments are needed to account for the interactions between the control-loops and to improve the closed-loop process performance. The resulting tuning parameters for the PZ CO_2 capture plant and the MEA CO_2 capture plant are presented in Tables 6.4 and 6.5. A sequential approach for automatic control structure selection which combines the RGA and IMC concepts with Parseval's theorem was presented by Jørgensen and Jørgensen (2000) In summary, this analysis indicates that, from the steady-state point of view, the control-loops of the liquid level have less effect from the other control loops while the control loops for $CC_%$ and θ_{Reb} have a high interaction between each other.

Table 6.4. Controllers tuning parameters for the PZ CO_2 capture plant

CV	MV	K_c	τ_I (min)
$CC_%$	Q_{Reb}	25048 (J/%)	50
L_{Sump}	F_{Rich}	-260 (mol/m)	10
θ_{Reb}	F_{Lean}	250 (mol)	15
L_{Reb}	F_{Reb}	-280 (mol/m)	8

Table 6.5. Controllers tuning parameters for the MEA CO_2 capture plant

CV	MV	K_c	τ_I (min)
$CC_%$	F_{Lean}	20 (mol/%)	17.5
L_{Sump}	F_{Rich}	-200 (mol/m)	5
θ_{Reb}	Q_{Reb}	-7.5E6 (J)	6.5
L_{Reb}	F_{Reb}	-80 (mol/m)	5

6.4   Performance evaluation and discussions

This section shows the performance of the proposed control structure for the CO_2 capture process using PZ and MEA solvents. A few scenarios has been considered in this work to test the performance of these plants, i.e. multiple ramp changes in the flue gas flow rate, V-1 valve stiction during load change, and steam flow shortage scenarios. These are frequent cases encountered in the day-to-day operation of a coal-based power station with integrated CO_2 capture plant. Each of these scenarios is discussed next. The focus is on the low energy PZ process since it has not been studied before.

6.4.1   Flue gas multiple ramp-changes scenario

It seems likely that in the future energy market with increasing share of intermittent renewable energy supplies, power plants may be required to operate with frequent and large power load changes on a daily and seasonal basis in order to balance electricity output and energy demand of the population (Chalmers et al., 2009). This mode of operation results in step-wise continuous changes in the flue-gas flowrate conditions using flexible operation (Chalmers and Gibbins, 2007; Chalmers et al., 2012; Lucquiaud et al., 2009; Wiley et al., 2011).

The performance of the developed control structures for multiple load changes using PZ and MEA solvents was considered. Figure 6.4 shows the multiple ramp increase (scenario 1A) and decrease (scenario 1B) imposed on the flue gas flow rate. As shown in this figure, three ramp changes consisting of ±10%, ±25% and ±50%, with respect to the nominal operation point, were applied to the processes. These ramp changes are introduced after 30 min, 210 min and 450 min for a period of 1 hour, respectively. Table 6.6 shows the performance of the CO_2 capture plant for both solvents, which has been measured in terms of the integral square error (ISE) and settling time for the CO_2 capture efficiency (*%CC*). The ISE for %CC is determined as follows:

$$ISE = \int_{t_0}^{t_{final}} \left(\%CC_{SP} - \%CC(t) \right)^2 dt \tag{10}$$

where *%CC$_{SP}$* is the set-point for the CO_2 capture rate (%) and *%CC(t)* is the CO_2 capture rate at any time *t*. Figures 6.5 and 6.6 show the response of the capture plant for scenarios 1A and 1B, respectively.
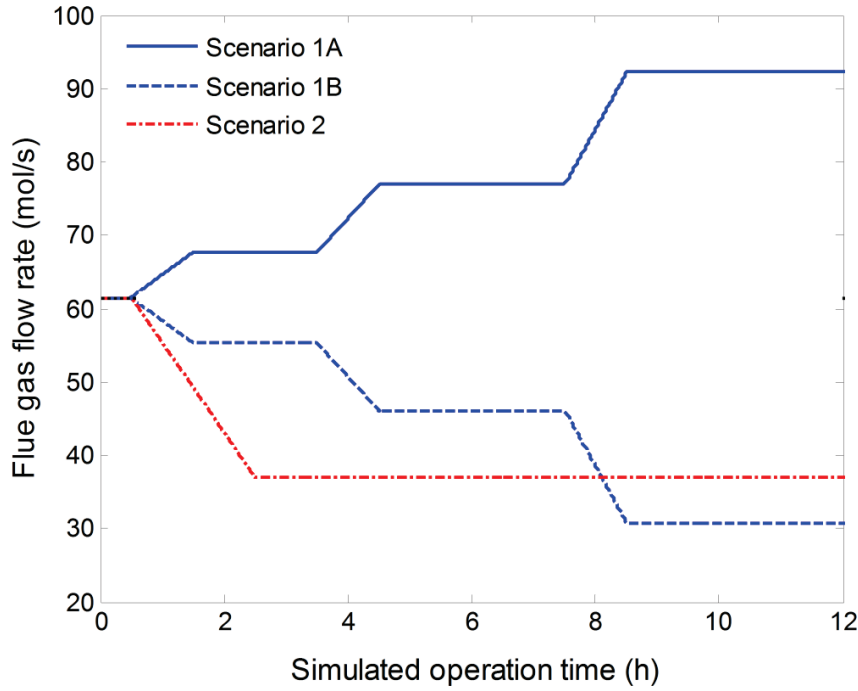
Figure 6.4. Flue gas flow rate versus time for the investigated dynamic operation scenarios: Scenario 1: multiple ramp changes; and Scenario 2: V-1 stiction

Figure 6.5a on MEA shows that the proposed control structure is able to maintain a tight control on the CO_2 capture efficiency (%CC) for 10% and 25% increases in the flue gas flow rate; however, the MEA control structure cannot track the %CC$_{SP}$ when a 50% ramp increase in the flue gas flow rate is introduced to the plant. The explanation for this observation is as follows. In figure 6.5b, small spikes can be observed in the reboiler loading (θ_{Reb}) due to the fast opening of V-1 to increase the lean solvent flow rate (figure 6.5c) once an offset in %CC is detected. However, the effect of increased solvent flow rate on θ_{Reb} is compensated by rapidly increasing the reboiler duty as shown in figure 6.5d. When the flue gas flow is increased 50% above its nominal value (at $t = 7.5$ h), the %CC suddenly decreases from 90% to 85%, as shown in figure 6.5a. The lean solvent flow rate (F_{Lean}) reaches its saturation limit at $t = 7.85$ h and the %CC-F_{Lean} control loop is unable to keep track of the %CC$_{SP}$. Figures 6.5b and 6.5d show that the θ_{Reb}-Q_{Reb} control loop reduces the offset in θ_{Reb} by further increasing the reboiler duty. However, Q_{Reb} also reaches its saturation limit at $t = 8.4$ h and this control loop is unable to reach the designated set point in θ_{Reb}. Based on the above, the proposed control structure for the MEA plant smoothly rejects flue gas flow rate changes of 10% and 25% but it cannot accommodate load changes of 50%, at which the lean solvent flow rate and reboiler duty saturate.

Table 6.6. Performance comparison of the control structures for the PZ and MEA plants

Scenario	ISE · 10^{-4}		Settling time (h) *	
	PZ	MEA	PZ	MEA
Multiple ramp increase	15.2	55.6	14.5	*INF*
Multiple ramp decrease	17.7	66.9	*INF*	*INF*
Valve stiction	20.2	8.39	10	3.5
Steam supply shortage	219.1	0.254	9.1	6

* Time required to reach the new steady state in %CC

INF – the plant did not reach its set-point

Figure 6.5 shows that the closed-loop response of the PZ plant for scenario 1A is faster and with less variability compared to that observed for the MEA plant. Table 6.6 outlines that the ISE of the CO_2 removal using PZ is approximately 3.5 times smaller than that obtained for the MEA plant. In addition, the PZ plant reached the final set-point in 14.5 hours for scenarios 1A while the final control objective of the MEA process was not met, i.e. *%CC* is 84.9% and θ_{Reb} is 0.193. As expected, an increase in the flue gas flow rate results in insufficient capture efficiency. Figure 6.5a illustrates that the deviation from the *%CC* set-point is more visible for PZ than for MEA: A 25% increase of the flue gas flow results in a *%CC* of 86.5% using PZ compared to a *%CC* of 89.1% using MEA. However, the *%CC-Q_{Reb}* control loop for the PZ process rejects the effect of flue gas flow increase by increasing the reboiler duty, as shown in figure 6.5d. Moreover, figure 6.5b on PZ illustrates that scenario 1A results in drops in the reboiler loading (θ_{Reb}), which is opposed to what was observed for the MEA process. This behaviour is due to the pairing between *%CC* and Q_{Reb}. The drop in *%CC* produces an increase of the reboiler duty, which increases CO_2 stripping and lowers θ_{Reb}. Further, the deviation from the θ_{Reb} set-point leads to the opening of V-1 which increases the lean solvent flow rate, as shown in figure 6.5c. Figures 6.5e and 6.5f show that the deviations in the liquid levels, i.e. sump and the reboiler drum are not significantly affected during multiple ramp changes in the load. In summary, the combined effect of the *%CC-Q_{Reb}* and *θ_{Reb}-F_{Lean}* PZ control loops correct the deviations from the set-points. Additionally, figures 6.5c and 6.5d show that the variability in the lean solvent flow rate (MV1) and reboiler duty (MV3) is lower for the PZ plant than for the MEA plant.
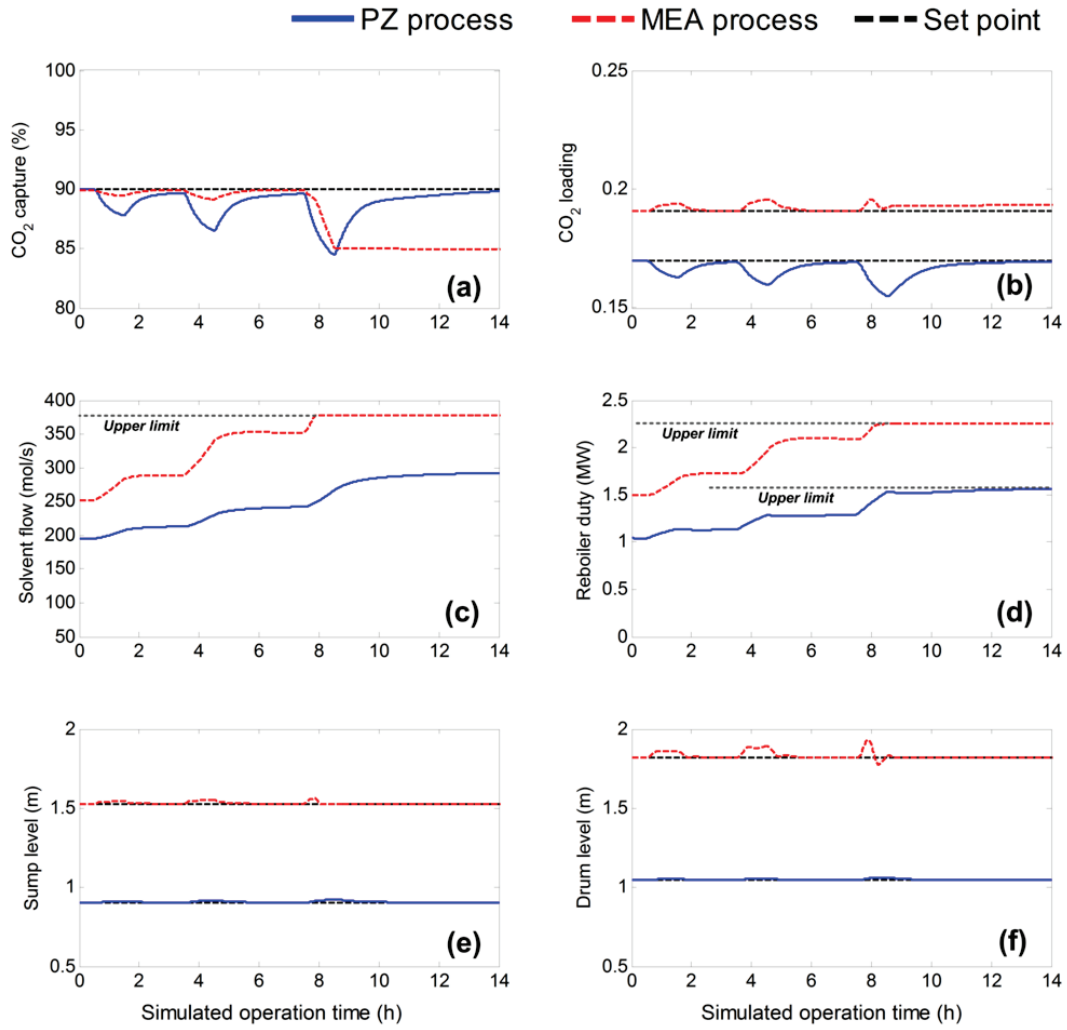
Figure 6.5. Closed-loop response to ramp increases of 10%, 25% and 50% in flue gas flow rate: (a) CO_2 capture efficiency; (b) reboiler outlet CO_2 loading; (c) lean solvent flow rate; (d) reboiler duty; (e) absorber's sump level and (f) reboiler's tank level

Figure 6.6 shows the response of the PZ and MEA plant for 10%, 25% and 50% ramp decreases in the flue gas flow rate (scenario 1B). Similar to scenario 1A, the PZ and the MEA plant can handle load changes of 10% and 25%. On the other hand, neither the PZ nor the MEA plant reach the control objectives of 90% CO_2 capture efficiency and the designated set point in reboiler lean loading for a ramp of -50%. This behaviour is less visible for the PZ solvent. The final deviation from the set-points in $\%CC$ and θ_{Reb} are larger for the MEA process since the MEA system reached its saturation limit at $t = 8.2$ hours whereas the PZ plant reached this condition at a later time, i.e. at $t = 10$ hours. As shown in Table 6.6, the ISE computed for the CO_2 removal is 3.8 times lower using PZ than that obtained for MEA. Figures 6.6e and 6.6f show that the

levels in the absorber's sump and the drum of the reboiler are tightly controlled using PZ and MEA solvents, i.e., the change in the levels is less than 0.1 m.
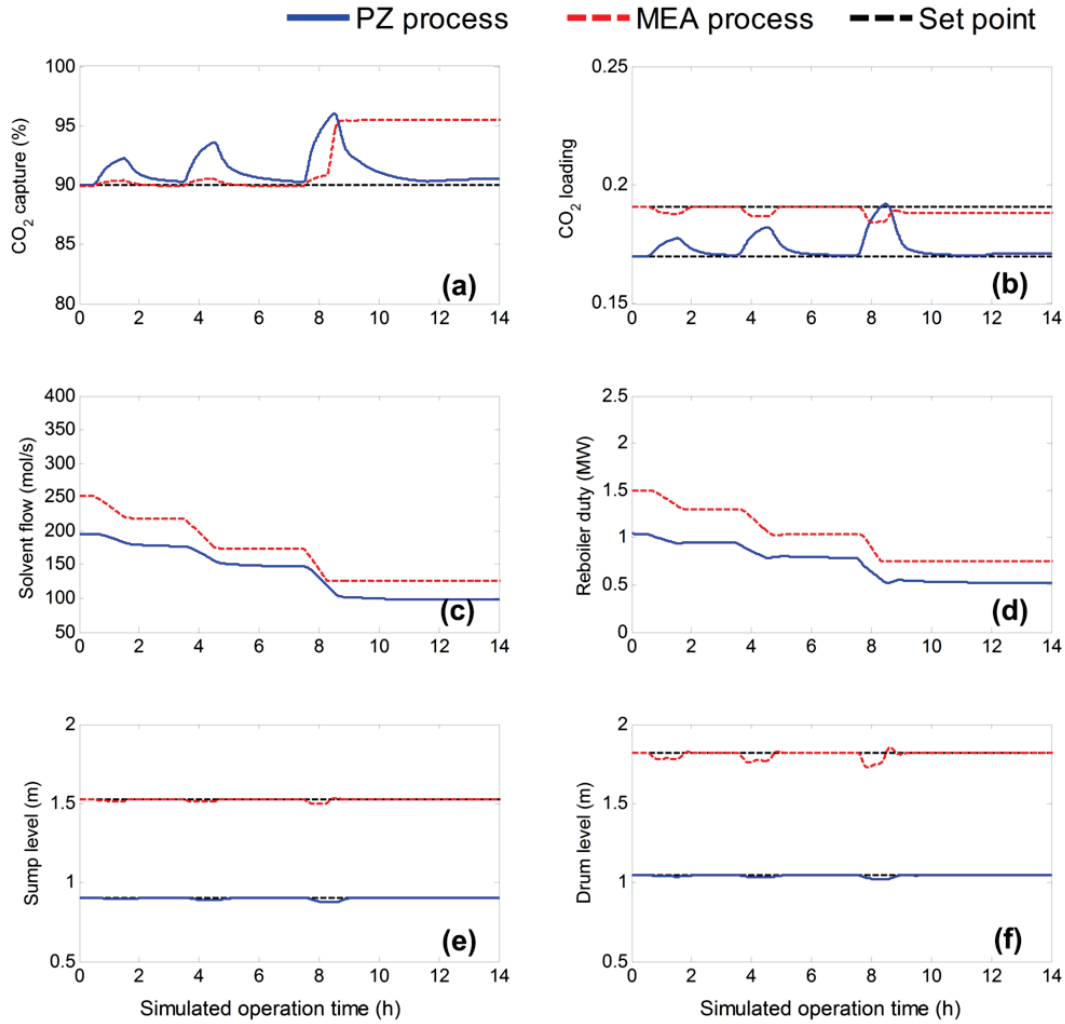

Figure 6.6. Closed-loop response to ramp decreases of 10%, 25% and 50% in flue gas flow rate: (a) CO_2 capture efficiency; (b) reboiler outlet CO_2 loading; (c) lean solvent flow rate; (d) reboiler duty; (e) absorber's sump level and (f) reboiler's tank level

The results shown above indicate that the control structure for PZ can accommodate load changes up to 50% whereas the MEA plant saturates and is not able to meet the control objectives for 50% change in the flue gas flow rate. Moreover, the variability in the MVs is less for the PZ plant compared to the MEA plant, i.e. the required changes in the lean solvent flow rate and the reboiler duty to reach the designated set-points are smaller in the PZ plant.

6.4.2 Flue gas ramp-change with valve stiction scenario

This operational scenario aims to investigate the effect of V-1 valve stiction on the performance of the CO_2 capture plant during ramp load decrease of the power plant. It resembles an operational scenario when the position of the V-1 valve cannot be modified due to failure of the actuator. The present scenario assumes that V-1 valve stiction occurs when the plants are in the presence of a 20% ramp decrease in the flue gas flow rate as shown in Figure 6.4 (scenario 2). Figure 6.7c illustrates that the lean solvent flow rate remains constant due to V-1 stiction during 1 hour after the introduction of the ramp change. After 1.5 hours from the start of the simulation, the V-1 valve becomes operational and all of the control loops operate normally. Figure 6.7 shows the closed loop response of the capture plant for scenario 2 using PZ and MEA solvents. Note that the simulated operation time of the MEA process is shorted than of the PZ process since neither the manipulated variables nor the control variables changed for more than 4 hours and the simulation has been terminated. Figure 6.7a illustrates that, as a consequence of the decrease in the flue gas flow in the presence of V-1 stiction, the MEA plant responds with a sudden increase in the CO_2 capture efficiency (*%CC*), from 90% to 95.7%. The continuous increase of the offset in *%CC* is due to the loss of the *%CC*-F_{Lean} control loop. On a long term, the malfunctioning of V-1 leads to a drop in the lean loading exiting the reboiler, θ_{Reb} (figure 6.7b). However, the offset in the loading is rapidly rejected by the θ_{Reb}-Q_{Reb} control loop and the plant ultimately converges to the designated set-points in 3.5 hours, as shown in figures 6.7a and 6.7b. The effect of V-1 stiction on the PZ capture plant is more significant compared to the MEA plant.

Figure 6.7a shows that the deviation from the 90% CO_2 capture set-point increases up to 98.2% using PZ whereas a 95.7% deviation was observed for the MEA plant. Figure 6.7d on PZ shows that the reboiler duty (Q_{Reb}) decreases rapidly from 1.04 MW to 0.68 MW in order to correct for the offset in the CO_2 capture efficiency. This drop in the reboiler duty produces a sudden increase in the reboiler lean loading, θ_{Reb}. Figure 6.7b illustrates that the reboiler outlet loading increases from 0.17 mol/mol alkalinity to 0.24 mol/mol alk. Note that Q_{Reb} is paired with *%CC* and θ_{Reb} with F_{Lean} in case of the PZ process while the pairing is the opposite for the MEA process. Thus, the increase of θ_{Reb} is due to the loss of the θ_{Reb}-F_{Lean} control loop in the presence of V-1 stiction. Figure 6.7a illustrates that the *%CC*-Q_{Reb} control loop ultimately manages to correct the deviation in *%CC*; however, the control actions of this control loop are delayed by the buffer tank located between the reboiler and the absorber units. Figures 6.7e and 6.7f show that the variability of the liquid levels in the tanks is not significantly affected with this scenario using PZ solvent. Moreover, the change in the level of the reboiler's drum is around 0.5 m for the MEA process. Therefore, stiction of V-1 for longer periods of time may eventually cause drying or flooding in the MEA plant under scenario 2. A possible approach to avoid flooding during malfunctioning of the lean flow valve (V-1) in presence of flue gas flow ramp scenario is by adding a bypass (or shunt) valve to shunt the excessive flue gas around the absorber.

This bypass valve practically ensure that the nominal 90% CO_2 removal rate can be met by maintaining the flue gas flow rate to the absorber near its nominal operating value (Zhang et al., 2016). However this control scheme leads to loss in the CO_2 capture rate.
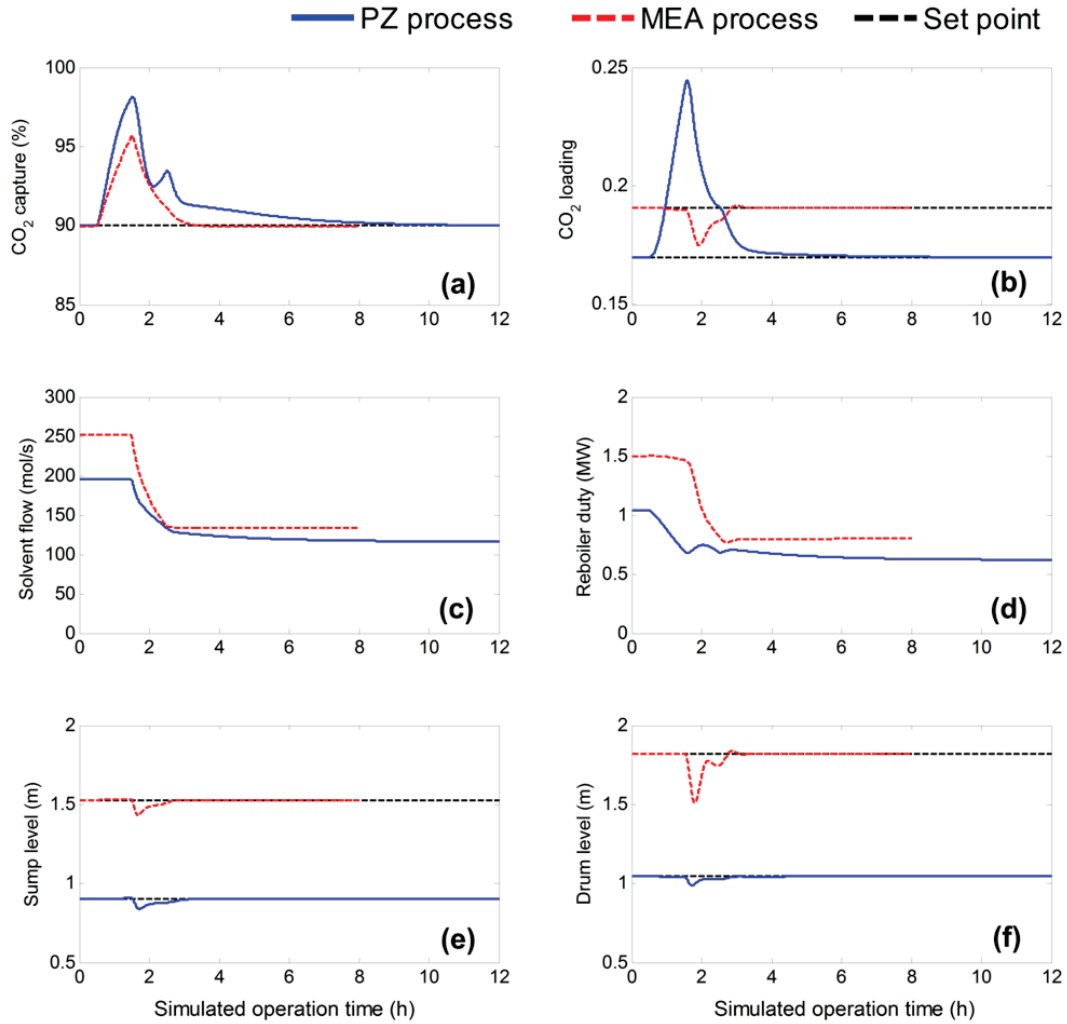

Figure 6.7. Closed-loop response to a 20% ramp change in flue gas flow rate in presence of V-1 lean solvent valve stiction: (a) CO_2 capture efficiency; (b) reboiler outlet CO_2 loading; (c) lean solvent flow rate; (d) reboiler duty; (e) absorber's sump level and (f) reboiler's tank level

Figures 6.7a and 6.7d suggest that the control structures proposed in this work correct the offsets in all the controlled variables when V-1 becomes operational. The impact of V-1 stiction has more significant effect on PZ than on MEA, i.e. the ISE of CO_2 removal is 2.4 times higher for the PZ process than that obtained for the MEA process (Table 6.6). In addition, table 6.6 highlights that the MEA capture plant requires 3.5 hours

to reject this disturbance. The settling time for the PZ capture plant is approximately 10 hours, almost three times the time needed by the MEA plant. These results are in agreement with the observations presented in figure 6.2, i.e. the PZ process is more sensitive to changes in the lean solvent flow rate compared to MEA.

6.4.3 Steam supply shortage under constant flue gas flowrate scenario

Power plants are required to accommodate scheduled and sudden changes in the electricity grid. A possible approach to suddenly increase the electricity output of a power plant with integrated CO_2 capture is to reduce the amount of steam supplied to the reboiler unit, which results in limited heat supply for the CO_2 capture process. Accordingly, this section details the response of the PZ and MEA capture plants for a 20% step reduction of the reboiler duty for a period of 2 hours, followed by unconstrained steam supply (scenario 3). The present scenario aims to reveal the response of each control-loop once the reboiler duty reaches its saturation limit using PZ and MEA solvents. Accordingly, the flue gas flow rate is kept constant in the present scenario while the maximum allowed utility (heat duty) for the reboiler, extracted from the power plant, is reduced from 1.04 MW to 0.83 MW for the PZ plant and from 1.5 MW to 1.2 MW to the MEA plant (figure 6.8d).

Figure 6.8a illustrates that the proposed control scheme for the MEA plant rejects the effect of heat supply shortage on the CO_2 capture efficiency (*%CC*) by increasing the lean solvent flow rate (F_{Lean}), as shown in figure 6.8c. However, figure 6.8d outlines that the lean CO_2 loading exiting the reboiler (θ_{Reb}) increases suddenly as the reboiler duty step decreases. The lean loading increases from 0.19 mol/mol to 0.28 in the presence of constraints in the reboiler duty and it rapidly reduces to its set-point when unconstrained steam supply is available ($t > 2.5$ hours). Furthermore, figure 6.8b demonstrates that the lean flow rate (F_{Lean}) increases in order to reject the effect of higher CO_2 loading of the absorber's feed and it slowly returns to its nominal value after $t > 2.7$ hours.

Figure 6.8 highlights that the effect of steam supply shortage on the PZ plant is critical, compared to the MEA plant. Not only the CO_2 loading of the reboiler deviates from its set-point (figure 6.8b) but the CO_2 capture efficiency reduces dramatically from 90% to 72.8% in the presence of steam shortage, as shown in figure 6.8a. As reported in Table 6.6, the ISE of the PZ plant is 860 times larger than that obtained for the MEA plant, while the settling time is 51% higher for PZ than for the MEA plant. This behaviour is in agreement with the observations presented in figure 6.3A, i.e. a step decrease in the reboiler duty leads to lower capture percentage and this effect is much more significant on the PZ plant than on the MEA plant.

Figure 6.8a on PZ shows that, as expected, the constraint in the reboiler duty leads to higher lean loadings, θ_{Reb}. In order to correct this offset in θ_{Reb}, the θ_{Reb}-F_{Lean} control loop decreases the lean solvent flow rate, as

shown in figure 6.8b. Consequently, the CO_2 capture percentage reduces pronouncedly due to higher lean CO_2 loading and lower lean solvent flow rate. On the other hand, the *%CC-Q_{Reb}* control loop is inhibited since Q_{Reb} is at its saturation limit. Figures 6.7e and 6.7f show that the variability of the liquid levels in the tanks is not significantly affected with this scenario regardless of the solvents being used.
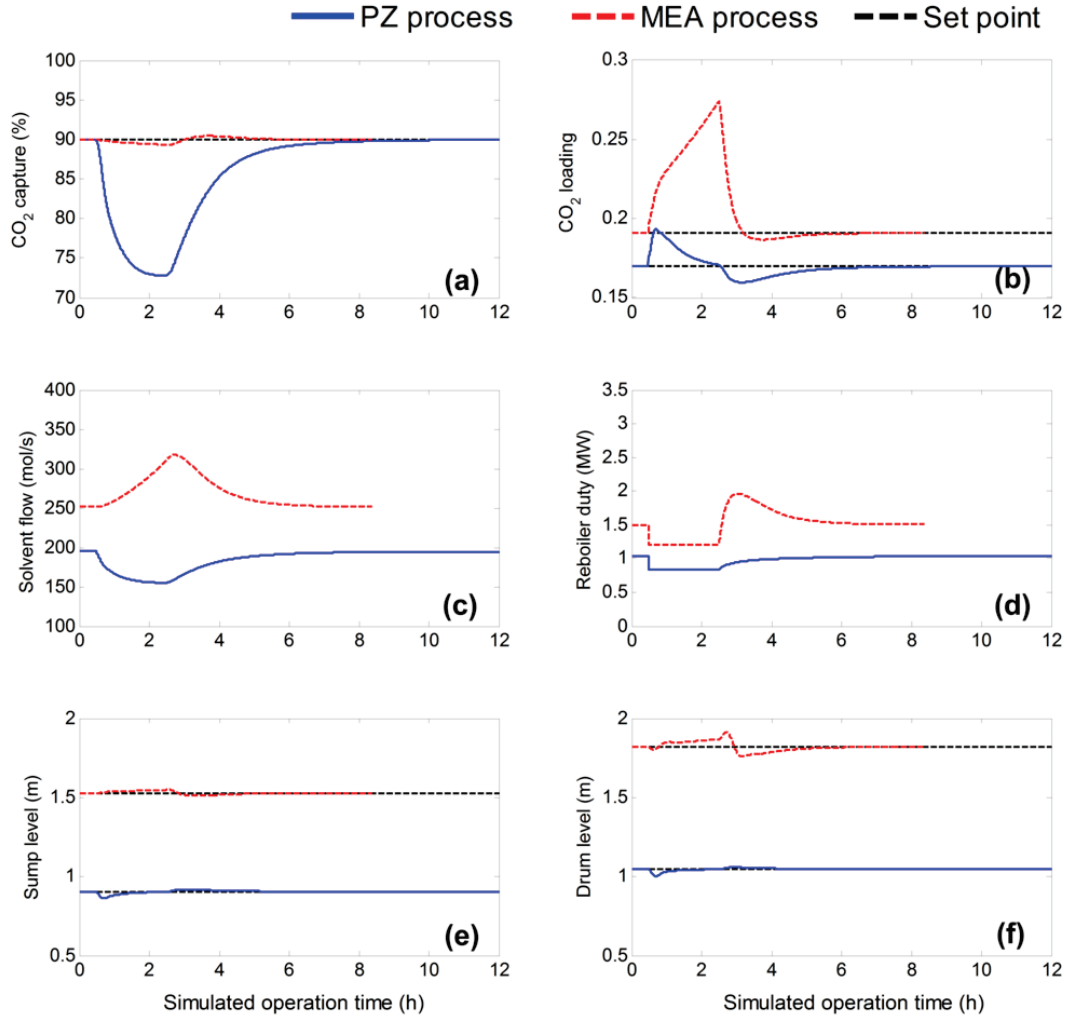

Figure 6.8. Closed-loop response to reboiler steam supply shortage: (a) CO_2 capture efficiency; (b) reboiler outlet CO_2 loading; (c) lean solvent flow rate; (d) reboiler duty; (e) absorber's sump level and (f) reboiler's tank level

Although the implemented control structure smoothly rejects the effect of steam supply shortage on CO_2 capture efficiency using MEA, this scenario may result in flooding in the absorber due to the significant increase in the solvent's flow rate. Moreover, the MEA plant can reject steam supply constraints only if V-1

does not reach its saturation limit. Furthermore, the performance of the PZ plant is strongly affected by this scenario; a shortage in the steam supply results in significant decrease of *%CC*, as a result of the loss of the *%CC*- Q_{Reb} control loop.

6.5   Conclusions

In this work, a decentralized control structure for the PZ and the MEA CO_2 capture processes was presented. The Relative Gain Array (RGA) analysis represents the base for the design of these control schemes. Additionally, the dynamic sensitivity of the process to step changes in the manipulated variables, i.e. lean solvent flow rate, reboiler duty, etc. was assessed. The dynamic sensitivity analysis showed that step changes in the lean solvent flow rate and reboiler duty have a significant impact on the performance of the CO_2 capture unit. The settling time is approximately 2 times slower in case of PZ compared to MEA. Thus, controllers with short time integrals are required to maintain the PZ plant within short closed-loop settling times.

The sensitivity analysis suggested to pair CO_2 removal efficiency (*%CC*) with reboiler duty (Q_{Reb}) and the reboiler lean loading (θ_{Reb}) with lean solvent flow rate (F_{Lean}) for the PZ process; this analysis also suggested the opposite pairing between these variables for the MEA process, i.e. *%CC*-F_{Lean} and θ_{Reb}-Q_{Reb}. The performance of the proposed control structures was evaluated for industrially-relevant operation scenarios. The controllability study showed that the control scheme specified for PZ rejects faster and with less variability changes in the power plant load, i.e. variation in the flue gas flow rate, compared to MEA. The PZ plant did not reach its saturation point and the control strategy was able to accommodate large changes in the load. The PZ and MEA plants can also accommodate V-1 valve stiction for a limited time interval. Initially, both of the plants deviate from their designated set-points in presence of V-1 failure; however, the CO_2 capture unit corrects these offsets when V-1 becomes operational.

Furthermore, this study has shown that a constraint in the steam supply (reboiler duty) represents a critical operation scenario, especially when PZ is being used. The performance of the PZ plant reduces drastically when the reboiler duty is reduced while the controllers of the MEA plant drive the system towards drying out/flooding. These findings suggest the need for advanced control strategies, e.g. MPC, which can explicitly account for constraints in process variables. Similar behaviour has been observed for V-1 valve-stiction scenario in presence of capture plant load decrease. A potential solution to avoid operability issues, i.e. drying out/flooding for this scenario using a PID control scheme is shunting the excess flue gas flow, as suggested by Zhang et al. (2016).

This study showed long settling time for PZ compared to MEA. Thus, use of PZ could lead to reduced flexibility of the capture plant. A possible solution to decrease the settling time is by pairing *%CC-F_{Lean}* and *θ_{Reb}-Q_{Reb}*. This approach would eliminate the delay introduced by the buffer tank in the control of *%CC*. A study similar to (Nittaya et al., 2014) seems relevant for further developing the PZ process. Other approaches, i.e. smaller buffer tanks, different pairing of MVs and CVs, cascade PID control may also increase operability of the plant. However, model based control is the most promising solution to improve operability pf post-combustion capture, i.e. reducing settling time and keeping the CVs at their designated set-points while meeting operational, environmental and economic constraints. The advantage of model based control for MEA has been previously demonstrated but there is a need to show the benefits of MPC for PZ.

Finally, this study suggests that PZ may be a better solvent than MEA since it can accommodate disturbances with less variability in the manipulated variables, i.e. lean solvent flow rate, recycle flow rate, reboiler duty and stripper's feed. In future work, the benefits of MPC strategy as well as the effect of process design on the process dynamics will be considered to enhance the performance of a CO_2 capture plant (Sahraei and Ricardez-Sandoval, 2014b; Sanchez-Sanchez and Ricardez-Sandoval, 2013; Trainor et al., 2013). In addition, the effect of uncertainties on the dynamic operation and economics of a CO_2 capture plant using piperazine (PZ), compared to the benchmark MEA solvent, will be investigated to increase the confidence in the design of a commercial-scale post-combustion plant.

References

Abdul Manaf, N., Cousins, A., Feron, P., Abbas, A., 2016. Dynamic modelling, identification and preliminary control analysis of an amine-based post-combustion CO2 capture pilot plant. J. Clean. Prod. 113, 635–653. doi:10.1016/j.jclepro.2015.11.054

Bui, M., Gunawan, I., Verheyen, V., Feron, P., Meuleman, E., 2016. Flexible operation of CSIRO's post-combustion CO2 capture pilot plant at the AGL Loy Yang power station. Int. J. Greenh. Gas Control. doi:10.1016/j.ijggc.2015.12.016

Chalmers, H., Gibbins, J., 2007. Initial evaluation of the impact of post-combustion capture of carbon dioxide on supercritical pulverised coal power plant part load performance. Fuel 86, 2109–2123. doi:10.1016/j.fuel.2007.01.028

Chalmers, H., Gibbins, J., Leach, M., 2012. Valuing power plant flexibility with CCS: the case of post-combustion capture retrofits. Mitig. Adapt. Strateg. Glob. Chang. 17, 621–649. doi:10.1007/s11027-011-9327-5

Chalmers, H., Lucquiaud, M., Gibbins, J., Leach, M., 2009. Flexible Operation of Coal Fired Power Plants with Postcombustion Capture of Carbon Dioxide. J. Environ. Eng. 135, 449–458. doi:10.1061/(ASCE)EE.1943-7870.0000007

Chen, E., 2015. Pilot Plant Results for 5 M Piperazine with the Advanced Flash Stripper. Abstr. from 3nd Post Combust. Capture Conf. Regina, Canada.

Ennio, M., Giampaolo, M., Rahul, A., Olav, B., Nick, B., Pfeffer, A., Flavio, F., 2011. D 4.9 European best practice guidelines for assessment of CO2 capture technologies.

Faber, R., Köpcke, M., Biede, O., Knudsen, J.N., Andersen, J., 2011. Open-loop step responses for the MEA post-combustion capture process: Experimental results from the Esbjerg pilot plant. 10th Int. Conf. Greenh. Gas Control Technol. 4, 1427–1434. doi:http://dx.doi.org/10.1016/j.egypro.2011.02.008

Faramarzi, L., Kontogeorgis, G.M., Thomsen, K., Stenby, E.H., 2009. Extended UNIQUAC model for thermodynamic modeling of CO2 absorption in aqueous alkanolamine solutions. Fluid Phase Equilib. 282, 121–132. doi:10.1016/j.fluid.2009.05.002

Fosbøl, P.L., Gaspar, J., Ehlers, S., Kather, A., Briot, P., Nienoord, M., Khakharia, P., Le Moullec, Y., Berglihn, O.T., Kvamsdal, H.M., 2014. Benchmarking and comparing first and second generation post combustion CO2 capture technologies. Energy Procedia 63, 27–44. doi:10.1016/j.egypro.2014.11.004

Gaspar, J., Cormos, A.-M., 2012. Dynamic modeling and absorption capacity assessment of CO2 capture process. Int. J. Greenh. Gas Control 8, 45–55. doi:10.1016/j.ijggc.2012.01.016

Gaspar, J., Fosbøl, P.L., 2016. Simulation and multivariable optimization of post-combustion capture using piperazine. Int. J. Greenh. Gas Control 49, 227–238. doi:10.1016/j.ijggc.2016.03.009

Gaspar, J., Fosbøl, P.L., 2015. A general enhancement factor model for absorption and desorption systems: A CO2 capture case-study. Chem. Eng. Sci. 138, 203–215. doi:http://dx.doi.org.globalproxy.cvt.dk/10.1016/j.ces.2015.08.023

Gaspar, J., Gladis, A., Jørgensen, J.B., Thomsen, K., von Solms, N., Fosbøl, P.L., 2016a. Dynamic Operation and Simulation of Post-Combustion CO2 Capture. Energy Procedia 86, 205–214. doi:10.1016/j.egypro.2016.01.021

Gaspar, J., Jorgensen, J.B., Fosbol, P.L., 2015a. Control of a post-combustion CO2 capture plant during process start-up and load variations. IFAC-PapersOnLine 48, 580–585. doi:10.1016/j.ifacol.2015.09.030

Gaspar, J., Jørgensen, J.B., Fosbøl, P.L., 2015b. A Dynamic Mathematical Model for Packed Columns in Carbon Capture Plants, in: Proceedings of ECC Conference. IFAC, http://www.ifac-papersonline.net/, pp. 2743–2748. doi:10.1109/ECC.2015.7330952

Gaspar, J., von Solms, N., Thomsen, K., Fosbøl, P.L., 2016b. Multivariable Optimization of the Piperazine CO2 Post-Combustion Process. Energy Procedia 86, 229–238. doi:10.1016/j.egypro.2016.01.024

Harun, N., Nittaya, T., Douglas, P.L., Croiset, E., Ricardez-Sandoval, L.A., 2012. Dynamic simulation of MEA absorption process for CO2 capture from power plants. Int. J. Greenh. Gas Control 10, 295–309. doi:10.1016/j.ijggc.2012.06.017

He, Z., Sahraei, M.H., Ricardez-Sandoval, L.A., 2015. Flexible operation and simultaneous scheduling and control of a CO2 capture plant using model predictive control. Int. J. Greenh. Gas Control. doi:10.1016/j.ijggc.2015.10.025

Jørgensen, J.B., Jørgensen, S.B., 2000. Towards automatic decentralized control structure selection. Comput. Chem. Eng. 24, 841–846. doi:10.1016/S0098-1354(00)00337-9

Lawal, A., Wang, M., Stephenson, P., Koumpouras, G., Yeung, H., 2010. Dynamic modelling and analysis of post-combustion CO2 chemical absorption process for coal-fired power plants. Fuel 89, 2791–2801. doi:10.1016/j.fuel.2010.05.030

Lin, Y.-J., Pan, T.-H., Wong, D.S.-H., Jang, S.-S., Chi, Y.-W., Yeh, C.-H., 2011. Plantwide Control of CO2 Capture by Absorption and Stripping Using Monoethanolamine Solution. Ind. Eng. Chem. Res. 50, 1338–1345. doi:10.1021/ie100771x

Lin, Y.-J., Wong, D.S.-H., Jang, S.-S., Ou, J.-J., 2012. Control strategies for flexible operation of power plant with CO2 capture plant. AIChE J. 58, 2697–2704. doi:10.1002/aic.12789

Lucquiaud, M., Chalmers, H., Gibbins, J., 2009. Capture-ready supercritical coal-fired power plants and flexible post-combustion CO2 capture. Energy Procedia 1, 1411–1418. doi:10.1016/j.egypro.2009.01.185

Luu, M.T., Abdul Manaf, N., Abbas, A., 2015. Dynamic modelling and control strategies for flexible operation of amine-based post-combustion CO2 capture systems. Int. J. Greenh. Gas Control 39, 377–389. doi:10.1016/j.ijggc.2015.05.007

Nittaya, T., Douglas, P.L., Croiset, E., Ricardez-Sandoval, L.A., 2014. Dynamic modelling and control of MEA absorption processes for CO2 capture from power plants. Fuel 116, 672–691. doi:10.1016/j.fuel.2013.08.031

Pachauri, R.K., Reisinger, A., on, C.C., 2008. Climate change 2007. Synthesis report. Contribution of Working Groups I, II and III to the fourth assessment report. IPCC.

Panahi, M., Skogestad, S., 2012. Economically efficient operation of CO2 capturing process. Part II. Design of control layer. Chem. Eng. Process. 52, 112–124. doi:10.1016/j.cep.2011.11.004

Panahi, M., Skogestad, S., 2011. Economically efficient operation of CO2 capturing process part I: Self-optimizing procedure for selecting the best controlled variables. Chem. Eng. Process. 50, 247–253. doi:10.1016/j.cep.2011.02.005

Posch, S., Haider, M., 2013. Dynamic modeling of CO2 absorption from coal-fired power plants into an aqueous monoethanolamine solution. Chem. Eng. Res. Des. 91, 977–987. doi:10.1016/j.cherd.2012.09.016

Puxty, G., Rowland, R., Allport, A., Yang, Q., Bown, M., Burns, R., Maeder, M., Attalla, M., 2009. Carbon Dioxide Postcombustion Capture: A Novel Screening Study of the Carbon Dioxide Absorption Performance of 76 Amines. Environ. Sci. Technol. 43, 6427–6433. doi:10.1021/es901376a

Sahraei, M.H., Ricardez-Sandoval, L.A., 2014a. Controllability and optimal scheduling of a CO2 capture plant using model predictive control. Int. J. Greenh. Gas Control 30, 58–71. doi:http://dx.doi.org/10.1016/j.ijggc.2014.08.017

Sahraei, M.H., Ricardez-Sandoval, L.A., 2014b. Simultaneous Design and Control of the MEA Absorption Process of a CO2 Capture Plant. 12th Int. Conf. Greenh. Gas Control Technol. GHGT-12 63, 1601–1607. doi:http://dx.doi.org/10.1016/j.egypro.2014.11.170

Sanchez-Sanchez, K.B., Ricardez-Sandoval, L.A., 2013. Simultaneous Design and Control under Uncertainty Using Model Predictive Control. Ind. Eng. Chem. Res. 52, 4815–4833. doi:10.1021/ie302215c

Seborg, D.E., Edgar, T.F., Mellichamp, D.A., 1989. Process dynamics and control. Wiley.

Trainor, M., Giannakeas, V., Kiss, C., Ricardez-Sandoval, L.A., 2013. Optimal process and control design under uncertainty: A methodology with robust feasibility and stability analyses. Chem. Eng. Sci. 104, 1065–1080. doi:10.1016/j.ces.2013.10.017

Valencia-Marquez, D., Flores-Tlacuahuac, A., Ricardez-Sandoval, L., 2015. Technoeconomic and Dynamical Analysis of a CO 2 Capture Pilot-Scale Plant Using Ionic Liquids. Ind. Eng. Chem. Res. 54, 11360–11370. doi:10.1021/acs.iecr.5b02544

Van Wagener, D.H., 2011. Stripper Modeling for CO2 Removal Using Monoethanolamine and Piperazine Solvents. The University of Texas at Austin, Austin, Texas.

Walters, M.S., Dunia, R.H., Edgar, T.F., Rochelle, G.T., 2013. Two-Stage Flash for CO2 Regeneration: Dynamic Modeling and Pilot Plant Validation. Energy Procedia 37, 2133–2144. doi:10.1016/j.egypro.2013.06.092

Wang, M., Lawal, A., Stephenson, P., Sidders, J., Ramshaw, C., 2011. Post-combustion CO2 capture with chemical absorption: A state-of-the-art review. Chem. Eng. Res. Des. 89, 1609–1624. doi:10.1016/j.cherd.2010.11.005

Wiley, D.E., Ho, M.T., Donde, L., 2011. Technical and economic opportunities for flexible CO2 capture at Australian black coal fired power plants. Energy Procedia 4, 1893–1900. doi:10.1016/j.egypro.2011.02.068

Yamaguchi, M., 2012. Climate change mitigation : a balanced approach to climate change. Springer.

Zhang, Q., Turton, R., Bhattacharyya, D., 2016. Development of Model and Model-Predictive Control of an MEA-Based Postcombustion CO 2 Capture Process. Ind. Eng. Chem. Res. 55, 1292–1308. doi:10.1021/acs.iecr.5b02243

Chapter 7. Conclusions and recommendations

This work aimed to develop a standardized approach for CO_2 post-combustion capture steady-state and dynamic modeling using in-house models and industrial process simulators. The focus was on the model for the packed columns as they represent the key units of a capture process and they greatly influence the capital and operational cost of a plant. Accordingly, first a steady-state rate-based model for CO_2 absorption and desorption has been developed and benchmarked using the baseline MEA solvent and promising solvents with high CO_2 capacity and low energy demand, e.g. PZ, PZ/K_2CO_3, CA/MDEA. The mass and energy balance equations and the mass transfer-, kinetic- and hydraulic- modules are implemented in Fortran 90 in a modular fashion. Then, this packed column model has been integrated into Aspen Plus for simulation and optimization of the complete post-combustion capture process. Furthermore, a dynamic model has been developed and applied to PZ and MEA to understand the transient behavior of a post-combustion plant and to investigate the controllability of a capture unit using PZ compared to MEA. This dynamic model is an extension of the steady-state model as it uses the same thermodynamic-, mass transfer-, kinetic- and physical property- modules. These are implemented in Fortran and interfaced with the Matlab implementation of the partial differential equations system. This approach ensures consistency between the dynamic and steady-state models, i.e. the solution of the dynamic and the steady-state model overlap when the plant reaches steady-state.

The steady-state and dynamic models for the absorber and for the desorber include: (1) the General Method (GM) enhancement factor model to calculate the CO_2 mass transfer rate across the gas-liquid interface; (2) the extended UNIQUAC thermodynamic model for vapor-liquid-solid equilibria and thermal properties and (3) correlations for physical properties needed in the mass transfer and hydraulic sub-models, e.g. diffusion coefficient, viscosity, surface tension, density, thermal conductivity, etc. The extended UNIQUAC model has been previously validated against several dataset for the solvents of interest and further development/adjustment of the model was not the intention of this work. The correlations for the physical properties have been obtained from literature and they have been re-evaluated by comparing to experimental data for absorption and desorption like conditions.

The column model uses the GM model as it eliminates many of the limitations of previous enhancement factor models. GM model connects the Onda's approximation for reversible reactions with the van Krevelen's approach for instantaneous irreversible reactions. The GM model has been successfully applied to single and parallel reaction systems. A study on MEA showed that GM predicts the numerical solution of the two-film model within 2% accuracy and the surface renewal model within 10% accuracy for absorption and desorption like conditions. The accuracy of the GM model has been further confirmed for single reactions (MEA) and parallel reactions (PZ and CA/MDEA) systems by comparing the model to a large number of wetted-wall column data. The absolute deviations between calculated and wetted-wall measured CO_2 fluxes are in the expected accuracy range, generally less than 20%. This is a noteworthy result considering the range of experimental conditions. This study demonstrated the GM model for MEA, PZ and CA/MDEA but we expect that it applies to other single and parallel reaction systems which can be approximated with multiple *(m+n)-th* order reversible reactions, e.g. reaction of CO_2 with blends of amines, promoted amines, etc.

The resulting steady-state model for the packed columns was compared against pilot absorber respectively desorber measurements using MEA, PZ, PZ/K_2CO_3, MDEA and CA/MDEA. This analysis showed that the model predictions are in the expected accuracy range. The relative deviations between simulated and measured CO_2 capture percentage, lean reboiler loading and specific reboiler duty are generally within ±10% for all of the solvents. Additionally, key performance parameters for the MEA closed-loop process, e.g. L/G-ratio, heat duty, CO_2 loading, stripper overhead composition, etc. confirmed the very good agreement between plant-wide capture model and pilot plant measurement. Generally, the model describes fairly well the shape of temperature and concentration profiles. However, the benchmarking study showed that profiles are less trustworthy, especially in the middle section of the column. As a result, it is important to evaluate the sensitivity of the composition and temperature profiles with respect to mass transfer, hydraulic, thermodynamic and kinetic sub-models for a set of design specifications to increase confidence in model based design. Furthermore, simulation results showed that precipitation of PZ decreases the performance of the solvent and it is important to consider the solubility window of PZ when evaluating and designing a capture process. These results were obtained with the developed hybrid capture model which considers slurry formation in the calculation of CO_2 mass transfer rate.

In terms of simulation results, it was found that PZ potentially reduces the energy demand of the solvent regeneration step with 0.4 to 0.8 GJ/t CO_2 compared to MEA (up to 20% lower energy demand). Additional energy savings of 0.2 GJ/t CO_2 can be realized by operating the capture plant closer to the solubility window of piperazine and/or by operating the absorber near the maximum (equilibrium) CO_2 rich loading. The solid-free operation window of a plant can be increased by maintaining the lean PZ solvent above ambient

temperatures, 25 °C in all of the units, e.g. condenser, storage tank, solvent reclaimer, pipes, etc. This option may require additional heating of units, especially in Nordic countries and during winter. The CO_2 loading of the rich solution exiting the absorber can be increased at the expenses of a greater process complexity and capital cost, for example by implementing intercooling in the absorber. These findings are expected to hold for natural gas cycle combined power plants (NGCC) as well as for coal-fired power plants (ASC). Note, the energy demand of an NGCC plant will be approximately 0.8 GJ/t CO_2 higher compared to an ASC case.

The developed dynamic model has been evaluated against dynamic pilot plant data using MEA and steady-state data using PZ. The agreement between model and experiment is good. The model predicts the transient evolution of the MEA pilot plant: it catches the fast responses of columns as well as the slow transient evolution with time delays. The dynamic model predicts well to the PZ pilot data for a broad range of L/G ratios, lean loadings and reboiler pressures. Additionally, a dynamic sensitivity study showed that step changes in the flue gas and the lean flow rate have a significant impact on the absorber with both solvents, MEA and PZ. The absorber settling time is roughly 2–3 times slower in case of PZ compared to MEA. Furthermore, this analysis revealed that the desorber evolves on a fast and a slow time-scale and it outlined the presence of inverse response of the PZ plant for increased rich loading or decreased feed temperature. Inverse response results in a challenging to control process.

Finally, a proportional-integral control structure has been implemented and the controllability of the plant has been investigated for PZ and MEA. These controllers are able to maintain the plant at the designated set-points when the manipulated variables do not reach their saturation limit. The PZ plant has less variability but with longer settling time compared to MEA; thus use of PZ could lead to reduced flexibility of the capture plant. Furthermore, the results outlined that limited steam supply and malfunctioning of the lean valve significantly impacts the performance of the PZ plant. A possible solution is invers pairing of the control and manipulated variables or implementing a model based control layer which can implicitly consider constraints in the process when computing the manipulated variables.

Recommendations for future work

Post-combustion CO_2 capture is a mature technology but further development of the process is essential to ensure the success of this technology in developing a green-sustainable energy sector. When simulating a complex process such as CO_2 post-combustion capture integrated with a power plant, several fundamental concepts must be considered, i.e. reaction kinetics, mass transfer and hydraulic characteristics, thermodynamics. Development and benchmarking of models and simulation software play an important role in increasing confidence in model based design and optimization. Based on this study, a first step could be verification of various mass transfer and hydraulic correlations against targeted pilot experiments. The

accuracy of these approximate mass transfer models should be evaluated against data obtained from small to large scale packed columns, various packing types, covering a broad range of operating conditions of interest for CO_2 capture. The confidence in these models is especially relevant for scale-up design. A better prediction will eliminate the need for conservative and uncertain design and therefore it will lead to more realistic cost estimations.

Furthermore, the GM and other approximate enhancement factor models for single and multiple parallel reactions should be compared against the full-numerical solution of the two-film model respectively the surface renewal model when using various single and promoted amines. These results should be compared to wetted wall column measurements to understand uncertainties related to both, experiments and models. Currently, the kinetic rate constants are generally obtained in the so called pseudo first order reaction zone and they are subject to the approach used for back-calculating the reaction rate-constant. A standard benchmarked approach is needed to eliminate uncertainties related to rate constants. Other experiments for physico-chemical properties, needed in the mass/heat transfer calculations need further evaluation, particularly at temperatures encountered in the desorber and the warmest part of the absorber. Then, using these benchmarked models, post-combustion capture can be optimization.

Flexibility and controllability of power-plants with integrated CO_2 capture is becoming a major topic when talking about the industrial deployment of post-combustion capture. There is a great need for dynamic models but also for real dynamic validation-data obtained with several innovative solvents. A better description of the transient behavior of the process is essential for control structure development and flexibility analysis. Moreover, the benefits of Model Predictive Control strategy as well as the effect of process design on the process dynamics need to be investigated to enhance the performance of a CO_2 capture plant.
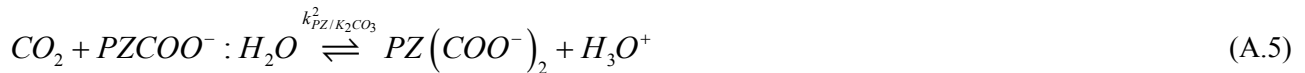
Post-combustion capture may be a promising solution for other industries, e.g. cement production, biogas cleaning, steal production, etc. which operate at different temperature-pressure and produce a flue gas with different composition. Post-combustion capture is potentially also applicable for off-shore CO_2 capture. The possible future applications of post-combustion need to be evaluated and optimized. Other development opportunities are complex process configurations, i.e. advanced heat integration, use of heat pumps and absorption enhancement.

Appendix

Appendix A - GM model applied to PZ promoted K_2CO_3 (PZ/K_2CO_3)

Reaction kinetics

The absorption/desorption of CO_2 with a PZ promoted K_2CO_3 involves several reactions. A simplified reaction kinetics was proposed by Cullinane and Rochelle (2006). This mechanism involves reactions (A.4) to (A.6). It is essentially the same mechanism as the zwitterion mechanism for the PZ-CO_2 system, i.e. it consists of two dominant reactions, the formation of the carbamate and bicarbamate ions, reactions (A.4) and (A.5). This is expected since neither the potassium ion (K^+) nor the carbonate ions are likely to react directly with CO_2. The reaction kinetics and the GM model for the PZ-CO_2 are presented in Chapter 2 - part B. Note that the reaction of CO_2 with the hydroxyl ion, reaction (A.6), is negligible for the PZ-CO_2 system since the reaction rate constant and the OH$^-$ concertation are small. However, the alkalinity of the PZ/K_2CO_3 system is much higher than the alkalinity of aqueous PZ, resulting in a correspondingly higher concentration of OH$^-$. As a result, reaction (A.6) could have a significant contribution to the absorption rate of CO_2, even though the rate constant, k_{OH} is much smaller than k^1_{PZ/K_2CO_3} respectively k^2_{PZ/K_2CO_3}

$$CO_2 + PZ:H_2O \overset{k^1_{PZ/K_2CO_3}}{\rightleftharpoons} PZCOO^- + H_3O^+ \tag{A.4}$$

$$CO_2 + PZCOO^-:H_2O \overset{k^2_{PZ/K_2CO_3}}{\rightleftharpoons} PZ(COO^-)_2 + H_3O^+ \tag{A.5}$$

$$CO_2 + OH^- \overset{k_{OH-}}{\rightleftharpoons} HCO_3^- \tag{A.6}$$

The reaction rate constants, k^1_{PZ} respectively k^2_{PZ} of the PZ-CO_2 system have to be corrected when using PZ promoted K_2CO_3 solvent. According to Cullinane and Rochelle (2006, 2004), the ionic strength potentially may alter the reaction rates through primary and secondary salt effects. This effect can be accounted for by introducing the ionic strength in the expression of the reaction rate constants:

$$k_{PZ,1/K_2CO_3} = k_{PZ,1}\exp(bI) \tag{A.7}$$

where b is an adjustable constant and I is the ionic strength. The ionic strength is defined as $I = 0.5\sum_i c_i z_i^2$

where c_i is concentration of ion i in kmol/m^3, and z_i is the charge of ions i. Cullinane and Rochelle (2006, 2004) found that the average value for b is 0.45 ± 0.10. In the present study b is set to . This value has been found to give a reasonable fit with experimental data an dit is in the range determined by Cullinane and Rochelle (2006, 2004). Similarly, the reaction rate constant k_{OH} is corrected for the ionic strength and it is Cullinane and Rochelle (2006, 2004):

$$k_{OH} = 10^{\left(13.635 - \frac{2895}{T(K)} + 0.08I\right)} \tag{A.8}$$

Mass transfer rate calculation

Reactions (A.4) to (A.6)are *(1+1)-th* order reactions where 1 mol of CO_2 reacts with *1* mole of base B ($B = PZ,PZ(COO-)_2$ and *OH-*). According to the GM model, the enhancement factor for this type of single reaction is the solution of the equations system (2.51) and (2.52).

$$E_{R_i} = Ha_{R_i} \sqrt{y^i_{B,R_i}} \frac{1 - y^*_{CO_2,R_i}}{1 - y^b_{CO_2}} \tag{A.9}$$

$$E_{R_i} = 1 + \left(E^*_{\infty,R_i} - 1 \right) \frac{1 - y^i_{B,R_i}}{1 - y^b_{CO_2}} \tag{A.10}$$

where E_{R_i} is the enhancement factor of the R_i-*th* individual reaction. Equations (2.51) and (2.52) form a system of nonlinear equations with two unknowns, E_{R_i} and y^i_{B,R_i}. Eliminating E_{R_i} leads to a single algebraic equation in y^i_{B,R_i} which can be solved numerically using methods such as the secant method, the Broyden method, the Newton method, etc.

The overall CO_2 mass transfer enhancement is the combination of all of the above reactions, as presented in chapter 2. The obtained overall enhancement factor, $E_{overall}$, is used to determine the CO_2 mass transfer flux across the gas-liquid interface according to:

$$J_{CO_2,gl} \simeq \frac{1}{1 / k^g_{CO_2} + H_{CO_2} / E_{overall} k^l_{CO_2}} \left(p_{CO_2} - p^*_{CO_2} \right) \tag{A.11}$$

$k^g_{CO_2}$ and $k^l_{CO_2}$ are the partial mass transfer coefficients for the gas side and for the liquid side and H_{CO_2} is the Henry law constant. The driving force for mass transfer is the difference between the partial pressure of CO_2 in the gas phase, p_{CO_2} and the equilibrium partial pressure of CO_2 exerted from the liquid phase, $p^*_{CO_2}$.

References

Cullinane, J.T., Rochelle, G.T., 2006. Kinetics of carbon dioxide absorption into aqueous potassium carbonate and piperazine. Ind. Eng. Chem. Res. Ind.Eng.Chem.Res, Ind Eng Res, Ind Eng Chem Res, Ind. Eng. Chem. Res. 45, 2531–2545. doi:10.1021/ie050230s

Cullinane, J.T.T., Rochelle, G.T., 2004. Carbon dioxide absorption with aqueous potassium carbonate promoted by piperazine. Chem. Eng. Sci. 59, 3619–3630. doi:http://dx.doi.org/10.1016/j.ces.2004.03.029

Appendix B - Benchmarking and comparing first and second generation post combustion CO₂ capture technologies

Philip Loldrup Fosbøl[1]1, Jozsef Gaspar[1], Sören Ehlers[2], Alfons Kather[2],
Patrick Briot[3], Michiel Nienoord[4], Purvil Khakharia[4],
Yann Le Moullec[5], Olaf T. Berglihn[6], Hanne Kvamsdal[6]

[1]*Center for Energy Resources Engineering, DTU Department of Chemical Engineering, The Technical University of Denmark (DTU), Søltofts Plads, 2800 Kongens Lyngby, Denmark*

[2]*Hamburg University of Technology, Institute of Energy Systems, Denickestr. 15, D-21073 Hamburg, Germany*

[3]*IFP Energies nouvelles, BP3 69360 Solaize, France*

[4]*TNO – Gas Treatment department, Leeghwaterstraat 46, 2628 CA Delft, the Netherlands*

[5]*EDF R&D, Fluid Dynamics Power Generation and Environment Department, 6 quai Watier, F-78401 Chatou, France*

[6]*SINTEF Materials and Chemistry, Department of CO2 Capture Process Technology, Post box 4760 Sluppen, N-7465 Trondheim, Norway*

Abstract

The Octavius FP7 project focuses on demonstration of CO₂ capture for zero emission power generation. As part of this work many partners are involved using different rate based simulation tools to develop tomorrow's new power plants. A benchmarking is performed, in order to synchronize accuracy and quality control the used modeling tools.

The aim is to have 6 independent partners produce results on simulation tasks which are well defined in this work. The results show the performance of a typical simulation tool ranging from in-house process simulator to Aspen Plus® and combination of the two, using CAPE-Open. Definitions of the models are outlined describing the used assumptions on mass transfer correlations, hydraulics, thermodynamic models, kinetics, and property packages.

A sensitivity study is carried out for absorption and desorption which shows the performance of capture percentage, specific reboiler duties, loading of rich and lean solutions, pressure drop, flooding, concentration and temperature profiles, product purity, and condenser performance.

The overall conclusion is that most predicted properties vary in the order of 5-10% percent, often more than accuracy in experimental pilot plant measurements. There is a general good resemblance between modeling results.

A few important properties like specific reboiler duty and reboiler temperature plus concentration and temperature profiles vary more than expected. Also high flooding scenarios in the stripper are difficult cases.

Efficiencies are discussed as part of the summary. Recommendations for modeling principles and best practice are given.

* Corresponding author. Tel.: +45-45252800; fax: +45-45882258
  E-mail address: plf@kt.dtu.dk

Introduction

This work is performed in relation to the OCTAVIUS FP7 project. The overall aim is to demonstrate integrated concepts for zero emission power plants covering all the components needed for power generation as well as CO_2 capture and compression. Pilot scale experiments of first and second generation post combustion processes are demonstrated by TNO, EnBW, and ENEL.

A task of the Octavius project is to perform a benchmarking of two power plants to estimate the energy foot print. The work entails several subcategories of tasks covering everything from process development, simulation extensions, optimizations, validation, evaluation, and control. An iterative procedure is applied between simulation and pilot scale testing. Knowledge is to flow from simulation and optimization into the pilot scale experiment and vice versa in order to benefit from several different types of information. The combined results will contribute to improving the capture units and the power integration.

It is not a trivial task to perform and therefore several partners are involved in validation and development of the process models. These partners have different preferences when it comes to modeling tool usage. Internal model synchronization is important in order to guarantee the correctness of the comparison in a later stage of the project. The work needs to be harmonized to secure the similarity of the produced results. The simulation benchmarking will show to which degree of accuracy the various properties can be modeled. It is expected that some variables will be very accurate, but others will tend to be less reliable. This is very important to the further work in OCTAVIUS but also to the general interpretation of the simulation results. It is vital that the partners are aware of which properties poses higher uncertainty. This is especially important when comparing results or carrying knowledge from one task to the other. It would not be beneficial to blindly trust already known inaccurate calculations. But at the same expectedly accurate results should also be appreciated and trusted which would greatly improve the application of the findings.

The core aim of this work is to prove the similarity of modeling principles spanning several different simulation tools. It is a quality control of the models to secure that the produced results are equivalent and do not deviate from expected behavior and from each other. A further aim is to outline which type of model results would often be accurate and which would tend to be less accurate.

The model comparison will be performed by SINTEF (Norway), TUHH (Germany), DTU (Denmark), IFPEN (France), EDF (France), TNO (Netherlands). It comprises anything from in house simulators to commercial tools.

The benchmarking

Benchmarking Basis

The basis of the benchmarking in this work builds on the knowledge of the European Benchmarking Task Force – EBTF [1] from the CESAR, CAESAR, and DECARBit projects. These groups developed a detailed description of capture and power plant cases which enabled them to construct similar and comparable results in terms of energy penalty and cost for specific power plant types using different CCS technologies. The focus on degradation, emission, operability and flexibility in OCTAVIUS requires additional criteria are used for the comparison. A new and proper reference capture process is established using criteria which are both of qualitative and of quantitative nature.

Two definitions are given in the OCTAVIUS benchmarking: The power plant base cases and the capture reference case. In this work the capture cases will be the main focus. Further simulation of the integrated first and second generation power base cases are bound for calculation through the next period in the OCTAVIUS project, a brief outline is given below, even though.

The benchmarking description is a very detailed documentation of the required information to perform the power simulations. It contains tables and notes on air composition and conditions plus fuel compositions. The outline is as follows.

The power plant base cases

Two new build base cases will be considered for the benchmarking in OCTAVIUS, an 800 MWe Bituminous Pulverised Coal and a 430 MWe Natural Gas Combined Cycle (NGCC) case.

The pulverized coal case has a net cycle efficiency of 45.5% while the specific CO_2 emission is 763 g/kWh$_{net}$ without post-combustion CO_2 capture. The steam turbines have extraction points, which deliver steam for nine feed water heaters. The live steam parameters are 300 bar at 600 °C, the parameters of the reheated steam are 60 bar at 620°C. For

the control of combustion product emissions, the power plant is equipped with SCR DeNOx plant, electrostatic precipitators and a wet limestone based desulphurization plant.

The NGCC case is based on a gas turbine where the exhaust gas is led to a heat recovery steam generator (HRSG), feeding its steam to a steam turbine. The net cycle efficiency is 58.1% while the specific CO_2 emission is 354 g/kWh$_{net}$ without post-combustion CO_2 capture.

The produced flue gases from the two power plants are very different and two non-similar capture setups need to be construction in connection to these two units.

Simulation synchronization methodology

The Benchmarking requires the simulation tools are reasonably well synchronized. To perform this, one of the Octavius partners described a flowsheet with relatively specific conditions for a basic CO_2 capture facility. It was a standard solvent based setup comprising a well-defined absorber and desorber using a typical heat exchange of the rich and lean solutions. 30 wt% MEA should be used as solvent, applying lean vapor recompression (LVC) and no absorber intercooling. This decision was taken based on the results of the CESAR FP7 project which showed that intercooling had no effect on the energy penalty of the MEA process. The project also showed that intercooling had positive effect on other solvents. The intent was to compare the calculated results.

Reasonably specific conditions were defined - everybody thought. Quickly problems arose when the partners set out to compare. Everybody had performed the simulation differently, and everybody tried to match the results of the one partner who originally produced a set of results. Some varied the height of the columns, other varied the reboiler temperature to match the heat duty. Even closing the loop of the solvent cycle posed room for interpretation. Some did not even try to match the reboiler duties but matched other properties. The group had basically produced 6 incomparable simulations using many different techniques and assumptions. It looked like almost any result could be produced, if the right variable where tuned accordingly. This is a noteworthy conclusion. Simulation results appearing in the open literature may very well describe and show results of specific reboiler duty, but even small differences in simulation design specification can give variations in the conclusions. Even missing information on packing type, column heights, temperature approaches etc. open room for unnecessary fatal interpretation.

The main conclusion was to create an extremely well-defined CO_2 capture simulation task, to establish the synchronization of the models. This meant that definitions needed to include information on flow input, what to compare for output, and which variables to fix. The capture plant was completely split up. The task was no longer to close the loop and prove a calculation of a flowsheet. The task was to perform an absorber calculation, and secondly to perform a desorber calculation. All room for interpretation and complexity was removed in order to secure that everybody were benchmarking the same information.
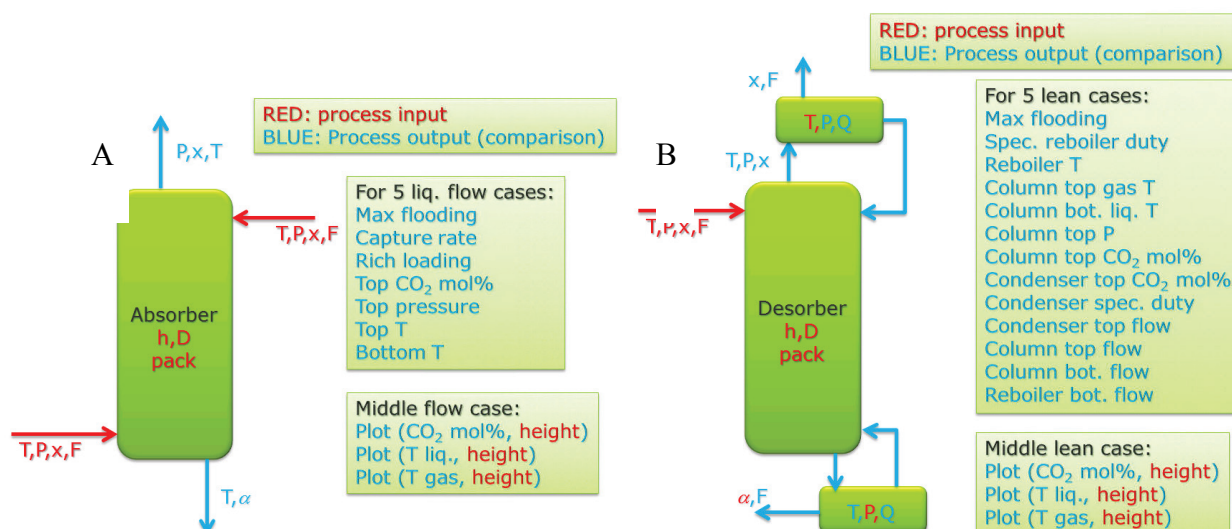

Fig. 1. (A) Absorber input and output specifications; (B) Desorber input and output specifications

The outline of the comparison is shown in Fig. 1. It contains the definition of input variables in red and calculated output results. As indicated in the figure, the absorber is supposed to be run at 5 lean flow rates, F, to study the effect of clean flue gas and the rich properties like loading ,(mol CO_2/mol MEA) α, temperature, T, and pressure P. Also maximum flooding % for a given height in the column was to be determined together with capture %. For the middle flow rate an additional analysis on column interior CO_2 mol% and temperatures were to be plotted. The column had a fixed height, h, diameter, D, and packing type. The inlet streams were given at fixed, T, P, F and compositions, x.

Similar conditions were defined for the desorber, except that flowsheet iteration had to applied for the calculations to succeed. The reason is that the partners decided, a bit unorthodox, to specify lean loading and calculate temperature and energy input to the reboiler, Q, instead of specifying them Similar to the absorber calculations, the middle lean specifications, was expected to present results on CO_2 mol% and temperatures as function of height. Note that LVC is not applied in this calculation scheme, in order to reduce the complexity, preventing partners to come up with new flowsheet assumptions. For the same reason wash sections for absorption and desorption were not included.

The second comparison was performed different to the first session. The intent was to perform a kind of round robin test where partners would go and perform calculations; DTU would collect and present the obtained results. In practice the testing was not completely blinded and some partners distributed the information internally before the final comparison.

The intent of this comparison was not to optimize or develop the CO_2 capture technology. The aim was to conclude if any of the partners modeling tools were giving unexpected results in core calculations of CO_2 capture.

The capture reference

The input variables defined above is summarized in the tables below. It contains detailed information in order to reproduce the results presented below. It has a general set of process criteria; an outline is given in table 1 for the absorber and desorber columns. It shows design specifications of the solvent type, packing, and dimensions.

Table 1. Absorber & desorber design specifications.

Parameter	Fixed values
Solvent	30 wt% MEA (CO_2 free)
Packing material (absorber & desorber)	Sulzer Mellapak 2X
Absorber height	20 m
Absorber diameter	13 m
Desorber height	13 m
Desorber diameter	8 m

Table 2. Absorber inlet flows specifications.

Parameter	Fixed values
Gas Inlet	
Temperature	43.5 °C
Pressure	104.5 kPa
CO_2 mole fraction	0.141
H_2O mole fraction	0.073
Inert mole fraction	0.786
Flow rate	46861.9 kmol/hr
Liquid inlet	
Temperature	40 °C
Pressure	102 kPa
CO_2 mol fraction	0.023
H_2O mol fraction	0.8675
MEA mol fraction	0.1095

Flow rate	180000 kmol/hr
CO₂ loading	0.21

Additional information is given in table 2 on inlet flows specifications for the absorber. It shows the variables on temperature, pressure, flow, and composition. The sensitivity carried out on lean flow rate is performed for 5 cases: 0%, ±10% and ±20% of the value given in table 2. The values were chosen according to the Octavius benchmarking definition.

Desorber design specifications are found in table 3. It contains definitions outlined in Fig. 1. The inlet pressure is defined as high pressure to prevent flashing in the pipes which would naturally occur at these conditions. No separate flash tank is used in this simulation and all flashing is expected to occur in the column. Pressure is defined in the reboiler at 190 kPa absolute. The pressure drop is considered upwards in the column. These properties together with the temperature in the condenser originate from the Octavius benchmarking definition.

The sensitivity of the lean loading is performed for 5 cases: -20%, - 15%, 0 %, 15%, and 30%. Originally -30% was used in the sensitivity but early calculation showed that some partners reached flooding at these conditions, therefore it was changed.

Table 3. Desorber inlet flow and design specifications.

Parameter	Fixed values
Rich feed solution	
Temperature	98 °C
Pressure	300 kPa (above bubble point)
CO₂ mol fraction	0.0578
H₂O mol fraction	0.8246
MEA mol fraction	0.1176
Flow rate	177400 kmol/hr
Rich loading (mol/mol)	0.4915 mol CO₂/mol MEA
Utilities(Condenser/Reboiler)	
Condenser temperature	30 °C
Reboiler pressure	190 kPa
Lean loading	0.21 mol CO₂/mol MEA

Table 4. Description of used simulation tools and setup.

	SINTEF	DTU	EDF	TUHH	IFPEN	TNO
Used tool	CO2SIM – in-house SINTEF simulator	DTU - CAPCO2 in Aspen Plus	Aspen Plus Standard Package	Aspen Plus V7.3	In-house model with ASPEN Plus V 8.4	Aspen Plus V8.2
Used simulation context	In-house flow sheet simulator with thermodynamic, kinetic, and unit operation models	Columns are DTU Cape-open modules in Aspen Plus. Other units Aspen Plus.	All Aspen plus.	All Aspen Plus. Columns Rad-Frac.	All Aspen Plus. Columns RateSep with kinetic models for absorber and desorber	All Aspen Plus. Columns Rad-Frac.
Modeling approach	Rate based columns. Other units: Equilibrium.	Rate based, identical column models. Other units: Equilibrium.	Rate based columns. Desorber: only transfer limitation, due to very fast kinetics. Other units: Equilibrium.	Rate based columns. Other units: Equilibrium.	Rate based, identical column models.	Rate based, identical column models. Internal reboiler and cond.
Solution approach	Columns are solved as BVPs using an adaptive	Columns are solved as a BVP. Dynamic height	Fixed 40 steps discretization for absorber, 30 for	Fixed 30 step discretization; non linear 15 step film	Discretization of columns heights in 20 stages.	20 stages for both absorber and desorber, standard

	collocation method.	discretization with min 30 steps and max 300.	desorber. 10 steps for the liquid film of absorber, no desorber film discretization.	discretization; default convergence options	Maximum number of iterations 30.	initialization. Sequential modular approach.
Thermodynamic model	Astarita-model [3-5] Henry parameter [6]. Heat of absorption [7]. Ideality of gas phase is assumed	Extended UNIQUAC for liquid phase and thermal properties. Ideality of gas phase is assumed.	ELEC-NRTL for liquid phase and thermal properties. Ideality of gas phase is assumed	ELEC-NRTL for liquid phase and thermal properties. Ideality of gas phase is assumed.	ELEC-NRTL for liquid phase and thermal properties. Ideality of gas phase is assumed.	ENRTL-RK and PC-SAFT. Henry's law for solubility of supercritical gases.

There are a number of additional detailed specifications for wash sections, coolers, pumps, and compressors and economy in the Octavius benchmarking document which is not relevant for this study.

Used simulation tools

The six partners involved in the comparison study used anything from pure in-house software to fully commercial solutions, but also principles in-between. SINTEF applied a fully in-house software package which constitutes a flowsheet simulator. DTU used a mixture of in-house and Aspen Plus. This means the core rate based columns where developed by DTU which applies to the CAPE-Open standard and the modules can be used in other process simulators implementing CAPE-Open. The remaining partners used Aspen Plus. IFPEN applied an external property package to Aspen Plus. Based on the description in table 4 it can be seen how EDF used a more fine-tuned version, and TNO took advantage of the work by Zhang et al. [2].

Table 5. Description of used simulation properties and correlations

	SINTEF	DTU	EDF	TUHH	IFPEN	TNO
Chemical properties	Correlations [5]	Correlations [8]	Aspen Plus DB	Aspen default settings	ASPEN PLUS Library (v 8.4)	Documented in [2]
Mass transfer model	Rocha et al. [9] mass transfer correlations	Rocha et al. [9] mass transfer correlations	Bravo et al. [12]	Bravo et al. [11]	Bravo et al. [12]	Bravo et al. [12]
Hydraulic model	Rocha et al. [10]. Holdup corrections for Sultzer packing	Rocha et al. [10]	Bravo et al [12]	Bravo et al. [11]	Bravo et al. [11]	Bravo et al. [11]
Heat transfer model	Chilton-Colburn analogy [13]	Chilton Colburn analogy	Chilton Colburn analogy	Chilton Colburn analogy	Chilton Colburn analogy	Chilton Colburn analogy
Reaction kinetics	Second order, Versteeg et al. [14].	Second order, Versteeg et al. [14] – zwitterion reaction mechanism	Second order. [19] derived from pseudo-first order assumption	Second order Plaza et al.[15] using Aboudheir [16] and Rochelle et al. [17]	[18]	Documented in [2]
Reaction rate constant	[14]	[14]	Hikita et al. [19]	Plaza et al.[15]	[14], modified by [18]	Documented in [2]
Kinetic model/approach	Enhancement factor based. penetration model in the absorber, instantaneous reversible model in the desorber.	General method enhancement factor based on the two-film theory	Resolution of diffusion reaction equation through the liquid film	Two film model with reactions taking place only in the liquid phase	Liquid Film discretization (6 points). No vapor phase discretization	Diffusion resistance and reaction in discretised (5) liquid film, diffusion resistance in vapor film
Other assumptions	MEA is considered non-volatile. Liquid	MEA is considered non-volatile. Liquid	MEA is volatile. All species can transfer MEA,	Diffusion resistance in liquid and		Stages: liquid phase well mixed, vapour is

side mass-transfer resistance of the volatile solvent is neglected. Adiabatic column. No pressure drop.	side mass-transfer resistance of the volatile solvent is neglected. Adiabatic column.	H_2O, CO_2 and N_2. Adiabatic column.	vapour film, reactions in liquid phase only		plug flow. Adiabatic column. MEA volatility not ignored.

In general all models used where rate based. SINTEF and EDF treated the absorber and desorber modelling principles differently. All applied an advanced activity coefficient model for the thermodynamic calculations. Some took more care to model the vapour phase. Note that the simulation are carried out at low pressure < 5bar. The simulation used equilibrium approaches for condenser and reboiler. TNO seem to have applied the principles slightly different compared to the other partners and decided to run columns with integrated units, even though this should not make a difference. There is a great variance on the detail for the solution and discretization of the model as outlined in the table.

Table 5 presents details of the simulation principles. The mass transfer correlations applied are reasonably the same, but the kinetic properties vary to a great extent. The theory applied for the enhancement factor is of cause very locked in Aspen Plus, where clearly there is more room for variety when the in-house software is applied.

Synchronization comparison and discussion

In practice the comparison study was performed as a two-step process. First the absorber calculations were performed and evaluated and secondly the desorber calculations were performed. Based on the discussions and the comparison of the results it was concluded that IFPEN deviated a bit due to misplaced definitions of the condenser specifications and similar issues. IFPEN therefore produced new improved results. Furthermore SINTEF wanted to improve the equilibrium modeling based on the comparison and they set out to improve the thermodynamic description and they were therefore allowed to produce new results as part of the test.

The results were constructed early 2014.

The discussion of calculations outcome is presented for the absorption and desorption process simulation below. It will be clear that some of the assumption outlined in table 4 and 5 are visible in the result and discussions below.

Absorption synchronization comparison

In absorption, one of the important variables for this study is the calculated capture percentage. It is a key property which is often compared to pilot scale tests. Model performance is often determined on its capability to reproduce this exact property. Fig. 2A indicates that a model output is ±10% accurate, even with almost identical modeling basis in Aspen Plus. Remember, pilot campaigns often strive to measure this property very accurately by making sure to close the mass balances.
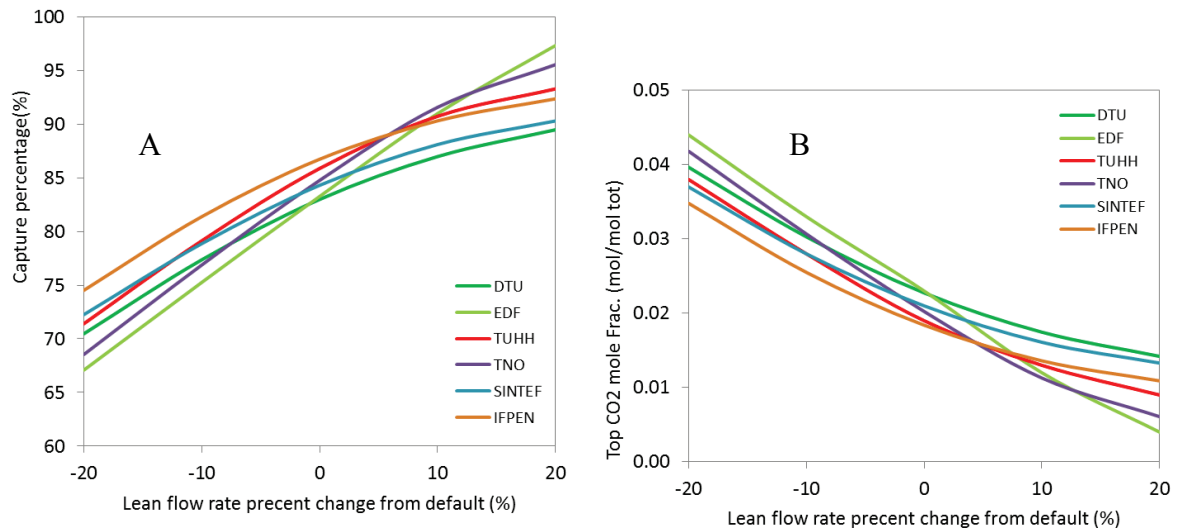
Fig. 2. (A) Absorber capture percentage; (B) absorber top gas phase mole fraction of CO_2 before washing.

The conclusion is that a model result of this kind is expected to be intermediate accurate. The results are as expected within the range of 70 to 95% capture corresponding to typical requirements for a CO_2 capture facility. The figure indicates that the results of EDF end IFPEN are outliers but nothing out of the ordinary. Fig. 2B supports the same conclusions and is basically a reflection of the same property because of mass balance conservation. It shows the top gas composition. The same variation is observed, ±10%.
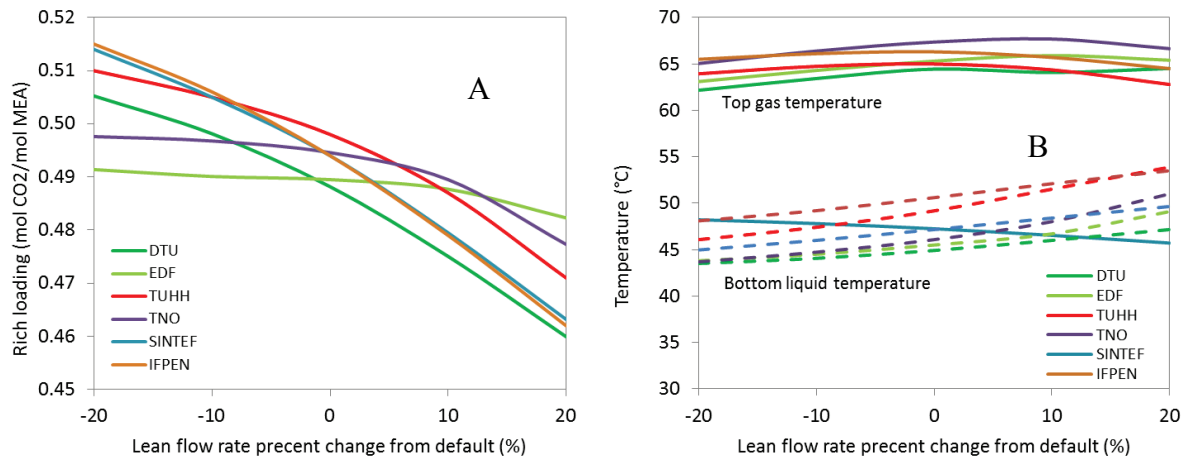
Fig. 3. (A) Absorber bottom rich loading; (B) Absorber top and bottom outlet temperatures.

The variation in capture percentage is not reflected in the bottom rich loading though, shown in figure 3A. It can be concluded that the obtained results of the partners are very similar and are reproduceable, within 4-5% accuracy. The typical equilibrium condition for these temperatures is approximately 0.52 in loading. This means the rich loading is not far from equilibrium. The main variation is most likely caused by the variability in the bottom temperaures shown in figure 3B. It shows a low predicted bottom liquid temperature of EDF and DTU. Figure 3A shows a low range rich loading. One would actually expect the opposite, that the low temperature would cause a high loading. The explanation is probably the thermodynamic model behind the calculations. It may have a tendency to give reasonbly high CO_2 partial pressures at low temperature for these two partners.
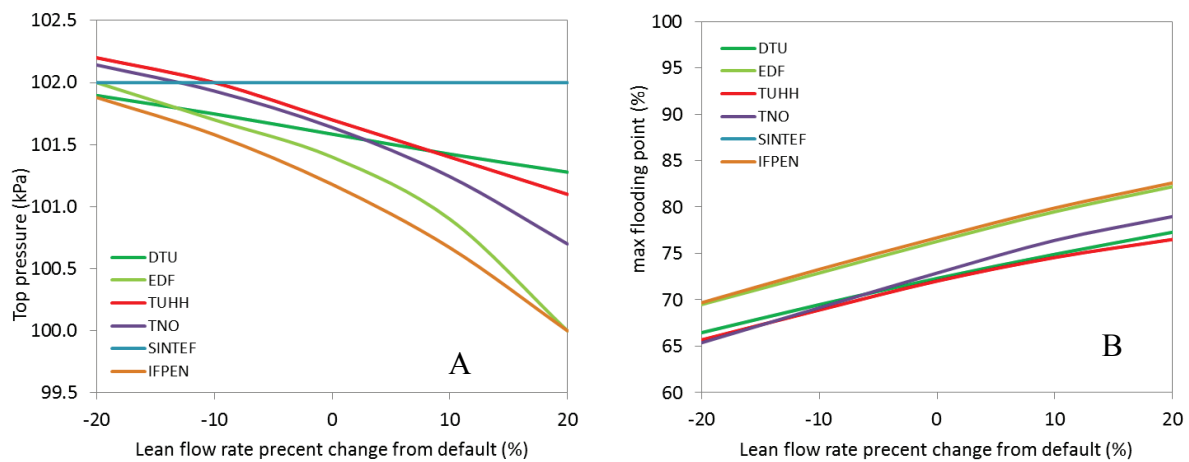
Fig. 4. (A) Absorber pressure at the top outlet; (B) Desorber input and output specifications

A conclusion on temperature accuracy can be drawn from figure 3B. In general the models seem to predict oulet temperatures within ±5 °C. This is also important to be aware off when comparing estimated temperaures. Later it can be seen that lower accuracy should be expected for temperaure profiles as function of column height.

The pressure drop is illustrated in figure 4A. SINTEF do no consider pressure drop as indicated. The inlet flue gas pressure is 104.5 kPa and the inlet liquid pressure is 102.0 kPa. A top outlet pressure of approximately 101.5 kPa is therefore a drop of 3 kPa over the 20 m. Only a small variation should be observed in pressure calculations of ±1%. It is closely linked to the amount of flooding presented in figure 4B. Here shown for the maximum flooding oberserved for any height in the column. Note flooding is not considered by SINTEF.

There seem to be two catagories of floodnig calculations. EDF and IFPEN in one group and the remaining in the other group. Table 5 summarises the hydrodynamic model used. It can not explain why here is a difference. TNO and TUHH uses the same model as IFPEN for this property, but the results are different.

Finally the gas concentration and liquid temperature profiles are shown in figure 5A and B. Liquid temperatuers are not shown but they are very similar to figure 5B. There is a direct link between 5A and B. As the gas flows upwards in the column, CO_2 is absorbed. The EDF calculations show at 12 m there is decrease in the CO_2 concentration which results in an increase of temperature. This is a well know phenomenon: The heat of absorption gives rise to temperature. It is a question of how quick the CO_2 is absorber. A high rate results in noticeable temperature increase. The CO_2 profiles by EDF and TNO indicates a high absorption efficiency in the top 8 m. The lower part of the column indicate that the bottom section is not efficient. The trend from these two calculations are similar. This is explainable from table 5, as the two partners use the same mass transfer correlation. DTU and SINTEF also use the same mass transfer correlation, even though, the temperature profile by SINTEF has a slightly different tendency in the range 0 to 2m. This could be water condensation from the gas phase which in the calculations could be slightly super-saturated.
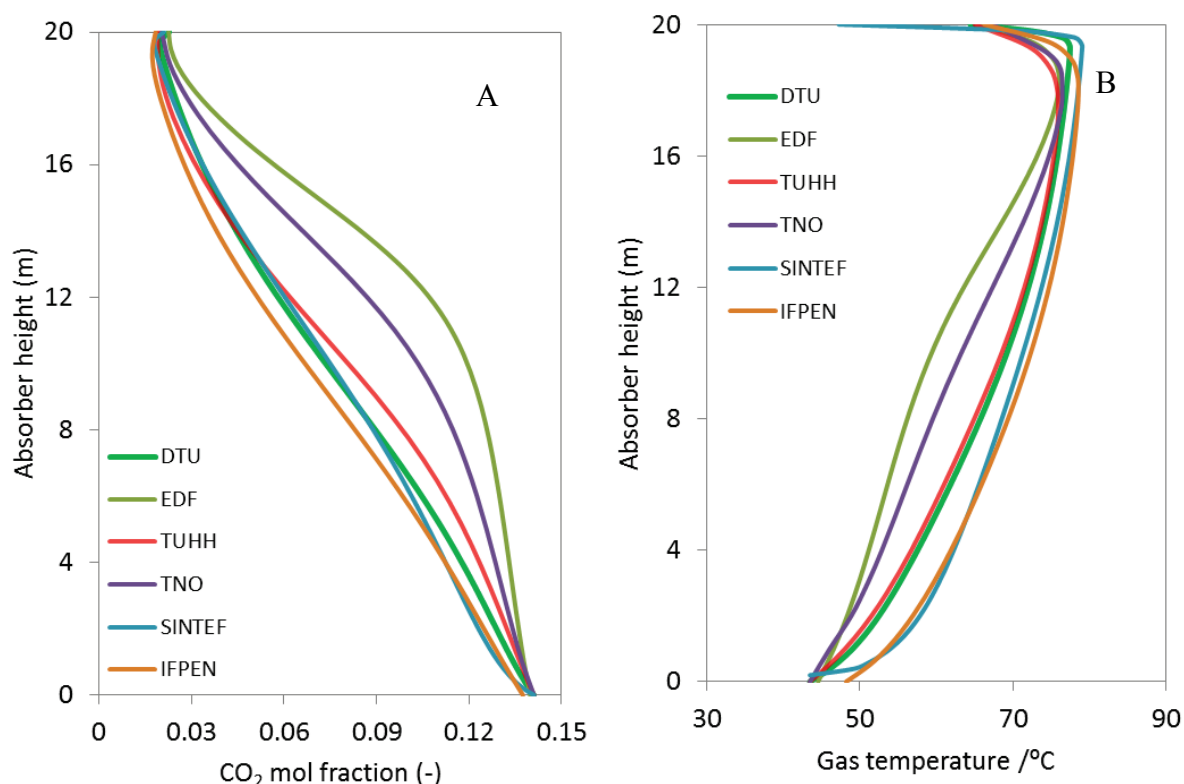
Fig. 5. (A) Absorber input and output specifications; (B) Desorber input and output specifications

It can be concluded that the majority of simulations for this specific problem gives linear concentration profiles as shown in figure 5A. There is obviously a great difference in the predicted concentrations, ±6%, in the mid column section, but the overall capture is the same, which is also substantiated by the results of figure 3A. There are no great outliers in the calculations.

The conclusions on the temperature profile are similar to the concentration profiles. The variation is greater in the mid section The properties are directly linked through the heat of absorption and the behaviour is therefore expected. Similar to the conclusions on the capture % above, it is noteworthy that many model validations in the literature are performed using pilot plant data showing plots similar to 5B. The observed termperature variance is in the order of ±10 °C. The experimental accuracy is expectedly in the order of 1-5 °C. This means that comparison of mid column temperature profiles may not be trustworthy to some extend and deviations should be expected.

The general conclusion is that reaonably similar and accepted results are obtained from the 6 partners. Variation are observed for column mid sections temperature, CO_2 concentrationsm, and capture % determinations. This is noteworthy during a comparison to experimental data. Further it can be concluded that even though 4 partners use Aspen Plus, off the shelf, the results are similar, but not in anyway identical.

Desorption synchronization comparison

The property most important to CO_2 capture is the specific reboiler duty (SRD), a variable determining the cost of operation. Figure 6A gives an outline of the obtained values. There is a high degree of variability, 10-15%. Some partners indicate a minimum in the energy consumption at 0% sensitivity. The calculations by TUHH and SINTEF seem to disprove this existence. The behavior of the SRD is reasonably homogenous, ±5%, for the 0 to 30% sensitivity. There is an indication that the TNO results give an energy consumption which could be 5% too high.

Pilot plant test often struggle to indicate reliable and accurate SRD values, where the truth is more likely that the modeling results are accurate to ±5-10%. The values are as expected in the order of 4 GJ/ton CO_2 which is comparable to the 3.9 GJ/ton CO_2 obtained in the CASTOR project.

In general the comparison is acceptable. The reason is found in figure 6B. The flooding results show that the sensitivity case -20 to 0 % gives flooding of the column close to 100%. Basically the majority of cases >70% flooding are not interesting from an industrial point of view. It would not be beneficial to operate the column at these conditions. The scatter observed in figure 6A is therefore not industrially interesting. SINTEF has not calculated flooding.
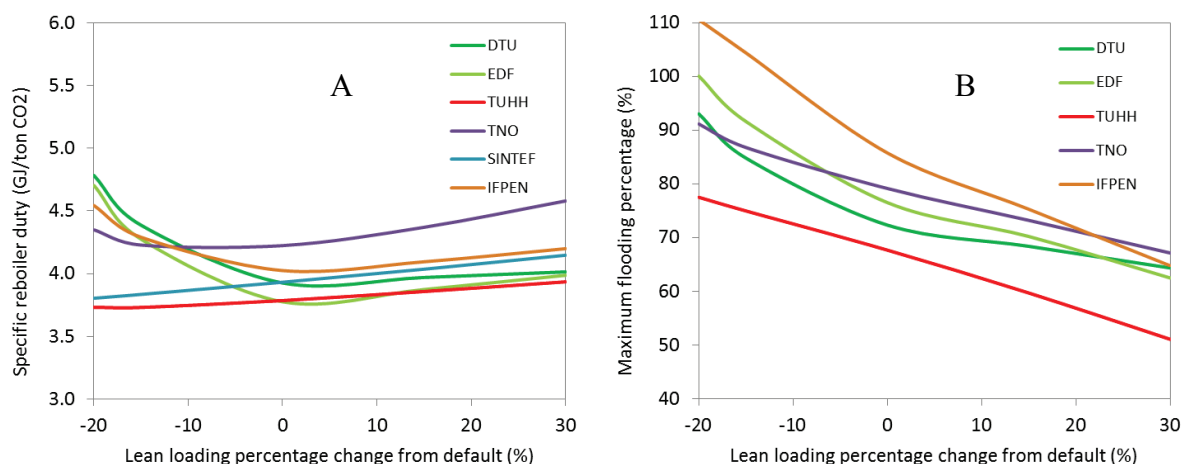

Fig. 6. (A) Reboiler specific heat duty; (B) Desorber flooding. Maximum indicates the maximum value, obtained at any height of the column.

It can be concluded that there is an unreasonably high variability in the SRD for cases close to flooding. A relative consistent reproduction is observed for lower flooding. A scatter in the order of 5% should be expected and results within this window should be seen as accurate. A comparison of model and pilot plant date would expectedly be accurate to 5%, based on these results.

The flooding calculations by IFPEN, performed with Aspen plus and KG Tower softwares, show that the column is flooded for the lean loading sensitivity cases <0%. Therefore they are unable to determine pressure loss of the column as indicated in figure 7A. SINTEF is not considering pressure loss and their stripper top pressure is the same as the reboiler pressure. A low pressure loss is calculated by most partners. Only IFPEN seem to calculate a reasonbly high pressure loss, but their calculations also indicate a realtive high degree of flooding, figure 6B.

Between partners the calculated pressures are very compareably. It has a low variability, and presuably a lower impact on the final SRD predictions.
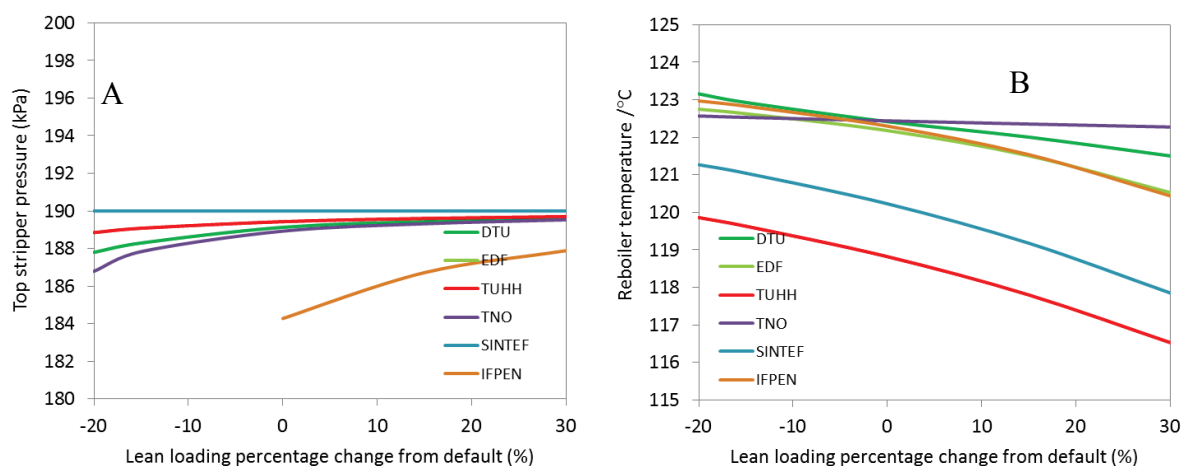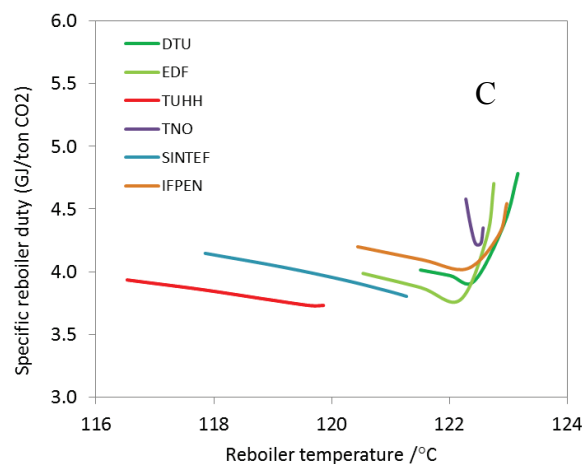
Fig. 7. (A) Pressure in stripper top (reboiler pressure is 190 kPa); (B) Reboiler temperature; (C) a combination of Fig. 6A and 7B

The reboiler temperature shown in figure 7B is a direct consequence of the pressure specification in the reboiler, 190 kPa. There is a slight correlation with the SRD shown in figure 6A: A lower temperature gives a lower SRD. The majority of partners obtain the same temperature. SINTEF and TUHH calculate a noticeable lower temperature. Naturally the same picture is seen for the stream coming into the reboiler, is has a lower temperature as shown in figure 8A, but is gives no explanation for the temperature differences. A reason could be the thermodynamic model used. Table 4 gives no indication of this difference. TUHH applies the same model as three other partners. Even DTU applies a completely different model but calculates the same as the electrolyte NRTL users.
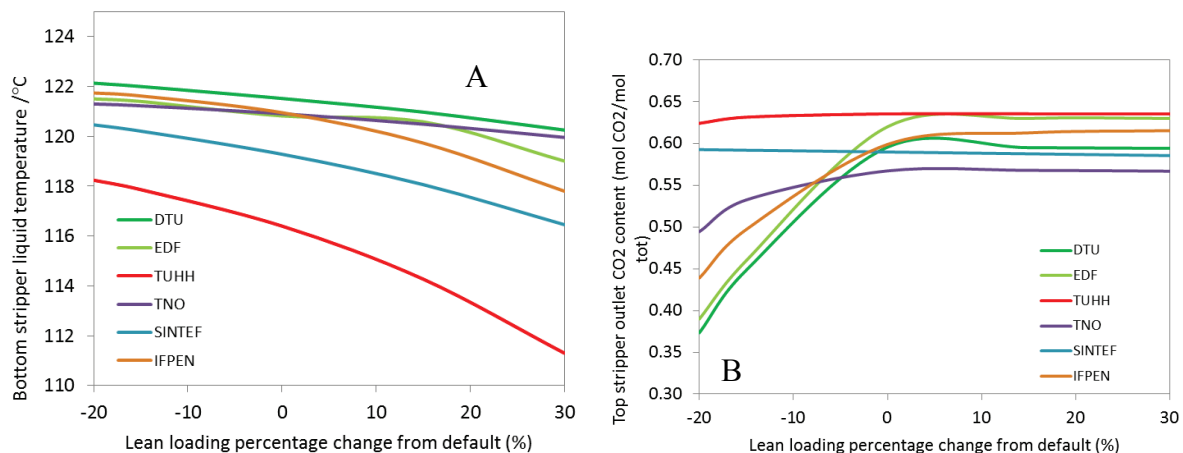
Fig. 8. (A) Outlet liquid temperature of the desorber bottom; (B) mole fraction of CO_2 in the stripped top gas.

It should be said that the reboiler temperature is sensitive to the composition of the fluids in the reboiler. Based on the methodology described above, the lean loading should be identically the same for all the calculations. The water/MEA concentration differences must be the only explanation. There is indication in the results which supports this: Figure 8B shows the top exiting gas. It mainly contains CO_2 and water. TUHH calculate values in the higher end, indicating a low water content. From mass balance conservation we know that the reboiler has more water. This would lower the boiling temperature and this would be the explanation for the observations. It is also supported by the SRD results which shows a lower energy consumption by TUHH. Most likely because they have less water evaporation.

The sensitivity of SRD to the reboiler temperature is obtained by combining figure 6A and 7B. Figure 7C shows the spread of the SRDs. There are no particular outliers, even though the results of TNO has a different shape compared to the other partners.

238

It can be concluded that accuracy of the calculated reboiler temperature is most likely ±1-5 °C. Very accurate benchmarking for this property can not be expected. This is important for comparisons to experimental data. Blindly picking up measured reboiler temperatures and using it for design specifications is not adviceable. On the other hand it is not important that the desorber bottom temperature is well-known it has the same accuracy, ±1-5 °C, which for this stream is acceptable.
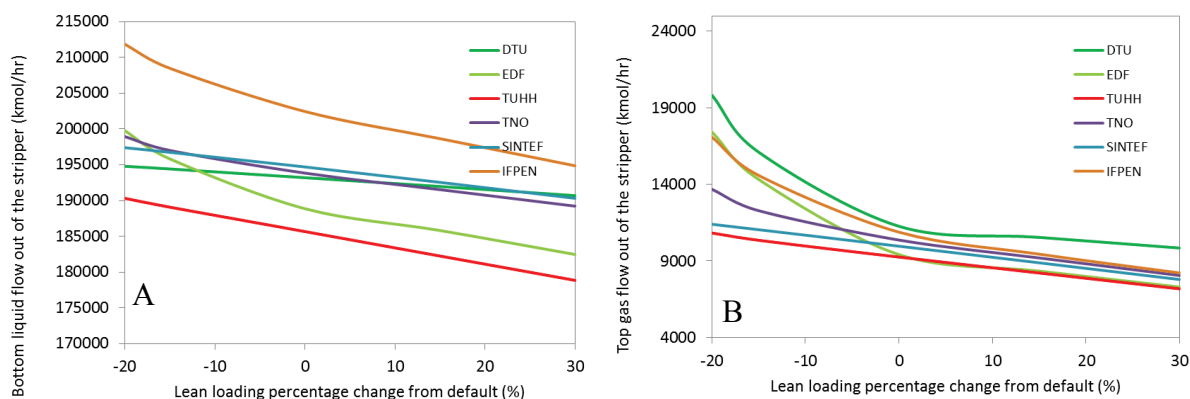

Fig. 9. (A) Desorber bottom liquid flow; (B) Desorber top gas flow.

Accuracy of mass balance is illustrated in figure 9. Bottom flow have a high expected accuracy, variability in the order of 10%. The trends of all the simulations are identical. The top gas flow is not as accurately determined. For the mentioned high flooding cases variability is significant. DTU seem to give values which are higher than other simulations. The observation is also visible in the clean CO_2 flow, figure 10A. Expected variability in the produced CO_2 flow is 10%. Many simulations give noticeable identical results as seen in figure 10A.
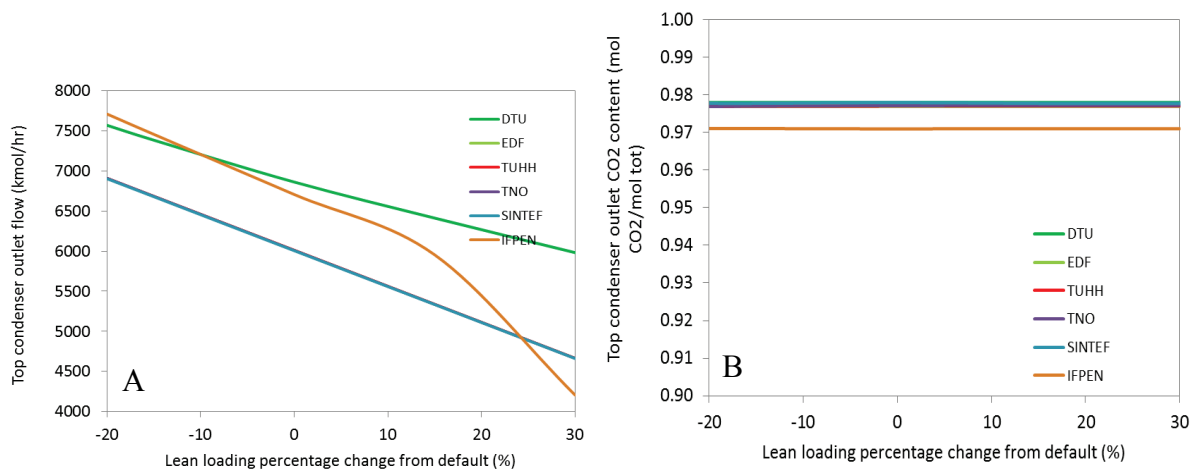
Fig. 10. (A) Clean CO_2 flow; (B) CO_2 flow purity

The purity of the produced CO_2 is shown in figure 10B. This property only depends on temperature for ideal gas systems. A very accurate value is expected since the condenser has a specified temperature of 30 °C. IFPEN shows a slightly different value compared to the other calculations due to an applied conservative pressure loss of 30 to 40 kPa.
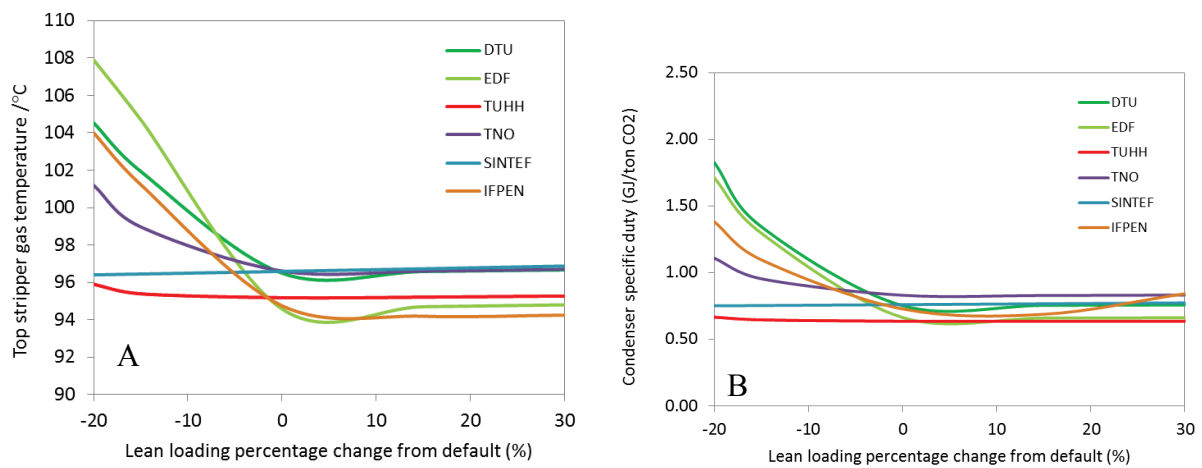
Fig. 11. (A) Desorber top outlet gas temperature; (B) Condenser specific heat duty.

The desorber top temperature and the condenser specific duty is shown in figure 11. The variation is identical to the observations in figure 6, 8B, and 9B - due to flooding. Accurate values are expected for desorber top temperature, ±2 °C, and condenser specific heat duty within 15%.
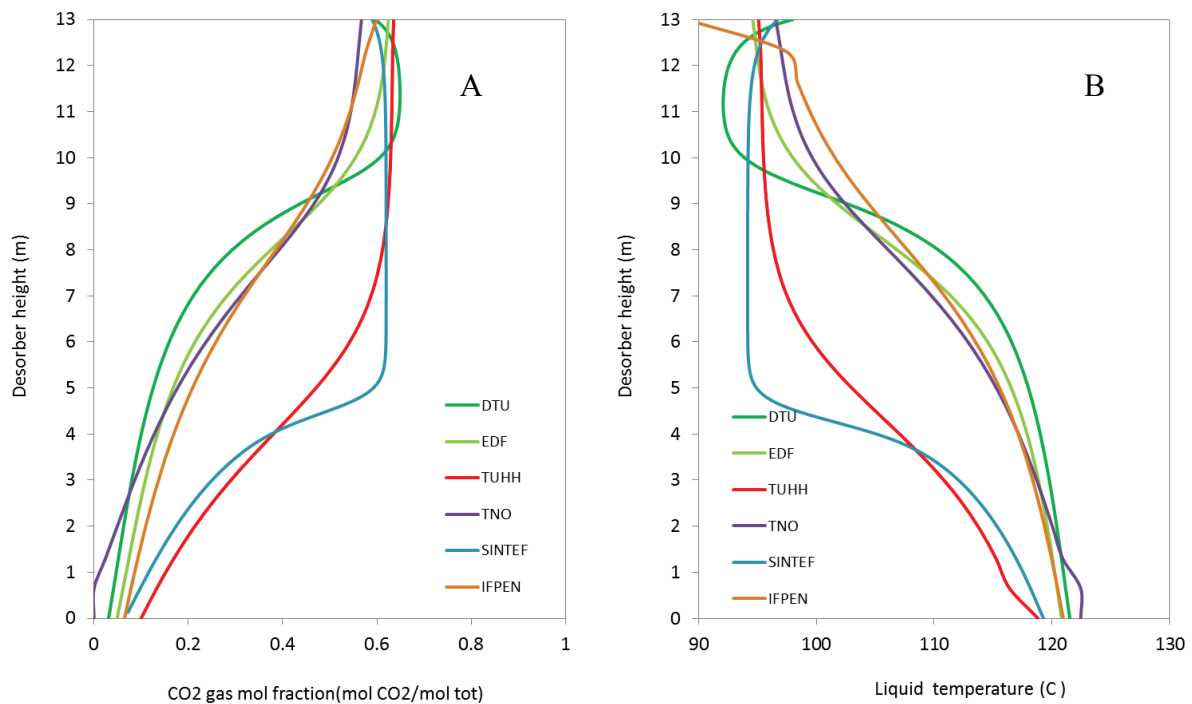

Fig. 12. Desorber CO_2 concentration profile (A) and liquid temperature profile for the case mentioned in table 3.

The desorber efficiency is illustrated in figure 12A, or more specifically the CO_2 gas concentration as function of height. The predictions by TUHH and SINTEF, show that the desorption is complete in the height of 5-7 m. Other partners show that the column is desorbing CO_2 more along the complete height. DTU specifically indicate absorption of CO_2 in the top part of the column. The explanation is found in figure 12B which show a temperature decrease in this section. The observed phenomenon is most likely due to flashing and therby evaporation and cooling – resulting in absorption. The same is observed by SINTEF though not to the same extent.

240

A great variability is predited for the conditions in the desorber. Carefulness should be taken while comparing profiles of model and pilot data. The accuracy very much depends on the accuracy of the mass transfer correlation. Figure 12 illustrates how desorption predictions by some partners can exstimate feasible height of the column in the order of anything from 5-13 m, conclusions which in practise would have a significant impact on the dicisions of economic investments.

The general conclusions on the desorber profiles is a reasonable accuracy of the top properties, but an unreasonable high scatter in the mid seciton. A number of the partners give consistent and similar results but few do have significantly different results. The reason is probably the applied mass transfer correlation. Within the partners that give reasonably the same results, there is an expected accuracy of 0.1 mol CO_2/mol total and 2 °C. It is noteworthy that Aspen Plus calculations obviously give very different results even though partners apply the same mass transfer model. The profiles obtained from experimental work should be carefuilly compared to the simulation data. There could be deep pitfalls in the prediction of these properties in some of the models used. The benefit is though, that properties in the top of the column are well estimated. Information which is most vital to the conclusions.

Main conclusions and summary

The aim of this study is two-fold: to outline the expected accuracy and variability of typical simulation tools for CO_2 capture and secondly to secure that partners in the Octavius project are synchronized with respect to modeling principles and calculations.

The work was initialized by letting people compare their calculations to a known case. The experience has shown that people will try by all efforts to match it. This is not beneficial to the comparison, since assumption and interpretations play a bigger role. Basically any result can be matched with the right kind of tuning. The only way to perform a benchmarking is to make sure all inputs are well defined and there is little room for interpretation.

In this work 6 simulation tools are summarized and modeling basis with assumptions described. Results are compared for absorption and desorption type conditions. A sensitivity study is carried out for each column, varying the lean flow rate in the absorber and the lean loading in the desorber.

Table 6. Expected predictability and variation of the calculated simulation properties

	Expected accuracy	Variability
Absorber results		
Capture %	Intermediate. Model scatter observed.	±10%
Top CO₂ molefraction	Intermediate. Model scatter observed.	±10%
Rich Loading	High. Deviation can be caused by inaccurate T meas.	±4%
Outlet temperature (top+bottom)	High, depends on accuracy of meas.	±5 °C
Pressure	High	±1kPa
Flooding	High reproducibility. Little scatter in model results.	±10%
CO₂ gas conc. profiles vs. height	Top + bottom conc. high accuracy. Mid column, less accurate	±6%
CO₂ temp. profiles vs. height	Top + bottom T high accuracy (1-5 °C). Mid column less accurate than meas.	±10 °C
Desorber results		
Specific reboiler duty	High, but low at >70-80% flooding.	5%
Flooding	Reasonable, but low at >70-80% flooding.	±10 %
Pressure	High	±1kPa
Reboiler temperature	Low	±1-5 °C
Bottom temperature	Reasonable	±1-5 °C
Column top CO2 mole fraction	Reasonable, but low at >70-80% flooding.	±10 %
Bottom liq. Flow	High	±10%
Column top gas flow	Low, lower at >70-80% flooding	20%
CO₂ outlet flow	High	10%
CO₂ purity	High	1%

Column top gas temperature	High	±2 °C
Condenser specific heat duty	High	±15%
CO_2 gas conc. profiles vs. height	Top conc. reasonable accuracy. Mid column, less accurate	NA
CO_2 temp. profiles vs. height	Top conc. reasonable accuracy. Mid column, less accurate	>2 °C

The findings of the sensitivity study are found in table 6. It outlines the expected accuracy of the predictions and the general variability among the 6 simulations.

There is a remarkable good agreement between the models. The majority of properties predictions vary between 5-10%, it indicates that approximately this order of accuracy should be expected for a comparison to experimental data. In a benchmarking study a 5-10% difference in calculation is therefore within the typical variability of the models. Note that experimental measurement may be more accurate than the 10% accuracy in the simulations.

A few properties can be picked out which should be treated with care if they are to be used for comparison. This is the CO_2 concentration and temperature profiles as function of height, plus the reboiler temperature. Especially the reboiler temperature is critical. It is a property often used for design specification. The profiles are less accurate in the mid sections of the column which is not critical to the simulation or comparison.

At high flooding, >70-80%, the following properties vary noticeably between simulation results: desorber SRD, flooding per cent, top CO_2 mole fraction, and the desorber top gas flow. The most important of these is the SRD which can not be reliably compared to experimental data at high flooding %.

The results have shown that the models predict the specific reboiler duty within 5-10% which is 0.2-0.4 GJ/ton CO_2 for the calculations performed. This is a significant contribution, and important to bear in mind, while doing a comparison to experimental data.

A good practice in process simulation and pilot experiments would be to meticulously define all inputs and process variables, even the packing type, insulation thickness, etc. Neglecting this would open up for future interpretation and tuning which is not beneficial to accurate model development. The minimum requirement for information is outlined in table 1 to 3.

The work presented creates a basis for future rate based model developers to characterize and compare their results to it may act as a baseline for modeling.

Acknowledgements

References

[1] N. Booth and al., European Best Practice Guidelines for Assessment of CO_2 Capture Technologies, CESAR Deliverable D2.4.3, March 2013

[2] Zhang Y, and Chen C-C., "Modelling CO2 absorption and desorption by aqueous monoethanolamine solution with Aspen rate-based model, Energy Procedia, 1584-1596, 2013.

[3] Astarita G, Savage DW, Bisnio A. Gas Treating with Chemical Solvents, Wiley, New York, 1983.

[4] Hoff, KA. Modeling and Experimental Study of Carbon Dioxide Absorption in a Membrane Contactor. Doctoral Thesis, The Norwegian University of Science and Technology (NTNU), Trondheim, Norway, 2003.

[5] Tobiesen, FA. Modelling and Experimental study of Carbon Dioxide Absorption and Desorption, Doctoral Thesis. The Norwegian University of Science and Technology (NTNU), Trondheim, Norway, 2006.

[6] Hartono A., Mba EO, Svendsen HF. Prediction of N2O solubility in alkanolamine solutions from the excess volume property. Energy procedia 37, 1744-1750, 2013.

[7] Kim I. Heat of reaction and VLE of post combustion CO2 absorbents. Doctoral Thesis, The Norwegian University of Science and Technology (NTNU), Trondheim, Norway, 2009.

[8] Gabrielsen J, CO2 Capture from Coal Fired Power Plants 2007; Ph.D. thesis.

[9] Rocha JA, Bravo JL, Fair JR. Distillation-Columns Containing Structured Packings - a Comprehensive Model for their Performance .1. Hydraulic Models. Ind Eng Chem Res 32, 641-51, 1993.

[10] Rocha JA, Bravo JL, Fair JR. Distillation columns containing structured packings: A comprehensive model for their performance .2. Mass-transfer model. Ind Eng Chem Res 35, 1660-7, 1996.

[11] Bravo JL, Rocha JA, Fair JR. A comprehensive Model for the performance of columns containig structured packings. Institution of Chemical Engineers Symposium Series 128, 489, 1992.

[12] Bravo JL, Rocha JA, Fair JR. Mass transfer in Gauze Packings. Hydrocaborn Process, 64 (1985), pp. 91–95

[13] Geankoplis CJ. Transport Processes, Separation Process Principles. 4th ed., Prentice-Hall, 2003.

[14] Versteeg GF, Van Dijck LAJ, Van Swaaij WPM. On the kinetics between CO2 and alkanolamines both in aqueous and non-aqueous solutions. An overview. Chem Eng Commun 144, 113-58, 1996.

[15] Plaza JM, Van Wagener D, Rochelle GT. Modeling CO2 Capture with Aqueous Monoethanolamine. International Journal of Greenhouse Gas Control 4 (2010), Nr.2, S. 161-166

[16] Aboudheir A. Kinetics. Modeling and Simulation of CO2 Absorption into Higly Concentrated and Loaded MEA Solutions. University of Regina, Canada, Dissertation, 2002.

[17] Rochelle GT, Bishnoi S, Chi S, Dang H, Santos J. Research Needs for CO2 Capture from Flue Gas by Aqueous Absorption/Stripping. Final Report for DOE of DE-AF26-99FT01029, 2001.

[18] Dugas R, Alix P, Lemaire E. Creation of an aspen ratesep absorber model for the evaluation of castor pilot plant data. 235th American Chemical Society (ACS) National Meeting, New Orleans, LA, April 6-10, 2008.

[19] Hikita H, Asai S, Ishikawa H, Honda M. The Kinetics of Reactions of Carbon Dioxide with Monoethanolamine, Diethanolamine, and Triethanolamine by a Rapid Mixing Method. Chem. Eng. J. 13, 7-12, 1977.

Appendix C - .NET based implementation of a CAPE-OPEN column model

This section presents the design and implementation of a CAPE-OPEN compliant unit (DTU-CAPCO2) for CO_2 absorption and desorption rate-based simulation. It discusses the functionalities of the CAPCO2 model and exemplifies an implementation of a CAPE-OPEN unit operation using the .NET platform in Microsoft Visual C#. In addition, the migration of the FORTRAN source code to .NET platform is discussed and exemplified.

Description of CAPCO2 rate-based column model

CAPCO2 is a general rate-based model for CO_2 absorption and desorption simulation. It is a versatile tool developed at the Technical University of Denmark. The great performance of the calculations is secured by incorporating a precise thermodynamic model and accurate estimation of mass transfer coefficients and hydraulic properties (Gabrielsen, 2007). CAPCO2 uses an in-house physical property package which was validated at both absorber and desorber conditions. It uses the extended UNIQUAC thermodynamic model to determine phase equilibria and thermodynamic properties (Faramarzi et al., 2010; Gaspar et al., 30, January, 2013). In addition, CAPCO2 uses the GM enhancement factor model which is valid at absorption and desorption conditions(Gaspar et al., 2014).
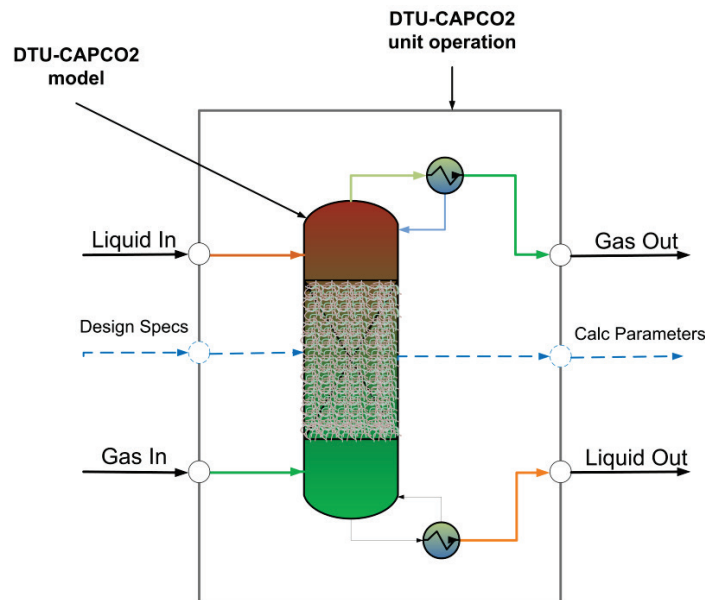
Figure C.1. Conceptual structure of the CAPCO2 rate-based column module.

Figure C.1 represents the conceptual structure of the CAPCO2 module. It illustrates how the module has two input ports and two output ports corresponding to a liquid and a gas feed plus a liquid and a gas outlet. Packing type, column characteristics, column configuration, etc. must be defined by the user as "design

specifications". The module returns calculated parameters such as capture rate, heat duty, etc. Note that the condenser and the reboiler are integrated into the rate-based model. It is therefore possible to configure the column as one of the five setups: absorber, absorber with integrated condenser, stripper with integrated reboiler, stripper with integrated condenser, plus stripper with integrated reboiler and condenser.

Implementation of CAPE-OPEN base classes: Procedure

This section provides an overview of the implementation procedure of a CAPE-OPEN unit in Microsoft Visual C#. The implementation relies on the CAPE-OPEN .NET class library. The CAPE-OPEN v.1.0 interface is used as a basis. It creates a namespace that contains all the CAPE-OPEN interface definitions and provides marshalling of data from the CAPE-OPEN COM objects to the .NET platform. Therefore, it can be used in the Visual C# and the Visual Basic compilers, as well as in other programing languages which support assemblies for the Microsoft .NET framework (Barrett Jr.& Yang, 2005). This class library is non-exclusive and royalty-free to publish or reproduce. It may be freely re-distributed and used for testing and evaluation purposes. The installation package can be found on United States Environmental Protection Agency (EPA) site (http://www.epa.gov/nrmrl/std/cape/cape.htm).
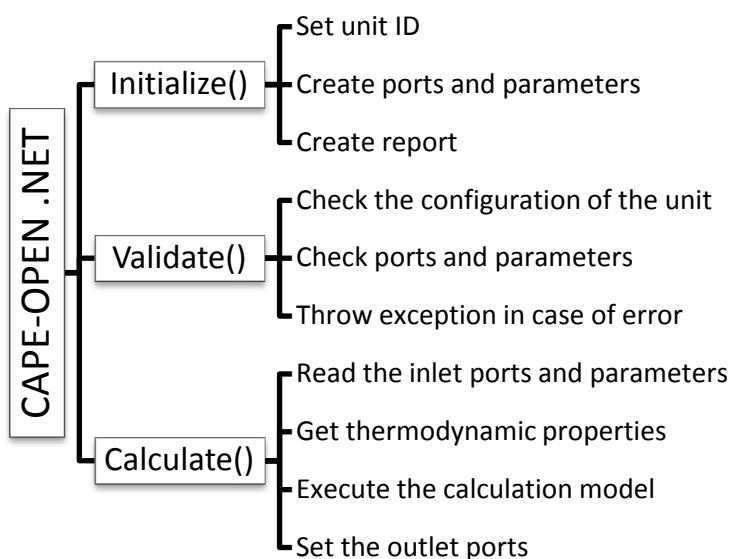
Figure C.2. Functionalities of the main base methods.

In order to create a CAPE-OPEN unit operation, three main methods need to be implemented: initialization, validation and calculation. An overview of these steps is shown in Figure C.2. The implementation details are discussed in the following. Besides these methods, the unit operation exposes an Edit() method that allows for developers to add a graphical user interface to the unit.

1. Initialization

The role of the Initialize() method is to reserve a unique ID for the unit and to allocate space for the ports and parameters. The creation and insertion of ports and parameters is realized by calling the Add() method which takes as input: name, direction, type and initial value for parameters. Parameters are used to set the design specs and operational conditions (column height and diameter, condenser/reboiler temperature and the packing type). An example of the implementation of the Initialize() method is shown in Figure C.3.

```
public override void Initialize()
{
    // Set unit ID
    this.ComponentName = "DTU-CAPCO2"

    // Create input ports
    this.Ports.Add(new CapeOpen.CUnitPort("pGasIn", "Gas In",CapeOpen.CapePortDirection.CAPE_INLET,
        CapeOpen.CapePortType.CAPE_MATERIAL));
    ...
    // Create outlet ports
    this.Ports.Add(new CapeOpen.CUnitPort("pGasOut", "Outlet Stream",
        CapeOpen.CapePortDirection.CAPE_OUTLET, CapeOpen.CapePortType.CAPE_MATERIAL));
    ...
    // Define parameters
    this.Parameters.Add(new CapeOpen.CRealParameter("Column height", "Column height", 17.0, 17.0, 0.0,
        100.0, CapeOpen.CapeParamMode.CAPE_INPUT, "m"));
    this.Parameters.Add(new CapeOpen.CBoolParameter("Inlcude Condenser",true
        CapeOpen.CapeParamMode.CAPE_OUTPUT));
}
```
*the listed code is with illustrative purpose and it is incomplete

Figure C.3. Visual C# code implementing the Initialize method

2. Unit operation state validation

A CAPE-OPEN unit operation can assume that the material objects, connected to the inlet ports, are fully specified. On the other hand, it is the responsibility for the unit operation to set the state of the outlet ports. However, the unit operation can check the suitability of the connected inlet and outlet port objects. The role of the Validate() method is to refuse the stream and throw appropriate exceptions if the connected objects do not expose a suitable interface. The state validation method can perform additional checks: to assure that the list and the order of the components on the inlet and outlet ports are the same; and to assure that the material object can support the thermodynamic calculations, etc.

The PME has to assure that the unit operation is valid before attempting to simulate the flow-sheet. Therefore, the PME can validate the unit operation at any time. However, these checks generally are performed before calculation time. Additional checks are performed by the PME after user changes to the unit operation object (van Baten& Szczepanski, 2011).

3. Calculation

During a flow-sheet simulation, the calculate function of the unit operation is called, in the order determined by the sequencing routine of the PME. The role of this method is to obtain pointers to the inlet and outlet material ports, to retrieve thermodynamic and physical properties from the selected servers and to determine and specify the outlet ports. The unit operation must set temperature, pressure and the total flow and composition of the ports, of all components flow. Figure C.4 shows an example of implementation of the mentioned steps.

As a good practice, it is recommended to use the "try" and "catch" structure for casting operation test. This approach allows evaluation of the object and it returns a valid pointer only if the material objects correspond to the requested type. Otherwise, if the material object attached to a port is invalid, the pointer will be null and a System Exception error is thrown. The CAPE-OPEN error handling interface takes care of these runtime errors by returning a message which indicates the source and the type of the error and/or exception.

```csharp
public override void Calculate()*
{
   // Get the inlet material object
   CapeOpen.ICapeThermoMaterialObject pLiquidIn = null;

   try{

      pLiquidIn = this.Ports[PortIndexArray].connectedObject as CapeOpen.ICapeThermoMaterialObject;
      }
   catch (System.Exception p_Ex)
      {
      CapeOpen.CapeInvalidOperationException ex = new CapeOpen.CapeInvalidOperationException("Does not
         support CAPE-OPEN 1.0.", p_Ex);
      this.throwException(ex);
      }

   try
      {
         // Retrieve components identifiers
         pLiquidInComps = pLiquidIn.ComponentIds as string[];

         // Read inlet ports(flow rate, temperature, pressure, etc.) and parameters
         pLiquidIn = this.Ports[PortIndexArray].connectedObject as CapeOpen.ICapeThermoMaterialObject;
         pLiquidInFlow = pLiquidIn.GetProp("flow", "Overall", pLiquidInComps, null, "mole") as double[];
         parameterInputVector[8] = (this.Parameters[(int)Parameterlist.plPressure]as CapeOpen.CRealParameter);

         // Read thermodynamic properties
          pGasInEnthalpy = pGasIn.GetProp("enthalpy", "Vapor", null, "Pure", "mole") as double[];
            ...
      }
   catch {...}
         ...
      RUN CAPCO2 model
         ...

   // get connected material object to the outlet ports
   CapeOpen.MaterialObjectWrapper pLiquidOut = new
   CapeOpen.MaterialObjectWrapper(this.Ports[PortIndexArray].connectedObject);

   try
      {
      // Set outlet ports (flow rate, temperature, pressure, etc.) and parameters
      pLiquidOut.SetProp("flow", "Overall", pLiquidInComps, null, "mole", LiquidPhaseComp);

      // perform equilibrium calculation and set the values
      pLiquidOut.CalcEquilibrium("TP", null);
      }
   catch {...}

   // Release the material object if it is a COM object
   if (pLiquidIn.GetType().IsCOMObject) System.Runtime.InteropServices.Marshal.ReleaseComObject(pLiquidIn)
}
  **the listed code is just with illustrative role and it is incomplete*
```

Figure C.4. Visual C# code implementing the Calculate method.

Development of a CAPE-OPEN module from a FORTRAN model

The main obstacle that may arise when implementing the CAPE-OPEN interface in the .NET platform is the use of a legacy (procedural) programing language, such as FORTRAN. To integrate a FORTRAN model in a .NET framework a code-migration process is needed. There are mainly two approaches: re-implementing the model from scratch or wrapping an object-oriented shell around the existing code. Figure C.5 shows the principle sketch of the code wrapping technique. CAPCO2 was implemented with this method. Re-

programming of the code is not a viable option since it may introduce bugs and the existing code has been extensively evaluated.
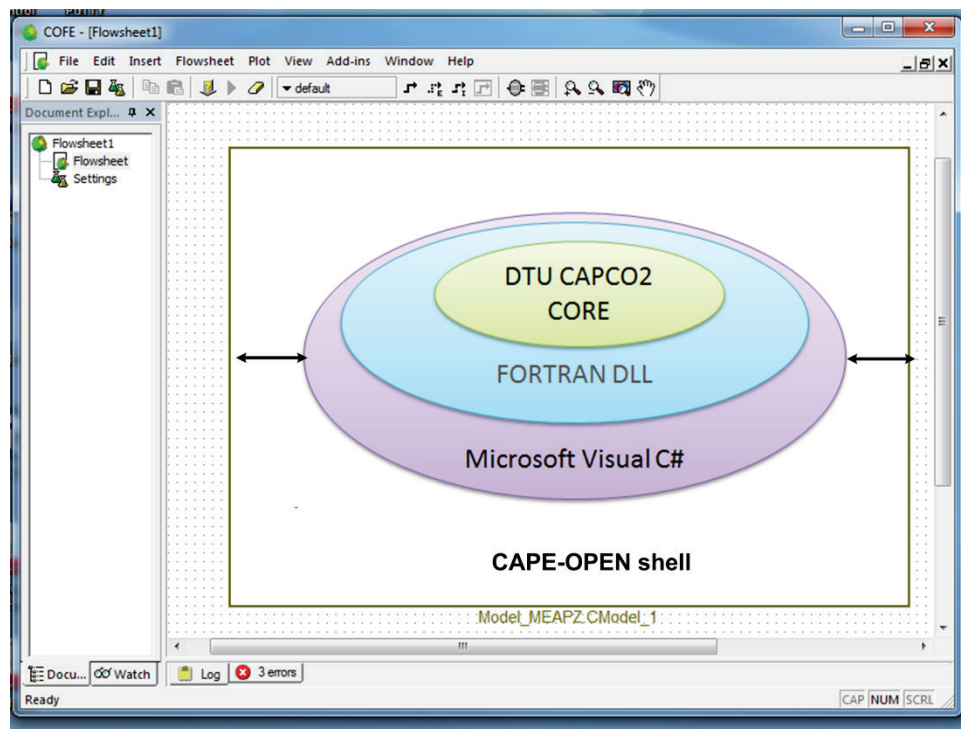

Figure C.5. Principle sketch of the code wrapping technique.

The DTU-CAPCO2 FORTRAN core contains the original functionality and routines of the system to be migrated. Note, outside dependencies of the core (e.g. thermodynamic and physical property packages) need to be migrated by introducing access points in the shell. A simple solution to migrate the source code together with its dependencies is by using the Dynamic Link Libraries (DLL) technology giving access to the functionalities of the model core. Therefore, the core code is separated from the CAPE-OPEN implementation and it is treated as a black box. This approach facilitates the maintenance of both subsystems, code core and the CAPE-OPEN interface.

The exterior layer in Figure C.5 is an object-oriented shell around the DLL, implemented in Visual C#. An example of its implementation is shown in Figure C.6. This shell ensures the communication between the DTU-CAPCO2 core and the CAPE-OPEN interface(COLaN, ; Domancich et al., 2010). This shell uses the LoadLibrary(), FreeLibrary(), GetProcessAddress() and GetLastError() functionalities of the "kernell32.dll" dynamic link library. These functions are used to get a handle and the address of the CAPCO2 FORTRAN DLL. Moreover, it returns an error message if an error occurs.

```csharp
[Serializable]
class DLLWrapper
{
  // Get a handle to a DLL
  [DllImport("kernel32.dll")]
  public static extern IntPtr LoadLibrary(string dllName);

  // Release the memory occupied for the DLL
  [DllImport("kernel32.dll")]
  public static extern bool FreeLibrary(IntPtr Handle);

  // Retrieve the address of the DLL
  [DllImport("kernel32.dll")]
  public static extern IntPtr GetProcAddress(IntPtr hModule, string procName);

  // Retrieves the calling thread's last-error code value
  [DllImport("kernel32.dll")]
  public static extern uint GetLastError();

  public static Delegate GetDelegateForFunction(IntPtr hDLL, string FunctionName, Type FunctionType){
        IntPtr ptr = DLLWrapper.GetProcAddress(hDLL, FunctionName);
        if (ptr == IntPtr.Zero)
            throw new Exception("Could not find entry point" + FunctionName + " in the DLL");
        else
            return Marshal.GetDelegateForFunctionPointer(ptr, FunctionType);}
  }
```

Figure C.6. Visual C# wrapper around a FORTRAN DLL.

It can be concluded that the code wrapping technique is a viable way to integrate source code from an unmanaged, procedural programing language into a managed, object-oriented programing language. Moreover, leaving the source code untouched ensures the bug-free migration of the source code and avoids the need for code optimization.

Installation of a CAPE-OPEN module

The .NET implementation of a CAPE-OPEN interface must be registered for COM interoperability. This allows the CAPE-OPEN module to interact with PMEs. This operation can be done on the Build page of the Visual C# Project Designer or using the "regasm.exe /codebase /tlb" " command in the Windows Command Window (CMD), running with administrator privileges.

In order to simplify the installation of the DTU-CAPCO2 model, an installer package was developed. This installation package creates a "CAPEOPEN - CAPCO2" program folder and copies the CAPE-OPEN module with all of the dependencies to this folder. Moreover, it registers the object for COM interoperability. Therefore, the tedious operation for COM registration is reduced to one click – like normal installation programs.
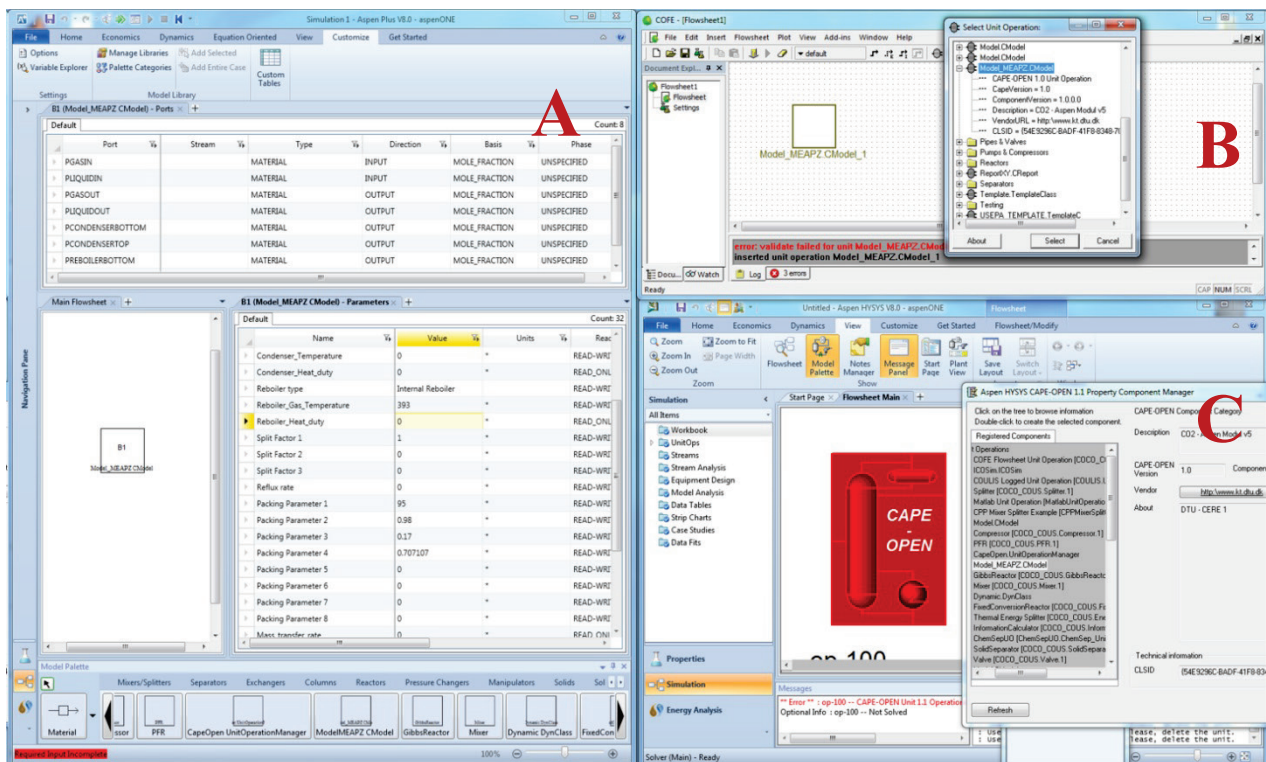
Figure C.7. DTU-CAPCO2 rate-based unit in Aspen Plus (A), COFE (B) and Hysys (C).

Once the FORTRAN source code is wrapped into a DLL, the CAPE-OPEN shell is created around the DLL and the module is registered for COM interoperability, the rate-based unit operation becomes available in all of the CAPE-OPEN compliant process modelling environments (COSE) as an extension to the built-in unit operation list. As an example, Figure C.7 shows the DTU-CAPCO2 unit operation in Aspen Plus (A), the freeware COFE simulator (B) and Hysys (C).

DTU-CAPCO2 and Aspen Plus

This section demonstrates the use of the DTU-CAPCO2 rate-based column model inside Aspen Plus for CO_2 post-combustion capture simulation. It presents the simulation of the Esbjerg pilot plant for Test 1A of the MEA campaign of the CESAR project. The purpose of Test 1A was to optimize the operation of the Esbjerg pilot with respect to the lean solvent flow rate. The pilot test was carried out in closed-loop. The aim of this simulation example is twofold: to verify the accuracy of the CAPE-OPEN implementation of the DTU-CAPCO2 module and to demonstrate the interoperability of Aspen and the CAPE-OPEN unit. The focus is on highlighting the benefits of the CAPE-OPEN interfaces. Details on how to set up and run a post-combustion capture simulation in Aspen Plus can be found on the Aspen support page, solution ID 123401 to 123408 (http://support.aspentech.com/).

Figure C.8 shows the post-combustion CO_2 capture process flow-sheet for the Esbjerg pilot plant. It substantiates that the DTU-CAPCO2 unit is used for absorption and desorption simulation, shown by the two white boxes to the left and right, in conjunction with built-in heat exchangers, mixers, pumps, and compressors. The communication basis between DTU-CAPCO2 and Aspen Plus is CAPE-OPEN. Therefore, the Aspen Plus simulation engines takes care of the convergence of the process flowsheet. The robustness and accuracy of the absorption and desorption calculation is secured by the CAPCO2 unit. Note that CAPCO2 benefits from the Aspen Plus features, e.g. flow, temperature, pressure can be specified in various units. Moreover, Aspen Plus includes various process analyses tools, such as sensitivity analyses, optimization, data fitting, etc.
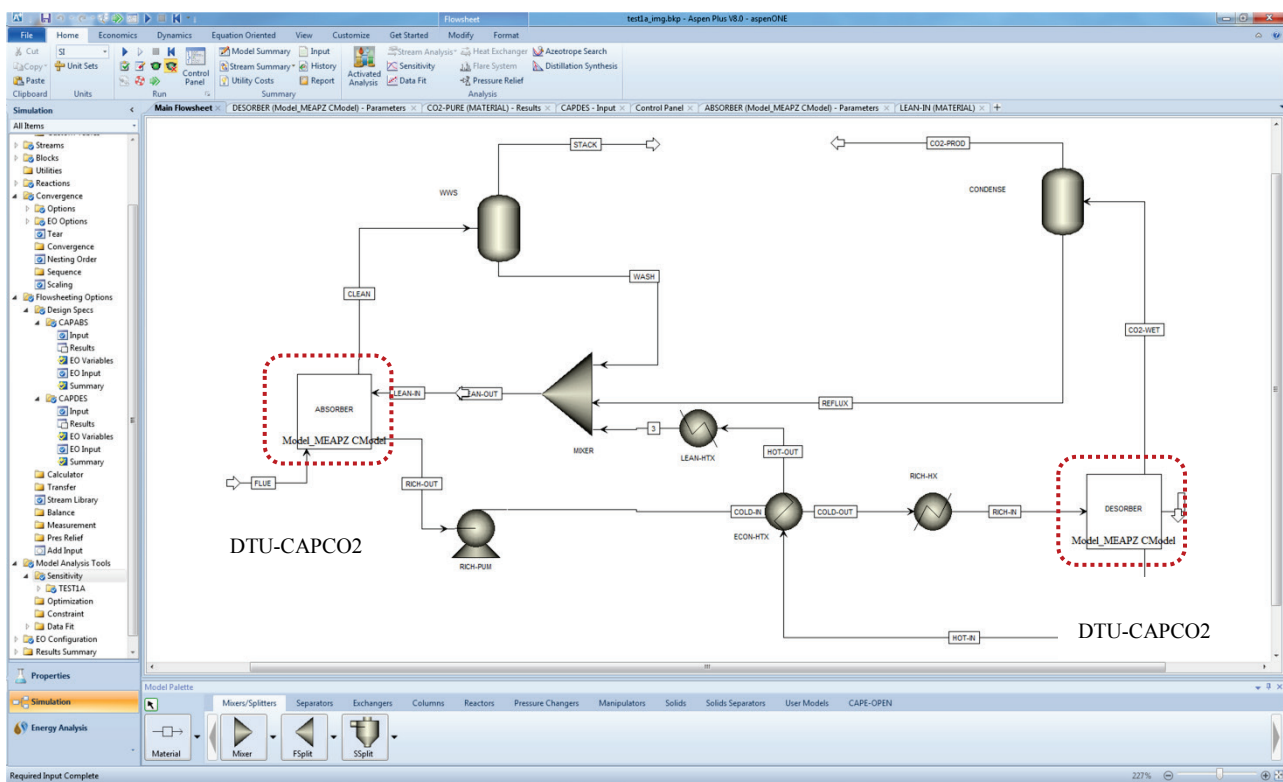
Figure C.8. Post-combustion capture process flow-sheet in Aspen Plus.

Figure C.9 shows the Graphical User Interface (GUI) of the DTU-CAPCO2 unit in Aspen Plus. This is a tailor-made GUI and it is used to set design specifications and to retrieve simulation results. For example, this interface takes as input column height and diameter, the configuration of the model (with or without condenser and/or reboiler), the applied enhancement factor model, etc. In addition, it returns the calculated lean/rich loading, the CO_2 mass transfer rate, CO_2 recovery percentage, reboiler energy penalty, etc. Other results, e.g. composition, temperature, etc. of a stream can be retrieved using the native GUI of Aspen Plus. Moreover, temperature and composition profiles may be saved in external files.
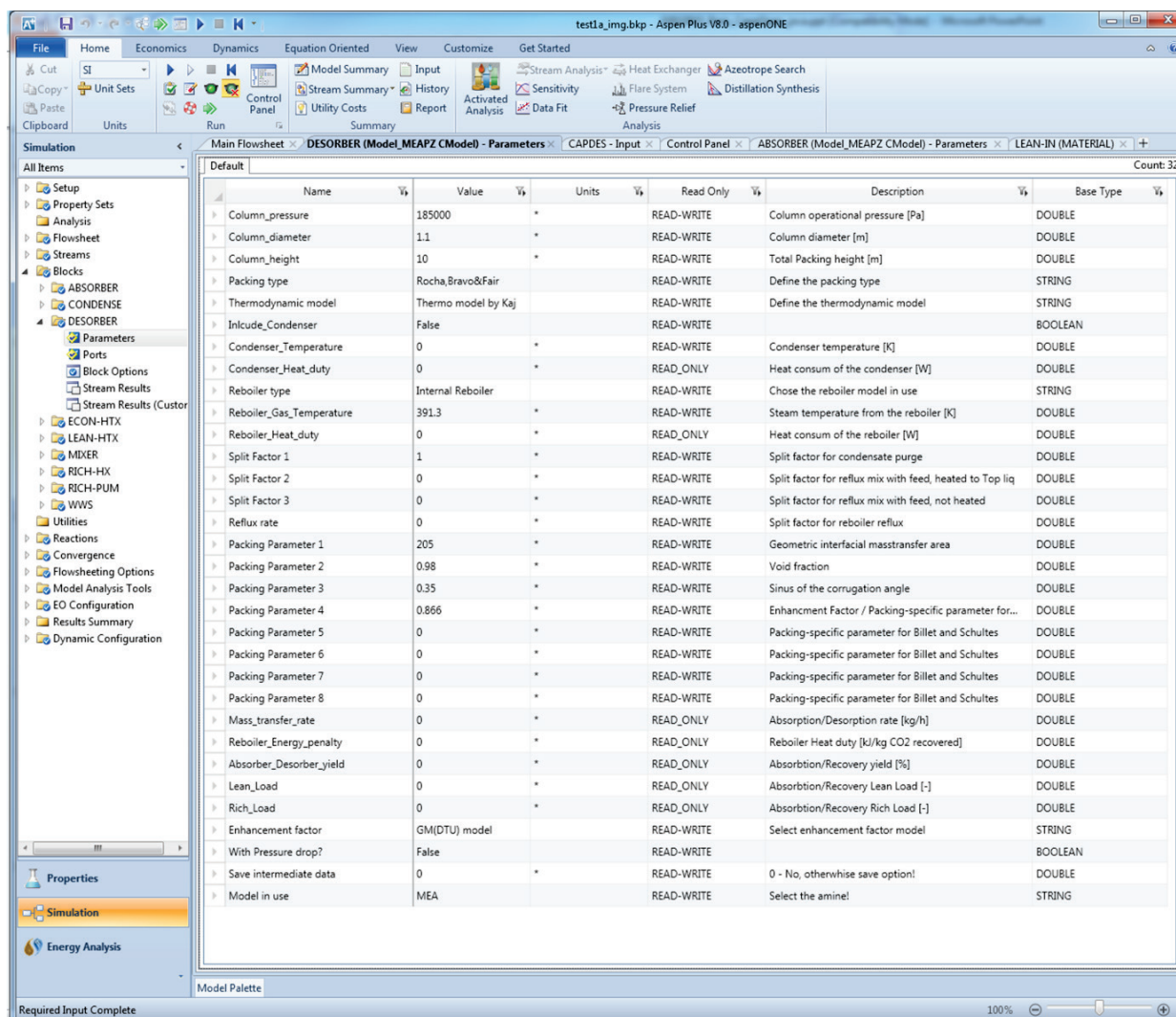
Figure C.9. Graphical User Interface of DTU-CAPCO2 unit in Aspen Plus.

In Test 1A of the CESAR-MEA campaign, the operation of the pilot plant was optimized with respect to the absorber liquid-to-gas ratio (L/G ratio) using fixed flue gas flow rate. At each solvent flow setting, the CO_2 recovery was tuned to 90% by manipulating the reboiler steam input. More details regarding the design specifications and pilot details used for input parameters can be found in the CESAR deliverable D3.2.4.

To re-create this case, a sensitivity study is carried out, using the "Sensitivity" model analysis tool in Aspen Plus. Uncertainties of measurements give rise to differences between model and real plant. Therefore, fine adjustments of the inlet variables are needed for the closed-loop simulation of the process. This is a tedious and time consuming process when done manually. The approach of the present work was to automatically fine tune the lean flow rate to obtain 90% absorption CO_2 capture. This task is performed by a simple "Design Specification" flowsheeting option in Aspen Plus. Moreover, a second "Design Specification" is

enforced to automatically maintain the CO_2 desorption recovery at 90% by changing the operating temperature of the reboiler. These options guarantee mass balance between the absorber and the desorber. In addition, a "Balance" flowsheeting option is set to maintain the CO_2, MEA and H_2O balance around the process. This option calculates the MEA and H_2O make-up streams. They are crucial for closed-loop simulation of a process. Figure C.10 shows an example of the GUI of the design specification and sensitivity tool in Aspen Plus. This particular setup is not fixed and allows for specification of any process variable, including the parameters of the DTU-CACO2 unit.
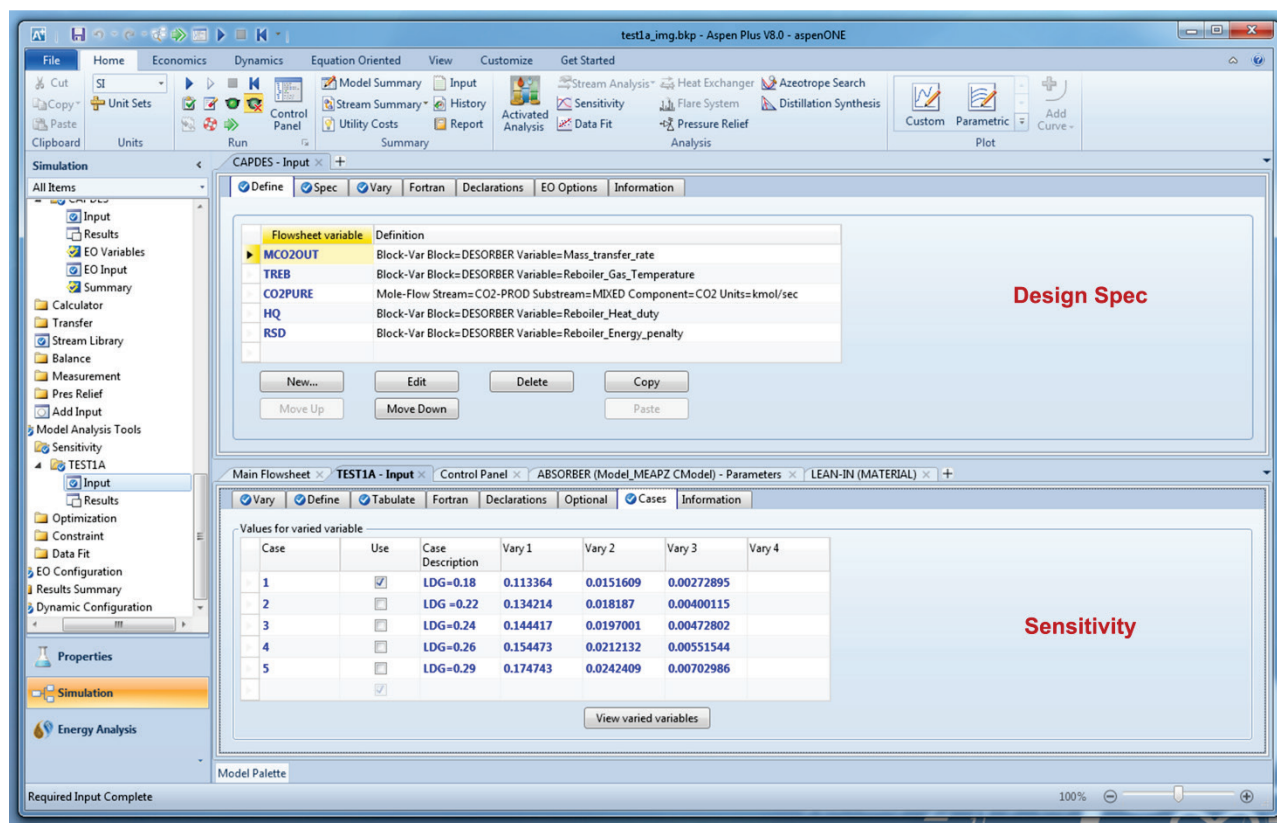
Figure C.10. Example of "Sensitivity" analysis tool and "Design Specs" options in Aspen Plus.

Figure C.11 shows a calculation example for the CESAR test series 1. It presents the calculated and measured reboiler heat duty and CO_2 recovery percentage at five different lean flow rates. The discrepancy between the model and the experiments is small, 2-10% as expected(Fosbøl et al., 2014), and they are in the accuracy range of the experimental measurements. The DTU-CAPCO2 model was extensively validated against various experimental measurements (Faramarzi et al., 2010; Gaspar et al., 30, January, 2013; Sønderby et al., 2013). Moreover, the model was benchmarked against the rate-based models used by SINTEF, IFP, TUHH, EDF and TNO (Fosbøl et al., 2014).

Table C.1. Validation calculation results for the DTU CAPCO2 absorber and desorber columns obtained before and after incorporating into CAPE-OPEN for case CESAR 1A

Parameter	Without CAPE-OPEN	With CAPE-OPEN
CO_2 capture % (absorber)	89.3067	89.3066
CO_2 recovery %	87.2900	87.2902
Reboiler specific duty (GJ/t CO_2)	3.9362	3.9362
Lean CO_2 loading	0.2004	0.2004
Rich CO_2 loading	0.4905	0.4905

Table C.1 shows a comparison between the results obtained before and after incorporating the DTU-CAPCO2 model into the CAPE-OPEN shell. The CAPE-OPEN is merely a shell around the CAPCO2 model and identical results are expected while performing calculations with either of the two interfaces. One can note that the implementations return the exact same result, Table C.1. Therefore, it can be concluded that the DTU-CAPCO2 CAPE-OPEN unit inherits the accuracy of the CAPCO2 model (Fosbøl et al., 2014). It substantiates that the interface is working properly and there were no obvious mistakes in the migration of the FORTRAN code to the CAPE-OPEN .NET platform.
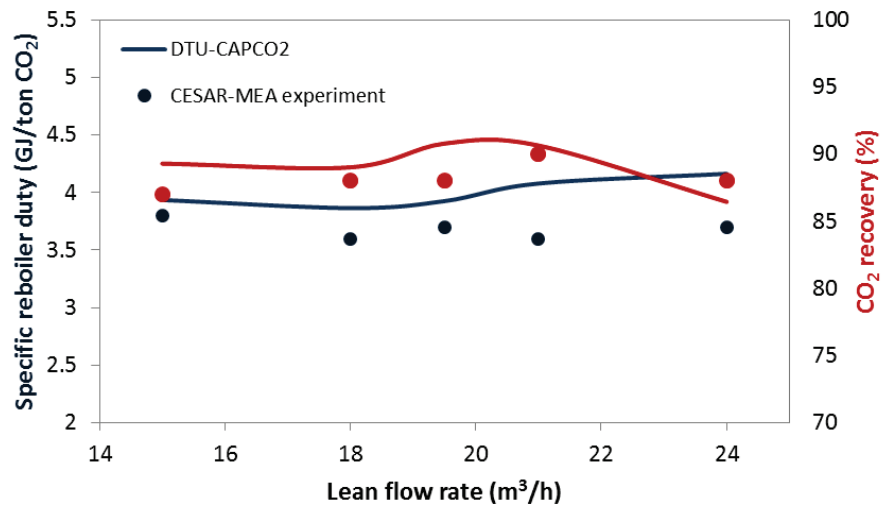
Figure C.11. Specific reboiler duty and CO_2 recovery rate as function of the lean flow rate.

It can be concluded that the CAPCO2 in-house model for CO_2 absorption and desorption is dynamically linked to Aspen Plus. In addition, the CAPE-OPEN interface makes it possible to use the CAPCO2 model in other software packages, such as gPROMS, CHEMCAD, PRO/II, Matlab, Excel etc. It demonstrates how 3rd party software developers can benefit from the built-in features of Aspen Plus but also highlights the advantage of using CAPE tools for accelerated process design and optimization.

References

Barrett Jr., W. M., & Yang, J. (2005). Development of a chemical process modeling environment based on CAPE-OPEN interface standards and the Microsoft .NET framework. Computers & Chemical Engineering, 30, 191-201.

COLaNMigration cookbook and Wizards. http://www.colan.org/index-9.html.

Domancich, A. O., Perez, V., Hoch, P. M., & Brignole, N. B. (2010). Systematic generation of a CAPE-OPEN compliant simulation module from GAMS and FORTRAN models. Chemical Engineering Research & Design, 88, 421-429.

Faramarzi, L., Kontogeorgis, G. M., Michelsen, M. L., Thomsen, K., & Stenby, E. H. (2010). Absorber Model for CO2 Capture by Monoethanolamine. Industrial & Engineering Chemistry Research, 49, 3751-3759.

Fosbøl, P. L., Gaspar, J., Ehlers, S., Kather, A., Briot, P., Nienoord, M., Khakharia, P., Le Moullec, Y., Berglihn, O., & Kvamsdal, H. M. (2014). Benchmarking and comparing first and second generation post combustion CO2 capture technologies. Energy Procedia.

Gabrielsen, J. (2007). CO2 Capture from Coal Fired Power Plants.

Gaspar, J., Thomsen, K., von Solms, N., & Loldrup Fosbøl, P. (30, January, 2013). Rate based CO2 post-combustion modeling in Aspen Plus using CERE Cape Open modules. University of Texas Carbon Capture Storage (UTCCS-2).

Gaspar, J., Thomsen, K., von Solms, N., & Fosbøl, P. L. (2014). Solid Formation in Piperazine Rate-based Simulation. Energy Procedia, 63, 1074-1083.

Sonderby, T. L., Carlsen, K. B., Fosbol, P. L., Kiorboe, L. G., & von Solms, N. (2013). A new pilot absorber for CO2 capture from flue gases: Measuring and modelling capture with MEA solution. International Journal of Greenhouse Gas Control, 12, 181-192.

van Baten, J., & Szczepanski, R. (2011). A thermodynamic equilibrium reactor model as a CAPE-OPEN unit operation. Computers & Chemical Engineering, 35, 1251-1256.

Appendix D - ACM implementation of the CAPCO2 column model

This section presents the design and implementation of an Aspen Custom Modeler (ACM) unit, DTU-CAPCO2, for CO_2 absorption and desorption rate-based simulation. It discusses the functionalities of the DTU-CAPCO2 model and exemplifies an implementation of the ACM unit operation. In addition, the wrapping of the FORTRAN source code to ACM platform is discussed and exemplified.

Description of CAPCO2 rate-based column model

The ACM implementation of the CAPCO2 has the same functionalities as the CAPE-OPEN implementation, presented in Appendix C. The ACM unit uses the same FORTRAN routines as the CAPE-OPEN unit, the DTU-CAPCO2 rate-based model. Thus, only a brief summary of the structure of the CAPCO2 unit is given.

Figure D.1 represents the conceptual structure of the DTU-CAPCO2 module. It illustrates how the module has two input ports and two output ports corresponding to a liquid and a gas feed plus a liquid and a gas outlet. Packing type, column characteristics, column configuration, etc. must be defined by the user as "design specifications". The module returns the calculated heat duties for the condenser and the reboiler. Note that the condenser and the reboiler are integrated into the rate-based model. It is therefore possible to configure the column as one of the five setups: absorber, absorber with integrated condenser, stripper with integrated reboiler, stripper with integrated condenser, plus stripper with integrated reboiler and condenser.
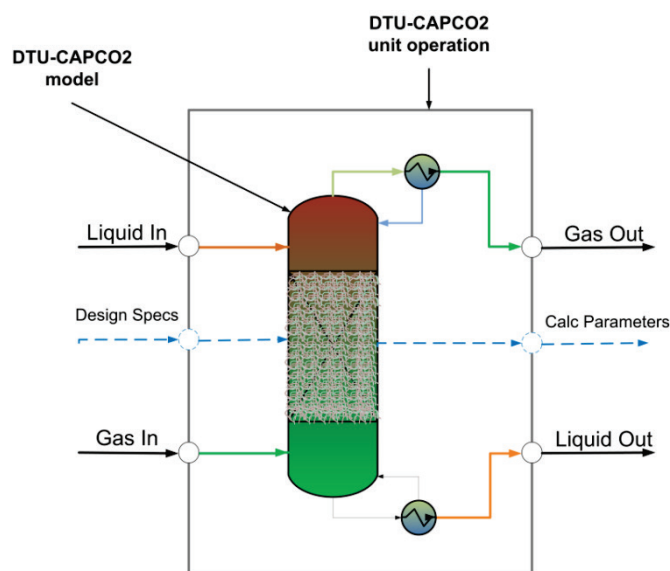

Figure D.1. Conceptual structure of the CAPCO2 rate-based column module.

Implementation of a unit operation using Aspen Custom Modeler

This section provides an overview of the implementation procedure of an Aspen Custom Modeler (ACM) unit. This implementation consists of three steps: (1) selection of properties, (2) implementation of the ACM model and (3) installation of the model.

<u>Selection of properties database</u>

Aspen Custom Modeler shares a common property database and set of thermodynamic models with Aspen Plus. This ensures consistency for all of the properties used in process simulation. There are options for setting up the properties in ACM: (1) from scratch in Aspen Properties and (2) export properties from an existing Aspen Plus simulation. In this work the 2nd option is preferred since it allows us to link the extended UNIQUAC thermodynamic model to ACM and therefore to Aspen Plus.

Before implementing the ACM model, a reference between the Aspen Plus and ACM must be defined. This is done by selecting *Component List,* then *Configure Properties* and *select Import Aspen Properties file* (see figure D.2). Note that this reference can be modified at any time, thus it is easy to keep consistency between the ACM model and Aspen Plus simulations (Tremblay and Peers, 2014).
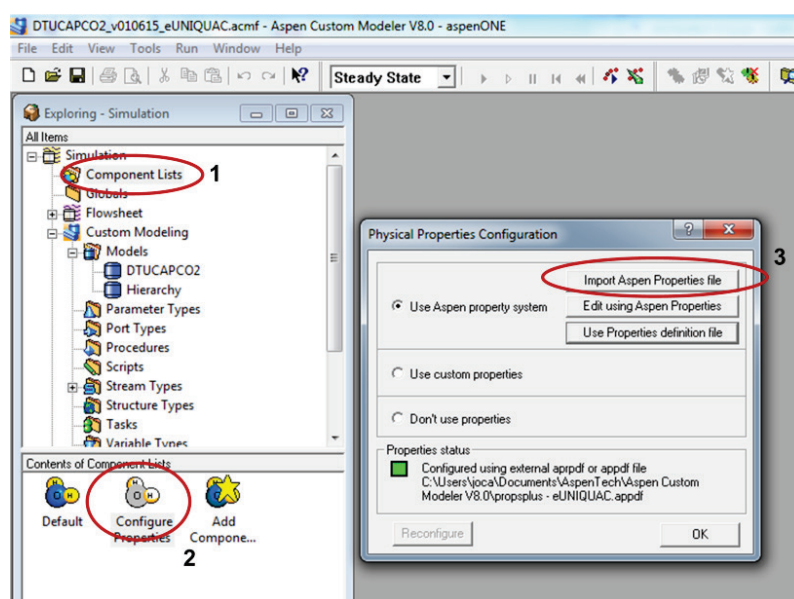

Figure D.2. Set up the component list in ACM based on Aspen Plus

Implementation of the ACM model

This section exemplifies the steps of implementing the CAPCO2 rate-based model in ACM. The code listening is illustrative aiming to provide an overview of the implementation procedure. A complete example for a flash ACM unit is describe in Tremblay and Peers (2014).

The first step is creating a custom model. This file will contain the implementation code. Then, we have to create the inlet/outlet ports and additional design variables, model parameters and procedures. In this work a procedure is used to wrap the rate-based model from FORTRAN to ACM. Finally, the mass and energy balance equations must be defined and outlet ports must be set.

Add ports

In order to generate a model for flowsheet simulation, ports must be defined. Ports allow connecting the DTU-CAPCO2 model to other units using streams. The developed model has 2 inlet ports (gas respectively liquid feed) and it has 3 outlet ports, i.e. gas outlet-, liquid outlet- and the condensate port. These ports are of _MoleFractionPort_ type for compatibility with Aspen Plus and Aspen Hysys.

```
//////////////////////////// PORTS SPECIFICATIONS ////////////////////////////////////////////////////////

// create input ports
GasInPort              as input  MoleFractionPort(description:"Gas feed to column");
LiquidInPort           as input  MoleFractionPort(description:"Solvent feed to column");
// create outlet ports
GasOutletPort          as output MoleFractionPort(description:"Gas outlet from condenser");
LiquidOutletPort       as output MoleFractionPort(description:"Liquid outlet reboiler");
CondensatePort         as output MoleFractionPort(description:"Liquid outlet from condenser");
```

Figure D.3. Define input/outlet ports

Add variables and parameters

The simplest way to add a parameter of a variable is using the built-in _Model Assistant_ tool. This tool inserts the code for the selected parameter/variable with the specified characteristics. Parameters and variables must have a name and type. Further possible specifications are: description, default value, lower/upper limits, etc. Variables can be of type _fixed_ and _free_. A fixed variable is held constant while a free variable is determined by the model calculations. A good practice is to specify all this fields with good initial values and specifications to ease the convergence of the model. An example for parameters and variables is given in figure D.4.
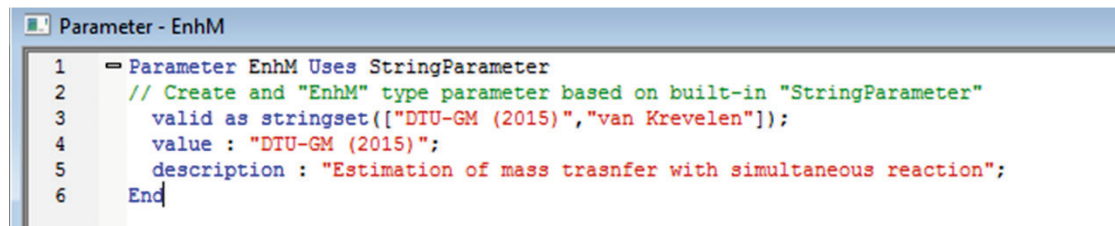
```
// Define variables
Diameter                as length (description:"Diameter of the column", lower:0, upper:30, value:8, spec:Fixed);
Height                  as length (description:"Heightof the column", lower:0, upper:100, value:8, spec:Fixed);
Reboiler_Temperature    as temperature (description:"Reboiler temperature", lower:0, upper:500, value:25, spec:fixed);
Reboiler_Pressure       as pressure (description:"Reboiler pressure", lower:0, upper:150, value:2, spec:fixed);
Condenser_Duty          as holdup_heat (description:"Condeser heat duty", lower:-1E10, upper:1E10, value:0, spec:Free);
colGasFlow              as hidden flow_mol (description:"Gas to condenser flow rate", value:1E-6, scale:1E-6, spec:free);

// define parameters
Enhancement_Factor      as EnhM;
Set_packing_type        as PckRBF;
Save_Parameters         as YesNo (description:"Save intermediate parameters", value:"No");
Surface_Area            as realparameter(description:"Packing surface area (m2/m3)", lower:0, upper:2000, value: 250);
```

Figure D.4. Define parameters and variables

Note that user made parameters and variables can be created using inheritance from existing parameters/variables. An example is shown in figure D.5.

```
Parameter - EnhM
1    ⊟ Parameter EnhM Uses StringParameter
2      // Create and "EnhM" type parameter based on built-in "StringParameter"
3        valid as stringset(["DTU-GM (2015)","van Krevelen"]);
4        value : "DTU-GM (2015)";
5        description : "Estimation of mass trasnfer with simultaneous reaction";
6      End
```

Figure D.5. Define parameters and variables

Add a procedure

Next a procedure need to be set up to simulate the absorber respectively desorber column. This procedure passes the values from the inlet streams and user specified parameters, e.g. height, packing characteristics, used mass transfer model, etc. to the CAPCO2 model and it retrieves the calculate values for the outlet streams (composition, temperature, pressure and flow rate) and it provides the calculated heat duty of the condenser/reboiler. Figure D.6 shows the ACM interface (procedure) to the CAPCO2 model and figure D.7 shows how to run the procedure inside the ACM model.

Figure D.6. Define a procedure to wrap the FORTRAN implementation of the CAPCO2 model

```
// call the pCAPCO2 procedure to run the CAPCO2 model with the given inlets and to retrieve the outlets
    CALL (colGasFlow,colGasYCO2,colGasYH2O,colGasPres,colGasTemp,
          condGasFlow, condGasYCO2,condGasYH2O,condGasPres,condGasTemp,
          condLiquidFlow,condLiquidYCO2,condLiquidYH2O,condLiquidPres,condLiquidTemp,Condenser_Duty,
          colLiquidFlow,colLiquidYCO2,colLiquidYH2O,colLiquidPres,colLiquidTemp,colSolidFraction,
          rebVapFlow,rebVapYCO2,rebVapYH2O,rebVapPres,rebVapTemp,
          rebLiquidFlow,rebLiquidYCO2,rebLiquidYH2O,rebLiquidPres,rebLiquidTemp,Reboiler_Duty,rebSolidFraction)
        = pCAPCO2(GIN, PACKING,Height, Diameter, Condenser_Temperature,Reboiler_Temperature,Reboiler_Pressure, dummy);
```

Figure D.7. Run the procedure to retrieve the CAPCO2 model calculations

Add mass and energy balance equations

Mass and energy balance equations are used to set the outlet gas and liquid ports. For compatibility with Aspen Plus and Aspen Hysys, the composition and flow rate of the liquid outlet flow is considered as a free variable and its composition is calculated by ACM, although conservation equations are implemented and solved in FORTRAN.

```
//**************************** MODEL EQUATIONS ****************************//
// set the gas outlet port: pressure, temeprature, composition and flow rate
      Eq_Pg:        GasOutletPort.P = condGasPres;
      Eq_Tg:        GasOutletPort.T = condGasTemp;
       IF((GasInPort.isConnected) OR (GasInPort.isLinked))THEN
         Eq_Y:      GasOutletPort.z(Componentlist - "CO2" - "H2O" - "N2" ) = 0;
       ELSE
         Eq_Y:      GasOutletPort.z(Componentlist - "CO2" - "H2O" - "N2") = 0;
       ENDIF
      Eq_YCO2:  GasOutletPort.z("CO2") = condGasYCO2;
      Eq_YH2O:  GasOutletPort.z("H2O") = condGasYH2O;
      Eq_Ysum:  sigma(GasOutletPort.z) = 1;
      Eq_GFlow:  GasOutletPort.F = condGasFlow;
// set the condensate outlet port if connected: pressure, temeprature, composition and flow rate
   IF(Condenser == "Internal")THEN
   // internal condenser is used
      Eq_Pc:        CondensatePort.P = condLiquidPres;
      Eq_Tc:        CondensatePort.T = condGasTemp;
      Eq_YC:        CondensatePort.z(Componentlist - "CO2" - "H2O" - "N2") = 0;
      Eq_YCO2c:  CondensatePort.z("CO2") = condLiquidYCO2;
      Eq_YH2Oc:  CondensatePort.z("H2O") = condLiquidYH2O;
      Eq_YN2:      CondensatePort.z("N2") = 0;
      Eq_LFlowc:  CondensatePort.F = condLiquidFlow;
   ELSE
      Eq_Pc:        CondensatePort.P = condLiquidPres;
      Eq_Tc:        CondensatePort.T = condLiquidTemp;
      Eq_YC:        CondensatePort.z(Componentlist - "H2O") = 0;
      Eq_cYsumc:  sigma(CondensatePort.z) = 1;
      Eq_LFlowc:  CondensatePort.F = condLiquidFlow;
   ENDIF
// set the liquid outlet outlet port: pressure, temeprature, composition and flow rate
   IF(Reboiler == "None")THEN
     Eq_Pl:        LiquidOutletPort.P = colLiquidPres;
     Eq_Tl:        LiquidOutletPort.T = colLiquidTemp;
     Eq_X:         LiquidOutletPort.z(Componentlist - "CO2" - "H2O" - "MEA") =  0;
     IF(Condenser == "Internal")THEN
       Eq_Y:         CondensatePort.z(["CO2","H2O"])*CondensatePort.F  + GasOutletPort.z(["CO2","H2O"])*GasOutletPort.F ...
         + LiquidOutletPort.z(["CO2","H2O"])*LiquidOutletPort.F = LiquidInPort.F*LiquidInPort.z(["CO2","H2O"])...
         + GasInPort.F*GasInPort.z(["CO2","H2O"]);
       Eq_TotBal:  LiquidOutletPort.F + GasOutletPort.F + CondensatePort.F = LiquidInPort.F + GasInPort.F;
     ELSE
       Eq_Y:         GasOutletPort.z(["CO2","H2O"])*GasOutletPort.F + LiquidOutletPort.z(["CO2","H2O"])*LiquidOutletPort.F = ...
         LiquidInPort.F*LiquidInPort.z(["CO2","H2O"]) + GasInPort.F*GasInPort.z(["CO2","H2O"]);
       Eq_TotBal:  LiquidOutletPort.F  + GasOutletPort.F  = LiquidInPort.F + GasInPort.F;
     ENDIF
   Eq_Xsum:      LiquidOutletPort.z("MEA") = 1 - LiquidOutletPort.z("H2O") - LiquidOutletPort.z("CO2");
   ELSE
     // The internal reboiler calculation is used
     Eq_Pl:        LiquidOutletPort.P = rebLiquidPres;
     Eq_Tl:        LiquidOutletPort.T = rebLiquidTemp;
     Eq_X:         LiquidOutletPort.z(Componentlist - "CO2" - "H2O" - "MEA") =  0;
     IF(Condenser == "Internal")THEN
       Eq_X:         CondensatePort.z(["CO2","H2O"])*CondensatePort.F  + GasOutletPort.z(["CO2","H2O"])*GasOutletPort.F ...
         + LiquidOutletPort.z(["CO2","H2O"])*LiquidOutletPort.F = LiquidInPort.F*LiquidInPort.z(["CO2","H2O"]);
       Eq_TotBal:  LiquidOutletPort.F + GasOutletPort.F + CondensatePort.F = LiquidInPort.F;
     ELSE
       Eq_X:         GasOutletPort.z(["CO2","H2O"])*GasOutletPort.F + LiquidOutletPort.z(["CO2","H2O"])*LiquidOutletPort.F = ...
         LiquidInPort.F*LiquidInPort.z(["CO2","H2O"]);
       Eq_TotBal:  LiquidOutletPort.F + GasOutletPort.F  = LiquidInPort.F;
     ENDIF
   Eq_Xsum:      LiquidOutletPort.z("MEA") = 1 - LiquidOutletPort.z("H2O") - LiquidOutletPort.z("CO2");
   ENDIF
```

Figure D.8. Mass balance in ACM

```
CALL (GasOutletPort.H) = pEnth_Mol_Vap (condGasTemp,condGasPres, GasOutletPort.z);
CALL (LiquidOutletPort.H) = pEnth_Mol_Liq (rebLiquidTemp,rebLiquidPres, LiquidOutletPort.z);
IF(Condenser == "Internal")THEN
  CALL (CondensatePort.H) = pEnth_Mol_Liq (condGasTemp,condLiquidPres, CondensatePort.z);
ENDIF
```

Figure D.9. Energy balance in ACM

Practically, the gas outlet stream (composition, temperature, pressure and flow rate) are set to the values retrieved form the CAPCO2 model and the outlet liquid stream is calculated based on overall total and component balances. Furthermore, the enthalpy of each outlet stream is calculated as shown in figure D.9. This enthalpy calculation will flash the outlet stream and will force Aspen Plus to set all the other variables

of the respective streams. If enthalpy calculation is not performed, the stream will have missing variables, leading to shut-down of Aspen Plus simulator. At this point the model can be compiled and used in Aspen Plus and Hysys.

Development of an ACM unit from a FORTRAN model

The DTU-CAPCO2 FORTRAN core contains the original functionality and routines of the system to be migrated. Note, outside dependencies of the core (e.g. thermodynamic and physical property packages) need to be migrated by introducing access points in the shell. A simple solution to migrate the source code together with its dependencies is by using the Dynamic Link Libraries (DLL) technology giving access to the functionalities of the model core. Therefore, the core code is separated from the ACM implementation and it is treated as a black box. This approach facilitates the maintenance of both sub-systems, code core and the ACM interface. An example of its implementation is shown in Figure D.10. This shell ensures the communication between the DTU-CAPCO2 core and the ACM interface. This shell uses the LoadLibrary(), FreeLibrary(), GetProcessAddress() and GetLastError() functionalities of the "kernell32.dll" dynamic link library. These functions are used to get a handle and the address of the CAPCO2 FORTRAN DLL. Moreover, it returns an error message if an error occurs.

```
!********************* BEGIN USER CODE ********************************
      IF (ICALL.EQ.IOutputs .OR. ICALL.EQ.IBoth) THEN
!     Load the DLL
      H_DLL = loadlibrary(dirpath(1:lrc-1) // "\\ColumnOU.dll"C)
!     Check for correct loading
      IF (H_DLL == 0) THEN
         errormsg = GetLastError();
         CALL ACM_PRINT(0,'  DLL was not hooked up correctly.',,0,0,0,0);
         CALL ACM_PRINT(0,'  Check if the PATH is set!',0,0,0,0,0);
         CALL ACM_PRINT(0,'  Error msg code =%f',errormsg,0,0,0,0);
         stop;
      ENDIF
!     Get the function address
         H_FUNC = getprocaddress(H_DLL,"ColumnUO"C);
!     Check for correct loading
      IF (H_FUNC == 0) THEN
         CALL ACM_PRINT(0,'  DLL was not loaded correctly.',0,0,0,0,0);
         CALL ACM_PRINT(0,'  Check if the PATH is set!',0,0,0,0,0);
      ENDIF

!!    Call the CAPCO2 module
      CALL ColumnUO(GCOL,PACKING,FlowOut,LiquidCompOut,
     &             GasCompOut,TemperatureOut,PressureOut,OutCondenser,
     &             OutCondSplit,InFeedWithCondensate,InReboiler,
     &             OutReboiler)
```

Figure D.10. ACM wrapper around the FORTRAN DLL.

It can be concluded that the code wrapping technique is a viable way to integrate source code from FORTRAN to ACM programing language. Moreover, leaving the source code untouched ensures the bug-free migration of the source code and avoids the need for code optimization.

DTU-CAPCO2 and Aspen Plus

This section demonstrates the use of the DTU-CAPCO2 rate-based column model inside Aspen Plus for CO_2 post-combustion capture simulation using the ACM interface. It presents how to set-up a post-combustion simulation using design specs for fixed 90% CO_2 removal and an optimized approach for simulation of lean-vapor-compression (LVC).

Post-combustion CO₂ capture process

The first step is building the flowsheet of the post-combustion capture process, as shown in Figure D.11. This flowsheet consist of: two DTUCAPCO2_UNIQUAC user models for CO_2 absorption (ABS) and desorption (DES); a pump (RICH-PUM); a heat exchanger (RICH-HX) and a flash unit for the condenser above the stripper (CONDENSE). The inlet flue gas stream is "GAS_FLOW" and the inlet lean stream is "LEAN-IN". The input specifications for all of the units and input streams are shown in Table D.1. How to configure the absorber and the desorber are detailed in the next sections.
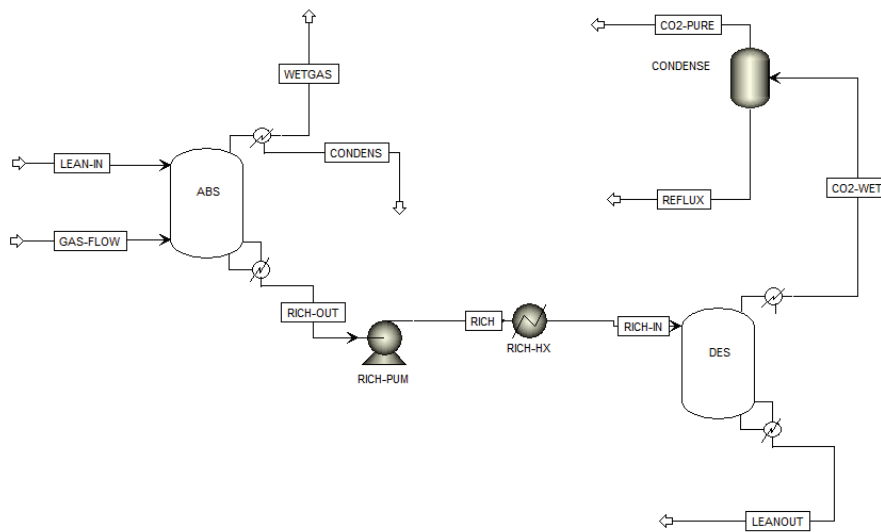

Figure D.11. Post-combustion CO_2 capture process flowsheet

In this example, we use an absorber with integrated condenser and a stripper with integrated reboiler. The condenser of the stripper is modelled with Flash 2 unit and the heat exchanger with a HeatX unit.

Table D.1. Input specifications for the inlet gas and lean stream respectively for the units

Input stream	Flue gas	Lean solvent	
Flow rate (kmol/h)	187.2	557.5522	
Temperature (°C)	48	40	
Pressure (bar)	1	1	
Mol fraction (mol %)			
MEA	0	0.115508	
H_2O	0.11	0.8637006	
CO_2	0.12	0.0207914	
N_2	0.77	0	
Unit	RICH-PUM	RICH-HX	CONDENSE
Pressure (bar)	1.85	1.85	1.85
Temperature (°C)	-	95	40

A.) Absorber Configuration

The first step is to configure the "*Variables*" of the ABS block. For this, right click on the *ABS* block and select "*Input*". Then set the values for the block variables as shown in Figure D.12.a. In this example, we use a 1.1 diameter column with 17 m height. The condenser above the absorber is operated at 40 °C. Here the condenser helps to recover water from the top part of the absorber. You can decide not to include the condenser. For now we include it. In case of an absorber, the reboiler pressure and temperature do not need to be specified. After running the simulation, the duty of the condenser will be given in the "*CONDESER_DUTY*" variable.
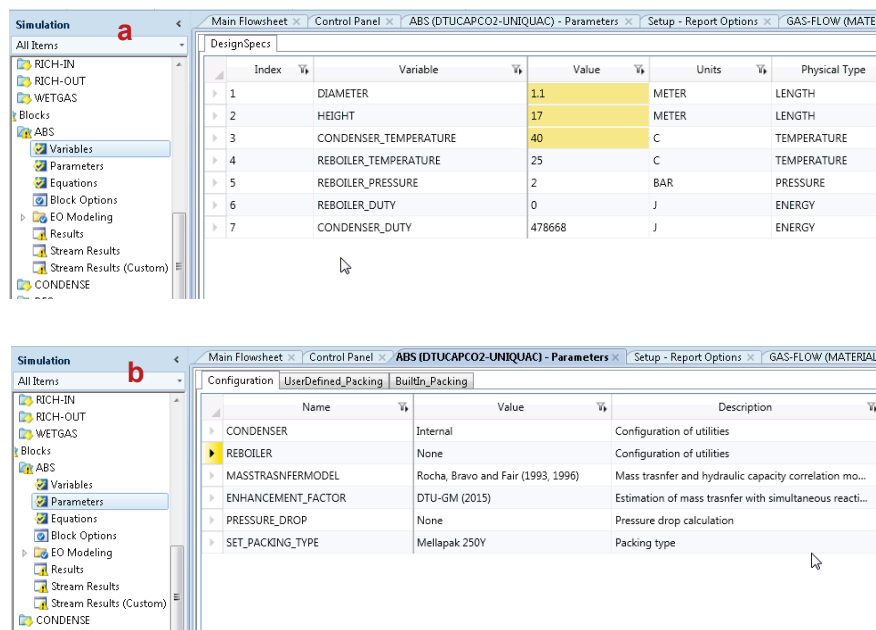

Figure D.12. Absorber configuration: (a) Variables and (b) Parameters.

Then, select the "*Parameters*" menu in the "*Simulation*" window and set the values in the "*Configuration*" tab as shown in Figure D.12.b. In this example, we use the integrated condenser and the "*Rocha, Bravo and Fair (1993, 1996)*" mass transfer model (Rocha et al., 1993). The enhancement factor is calculated using the "*DTU-GM (2015)*" model (Gaspar and Fosbøl, 2015). In addition, we assume constant pressure along the column height and we use the Mellapak 250Y packing.

B.) Desorber Configuration

The procedure for configuring the desorber is similar to the above described procedure for the absorber. First, set the diameter (1.1 m), height (10 m), and the reboiler operating temperature (121 ℃) and pressure (1.85 bar), as shown in Figure D.13a. The condenser temperature does not need to be specified. The "*REBOILER_DUTY*" variable shows the calculated reboiler heat duty. Note, the CAPCO2 model with integrated reboiler configuration is used. It significantly reduces the simulation time.

Then, select the "*Parameters*" menu in the "*Simulation*" window and configure the model as shown in Figure D.13.b. Note, a user defined packing is used in the desorber. To specify the packing specific parameters, select the "*UserDefined_Packing*" tab and introduce the following values: 250 (surface area), 0.95 (void fraction), 0.35 (surface enhancement) and 0.707107 (corrugation channel). The remaining parameters are used when the "*Billet and Schultes (1999)*" mass transfer model is selected (Billet and Schultes, 1999). More details about specifications of the packing can be found in "*Packing specifications*" section.
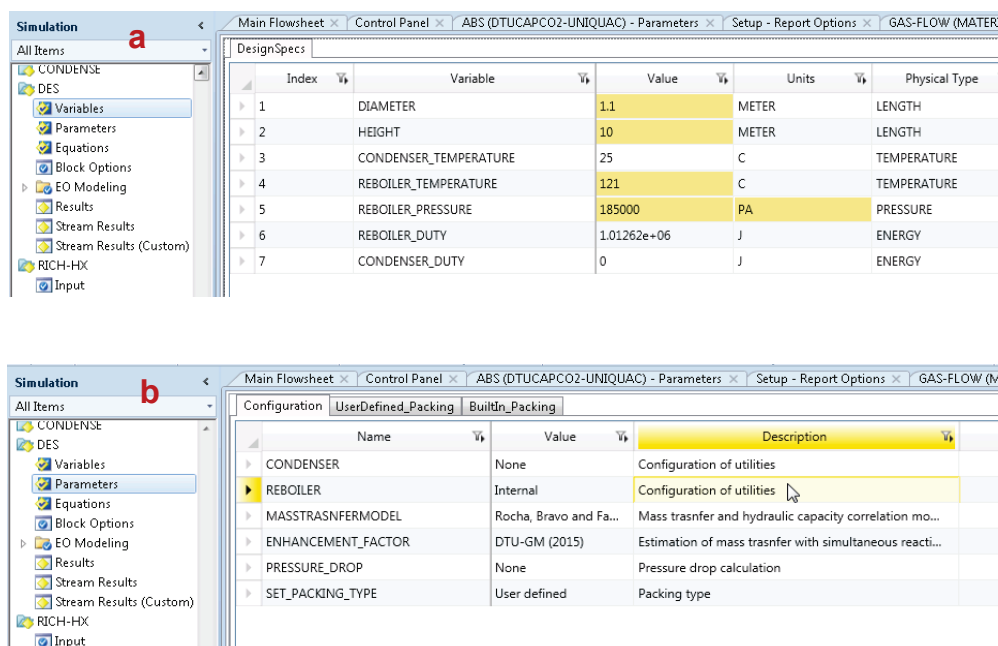

Figure D.13. Desorber configuration: (a) Variables and (b) Parameters.

These are the steps of building and specifying a basic post-combustion capture process using the DTU CAPCO2 rate-based model. At this point the simulation is ready to be run.

The simulation results show that 4.839428 kmol/h CO_2 will be released to the atmosphere in the WETGAS stream and 16.75662 kmol/h CO_2 will be recovered in CO2-WET stream. The heat demand of this process is 0.888704 MW. Therefore, the capture process is not operated neither at optimal nor at 90% CO_2 capture percentage. In the following, a possible approach for preparing a closed loop simulation is described. This approach uses Aspen Plus design specs to recover the same amount of CO_2 in the desorber as captured in the absorber.

Design specs for fixed 90% CO_2 removal

It is a good practice to set up design specifications for keeping 90% CO_2 absorption and CO_2 stripping percentage. For this, design specifications are needed. In this example, we will keep the 90% CO_2 removal rate by modifying the lean solvent flow rate to the absorber and by modifying the operating temperature of the reboiler.

Note, the parameters from the "*Variables*" menu, e.g. diameter, height, condenser temperature, reboiler temperature and pressure respectively condenser and reboiler duty, can be accessed in the design spec window of Aspen Plus, as shown in Figure D.14.
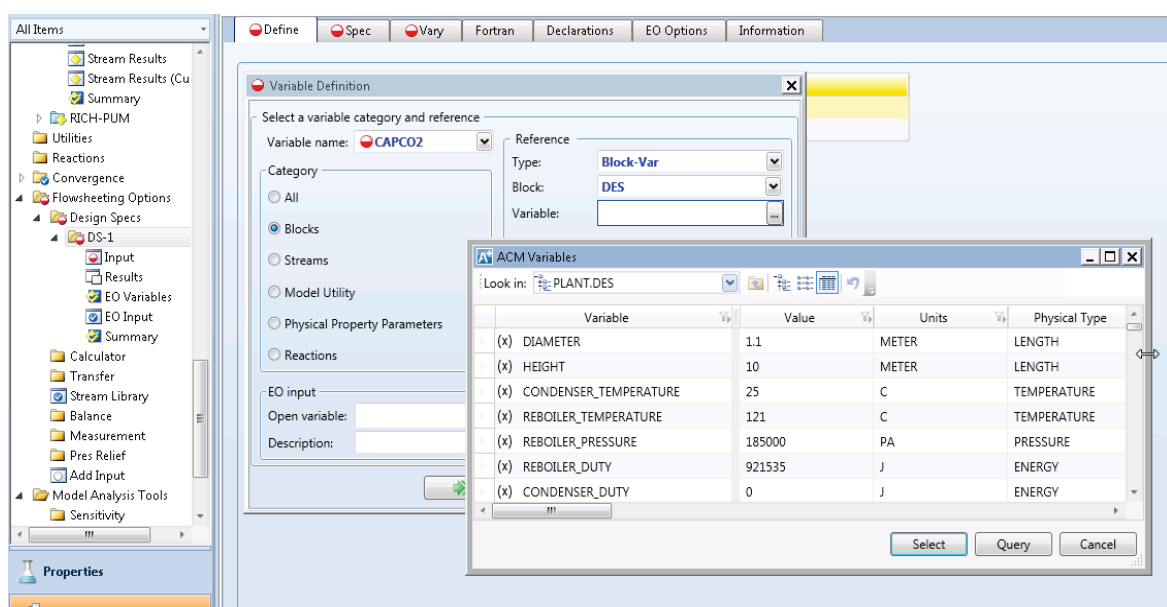

Figure D.14. CAPCO2 user model parameters in Aspen Plus

90% CO₂ absorption

Set up a design specification which modifies the lean solvent flow rate in order to maintain 90% CO_2 absorption percentage. Figure D.15 shows the settings for "Define", "Spec" and "Vary" tabs.

90% CO₂ stripping

Set up a design specification which modifies the reboiler temperature in order to maintain 90% CO_2 removal percentage. Figure D.16 shows the settings for the "Define", "Spec" and "Vary" tabs.

Figure D.15. Design Spec for 90% CO_2 absorption

Figure D.16. Design Spec for 90% CO2 removal rate

The simulation is configured and ready to be executed. Some calculation results are shown in Table D.2.

Table D.2. Simulation results for the CO_2 post-combustion capture process

Parameter\Stream	WET-GAS	CO2-WET	LEAN-OUT
Temperature (°C)	40	83.48761	118.827
Pressure (bar)	1	1.85	1.85
Mol flow (kmol/h)			
MEA			64.40188
H2O	11.72075	6.707272	444.2738
CO2	2.363239	19.13511	12.7275
N2	144.1438	6.4922E-11	
Calculated duties			
Heat duty of the absorber condenser (MJ)	0.414092		
Heat duty of the desorber reboiler (MJ)	0.959967		
Reboiler temperature (°C)	121.03		
Heat duty of RICH-HX (MW)	0.6847882		
Heat duty of CONDENSE (MW)	-0.133266		

Simulation of Lean-Vapor-Compression

This section presents an optimized approach to simulate Lean-Vapor-Compression (LVC) using the DTU-CAPCO2 model in Aspen Plus. The flowsheet for LVC as used in this work is presented in Figure D.17.
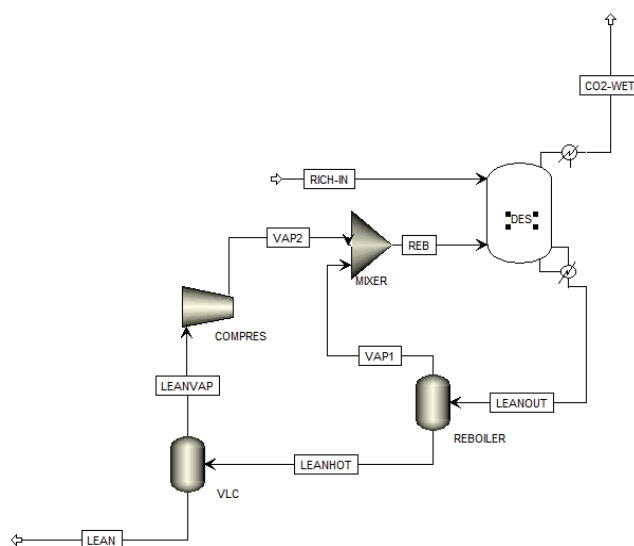
Figure D.17. Flowsheet for the LVC configuration

First, configure the desorber column as shown in Figure D.18.a and Figure D.18.b. Set the "REBOILER" field to "*None*" in the "*Parameters*" menu (Figure D.18.a) and set the diameter and height of the column respectively the reboiler pressure as shown in Figure D.18.b.

Figure D.18. Desorber configuration for LVC simulation

Furthermore, in *Blocks* of the *Simulation* window select the *DES* unit. In the B*lock Options* of click on "*Simulation options*" and **uncheck** the **"*Bypass the block if the total flow is zero*"** option, see Figure D.19.

Figure D.19. Modifying the block options of the desorber column

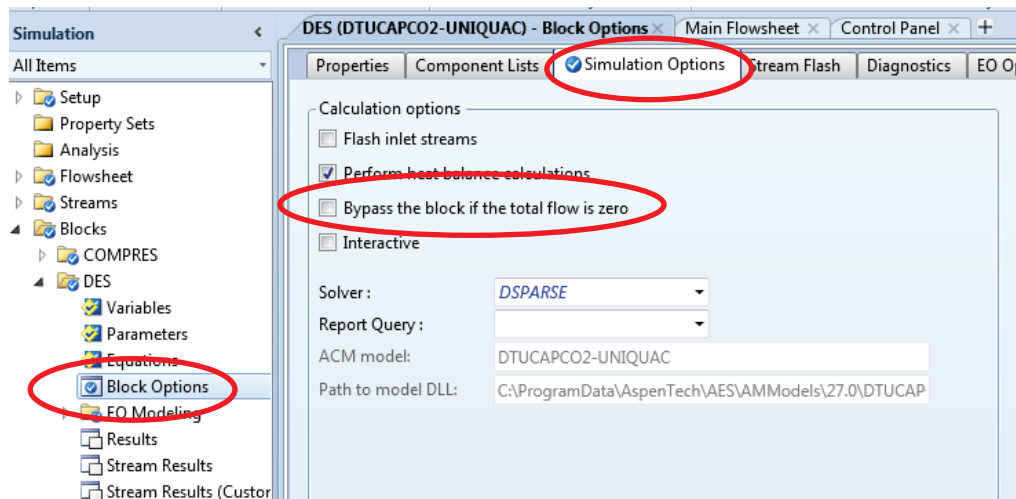Afterwards, in the *Convergence* block of the *Simulation* window select *Tear* and specify the LEANOUT stream as tear stream, see Figure D.20. Note, the lean exiting the desorber must be specified as tear stream. We recommend using a tolerance of 1E-4.
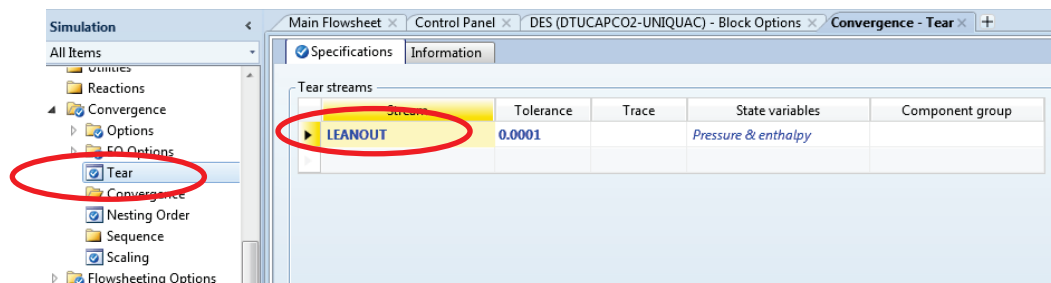
Figure D.20. Setting a tear stream in Aspen Plus

Finally, set the other units using the specifications in Table D.3 and run the simulation.

Table D.3. Specifications for the Aspen Plus built-in units

Unit	Parameter
REBOILER	Temperature = 121 C; Pressure = 1.85 bar
VLC	Duty = 0 W; Pressure = 1.2 bar
COMPRES	Type : Isentropic; Discharge Pressure = 1.85 bar
MIXER	PRESSURE = 1.85 bar

References

Billet, R., Schultes, M., 1999. Prediction of mass transfer columns with dumped and arranged packings - Updated summary of the calculation method of Billet and Schultes. Chem. Eng. Res. Des. 77, 498–504. doi:10.1205/026387699526520

Gaspar, J., Fosbøl, P.L., 2015. A general enhancement factor model for absorption and desorption systems: A CO2 capture case-study. Chem. Eng. Sci. 138, 203–215. doi:http://dx.doi.org.globalproxy.cvt.dk/10.1016/j.ces.2015.08.023

Rocha, J.A., Bravo, J.L., Fair, J.R., 1993. Distillation-Columns Containing Structured Packings - a Comprehensive Model for their Performance .1. Hydraulic Models. Ind. Eng. Chem. Res. 32, 641–651. doi:10.1021/ie00016a010

Tremblay, D., Peers, Z., 2014. Jump Start: Aspen Custom Modeler V8. Burlington, MA Aspen Technol. Inc.

Appendix E - Multivariable Optimization of the Piperazine CO$_2$ Post-Combustion Process

Jozsef Gaspar[a], Nicolas von Solms[a], Kaj Thomsen[a], Philip Loldrup Fosbøl[a2]

^{a}Technical University of Denmark, Department of Chemical Engineering, Center for Energy Resource Engineering (CERE), Søltofts Plads, 2800, Kgs. Lyngby, Denmark

Abstract

8 molal piperazine (PZ) is a promising solvent for developing an energy efficient CO$_2$ post-combustion capture process. However, it has a limited operating range due to precipitation. The operating range can be extended by decreasing the piperazine concentration and/or increasing the CO$_2$ loading of the lean solvent. However, optimal solvent composition must be determined taking into account the solvent circulation rate and the heat demand of the solvent regeneration.

In this paper, we determine and generalize trends of performance for a broad range of operating conditions: 1.8 to 9 mol PZ/ kg water, 0.2 to 0.6 lean loading, and for two flue gas sources: natural gas combined cycle power plant (NGCC, 3.9 mol% CO$_2$) and a coal based power plant (ASC, 13.25 mol% CO$_2$). Special attention is given to the boundaries where precipitation may occur. The results are created by the hybrid CAPCO2 rate-based model which accounts for precipitation when estimating the heat and mass transfer rates. The results show that the 7 molal piperazine gives the lowest specific reboiler duty at 0.40 CO$_2$ lean loading: 3.32 GJ/t CO$_2$ and 4.05 GJ/t CO$_2$ for the ASC case and NGCC cases. The analysis also reveals that the capture process needs to be operated up to 7.8 % above the minimum duty to avoid the risk of clogging due to solid formation. Note, this analysis assumes a 25 °C minimum solvent temperature. The energy requirement of the capture process can be further improved by assuming a minimum solvent temperature of 30 ºC which gives a specific reboiler duty of 3.23 GJ/t CO$_2$ (ASC case) and 3.80 GJ/t CO$_2$ (NGCC case).

Keywords: CO$_2$ capture; piperazine; rate-based simulation and optimization; solubility; extended UNIQUAC; specific reboiler duty; L/G ratio.

Introduction

   Flexibility is a core benefit of the post-combustion CO$_2$ capture technology. It offers adaptabilities through scale-up possibilities, part-load operation during peak electricity price periods, and retrofit to existing power plants. Currently it is an energy efficient and mature solution. Thus, post-combustion capture is the most promising short and mid-term solution for decreasing the CO$_2$ emissions.

   The focus of this study is the piperazine (PZ) based CO$_2$ post-combustion capture process. Recent modeling and experimental studies have shown that 8 m PZ has double the CO$_2$ absorption rate and capacity compared to 7 m MEA [1]. There are other benefits of PZ such as moderate heat of absorption and thermal stability. However, the 8 m PZ solution has a limited operating range due to solubility issues. It precipitates at both lean and rich process conditions [2-4].

   The operating range can be extended by decreasing the piperazine concentration of the solvent. 5 molal PZ is a promising alternative to eliminate the limitations but still retain the benefits of 8 m PZ. Chen et al. [1] demonstrates that the absorption rate of 5 m PZ is approximately 30% higher than 8 m PZ. However, the absorber must be operated at a higher L/G ratio to achieve 90% CO$_2$ removal. Furthermore, precipitation can be avoided by using a higher lean loading. Fosbøl et al. presents how the precipitation-free operational range grows exponentially with CO$_2$ loading

indifferent of piperazine composition [4]. They show that an 8 molal PZ solution does not precipitate above 0.40 CO_2 loading at 25°C.

The optimum solvent composition needs to be determined based on a circulation rate and energy demand, considering the solubility limit of PZ. It is worth noting that process conditions needs to be (re)optimized for each concentration value to assure a consistent and fair comparison of the solvent capacity and energy demand of the process. This analysis requires a systematic and thorough study showing the performance of PZ for a broad concentration and CO_2 loading range.

The aim of this study is to perform a systematic and comprehensive evaluation of the absorption capacity and mass transfer benefits of a 1.8, 3, 5, 7, 8 and 9 m PZ solution, for two flue gas sources: natural gas combined cycle (3.9 mol% CO_2) and a coal based power plant (13.25 mol% CO_2). In this work, optimum process conditions, e.g. L/G ratio, lean loading, column specifications are determined for each PZ concentration. The results are created using the DTU in-house hybrid CAPCO2 rate-based model for CO_2 absorption and desorption calculations [3]. Hybrid CAPCO2 is to our knowledge a first-of-its-kind rate-based model which includes solid precipitation in the mass and heat transfer estimation.

The rate-based model of a precipitating CO_2 capture process

In this work, the hybrid CAPCO2 in-house rate-based model is implemented to simulate CO_2 absorption and desorption. Compared to traditional rate-based models, hybrid CAPCO2 includes solid-liquid phase change when predicting the CO_2 mass and heat transfer rate between the gas phase and the liquid phase. This model was compared to pilot plant data. The analysis reveals a good agreement between the model and experiments [3].

The hybrid rate-based model is built on the core of the original CAPCO2 model. It is formulated as a boundary value problem with specified inlet conditions and calculated outlet conditions. The lean temperature, pressure, composition and flow rate are specified at the top of the column. The temperature, pressure, composition and flow rate of the gas are fixed at the bottom of the column. In case of a desorber, the gas stream results from an integrated reboiler unit and only the reboiler temperature and pressure have to be specified. The rate-based model is built on mass and energy balances for the liquid phase and gas phase. They are solved simultaneously with algebraic equations for mass and hydraulic properties, mass and heat transfer fluxes, and the extended UNIQUAC thermodynamic model. Extended UNIQUAC is a rigorous model which is able to accurately predict solid precipitation [4-6]. This model gives the phase equilibria and thermal properties. The numerical approach and the equation system of CAPCO2 are presented in previous works [7,8].

The mass and heat transfer fluxes are determined in a film theory approach, using the General Method (GM) enhancement factor model [3,9]. GM connects the Onda's approximation for reversible reactions with the van Krevelen's approach for instantaneous irreversible reactions. Therefore, it is valid for both, absorber and desorber conditions, and for high driving forces and pinch conditions. It eliminates many of the limitations of existing enhancement factor models. Note that this is of crucial importance since absorption of carbon dioxide involves finite rate reactions [10].

Table 1. Used physical properties correlations for aqueous piperazine

Parameter	Expression/Source	Validation data
Density	$\rho = \rho_{H_2O} + 0.04796 \cdot w_{PZ}$	[11-16]
Viscosity	Dugas, 2009 [17]	[11-16]
Surface tension	$\sigma = 71.8623 - 0.1255\left(T - 293.15\right) - 17.9983 \cdot w_{PZ}$	[12,14,15]
Diffusivity of CO_2 and PZ in unloaded solution	Dugas and Rochelle, 2011 [18]	[10,11,19,20]

In this work, the Rocha et al. model predicts the mass transfer coefficients, the liquid hold-up and the interfacial area [21,22]. The necessary physical property parameters, e.g. diffusivities, surface tension, viscosity, conductivity, density and etc. entering this model has been evaluated and validated against experimental data. The physical properties describing the gas phase are presented in [7]. Table 1 gives an overview of these correlations for the liquid phase.

Process boundaries and design specifications

The absorber and the desorber are designed for a nominal theoretical 250 MWe capacity advanced supercritical pulverized coal power plant (ASC) respectively a 250 MWe capacity natural gas combined cycle power plant (NGCC). The ASC plant produces 238 kg/s flue gas, with a CO_2 concentration of 13.25 mol%. The NGCC plant produces 386.33 kg/s flue gas with 3.90 mol% CO_2. We assume that the gas from ASC respectively NGCC passes through a DeNOx plant, a wet limestone based desulphurization plant and a direct contact cooler for the control of combustion products. Therefore, the flue gas contains only CO_2, inert gases and it is saturated with water at the absorber inlet temperature, 40 °C.

Table 2. Main inlet and outlet specifications for the absorber and the desorber

Parameter	Unit	ASC	NGCC
Flue gas flow rate	kg/s	238.46	386.33
Flue gas temperature	°C	40	40
Flue gas pressure	kPa	101.6	101.6
Flue gas CO_2 composition	mol%	13.25	3.90
Flue gas H_2O composition	mol%	12.11	8.20
Lean inlet temperature	°C	40	40
Lean loading	mol/mol	0.2 – 0.6	0.3 – 0.6
Rich loading	mol/mol	0.65 – 0.8	0.6 – 0.7
Piperazine concentration	mol/kg water	1.8 – 9	1.8 – 7
L/G ratio	mol/mol	2 – 12	0.5 – 5
Reboiler pressure	kPa	190	190

In the absorber the flue gas is washed with lean piperazine solution. The concentration of the lean solvent for the ASC case is varied between 1.8 and 9 mol PZ/kg H_2O and 0.20 to 0.60 CO_2 loading. The covered PZ concentration range for the NGCC case is from 1.8 to 7 mol PZ/kg H_2O. Higher piperazine concentrations are not feasible and results in insufficient wetting of the column due to the low solvent flow rate. Note that the lean loading and the operating temperature range are chosen taking into account the solubility window of the loaded piperazine solution. Table 2 summarizes the main operating conditions for the absorber and the desorber.

The absorber and the stripper are packed columns equipped with Sulzer Mellapak 2X structured packing. This packing offers low pressure drop and can be used for wide range of liquid loads. The carbon capture plant is designed for 90% CO_2 removal percentage. The diameter of the columns is calculated for an operating velocity of 70% flooding and it varies between 10 and 15 m. A minimum diameter of 10 m is required to accommodate the gas flow resulting from the ASC and NGCC plant. In this work, an 18 m tall absorber column is used. A sensitivity study has shown that the CO_2 capture efficiency increases with the column height up to 18 m, and then it remains unchanged. A similar behavior is shown in [23]. Based on the approach for the absorber, the height of the stripper is set to 14 m.

Results and discussion

This section shows a parametric sensitivity study to determine the effect of the lean solvent PZ and CO_2 concentration on energy demand and solvent recirculation flow rate. Moreover, it presents the effect of pressure on the energy performance of stripping and compression and it underlines the operating conditions where precipitation may occur. The present analysis demonstrates how the CO_2 capture process must be operated above optimal conditions to avoid clogging due to solid formation.

Thermodynamic analysis

We perform a thermodynamic analysis to determine the precipitation boundary and the maximum capacity of the solvents. This analysis gives the upper and the lower limit for the CO_2 loading range. The approach of this work is to determine the CO_2 loading at which the first solid particle appears for a given piperazine concentration at 25 °C. It corresponds to the minimum loading value required for solid-free operation. Here it is determined using the extended

UNIQUAC thermodynamic model [4-6]. Note that 25 °C is chosen as the minimum temperature and any colder condition will results in solid formation at lower loadings. In this work, the loading is defined as moles of CO_2 per 1 mol of piperazine.

Table 3 shows the results for various PZ concentrations. In general the concentrations 3 molal piperazine or above will precipitate a solid. A high loading removes precipitation. This is reflected in the thermodynamic analysis which reveals how the minimum CO_2 loading exponentially increases with respect to piperazine concentration. A 1.8 molal solution will not precipitate at 25 °C, while a 9 molal needs 0.42 loading or else it will precipitate piperazine.

Table 3. Lower and upper limit of the CO_2 loading range for the ASC and the NGCC case

Solvent concentration (mol PZ/kg water)	1.8	3	5	7	8	9
Solvent concentration (wt. %)	13.4	20.5	30.1	37.6	40.8	43.7
Minimum CO_2 loading at 25 °C (mol/mol)	0	0.169	0.339	0.400	0.414	0.422
Maximum rich loading – ASC at 50 °C (mol/mol)	0.833	0.808	0.804	0.796	0.792	0.781
Maximum rich loading - NGCC at 50 °C (mol/mol)	0.720	0.716	0.712	0.707	0.735	0.670

Furthermore, a thermodynamic analysis is carried out which shows the maximum rich loading, corresponding to an isothermal absorber at 50 °C. It is reached when equilibrium prevails in the bottom of the absorber. The value, called rich loading, is an expression of the solvent capacity. A low rich loading results in less captured CO_2 and a high rich loading gives more removal of CO_2 per solvent. Table 3 gives the value for both the ASC and the NGCC cases for different piperazine concentrations. It outlines that the solvent capacity (rich loading) linearly decreases with respect to the piperazine concentration. It underlines how the rich loading for the NGCC case is smaller than for the ASC case. It is approximately 0.80 mol/mol for the ASC case and it is roughly 0.70 mol/mol for the NGCC case. The decrease of the maximum rich loading is due to the lower partial pressure of CO_2 in the flue gas.

There is a clear link between the piperazine concentration and the CO_2 loading of the solvent for determining the solid-free operation window. The risk of clogging due to solid formation is higher in concentrated piperazine solutions. The minimum loading, to avoid solid formation above 25 °C, increases from 0 to 0.42 mol CO_2/mol PZ, when the concentration increases from 1.8 to 9 mol PZ/kg water. Basically, the solid-free loading range shrinks when increasing the piperazine concentration due to the lower maximum rich loading values. The specific ranges are smaller for the NGCC case compared to the ASC case.

Effect of lean composition on L/G ratio

This section utilizes a thorough rate-based calculation strategy. It shows the importance of lean composition on the L/G ratio, required for 90 % CO_2 capture. The focus is on evaluating the benefits of increasing the PZ concentration and/or decreasing the CO_2 loading of the lean. The 90% CO_2 capture is reached by adjusting the lean solvent flow rate. It is important to note that a higher L/G ratio results in greater pump work and it requires a wider column to keep a constant 70% of flooding.

Fig. 1A and Fig. 1B show the L/G ratio and the lean solvent flow rate at 90% CO_2 capture for the ASC and NGCC cases using 3, 5, and 7 molal piperazine as function of the lean CO_2 loading. Note that the flue gas flow rate for the ASC case is 238.46 kg/s respectively 386.33 kg/s for the NGCC case. These figures outline that both, PZ concentration and the CO_2 lean loading, have a great impact on the L/G ratio, independent of the flue gas source. The L/G ratio slowly increases up to 0.40 lean CO_2 loading, followed by a sudden rise up to 0.50 CO_2 load. Furthermore, Fig. 1A underlines that the L/G ratio reduces significantly when increasing the solvent concentration. An increase of the PZ content from 3 to 5 molality decreases the L/G ratio with approximately 2 units (ASC case) respectively 0.5 units (NGCC case).
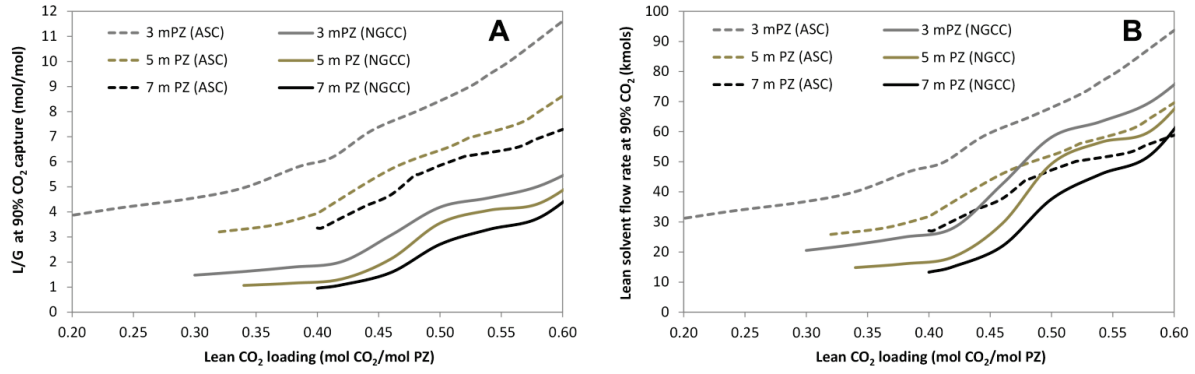
Fig. 1. (A) L/G ratio at 90% CO$_2$ capture and (B) lean solvent flow rate as function of lean loading for different solvent concentrations for the ASC and the NGCC case

In addition, Fig. 1A shows that the L/G ratio is more than double for the ASC case compared to the NGCC case. However, looking at the solvent flow rate, Fig. 1B, it can be seen that, at high lean loadings, the lean solvent flow is comparable between the ASC and the NGCC scenarios. Fig. 1B underlines that the solvent flow required for 90 % CO$_2$ capture increases suddenly from 0.40 to 0.50 loading. This sudden change in the flow rate is more visible for the NGCC case. This unexpected behavior was analyzed by Plaza et al. [24] and Darshan et al. [25]. They show how mass transfer pinch occurs at the location of the temperature bulge for intermediate lean loadings and it results in capture capacity penalties. It has to be noted that the temperature bulge is located near to the top of the column at the low lean loadings. This phenomenon can be avoided by implementing intercooling. At high lean loading, the L/G ratio is sufficiently large to reduce the magnitude of the temperature bulge. Therefore, temperature related mass transfer limitations are avoided at low and high loadings for these conditions.

Note in Fig. 1A and Fig. 1B how the lines are not drawn below approximately 0.3 and 0.4 lean loading due to precipitation issues, see Table 3.

Effect of pressure on energy performance

The effect of the reboiler operating pressure on energy performance is evaluated in this section. The performance of the system is described in terms of equivalent work which shows the work lost from the turbine upstream of the power plant plus the work needed to compress the pure CO$_2$ product stream. Thus, it contains the heat used in the stripper and the electricity needed by the compressors.

The focus is on exemplifying the correlation between pressure and equivalent work as function of piperazine concentration using the specifications of the ASC and the NGCC cases. In this analysis, the operating pressure of the reboiler is chosen (190 and 250 kPa) and the steam input to the reboiler is varied to reach 0.30 respectively 0.42 CO$_2$ lean loading. These loadings correspond to the minimum CO$_2$ loading for solid-free operation of a 4.5 molal respectively 9 molal piperazine solution at 25 ºC. Note that all of the other variables, e.g. diameter, feed flow rate, rich loading, etc. are kept constant to purely isolate the effect of pressure on the performance of the system.

The equivalent work is given by eq. (1). A typical value for the Carnot cycle efficiency with a turbine cycle efficiency of $\eta = 75\%$ is assumed. In addition, we use $\Delta T = 5K$ temperature difference and the temperature of the sink, T_{sink}, is taken as 313 K. The compression work, $W_{compression}$, is estimated using the correlation from [26].

$$W_{eq} = \eta \left(\frac{T_{source} + \Delta T - T_{sink}}{T_{source} + \Delta T} \right) Q_{reboiler} + W_{compression} \tag{12}$$

Fig. 2 shows the equivalent work as function of solvent concentration at 190 kPa and 250 kPa for 0.30 and 0.42 loadings. The results outline the benefits of increasing the piperazine concentration. The equivalent work exponentially decreases all the way up to 7 molality for all reboiler pressures and lean loadings. Further increase of the concentration to 9 molal only leads to minor reduction of the energy demand.
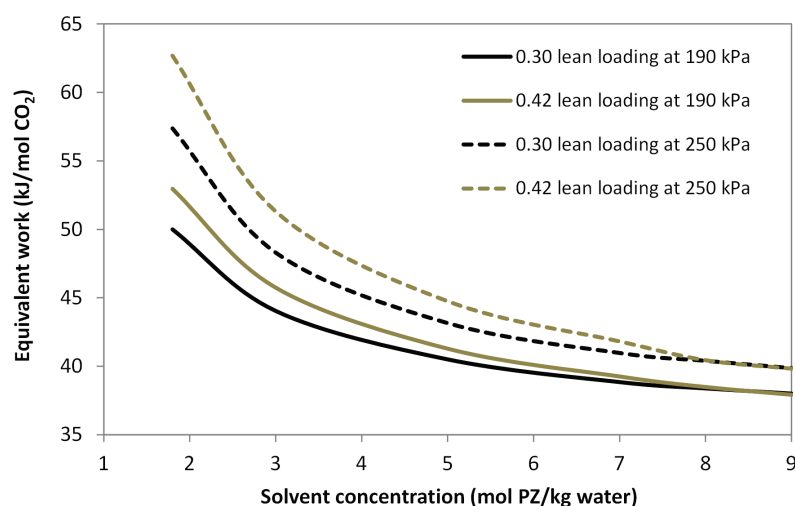
Fig. 2. . Equivalent work as function of solvent concentration at 190 and 250 kPa for the ASC and NGCC cases.

In addition, this figure emphasizes that the energy demand of CO_2 stripping and compression is generally lower at 0.30 loading compared to 0.42 CO_2 load. However, the difference between the isobars diminishes for more concentrated solutions and they overlap above 8 molality. Furthermore, this figure outlines that the equivalent work is 7 to 20% less at 190 kPa compared to 250 kPa. Based on the experience with monoethanolamine (MEA), the opposite would be expected. However the same behavior was shown experimentally by van Wagener et al. for 8 molal PZ [27].

It can be concluded that it is less energy intensive running the stripper at 190 kPa than at 250 kPa. In addition, the 5 molal piperazine case seems to be the most promising solvent since further concentrating the solvent results in minor energy improvement but exponential increase of the minimum CO_2 loading due to solid formation.

Effect of lean composition on energy performance

We now investigate the performance of the stripper for various operating conditions using solvents with different piperazine concentrations. The performance of the stripper is quantified in terms of specific reboiler duty (SRD), the heat (GJ) needed to strip out 1 ton of CO_2. In this analysis, the steam input to the reboiler is varied at fixed rich loading and reboiler pressure of 190 kPa. Other parameters which influence the performance of the system, e.g. pressure, height, diameter, are kept constant to isolate the effect of lean composition on the heat demand. Note that the rich loading for the ASC case is 0.8 mol CO_2/mol PZ and it is 0.7 for the NGCC case. These values correspond to the maximum rich loading. Therefore, the heat demand of the stripper may be slightly higher for integrated simulations. However, we adopt this approach to isolate the effect of the absorber from the desorber.

Fig. 3 presents the specific reboiler duty (SRD) versus the lean loading for the ASC and NGCC case using 3, 5 and 7 molal piperazine solutions. This figure highlights that the heat demand of the solvent regeneration reduces exponentially with respect to lean loading. It reduces until it reaches a minimum around 0.25 CO_2 loading. This minimum corresponds to the optimum operating conditions and it is reached when the water condensation balances the heat required for solvent regeneration. Below the optimum lean loading, the heat input to the stripper is too high and the excess of heat is mostly consumed by evaporation of water. Above the optimum point, the steam flow to the reboiler is insufficient and it results in a low CO_2 recovery rate. This case corresponds to a low energy input system. Even though it requires a low energy input it is not feasible as seen in Fig. 3 by the higher SRD compared to the minimum.
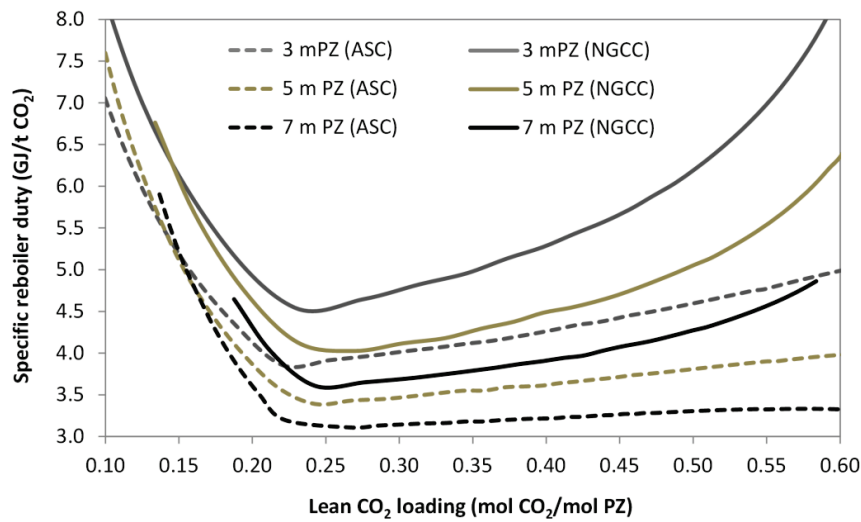
Fig. 3. Specific reboiler duty as function of lean loading for the ASC and the NGCC case.

Furthermore, Fig. 3 demonstrates that the reboiler duty varies with respect to piperazine concentration and flue gas type. It shows how the energy demand of the NGCC case is roughly 0.7 GJ/t CO_2 higher compared to the ASC case. This is due to the lower rich CO_2 loading of the desorber feed.

The figure demonstrates that the 7 molal solution has the best energy performance for both cases (ASC and NGCC) and it is approximately 15 – 20 % smaller compared to the 3 molal case. The optimum lean loading and optimum SRD for 3, 5 and 7 molal solutions are shown in Table 4. The feasible SRD can be further reduced to 3.15 GJ/t CO_2 for the ASC case when using a 9 molal PZ solution. However, the risk of solid formation becomes considerably higher and the safe operation range shrinks to the 0.42 – 0.78 loading range. Moreover, the full benefit of highly concentrated solutions can be reached only using intercooling. A 0.18 GJ/t CO_2 saving seems to be insignificant compared to the capital and operational cost of an absorber with intercooling.

Table 4. Optimum and feasible energy performance of the stripper for 3, 5 and 7 m PZ solution for the ASC and the NGCC scenario

Flue gas source	Piperazine concentration	Optimum lean loading	Optimum SRD	Minimum lean loading	Feasible SRD	Energy penalty
	mol PZ/kg water	mol CO_2/mol PZ	GJ/ ton CO_2	GJ/ ton CO_2	GJ/ ton CO_2	(%)
ASC	3	0.221	3.855	0. 169	3.854	0
	5	0.242	3.389	0.339	3.519	3.7
	7	0.258	3.173	0.400	**3.327**	4.6
NGCC	3	0.229	4.545	0. 169	4.545	0
	5	0.269	4.025	0.339	4.484	10.2
	7	0.271	3.736	0.400	**4.051**	7.8

* Energy penalty(%) = (Feasible SRD – Optimum SRD)/ Feasible SRD · 100

It can be seen by comparing the optimum lean loading, Table 4, with the minimum lean loading, Table 3, that generally the minimum lean loading is greater than the optimum value. Note the minimum lean loading is the limit at which the first precipitate appears at 25 °C. The optimum lean loading corresponds to the best SRD, as shown in Fig. 3. For example, a 5 molal solution has an optimum lean loading of 0.24 but the minimum lean loading is 0.34. Therefore, the stripper must be operated above the optimum loading to avoid solid formation. This energy penalty is quantified as the relative difference between the feasible SRD and optimum SRD and it is given in Table 4. The feasible SRD corresponds to the specific reboiler duty in the solid-free domain. The solid free domain is above the minimum lean loading.

Table 4 shows the energy penalty for 3, 5 and 7 molal solution for the ASC and NGCC cases. It illustrates that the energy penalty is greater for the NGCC scenario. It can be seen that the lowest feasible specific duty is 3.32 GJ/t CO_2

and 4.05 GJ/t CO_2 for the ASC and NGCC case respectively. This value corresponds to the 7 molal PZ for both cases. A possible approach to expand the safe and precipitation-free domain is to assume a minimum solvent temperature (precipitation boundary) of 30 °C. However, additional heating of the storage and buffer tanks and appropriate control structures are needed. Operational challenges may appear especially in Nordic countries or during winter. However, a greater minimum solvent temperature allows the operation of the plant at 3.13 GJ/t CO_2 respectively 3.74 GJ/t CO_2 reboiler duty for the ASC and NGCC cases.

Conclusions

This work shows a systematic evaluation of a CO_2 post-combustion capture process for 1.8, 3, 5, 7, 8, and 9 molal piperazine solutions. It shows the results for two flue gas sources: an advanced supercritical pulverized coal power plant (ASC) with 13.25 % CO_2 and a natural gas combined cycle power plant (NGCC) with 3.90 % CO_2. The results are created using the hybrid CAPCO2 in-house rate-based model for CO_2 absorption and desorption. This model takes into account precipitation of piperazine in the description of mass transfer and in the calculation of the equilibrium composition. They are determined using the extended UNIQUAC thermodynamic model. The mass and heat transfer fluxes are described in a film-theory approach, using the General Method (GM) enhancement factor model. This model is valid for both absorption and desorption conditions.

This study shows the optimum PZ concentration, CO_2 loading and the corresponding solvent flow rate. It underlines that the L/G ratio and the reboiler duty strongly depend on the piperazine concentration and CO_2 loading. Furthermore, it underlines that the energy demand of the process is a strong function of CO_2 partial pressure of the flue gas due to the decrease of the solvent capacity (maximum rich loading). Higher partial pressure gives a greater maximum rich loading corresponding to greater solvent capacity. Furthermore, we demonstrate how the value of the rich loading greatly influences the performance of the stripper and it is an important criterion for the design of an absorber. A rich loading of 0.70 mol CO_2/mol PZ, corresponding to NGCC case, gives 0.7 GJ/t CO_2 higher energy demand compared to a 0.80 rich loading, ASC case. Other important parameter for the performance of the system is the operating pressure of the reboiler. The simulations show how a greater pressure results in higher energy demand, especially at lower CO_2 lean loading and piperazine concentration. The effect of pressure on energy demand diminishes when increasing the piperazine concentration above 7 molal.

This analysis demonstrates that the 7 molal solution has the best energy performance for both cases (ASC and NGCC) and it is approximately 15 – 20 % smaller compared to the 3 molal case. The lowest feasible specific reboiler duty can be reached at 0.40 CO_2 lean loading: 3.32 GJ/t CO_2 and 4.05 GJ/t CO_2 for the ASC case and NGCC cases. The analysis also reveals that the capture process needs to be operated up to 7.8 % above the minimum duty to avoid the risk of clogging due to solid formation. Note this analysis assumes a 25 °C minimum solvent temperature. The energy requirement of the capture process can be further improved by assuming a greater minimum temperature when the reboiler duty lowers to 3.17 GJ/t CO_2 (ASC case) and 3.73 GJ/t CO2 (NGCC case). However, it may require additional heating of storage tanks and more complex control structure, especially in cold-winter conditions. The energy demand of stripping reduces to 3.15 GJ/t CO_2 for coal based cases when using a 9 molal solution and absorber with intercooling. However, the solid-free operation window of this system is significantly smaller compared to the 7 molal solution.

The SRD calculations performed in this work are deliberately based on process calculations without any particular optimization or heat integration in mind. This is purely set up with the strategy to perform a basic comparison of the process conditions, without too much interference from other types of optimization. There is still at great potential for further decreasing the SRD by more advanced heat integration. The local design optima found in this work will most likely remain optima in more advanced heat integration scenarios.

Since implementation of CO_2 capture in a coal-fired power plant will introduce significant capital and operating cost, other process configurations as well as dynamic-optimal scheduling of a capture process should also be studied. This study provides the base to build on by emphasizing the benefits and drawbacks of piperazine for the relevant operating process conditions.

References

[1] Chen E, Fulk S, Sache D, Lin Y, Rochelle GT. Pilot Plant Activities with Concentrated Piperazine. Energy Procedia 2014;63:1376-91.
[2] Fosbol PL, Neerup R, Arshad MW, Tecle Z, Thomsen K. Aqueous Solubility of Piperazine and 2-Amino-2-methyl-1-propanol plus Their Mixtures Using an Improved Freezing-Point Depression Method. J Chem Eng Data 2011;56:5088-93.
[3] Gaspar J, Thomsen K, von Solms N, Fosbøl PL. Solid Formation in Piperazine Rate-based Simulation. Energy Procedia 2014;63:1074-83.

[4] Fosbøl PL, Maribo-Mogensen B, Thomsen K. Solids Modelling and Capture Simulation of Piperazine in Potassium Solvents. Energy Procedia 2013;37:844-59.

[5] Thomsen K, Rasmussen P. Modeling of vapor–liquid–solid equilibrium in gas–aqueous electrolyte systems. Chemical Engineering Science 1999;54:1787-802.

[6] Thomsen K, Rasmussen P, Gani R. Correlation and prediction of thermal properties and phase behaviour for a class of aqueous electrolyte systems. Chemical Engineering Science 1996;51:3675-83.

[7] Gabrielsen J. CO2 Capture from Coal Fired Power Plants. 2007.

[8] Fosbøl PL, Thomsen K, Stenby EH. Energy demand for CO2 solvent regeneration. 2009;Proceedings:242-252.

[9] Gaspar J, Fosbøl PL. A general enhancement factor model for absorption and desorption systems: A CO2 capture case-study. AIChE Journal (under review).

[10] Derks PWJ, Kleingeld T, van Aken C, Hogendoom JA, Versteeg GF. Kinetics of absorption of carbon dioxide in aqueous piperazine solutions. Chemical Engineering Science 2006;61:6837-54.

[11] Sun WC, Yong CB, Li MH. Kinetics of the absorption of carbon dioxide into mixed aqueous solutions of 2-amino-2-methyl-l-propanol and piperazine. Chemical Engineering Science 2005;60:503-16.

[12] Derks P, Hogendoorn K, Versteeg G. Solubility of N2O in and density, viscosity, and surface tension of aqueous piperazine solutions. J Chem Eng Data 2005;50:1947-50.

[13] Samanta A, Bandyopadhyay S. Density and viscosity of aqueous solutions of piperazine and (2-amino-2-methyl-1-propanol + piperazine) from 298 to 333 K. J Chem Eng Data 2006;51:467-70.

[14] Muhammad A, Mutalib MIA, Murugesan T, Shafeeq A. Thermophysical Properties of Aqueous Piperazine and Aqueous (N-Methyldiethanolamine plus Piperazine) Solutions at Temperatures (298.15 to 338.15) K. J Chem Eng Data 2009;54:2317-21.

[15] Murshid G, Shariff AM, Keong LK, Bustam MA. Physical Properties of Aqueous Solutions of Piperazine and (2-Amino-2-methyl-1-propanol + Piperazine) from (298.15 to 333.15) K. J Chem Eng Data 2011;56:2660-3.

[16] Freeman SA, Rochelle GT. Density and Viscosity of Aqueous (Piperazine plus Carbon Dioxide) Solutions. J Chem Eng Data 2011;56:574-81.

[17] Dugas RE. Carbon Dioxide Absorption, Desorption and Diffusion in Aqueous Piperazine and Monoethanolamine. 2009, December;University of Texas at Austin.

[18] Dugas RE, Rochelle GT. Modeling CO2 absorption into concentrated aqueous monoethanolamine and piperazine. Chemical Engineering Science 2011;66:5212-8.

[19] Samanta A, Bandyopadhyay SS. Kinetics and modeling of carbon dioxide absorption into aqueous solutions of piperazine. Chemical Engineering Science 2007;62:7312-9.

[20] Bindwal AB, Vaidya PD, Kenig EY. Kinetics of carbon dioxide removal by aqueous diamines. Chem Eng J 2011;169:144-50.

[21] Rocha JA, Bravo JL, Fair JR. Distillation-Columns Containing Structured Packings - a Comprehensive Model for their Performance .1. Hydraulic Models. Ind Eng Chem Res 1993;32:641-51.

[22] Rocha JA, Bravo JL, Fair JR. Distillation columns containing structured packings: A comprehensive model for their performance .2. Mass-transfer model. Ind Eng Chem Res 1996;35:1660-7.

[23] Dash SK, Samanta AN, Bandyopadhyay SS. Simulation and parametric study of post combustion CO2 capture process using (AMP plus PZ) blended solvent. International Journal of Greenhouse Gas Control 2014;21:130-9.

[24] Plaza JM, Rochelle GT. Modeling pilot plant results for CO2 capture by aqueous piperazine. 10th International Conference on Greenhouse Gas Control Technologies 2011;4:1593-600.

[25] Sachde D, Rochelle GT. Absorber Intercooling Configurations using Aqueous Piperazine for Capture from Sources with 4 to 27% CO2. Energy Procedia 2014;63:1637-56.

[26] Madan T, Van Wagener DH, Chen E, Rochelle GT. Modeling pilot plant results for CO2 stripping using piperazine in two stage flash. Ghgt-11 2013;37:386-99.

[27] Van Wagener DH, Rochelle GT, Chen E. Modeling of pilot stripper results for CO2 capture by aqueous piperazine. International Journal of Greenhouse Gas Control 2013;12:280-7

Appendix F - Dynamic mathematical model for packed column in carbon capture plants

A Dynamic Mathematical Model for Packed Columns in Carbon Capture Plants

Jozsef Gaspar[1], John Bagterp Jørgensen[2], Philip Loldrup Fosbøl[1]

Abstract— In this paper, we present a dynamic mathematical model for the absorption and desorption columns in a carbon capture plant. Carbon capture plants must be operated in synchronization with the operation of thermal power plants. Dynamic and flexible operation of the carbon capture plant is important as thermal plants must be operated very flexibly to accommodate large shares of intermittent energy sources such as wind and solar in the energy system. To facilitate such operation, dynamic models for simulation, optimization and control system design are crucial. The dynamic model developed in this paper is suitable for gas-liquid packed columns, e.g. for CO_2 absorption and desorption. The model is based on rigorous thermodynamic and conservation principles and it is set up to preserve these properties upon numerical integration in time. The developed model is applied for CO_2 absorption and desorption simulation using monoethanolamine (MEA) and piperazine (PZ) as solvent. MEA is considered as the base-case solvent in the carbon capture business. The effect of changes in the flue gas flow rate and changes in the available steam are investigated to determine their influence on the performance of the capture process. The response of the model is shown in terms of capture efficiency and purity of the CO_2 product stream. The model is aimed for rigorous dynamic simulation in the context of optimization and control strategy development.

I. INTRODUCTION

Carbon Capture and Storage (CCS) has emerged as one of the main alternatives for sustainable energy infrastructure development and it is moving towards industrial deployment. Post-combustion capture (PCC) is a mature technology which is suitable for various processes in power plants, the steel industry, cement production, petroleum refining, and the bio-chemical industry, etc. In October, the first implementation of CCS on a commercial scale, the Canadian Boundary Dam coal-fired power plant with integrated PCC, started to capture and transport 1 million tonnes of CO_2/year.

The growing focus to reduce CO_2 emissions imposes the need to implement CO_2 capture technologies in fossil fuel-fired power plants. However, issues related to the large cost and high energy use of the CCS technology still need to be overcome. One possible solution is the part load operation of capture units during periods of high peak electricity prices which leads to the increase of the energy output of thermal power plants. In addition, the increasing use of renewable sources, e.g. wind and solar energy also imposes the need for flexible operation of power plants. Power plants already operate with large and frequent load changes on a daily basis to balance the power production and the electricity demand.

Therefore, the understanding of the capture unit transient behavior is required in order to maintain the flexibility of the power plant with the integrated capture unit.

To enable flexible and economically efficient operation of power plants with integrated carbon capture plants, they should be optimized and controlled in a coordinated fashion. Model based optimization and control technologies are needed for this coordination. These technologies require dynamic models of the individual units and of the entire plant to coordinate and optimize the process. The main unit operations of a post combustion plant are the columns for absorption of CO_2 and desorption of CO_2. In this paper, we derive dynamic mathematical models and investigate the dynamic response of such columns. Understanding the transient behavior of the CO_2 capture process will contribute to the industrial deployment of the CCS technology by assuring flexible and economically feasible operation of the thermal power plant with integrated CO_2 capture units.

Studies that propose a dynamic model for CO_2 capture simulation have recently started to appear in the open literature [1]-[3]. However, most of the dynamic models for CO_2 absorption and desorption have been implemented in specialized simulation software packages e.g. gPROMS, Aspen Plus Dynamics, UniSim, etc [4]. The further development of these models might be limited due to the locked architecture of the software package. Åkesson et al. [5] show that rigorous models for model based online optimization and control are computationally demanding. To be computationally tractable, reduced order models must be used. The best approach to maintain reliability is to approximate the mass and heat transfer models with correlations. Rigorous solution of mass and heat transfer models requires the computation of steady-state or transient differential equation systems coupled with the evaluation of the thermodynamic, kinetic and physical property model. Generally, heat and mass transfer correlations are algebraic equations and give reasonable approximation of the exact model.

The purpose of the present paper is to present a dynamic model for transient simulation of packed columns. The model uses heat and mass transfer correlation models and it is based on rigorous thermodynamics. It is specific for solvent based post-combustion capture system and it is applied for CO_2 absorption and desorption simulation. The key novelty introduced by the present study is the development, implementation and validation of a mechanistic first principle based dynamic model for CO_2 absorption and desorption columns. The differential equation scheme is kept in standard and modular form to maintain the flexibility of the system

[1]Department of Chemical and Biochemical Engineering,Technical University of Denmark, Kgs. Lyngby, Denmark `joca,plf @kt.dtu.dk`
[2]Department of Applied Mathematics and Computer Science,Technical University of Denmark, Kgs. Lyngby, Denmark `jbjo@dtu.dk`

and to make it easy to implement for various processes. The developed model is demonstrated for CO_2 absorption and desorption using the base case MEA and the more promising PZ solvent. The dynamic behavior of the model is investigated for two simulation scenarios: (1) changes in the power plant load and (2) insufficient and/or low quality steam for the reboiler. To the authors' knowledge, this is the first study that presents, compares, validates and analyses a dynamic mechanistic model for MEA and PZ. The paper is organized in two main sections. The first part shows the derivation of a dynamic model for packed columns. The second part of the paper describes a case study illustrating the dynamic behavior of CO_2 absorption and desorption columns using MEA and PZ.

II. Dynamic Model Development

This section presents a dynamic model for CO_2 absorption and desorption calculation. It first introduces the system boundaries and the basic assumptions for the rate based CO_2 capture model. The material and energy balances are stated in the following two subsections. The last two sub-sections focus on the core thermodynamics and simultaneous mass transport and reaction description. The focus is on the main practical simplifications which can be considered for the development of the post-combustion capture process. These assumptions aim to reduce the computational load of the numerical scheme.

A. Assumptions and boundaries

The plug-flow reactor (PFR) model is a common way to represent packed columns, e.g. the CO_2 absorber and desorber. The PFR model assumes that there is no radial distribution of properties e.g. temperature, concentration, velocity. A PFR is a combination of well-mixed units which corresponds to the so called control volume. Fig. 1 illustrates a packed column and the transport phenomena in a control volume of this column. The conservation of mass and energy is applied to this control volume with fixed boundaries. The liquid inlet concentration, temperature and flow rate are fixed at the top ($h = H$) of the column. The gas inlet conditions are fixed at the bottom ($h = 0$) of the column. The liquid bottom and gas top stream are determined using the conservation laws. Fig. 1 illustrates that the column is divided into a gas and a liquid side. The volume occupied by the liquid is $dV_l = \varepsilon h_l dV$, where ε is the void fraction and h_l is the liquid hold-up.

A few idealizations are imposed to facilitate the application of the thermodynamic principles. An adiabatic column with counter flow is considered. It is assumed that the mass transfer between the phases is bi-directional, to develop a flexible and generic model. Positive sign shows mass transfer from gas to liquid, i.e. absorption or condensation and negative sign refers to desorption and evaporation.

B. Conservation of mass for the gas and liquid phase

Mass transfer is a result of molecular diffusion and convection. The flow fields of an industrial packed column are
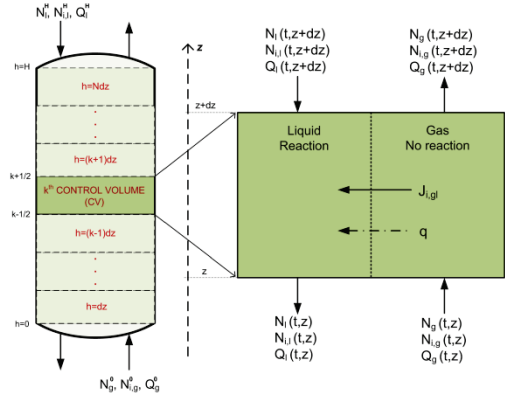

Fig. 1: Packed column with a control volume of height dz

strongly turbulent in both phases, and it is reasonable to assume that the mass transfer rate by molecular diffusion is negligible compared to the convective flux. Therefore, the total mole balance for a control volume is given in (1a), where the left hand side represents the accumulation of moles, $\triangle n_l$ within $dV_l = \varepsilon h_l S dz$. The right-hand side gives the convective mass transfer flux, where N_l denotes the total liquid flux, $u_{el} = \frac{F_l}{\varepsilon h_l S}$ is the effective liquid velocity and F_l is the volumetric flow rate [7]. The net liquid flux is (2b). The mass transfer flux through the gas-liquid interface, $J_{i,gl}$ is calculated using (12a). Note that all of the mass transfer fluxes are expressed in mole bases, $mol/m^2 s$. When the control volume becomes infinitesimal, (1a) reduces to the differential form of the total liquid phase mole balance equation, as shown in (1b). The total mole balance is expressed in mole-density, C_l. It is assumed that the liquid hold-up is constant in time.

$$\triangle n_l = \triangle N_l \varepsilon h_l S dt + a_{eff} dt \sum J_{i,gl} \qquad (1a)$$

$$\frac{\partial C_l}{\partial t} = \frac{\partial N_l}{\partial z} + \frac{a_{pck}}{\varepsilon h_l} \sum J_{i,gl} \qquad (1b)$$

where

$$\triangle n_l = (C_l dV_l)|_{t+dt,z} - (C_l dV_l)|_{t,z} \qquad (2a)$$

$$\triangle N_l = (C_l u_{el})|_{t,z+dz} - (C_l u_{el})|_{t,z} \qquad (2b)$$

Substitution of the total mole, n_l by the moles of component i in a control volume, $n_{i,l}$, leads to (3a). The component mole balance equation for component i in liquid phase is shown in (3b). The molar flux of component i is $N_{i,l} = C_{i,l} u_{el}$, where $C_{i,l}$ refers to the molar concentration and u_{el} is the effective velocity of the liquid.

$$\triangle n_{i,l} = \triangle N_{i,l} \varepsilon h_l S dt + a_{eff} dt J_{i,gl} \qquad (3a)$$

$$\frac{\partial C_{i,l}}{\partial t} = \frac{\partial N_{i,l}}{\partial z} + \frac{a_{pck}}{\varepsilon h_l} J_{i,gl} \qquad (3b)$$

where

$$\triangle n_{i,l} = (C_{i,l} dV_l)|_{t+dt,z} - (C_{i,l} dV_l)|_{t,z} \qquad (4a)$$

$$\triangle N_{i,l} = (C_{i,l} u_{el})|_{t,z+dz} - (C_{i,l} u_{el})|_{t,z} \qquad (4b)$$

The total and component mole balance equations can be deduced in a similar way for the gas phase and they are stated in (5) and (6). Note that the volume occupied by the gas is $dV_g = \varepsilon h_g S dz$, where $h_g = 1 - h_l$. The molar flux of component i, in and out of the control volume is $N_{i,g} = C_{i,g} u_{eg}$ where $C_{i,g}$ refers to the concentration of component i in the gas phase and u_{eg} is the effective velocity of the gas.

$$\frac{\partial C_g}{\partial t} = -\frac{\partial N_g}{\partial z} - \frac{a_{pck}}{\varepsilon(1 - h_l)} \sum J_{i,gl} \qquad (5)$$

$$\frac{\partial C_{i,g}}{\partial t} = -\frac{\partial N_{i,g}}{\partial z} - \frac{a_{pck}}{\varepsilon(1 - h_l)} J_{i,gl} \qquad (6)$$

Equations (1b), (3b), (5) and (6) are based on the enhancement factor approach. Therefore, the reaction term is included in the mass transfer flux, $J_{i,gl}$ which is a sum of the physically and chemically bounded reactive component, e.g. CO_2. Section II-D provides more details about the enhancement factor approach and gives a correlation for the mass transfer flux calculation (12a).

C. Conservation of energy for the gas and liquid phase

Heat transfer is a result of convection, conduction and radiation. Heat transfer by radiation is neglected since packed columns are operated at relatively low temperatures. For practical applications, it is realistic to assume that the active solvent has low volatility and the reaction takes place only in the liquid film. Moreover, the mass and heat transfer area are presumed equal and the volatile components condense at the gas-liquid interface releasing the heat to the liquid. Based on these assumptions, the conservation of the energy for a control volume for the liquid phase is expressed by

$$dV_l \triangle \widetilde{E}_l = \triangle \widetilde{Q}_l \varepsilon h_l S dt - a_{eff} dt (q_{conv} + q_{cond} + q_{gen}) \quad (7)$$

where

$$\triangle \widetilde{E}_l = (C_l E_l)|_{t+dt,z} - (C_l E_l)|_{t,z} \qquad (8a)$$

$$\triangle \widetilde{Q}_l = (N_l Q_l)|_{t,z+dz} - (N_l Q_l)|_{t,z} \qquad (8b)$$

q_{conv} refers to the heat transported through the gas-liquid interface by the volatile components, i.e. CO_2, H_2O; q_{cond} is the heat flux by conduction; and q_{gen} gives the generated heat by reaction or condensation/evaporation. Note that the heat transfer by conduction results from the temperature difference between the phases. The source term, q_{gen} gives the heat generated by the reaction between the active components, i.e. CO_2 and MEA and the latent heat of condensation/vaporization of the volatile components, i.e. MEA, H_2O. The sign of the source term is negative for exothermic reactions and condensation. It is positive for endothermic reactions and vaporization. The gas phase is the reference phase. Therefore, the direction of the mass and heat transfer fluxes is positive for absorption and condensation. The heat transfer fluxes are calculated at the gas phase temperature. The energy of a system is the sum of internal, kinetic and potential energy (9a). The energy carried by the liquid

stream, Q_l through the entrances and exits of the control volume is given in (9b).

$$E_l = U_l + \frac{u_l^2}{2g_c} + \frac{zg}{g_c} \approx U_l \qquad (9a)$$

$$Q_l = H_l + \frac{u_l^2}{2g_c} + \frac{zg}{g_c} \qquad (9b)$$

$\frac{u^2}{2g_c}$ gives the kinetic energy of the system and $\frac{zg}{g_c}$ refers to the potential energy. In the expression of the kinetic respectively potential energy, $g_c = 1[kg - m/N - s^{-2}]$ is the gravitational conversion factor, g is the gravitational acceleration and z gives the height. Note that the internal energy, U and enthalpy, H are thermodynamic state properties. They can be calculated using thermodynamic models or they may be approximated by empirical correlations. By introducing (9a) and (9b) in (7), in the limits when dz approaches zero, the energy balance transforms to:

$$\frac{\partial \widetilde{E}_l}{\partial t} = \frac{\partial \widetilde{Q}_l}{\partial z} + \frac{a_{pck}}{\varepsilon h_l} (q_{conv} + q_{cond} + q_{gen}) \qquad (10)$$

where $\widetilde{E}_l = C_l E_l$ and $\widetilde{Q}_l = N_l Q_l$.

The derivation of the energy balance for the gas phase is similar to the liquid phase, shown in (11), with the exception that the source term, q_{gen}, is set to zero.

$$\frac{\partial \widetilde{E}_g}{\partial t} = -\frac{\partial \widetilde{Q}_g}{\partial z} - \frac{a_{pck}}{\varepsilon(1 - h_l)} (q_{conv} + q_{cond}) \qquad (11)$$

The aim is to end up with a dynamic model which is fast and accurate enough for online optimization and control studies. Therefore, simplification of the mass-heat transfer models is needed to overcome the computational time and memory constraints. The approach of this work is to approximate the mass and heat transfer models using the [7] correlations with an enhancement factor and the Chilton-Colburn analogy [14]. The suitability of these correlations for amine based capture systems is demonstrated in [6].

D. Mass transport phenomena

Three models are typically used in the description of gas-liquid mass transport phenomena. The models are the two-film theory, the penetration theory and the surface renewal model. The mass transfer fluxes are computed by the solution of second order non-linear partial differential equation system. In addition, the mass transfer flux depends on the re-action kinetics for rate based models, e.g. CO_2 absorber and desorber [8]. The complexity of these models can be reduced by introducing the so called enhancement factor (E), which describes the increase in mass transfer rate using reactive solvents compared to non-reactive solvents. An approximate analytical method for predicting the enhancement factor is presented in [9]. This model is based on the penetration theory. A similar approach is adopted in [10] and [11] for the two-film model theory. The enhancement factor approach is preferred since it reduces the computational times and complexity of the numerical scheme. In this basis, the mass

transfer flux of component i, $J_{i,gl}$, through the gas-liquid interface $(x = 0)$ is calculated by

$$J_{i,gl} = -D_i \frac{\partial C_{i,g}}{\partial x}\Big|_{x=0} \approx K_{i,g}^{tot}(p_i^g - p_i^{eq}) \qquad (12a)$$

$$\frac{1}{K_{i,g}^{tot}} = \frac{1}{k_{i,g}} + \frac{H_i}{E k_{i,l}} \qquad (12b)$$

where p_i^g denotes the partial pressure of component i in the gas phase and p_i^{eq} gives the equilibrium partial pressure of component i, and $J_{i,gl}$ gives the mass transfer flux in $(mol/m^2 s)$. Eq. (12b) gives the total mass transfer coefficient, $K_{i,g}^{tot}$, where $k_{i,g}$ and $k_{i,l}$ denote the partial mass transfer coefficients in the gas and liquid film [7]. E is the enhancement factor and H_i is the Henry coefficient for component i.

E. Applied thermodynamics

The extended UNIQUAC thermodynamic model proposed by Thomsen and Rasmussen [12] is applied in the present work to accurately describe the liquid-vapor equilibrium as well as the thermal properties. The phase equilibrium is calculated in a γ-ϕ approach coupled with equilibrium speciation reactions. Therefore, liquid phase activity coefficients are calculated with the extended UNIQUAC model, and the gas phase fugacity coefficients are estimated with the Soave-Redlick-Kwong equation of state.

A realistic approach to simplify the energy balance for the absorber and desorber is to neglect the volume derivative of the internal enthalpy and the pressure derivative of the enthalpy. Therefore, the internal energy and enthalpy of a mixture may be calculated with (13a) and (13b). Note, equation (13a) and (13b) are true for ideal gases and incompressible fluids. Equation (13b) is a reasonable approximation for low-pressure gases, for solids and for liquids outside the critical region [13]. Basically, (13a) and (13b) show the temperature-composition dependence of the internal energy and of the enthalpy of a mixture.

$$dU(T,V,n) \approx \sum n_i C_{v,i} dT \qquad (13a)$$

$$dH(T,P,n) \approx \sum n_i C_{p,i} dT \qquad (13b)$$

where i = CO_2, H_2O and amine, e.g. MEA, PZ, etc. In many cases, the relation between the conductive heat flux, q_{cond} and the temperature gradient is linear and it is given by (14), where λ denotes the interface heat transfer coefficient. The Chilton-Colburn analogy [14] describes the heat transfer coefficient, λ. In case of CO_2 absorption or desorption, the heat of the reaction may be calculated with (15), where $\triangle_r H$ refers to the heat of reaction including physical absorption and $\triangle_{vap} H$ is the heat of vaporization of the volatile compound. The heat of reaction and the heat of vaporization are calculated with the extended UNIQUAC thermodynamic model [12].

$$q_{cond} \approx \lambda (T_g - T_l) \qquad (14)$$

$$q_{gen} = \sum J_{CO_2,gl} \triangle_r H + \sum J_{i,gl} \triangle_{vap} H \qquad (15)$$

where i = H_2O and amine, e.g. MEA, PZ, etc.

TABLE I: Inlet parameters for the base case configuration

Flue gas flow rate	9.64 kmol/s
Flue gas inlet temperature	43.5 C
Flue gas inlet CO_2 mol fraction	14.1 %
Lean solvent flow rate	39.02 kmol/s
Lean solvent inlet temperature mol fraction	40 °C
MEA inlet concentration	7 molal
PZ inlet concentration	5 molal
Lean solvent loading	0.21 mol/mol alk.

F. Solution of the dynamic model

The dynamic model may be represented by the differential equation system (16). This standard form is preferred to preserve the conservation principles upon numerical integration in time and to keep the model in a compact and general applicable form [15].

$$\frac{d}{dt} g(x(t)) = f(x(t), u(t)) \qquad (16)$$

with the initial conditions $x(t_0) = x_0$. The term $g(x(t))$ gives the conserved properties i.e. mass, concentration, energy, $x(t)$ are the system states and $u(t)$ are the manipulated variables, given by

$$x = \begin{bmatrix} C_l & C_{CO_2,l} & C_{H_2O,l} & T_l & C_g & C_{CO_2,g} & C_{H_2O,g} & T_g \end{bmatrix}^T$$

$$g(x) = \begin{bmatrix} C_l & C_{CO_2,l} & C_{H_2O,l} & \widetilde{E}_l & C_g & C_{CO_2,g} & C_{H_2O,g} & \widetilde{E}_g \end{bmatrix}^T$$

The right-hand side of (16) has the usual meaning. It contains the convective-conductive terms along the column height. Note that in the expression of $f(x(t), u(t))$, the divergence of the property, e.g. mass and heat fluxes is invariant in the radial direction. In the present work, the finite difference method is used for the discrete representation of the spatial derivatives in (1b), (3b), (5), (6), (10) and (11). The resulting stiff differential equation system is solved in Matlab using the ode23s solver. However, the computational cost can be improved by using singly diagonally implicit Runge-Kutta methods, such as SDIRK or ESDIRK methods, as shown by [15].

III. RESULTS AND DISCUSSION

The present study investigates the accuracy of the developed dynamic model for CO_2 absorption and desorption. Fig. 2 shows the comparison of the model developed in this work with the CAPCO2 steady-state results [14]. In addition, Fig. 3 and 4 illustrate the effect of changes in the flue gas flow rate conditions and the reboiler operating temperature, to determine their influence on the performance of the CO_2 capture process. Table I summarizes the inlet process parameters and main design specifications for the base case scenario.

The simulation case corresponds to a 200 t/hr CO_2 capacity post-combustion capture plant using 7 molal MEA respectively 5 molal PZ solution. The equivalent loading of the solution is set to 0.21 mol CO_2/mol alkalinity. In the present work, the solvent flow rate is adjusted to capture 90% CO_2 for the base case scenario and the column diameter is determined assuming 70% of flooding [7].
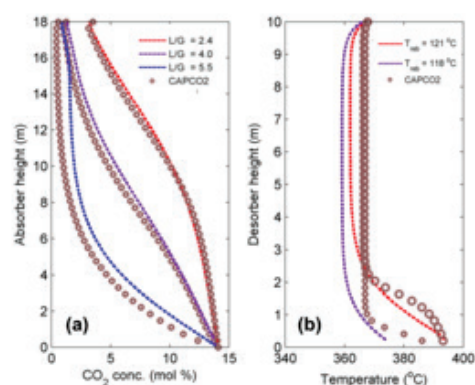
284

Fig. 2: Comparison of the dynamic model with the steady state CAPCO2 model: (a) CO_2 profile vs. absorber's height (b) Temperature profile vs. desorber's height. The o represents the corresponding results with CAPCO2.

Fig. 3: CO_2 capture percentage during ramp changes in the liquid to gas ratio as function of time

A. Model validation

The dynamic model implemented in this study is validated at steady state using the CAPCO2 model, which has been bench-marked in the OCTAVIUS FP7 project [16]. Table I presents the inlet conditions for the validation study.

Fig. 2 presents the performance of the developed model for simulation of CO_2 absorption and desorption. Fig. 2a shows the CO_2 concentration profiles, calculated with the dynamic model and CAPCO2, at three liquid to gas flow ratios (L/G) as function of the column height. This figure underlines that the results obtained by the dynamic model and the steady-state model overlap. Fig. 2b. presents the performance of the implemented model for desorption simulation. This figure illustrates the liquid temperature profiles as function of the height of the desorber when the reboiler temperature is set to 121^oC and 118^oC. The comparison underlines the good agreement between the two models. The deviation between the dynamic model and CAPCO2 are up to 7^oC. This discrepancy in the temperature values is due to the sensitivity of the temperature with the water evaporation rate in the reboiler [17].

B. Dynamic simulation and analysis

The dynamic response of the CO_2 capture model is evaluated using MEA and PZ, for two case studies:

- ramp changes in the flue gas flow rate
- step changes in the reboiler operating temperature

The dynamic simulation is initialized using the base case operating conditions, shown in Table I.

1) Ramp changes in the flue gas flow rate: To understand the effect of changes in the gas flow rate, which might occur due to changes in the output of a thermal power plant, the CO_2 capture percentage is calculated for two ramp scenarios. Fig. 3 shows the simulation results when the flue gas flow rate increases (case 1) and decreases (case 2) linearly after 30 minutes of steady-state operation. The
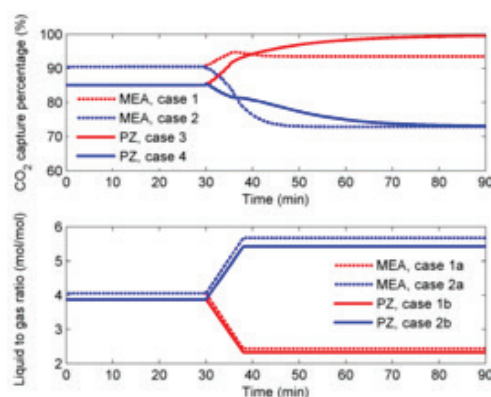
rate of increase respectively decrease of the gas flow rate is 5%/min respectively -5%/min for a period of 8 min. Therefore, the liquid to gas ratio (L/G) changes from 4 to ~ 2.4 (case 1) and ~ 5.6 (case 2). The analysis reveals that a decrease of the L/G ratio results in the increase of the capture percentage and vice verso. Moreover, it underlines the degree of non-linearity in the process for both solvents, MEA and PZ. For the MEA case, a 3.33% change in the capture percentage is observed for case 1a and 19.46% change in the same process variable is observed for case 2a. Even more, the effect of changes in the flue gas flow rate differs between solvents. For the PZ case, CO_2 capture percentage increases with 16.88% for case 1b and decreases with 13.78% for case 2b. Note that the time needed to reach a new steady-state varies with the solvent. MEA reaches a new steady state in ~ 20 min (case 1a and 2a) and PZ in ~ 40 min (case 1b and 2b). One possible explanation is the dependence of the liquid hold-up and therefore residence time on the L/G ratio and solvent physical properties, e.g. viscosity, surface tension, etc. In addition, the simulation reveals that the L/G ratio has a stronger influence on the temperature for the PZ simulation scenario, case 1b and 2b.

2) Step changes in the reboiler temperature: The heat duty and therefore the temperature in the reboiler is a key process variable that can be optimized and controlled. This variable determines the CO_2 removal rate and directly affects the operating cost of the capture plant. Thus, the present work analyses the effect of reducing the reboiler temperature. Note that small decrease of temperature, from 0.25 to $2°C$ may occur due to poor performance of the temperature control loop or due to the inaccuracy of the temperature probe. Greater temperature reductions may appear due to oscillations of the heat supply from the power plant or a change in priority for the use of the steam.

The present analyses evaluates the effect of step changes in the reboiler temperature with respect to the base case value, using MEA and PZ. Note that the first temperature reduction appears after 30 min of steady-state operation. Afterward, the
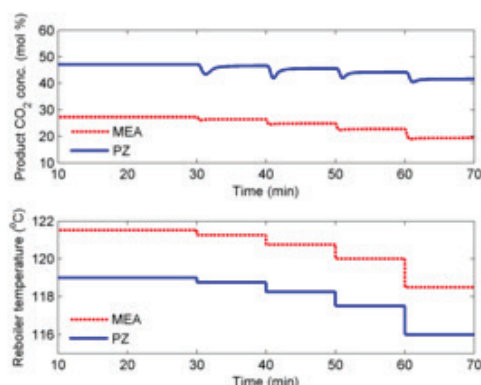
Fig. 4: CO_2 concentration of the product stream above the desorber during step changes in the reboiler operating temperature

temperature is reduced every 10 minutes. Fig. 4 shows the dynamic responses of the process for step changes of -0.25, -0.75, -1.5 and $-3°C$. This figure illustrates the reboiler temperature as function of time and the concentration of the CO_2 product stream, above the desorber, as function of time. As expected, the CO_2 composition of the gas stream at the top of the desorber decreases with the reduction of the temperature of the reboiler. For example, a $1.5°C$ reduction of the temperature results in 16.50% and 6.34% decrease of the CO_2 content when using MEA and PZ. Fig. 4 underlines the non-linearity of the desorber model with respect to the operating conditions of the reboiler. Moreover, it demonstrates that the new steady-state is reached faster with MEA than PZ. This might be due to the differences in the desorber hold-up and the vapor production of the reboiler.

Based on the result in Fig. 4, it can be concluded that even a small drop in the reboiler temperature causes the decrease of the CO_2 recovery since less CO_2 is being collected at the outlet gas stream. Therefore, accurate and robust control of the steam flow rate to the reboiler is essential to maintain the desorber column at desired set point.

IV. Conclusions

This work presents a dynamic mathematical model for the absorption and desorption column in a carbon capture plant. It is set up in a standard form to preserve mass and energy conservation upon numerical integration in time. We have demonstrated the performance of the model for a 200t/h CO_2 capacity absorber and desorber column using as solvent monoethanolamine (MEA) and piperazine (PZ). We have evaluated the accuracy of the model against the CAPCO2 steady-state simulator. The paper shows the results for three liquid to gas flow ratio (L/G) and for two temperature of the reboiler. Moreover, a ramp and step response study is also performed to investigate the effect of changing the L/G ratio and the temperature of the reboiler on the process variables. This study underlines that the decrease of the L/G ratio has

a more pronounced effect on the CO_2 capture percentage than the increase of the L/G ratio. The desorber analysis reveals that even small changes in the reboiler temperature, from 0.25 to 3 $°C$, reduces the CO_2 removal rate. It can be concluded that the implemented model describes the transition from one steady state to another. The model is aimed for robust and rigorous dynamic simulation but also for online optimization and control strategies development. For this, we intend to couple the dynamic model for CO_2 absorption and desorption with models of other sub-units (heat exchangers, sumps, pumps) to form a complete model of a post-combustion capture plant.

References

[1] H.M. Kvamsdal, J.P. Jakobsen, K.A. Hoff, Dynamic modeling and simulation of a CO_2 absorber column for post-combustion CO_2 capture. Chemical Engineering and Processing: Process Intensification, vol. 48(1), pp. 135144, 2009.

[2] T. Greer, A. Bedelbayev, J.M. Igreja, J.F. Gomes, B Lie, A simulation study on the abatement of CO_2 emissions by de-absorption with monoethanolamine, Environmental Technology, vol. 31(1), pp. 107115, 2010.

[3] A. Lawal, M. Wang, P. Stephenson, H. Yeung, Dynamic modelling of CO_2 absorption for post combustion capture in coal-fired power plants, Fuel, vol. 88(12), pp. 24552462, 2009.

[4] M. Bui, I. Gunawan, V. Verheyen, P. Feron, E. Meuleman, S. Adeloju, Dynamic modelling and optimization of flexible operation in post-combustion CO_2 capture plants - A Review, Computer and Chemical Engineering, vol. 61, pp. 245-265, 2014.

[5] J. Åkesson, C.D. Laird, G. Lavedan, K. Prölß, H. Tummescheit, S. Velut, et al., Nonlinear model predictive control of a CO_2 post-combustion absorption unit, Chemical Engineering and Technology, vol. 35, pp. 445-454, 2012.

[6] A.M. Cormos, J. Gaspar, Assessment of mass transfer and hydraulic aspects of CO_2 absorption in packed columns, International Journal of Greenhouse Gas Control, vol. 6, pp. 201-209, 2012.

[7] J.A. Rocha, J.L. Bravo, J.R. Fair, Distillation columns containing structured packings: A comprehensive model for their performance, Industrial & Engineering Chemistry Research, vol. 35(5), pp. 1660-1667, 1996.

[8] D.A. Glasscock, G.T. Rochelle, Numerical simulation of theories for gas absorption with chemical reactions, A.I.Ch.E. Journal, vol. 35(8), pp. 1271-1281, 1989.

[9] W.J. DeCoursey, R.W. Thring, Effects of unequal diffusivities on enhancement factors for reversible and irreversible reaction, Chemical Engineering Science, vol. 44(8), pp. 1715-1721, 1989.

[10] J. Gaspar, K. Thomsen, N. von Solms, P.L. Fosbøl, Cape-open standard for plant wide carbon capture simulation, University of Texas 2nd Conference on Carbon Capture and Storage (UTCCS-2), Austin, Texas, Jan. 2014.

[11] J. Gaspar, K. Thomsen, N. von Solms, P.L. Fosbøl, Solid formation in piperazine rate-based simulation, Proceedings of Greenhouse Gas Control Technologies (GHGT-12) conference, Austin, Texas, 2014

[12] K. Thomsen and P. Rasmussen, Modelling of vapour-liquid-solid equilibrium in gas-aqueous electrolyte systems. Chem. Eng. Science, vol. 54(12), pp. 1787-1802, 1999.

[13] J.M. Smith, H.C. Van Ness, Introduction to chemical engineering thermodynamics, McGraw-Hill International editions, Chemical Engineering Series, Singapore, 4th edition, 1987.

[14] J. Gabrielsen, CO_2 capture from coal fired power plants, Ph.D. Thesis, Technical University of Denmark, 2007.

[15] C. Völcker, J.B. Jørgensen, P.G. Thomsen, E.H. Stenby, Simulation of Subsurface Two-Phase Flow in an Oil Reservoir, Proceedings of European Control Conference, Budapest, Hungary, 2009.

[16] P.L. Fosbøl, J. Gaspar, S. Ehlers, P. Briot, C.S. Sanchez, Y Le Moullec, H Kvamsdal, Benchmarking and comparing first and second generation post combustion CO_2 capture technologies, Proceedings of Greenhouse Gas Control Technologies (GHGT-12) conference, Austin, Texas, 2014

[17] P.L. Fosbøl, K. Thomsen, E.H. Stenby, Energy demand for CO_2 solvent regeneration, Proceedings, pp. 242-252, 2009.

286